A comparative analysis of G-protein- coupled receptor and peptide ligand expression within human and mouse islets of Langerhans, and its application in exploring the role of CXCL14 in islet function

Hawkes, Ross Graham

Awarding institution:
King's College London

A comparative analysis of G-protein-coupled receptor and peptide ligand expression within human and mouse islets of Langerhans, and its application in exploring the role of CXCL14 in islet function

A thesis submitted by

Ross Graham Hawkes

For the degree of Doctor of Philosophy from

King's College London

Diabetes Research Group

Division of Diabetes and Nutritional Sciences

Faculty of Life Sciences and Medicine

King's College London

ACKNOWLEDGEMENTS

I would firstly like to thank Professor Shanta Persaud and Professor Peter Jones for providing me with the opportunity to work for the Diabetes Research Group, and for creating a working environment that was perfect for undertaking a PhD in. The Diabetes Research Group at King's College London is a unique and special place to work, and one that I will look back on fondly.

An extended thank you to Professor Shanta Persaud for her guidance and support during my time at King's, not only in relation to her supervisory role, but as someone who has lent an ear and provided sound advice in times that have required clarity and perspective.

A very special thank you to Dr Stefan Amisten for the opportunity to undertake a PhD under his supervision. His patience, positivity, trust, contagious curiosity and open-mindedness have made these last years a truly interesting and enjoyable experience. I will be forever grateful to Stefan for this opportunity and look forward to celebrating over a slice of blueberry pie!

In addition to my supervisors, I would also like to thank the entire Diabetes Research Group, past and present, especially Patricio Atanes, Amazon Austin, Zara Franklin, Zoheb Hassan, Robert Drynda, Alan Kerby, Ahmed Arzouni, Kerry Mclaughlin, Carolyn Johnson, Astrid Hauge-Evans, Bo Liu, Anastasia Tsakmaki, Inmaculada Ruz Maldonado, Thomas Hill and Jai David. Having fellow colleagues like these made every day that bit more enjoyable.

Lastly, I would like to thank my wife Becky. Her continuous support during the ever changing course that my career has taken us on has been inspiring. Here's to us and the future.

ABSTRACT

G protein-coupled receptors (GPCRs) are a diverse super family of seven transmembrane spanning proteins whose primary function is to initiate the activation of intracellular signalling pathways following stimulation by extracellular stimuli, which include photons, amines, lipids, ions, peptides and proteins. Due to the ubiquitous expression of GPCRs throughout various tissues, they are implicated in the regulation of a variety of diverse physiological processes, such as secretion of the blood glucose controlling hormones insulin, glucagon and somatostatin from islets. As a result, GPCRs are being identified as therapeutic targets for the treatment of type-2 diabetes.

Despite the large array of potential GPCR targets available, only a handful of GPCRs have proven to be successful clinical targets, which may partially be due to the lack of availability of suitable translational models that reflect the human GPCR landscape. The aim of the experiments described in this thesis was to compare the mRNA expression profiles of all GPCRs (the GPCRome) and all GPCR peptide ligands (the Secretome) in human and mouse islets in order to determine the suitability of using mouse islets as a translational model for predicting the role of islet GPCRs and GPCR peptide ligands in human islet function. In addition, some experiments demonstrate how the GPCRome and Secretome data were used to assess the role of CXCL14 in islet function.

Quantitative real-time PCR (qPCR) was used to compare the mRNA expression profiles of 376 GPCRs and 159 GPCR peptide ligands in human islets with their orthologous counterparts in islets isolated from two strains of mice (outbred ICR mice and inbred C57/BL6 mice). A reasonable degree of similarity in GPCR mRNA expression between human islets and islets from each mouse strain was found ($r^2 = 0.360$ vs. ICR; $r^2 = 0.304$ vs C57), with a highly similar expression profile observed between the ICR and the C57 mouse strains ($r^2 = 0.946$). Regression analysis of GPCR peptide ligand mRNA expression revealed that human islets exhibit a reasonable degree of similarity compared to islets of both mouse strains ($r^2 = 0.245$ vs. ICR; $r^2 = 0.225$ vs. C57) with a highly similar expression profile observed between the two mouse strains ($r^2 = 0.968$).

In the process of quantifying the GPCR peptide ligand mRNA expression profiles, it was revealed that the orphan chemokine CXCL14 is expressed by both mouse and human islets. Studies have shown that CXCL14 knockout mice are protected from hyperglycaemia and hyperinsulinemia and they have improved insulin sensitivity. However, CXCL14's role in islet function has yet to be explored. The experiments described in this thesis demonstrate that CXCL14 inhibits insulin secretion from mouse islets and the MIN6 mouse β-cell line by a

mechanism that is not transduced through a Gαi-mediated reduction in intracellular cAMP, but is likely to occur through an inhibition of glucose uptake or glucokinase activity. Further experiments designed to elucidate the target involved in CXCL14 function revealed that CXCL14 is neither an agonist nor an antagonist for the CXCR7 receptor and the putative CXCR4 receptor, and thus these receptors are not responsible for mediating CXCL14 function.

In summary, the experiments described in this thesis reveal that human and mouse islets exhibit some degree of similarity in GPCR and GPCR peptide ligand mRNA expression, but the suitability of using mouse islets as surrogates for predicting human islet physiology is receptor/receptor family specific. This thesis also reveals how the GPCRome and Secretome data can be employed to investigate the role of particular ligands, such as CXCL14, and potential GPCRs responsible for mediating the actions of such ligands in islet function.

Abbreviation	Definition
18S	18S ribosomal rRNA
2DG	2-deoxy-D-glucose
α	Alpha
Ab	Antibody
ATP	Adenosine triphosphate
β	Beta
bp	Base pair
BrdU	5-bromo-2'-deoxyuridine
BSA	Bovine serum albumin
^{o}C	Degrees centigrade
Ca^{2+}	Calcium
cAMP	Cyclic adenosine 3', 5' - monophosphate
cDNA	Complementary DNA
CO_2	Carbon dioxide
Conc.	Concentration
cpm	Counts per minute
Ct	Threshold cycle
CXCL12	Chemokine (C-X-C motif) ligand 12
CXCL14	Chemokine (C-X-C motif) ligand 14
dH_2O	Distilled water
DMEM	Dulbecco's modified Eagle's medium
DMSO	Dimethyl sulphoxide
DNA	Deoxyribonucleic acid
ECM	Extracellular matrix

EDTA	Ethylenediaminetetraacetic acid
ELISA	Enzyme-linked immunosorbent assay
E_{max}	Maximum efficacy
ER	Endoplasmic reticulum
FBS	Foetal bovine serum
FLIPR	Fluorescent light imaging plate reader
FRET	Fluorescence resonance energy transfer
Fura-2-AM	Fura-2-acetoxymethyl derivative
γ	Gamma
GAPDH	Glyceraldehyde 3-phosphate dehydrogenase
G6P	Glucose-6-phosphate
G6PDH	Glucose-6-phosphate dehydrogenase
GDP	Guanosine diphosphate
GLP-1	Glucagon-like peptide-1
GLUT	Glucose transporter
GPCR	G-protein-coupled receptor
Grb2	Growth factor receptor-bound protein 2
GTP	Guanosine triphosphate
HbA_{1c}	Glycated haemoglobin A1c
HCl	Hydrochloric acid
Hr	Hour
HTRF	Homogeneous time-resolved fluorescence
IBMX	3-isobutyl-1-methylxanthine

INS-1	Rat insulinoma cell line
IP_3	Inositol 1,4,5-triphosphate
IR	Insulin receptor
IRS	Insulin receptor substrate
µ	Micro
µg	Microgram
µM	Micromolar
mg	Milligram
Min	Minute
MIN6	Mouse insulinoma cell line
mM	Millimolar
ml	Millilitre
mRNA	Messenger RNA
MuLVRT	Murine Leukaemia Virus Reverse Transcriptase
Mwt	Molecular weight
NaOH	Sodium hydroxide
NCS	Newborn calf serum
ng	Nanogram
nM	Nanonmolar
NSB	Non-specific binding
PBS	Phosphate-buffered saline
PCR	Polymerase chain reaction
PEG	Polyethylene glycol
PI3K	Phosphatidylinositol-3-kinase

PIP_2	Phosphatidylinositol 4,5-biphosphate
PKA	Cyclic-AMP-dependent protein kinase A
PKC	Protein kinase C
PLA_2	Phospholipase A_2
PLC	Phospholipase C
PLD	Phospholipase D
PPIA	Peptidylprolyl isomerase A
RIA	Radioimmunoassay
RLU	Relative luminescent units
RNA	Ribonucleic acid
RT	Reverse transcription
SAB	Secretion assay buffer
SDF-1α	Stromal derived factor-1α
SH2	Src homology 2
SOS	Son of sevenless
TR	Time resolved
UV	Ultraviolet

CHAPTER 1 - Introduction

1.1 The islets of Langerhans

1.1.1 Islet structure

The islets of Langerhans, which are the endocrine component of the pancreas, constitute 1-4% of the total pancreatic mass, whilst the remaining proportion of the pancreas is comprised of exocrine tissue (Dolensek et al., 2015). Each islet is approximately 100-200μm in diameter (Jo et al., 2007) with approximately a million islets found in the healthy human pancreas and approximately 1000 islets found in the mouse pancreas (Bonnevie-Nielsen et al., 1983). Whilst the pancreas size and therefore number of islets is proportional to the size of the species, the actual size of islets remains similar between species (Kim et al., 2009). Each mammalian islet contains approximately 50 to 3000 cells, which can be categorised into five cell types: glucagon secreting α-cells; insulin secreting β-cells, somatostatin secreting δ-cells; pancreatic polypeptide releasing cells and ghrelin expressing ε-cells (Rutter et al., 2015). Despite similarities in size and cell type presence of islets between human and rodent islets, the proportion and distribution of the five cells types of the islet varies. For instance, the proportions of α-, β-, δ-cells within the human islet are approximately 40, 50, 10% respectively, whereas in mouse islets the proportions are approximately 15-20, 60-80, 10% respectively (Steiner et al., 2010). Not only do the proportion of islet cells differ between human and rodent islets but the arrangement of these cells within islets also varies. Within rodent islets a core of β-cells surrounded by a mantle of α-cells and δ-cells is observed, whereas the arrangement of such cells within human islets is less defined and found to be more interspersed with each other (Cabrera et al., 2006) (Figure 1.1.1).

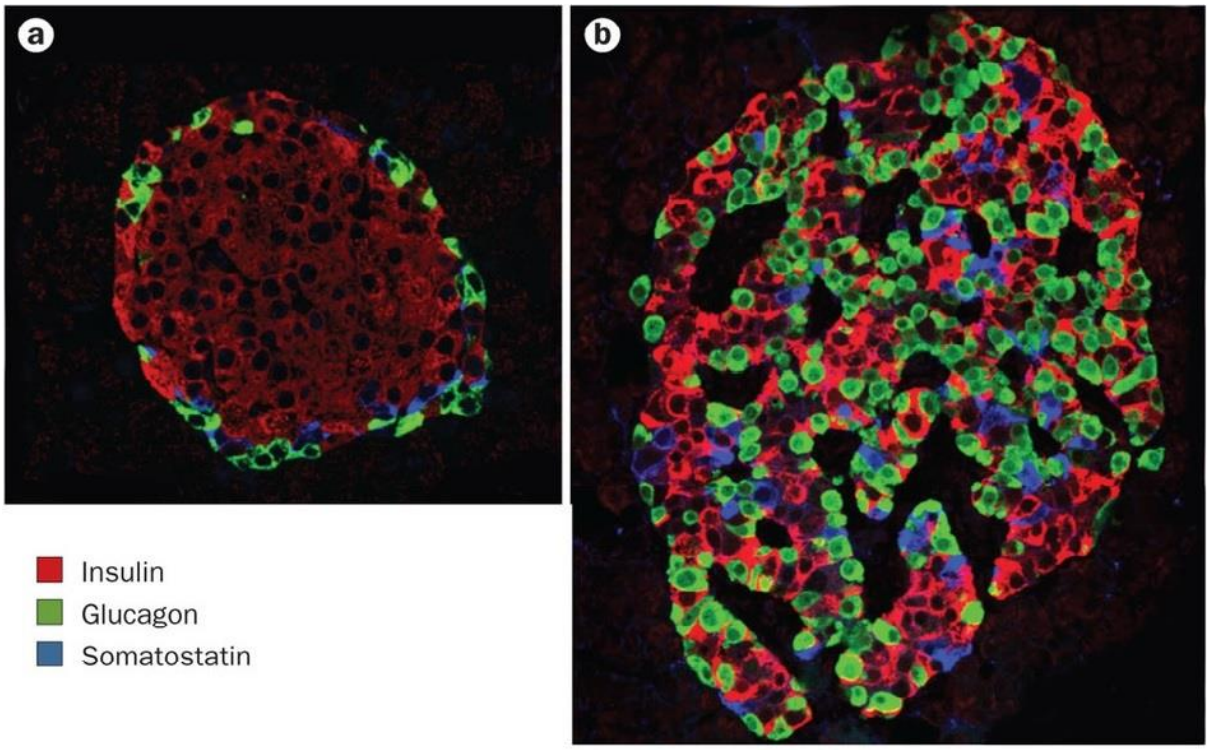

Figure 1.1.1 Architecture of the islets of Langerhans. The figure depicts a cross section of a (a) mouse and (b) human islet stained for insulin, glucagon and somatostatin as indicated by red, green and blue immunofluorescence respectively (Wang et al., 2015).

Islets are highly vascularised (see Figure 1.1.2) and despite only accounting for approximately 3% of the pancreatic mass, receive 15% of the total pancreatic blood supply (Jansson et al., 2016). There are two distinct blood flow patterns within the mouse islet: inner to outer, in which flow travels from the β-cell core to the outer layer of other cell types, and top to bottom, in which flow travels from one side of the islet to the other irrespective of cell type. The inner to outer flow is proposed to support the concept that β-cell secretory products can regulate the function of cells downstream, for example the regulation of glucagon secretion from α-cells (Nyman et al., 2008). Whilst these blood flow patterns have been observed in mouse islets, the fact that cell type distribution varies more in human islets suggests the pattern of flow in human islets may differ compared to mouse islets.

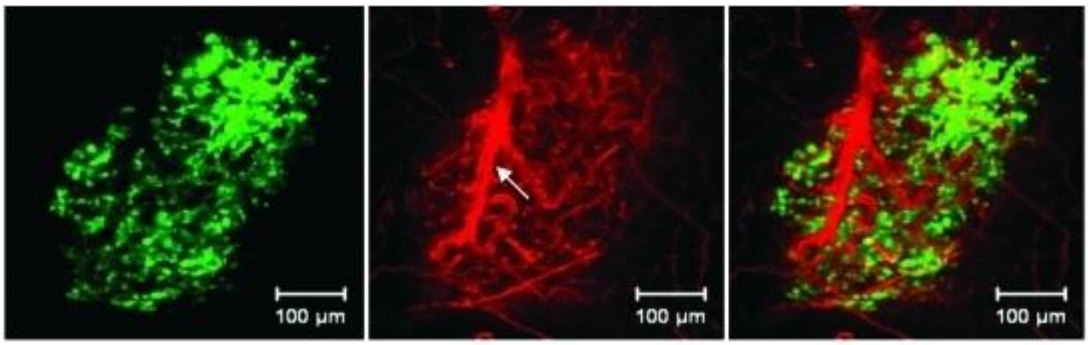

Figure 1.1.2 Visualisation of islet vasculature. Islet β-cells highlighted with GFP fluorescence and islet vasculature observed by Rhodamine dextran infusion (red) in the left and centre panels respectively. Right panel depicts a superimposed image. (Nyman et al., 2008).

The extensive vascularisation of islets is an integral component of their primary role to sense fluctuations in blood nutrients and respond accordingly in an endocrine manner to maintain glucose homeostasis.

1.1.2 The regulation of glucose homeostasis

Mammalian cells, in particular the brain, utilise glucose as a primary source of energy in the form of ATP, which is necessary for many metabolic processes (Hoyer, 1990). Due to the significant involvement of glucose in essential cellular processes, the circulating levels of glucose are meticulously monitored and controlled in order to maintain euglycemia, i.e. ~3-5mM blood glucose. The maintenance of glucose homeostasis is a co-ordinated and complex series of processes that involves the endocrine pancreas, liver, adipose tissue, skeletal muscle, gastro-intestinal tract and the central nervous system. The principal pancreatic endocrine hormone involved in the reversal of postprandial elevation in blood glucose is insulin, which functions by

enhancing glucose uptake into insulin-sensitive tissues and promoting it's storage in macromolecules.

Following elevations in blood glucose, the β-cells of the islets of Langerhans secrete insulin, which functions by binding to cell surface insulin receptors within target tissues. The insulin receptor (IR) is a membrane bound $(\alpha\beta)_2$-type receptor tyrosine kinase, which is composed of two αβ-heterodimers. Each heterodimer consists of an extracellular hormone-binding α-subunit and a transmembrane spanning β-subunit containing an intracellular tyrosine kinase binding domain. The α- and β-subunits of each heterodimer are linked by a disulphide bridge and the two heterodimers linked by four disulphide bridges between the α–subunits (Tatulian, 2015).

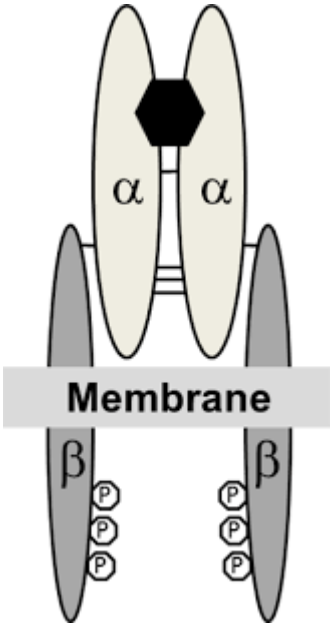

Figure 1.1.3 An illustration of the structure of the insulin receptor (Tatulian, 2015). The two α-subunits of the receptor are quadruply disulfide-linked, and each α-chain is disulfide-linked to a β- chain. Once bound to insulin (black hexagon), each β-chain phosphorylates its counterpart at tyrosines 1158, 1162, and 1163.

Upon insulin binding, the receptor undergoes a conformational change which promotes the autophosphorylation of three tyrosine residues located on each β-subunit

of the heterodimer, thus disinhibiting the tyrosine kinase activity of the receptor. This allows for the phosphorylation of downstream signalling molecules such as the insulin receptor substrate proteins (IRS) of which there are four members, IRS1-4 (Sesti, 2000). IRS1 and 2 are ubiquitously expressed throughout insulin sensitive tissues whereas IRS3 is predominantly expressed within adipocytes (Zhou et al., 1999). IRS proteins are classed as adapter proteins that have no intrinsic catalytic activity, but once phosphorylated reveal sites of binding for Src homology proteins, such as phosphatidylinositol-3-kinase (PI3K) and growth factor receptor-bound protein 2/son of sevenless (Grb2/SOS). The PI3K pathway mediates translocation of glucose transporter 4 (GLUT4) to the plasma membrane of adipocytes and myocytes following phosphorylation of the membrane lipid phosphatidylinositol 4,5 bisphosphate (PIP_2) to phosphatidylinositol 3,4,5 trisphosphate (PIP_3,) the recruitment of Akt2 and the subsequent phosphorylation of Akt2 by PDK1 (Tatulian, 2015). The increased translocation of GLUT4 to the plasma membrane facilitates glucose uptake, thus reducing circulating blood glucose levels. In addition to GLUT4 translocation, the interaction of IRS with Grb2 induces the binding of Grb2 to SOS and the activation of Ras protein, resulting in the nuclear translocation of MAPK and the regulation of transcription factors which modulate gene expression, proliferation and differentiation (Brown et al., 2015). Thus, the role of IRS proteins are essential to insulin's mechanism of action in regulating cell metabolism and growth.

As previously mentioned, the process of glucose uptake is facilitated by glucose uptake transporters. The GLUT protein family consists of 14 members grouped into three major classes based on sequence homology and substrate selectivity (Aparicio et al., 2010). GLUT4 is predominantly expressed in myocytes and adipocytes and is responsible for the majority of total glucose uptake during periods of elevated blood

glucose; muscle ~85%, adipose tissue ~15% (Govers, 2014). Cellular uptake of glucose via GLUT4 is an energy-independent process that can only occur down a concentration gradient. The GLUT2 isoform, on the other hand, is expressed in the intestine, kidney, liver and β-cells of pancreatic islets and it has a distinctly different glucose uptake kinetic profile to GLUT4 (Mueckler, 1994). GLUT2 is a high capacity, low affinity transporter with a K_m for glucose of ~17mM. This high capacity and low affinity allows for a large influx of glucose and is one of the key underlying factors responsible for mediating the secretion of insulin from β-cells during hyperglycaemic episodes (Leturque et al., 2009).

In contrast to maintaining glucose homeostasis during hyperglycaemia, processes also exist to modify glucose homeostasis during periods of hypoglycaemia. In the event of hypoglycaemia, glucagon is secreted from the α-cells of the islets to promote hepatic glucose production by promoting glycogenolysis and gluconeogenesis. These events are mediated through the glucagon receptor (GCGR), which couples principally through the Gαs-coupled signalling cascade but also through Gαq (Han et al., 2015). Activation of the Gαs pathway promotes activation of the membrane bound adenylate cyclase enzyme which increases intracellular cAMP generation and subsequently activates protein kinase A (PKA). PKA phosphorylates glycogen phosphorylase kinase, which subsequently phosphorylates the serine-14 residue of glycogen phosphorylase resulting in glycogenolysis (Jiang and Zhang, 2003).

1.1.3 Insulin biosynthesis and storage

The ability of β-cells to release insulin quickly in response to elevated blood glucose levels and to replenish insulin stores in preparation for the next episode of elevated

blood glucose means that they are highly specialised for the production and storage of insulin. The human insulin gene is located on the short arm of chromosome 11 and is comprised of 1335 base pairs (Bell et al., 1980). Transcription of the gene encodes an mRNA molecule of 600 nucleotides which when translated produces the 11.5kDa polypeptide preproinsulin. Following production, preproinsulin is released into the lumen of the rough endoplasmic reticulum (Halban, 1991) and cleaved by proteolytic enzymes to generate a 9kDa peptide, proinsulin, which is comprised of an A chain (21 amino acids) and a B chain (30 amino acids) of insulin linked by a 31 amino acid C-peptide (Orci et al., 1988). The purpose of the C-peptide is to contribute to the post-translational modification of proinsulin before it is transported in microvesicles to the Golgi apparatus and packaged into secretory granules. Conversion of proinsulin into insulin occurs within the calcium-rich acidic environment of the maturing secretory granule (Hutton, 1982), a process which is mediated by two endopeptidases: pro-hormone convertase 2 and 3, and carboxypeptidase H (removes C-peptide) (Davidson and Hutton, 1987). The newly synthesised 5.8kDa insulin peptide and the C-peptide are stored together in secretory granules along with divalent cations such as magnesium (70mM), calcium (120mM), and importantly, zinc (20mM), which is essential for the crystallisation and stabilisation of mature insulin protein within the secretory granule.

1.1.4 Regulation of insulin secretion from islets of Langerhans

The release of insulin from secretory vesicles is a multistep process that requires the translocation of vesicles to the plasma membrane, vesicle docking and the fusion of vesicles with the plasma membrane. Regulation of this process is mediated by a variety of mediators including nutrients, hormones, and neurotransmitters.

1.1.4.1 Glucose-induced insulin secretion

Glucose is the principal physiological secretagogue for insulin secretion. Glucose-induced insulin secretion is mediated through the uptake of glucose into the β-cells via insulin-independent glucose uptake transporters (GLUTs), in particular GLUT-2, whilst GLUT-1 and -3 in have also been implicated in glucose uptake into human β-cells (Thorens, 2015). GLUT2 is a high capacity low affinity transporter with a K_m for glucose of ~17mM. This high capacity and low affinity allows for a large influx of extracellular glucose, thus promoting a rapid equilibration of extracellular glucose with that present inside the cell and it is therefore fundamental in mediating insulin secretion from β-cells during periods of elevated blood glucose levels (Leturque et al., 2009). During these periods, glucose is taken up into the β-cell and is phosphorylated to glucose-6-phosphate (G6P) by the rate-limiting intracellular enzyme glucokinase (Matschinsky, 1996), which is the first step in the glycolytic pathway. The end product of glycolysis is the generation of pyruvate which is fed into the tricarboxylic acid (TCA) cycle in the mitochondria, resulting in increased ATP production and subsequent elevations in cytosolic ATP levels. This surge in cytosolic ATP increases the ATP:ADP ratio and subsequently leads to closure of ATP-sensitive K^+ (K_{ATP}) channels following binding of ATP to the Kir6.2 subunit. Consequently, a reduction in intracellular K^+ efflux induces depolarisation of the plasma membrane and activation of voltage-gated Ca^{2+} channels (Yang and Berggren, 2006). The resulting effect is an influx of extracellular calcium which in turn prompts the activation of calcium sensing secretory granule-associated small N-ethylmaleimide-sensitive factor receptor (SNARE) proteins, which promote fusion of the vesicle with the plasma membrane (Sudhof and Rothman, 2009).

Glucose-induced insulin release displays a biphasic pattern consisting of a prompt short-lived (0-10mins) release of insulin followed by a stable and prolonged phase of release (Del Prato et al., 2002). First-phase insulin release has a lower glucose threshold than the late-phase suggesting that alternative mechanisms exist for each phase (Nesher and Cerasi, 1987). The mechanisms underlying this biphasic pattern of insulin release are not entirely understood but it has been proposed that the β-cell contains two distinct pools of insulin granules: 1) a small labile pool that is primed for immediate release and 2) a larger pool that feeds slowly into the labile pool (Grodsky et al., 1969). Following exhaustion of the labile pool and subsequent ending of first phase release, translocation of granules from the large pool replenishes the system and initiates the second phase of insulin release (Nesher and Cerasi, 2002).

Glucose-induced increases in cytosolic calcium within β-cells also promote the activation of additional effector molecules, such as calcium-calmodulin-dependent protein kinases (CaMKs), phospholipase C (PLC) and cytosolic phospholipase A_2 ($cPLA_2$):

Calcium/calmodulin-dependent protein kinases (CaMKs)

Calcium/calmodulin-dependent protein kinases (CaMKs) are a class of calcium-sensitive enzymes that are activated in the presence of intracellular Ca^{2+} and the Ca^{2+}-binding protein calmodulin (CaM). The β-cells express several kinases that are activated by Ca^{2+} and CaM, including the myosin light chain kinase (MLCK), CaMK II, CaMK III and CaMK IV (MacDonald and Kowluru, 1982), (Jones and Persaud, 1998) (Hughes et al., 1993) (Persaud et al., 2011). CaMK II has been implicated in the modulation of Ca^{2+}-induced insulin secretion following results indicating that a loss of secretory responsiveness is accompanied by a reduction in Ca^{2+}-dependent

phosphorylation of endogenous islet substrates for CaMK II (Jones et al., 1992). Such substrates for CaMK II include MAP-2 and synapsin I, which facilitate the trafficking of insulin secretory granules (Easom, 1999).

PLC/ protein kinase C (PKC) signalling pathway

PLC is a membrane bound phospholipase that plays a key role in the PLC/PKC intracellular signalling pathway, which is also implicated in non-nutrient induced insulin secretion following Gαq-coupled GPCR activation. In brief, PLC hydrolises membrane-bound phosphatidyl-4,5,-biphosphate (PIP_2) into two second messengers: inositol 1,4,5-triphosphate (IP_3) and diacylglycerol (DAG). The generation of IP_3 activates IP_3-receptor gated calcium channels on the endoplasmic reticulum resulting in mobilisation of calcium from internal stores and consequently potentiating glucose-induced insulin secretion. DAG generation results in translocation of DAG sensitive protein kinase C isoforms to the β-cell plasma membrane. The role of PKC in glucose-induced insulin secretion is unclear, with reports suggesting that down regulation of PKC isoforms in β-cells does not affect glucose-induced insulin secretion (Persaud and Jones, 1993), whereas the potentiation of insulin secretion with Gαq-coupled receptor agonists was abolished following down regulation of PKC (Persaud et al., 1991). This suggests that DAG-sensitive PKC isoforms are not important for glucose-induced insulin secretion but are for non-nutrient potentiation of insulin secretion.

cPLA$_2$

Elevations in intracellular calcium levels within β-cells can activate the calcium-sensitive cytosolic PLA_2 ($cPLA_2$) enzyme, which hydrolyses membrane

phosphatidylcholine to generate arachidonic acid. By itself, arachidonic acid stimulates insulin secretion from dispersed rat endocrine-enriched pancreatic cells (Metz et al., 1983). However, metabolism of arachidonic acid via the cyclooxygenase and lipoxygenase pathways results in the generation of prostaglandins, thromboxanes, hydroxyeicosatetrenoic acids (HETES), hydroperoxyeicosatretenoic acids (HPETES), which have unclear effects on insulin release (Walsh and Pek, 1984) (Metz et al., 1984). This lack of clarity on the role of arachidonic acid metabolites on islet function is in part due to the reliance on the usage of poorly selective COX and LOX inhibitors.

While glucose is the principal stimulus for insulin release from β-cells, alternative mechanisms exist to potentiate and modulate this effect, for example through, GPCR-mediated mechanisms.

1.1.4.2 GPCR-mediated regulation of insulin secretion

G-protein-coupled receptors are a diverse family of seven transmembrane bound proteins whose primary function is to initiate the activation of intracellular signalling pathways following the binding of extracellular ligands (Bohme and Beck-Sickinger, 2009). Examples of GPCR ligands that regulate insulin secretion include intra-islet peptides (glucagon and somatostatin), neurotransmitters (acetylcholine and adrenaline), neuropeptides (VIP, PACAP and galanin), incretins (GLP-1 and GIP), divalent cations (Ca^{2+}, Zn^{2+}) and free-fatty acids. Ligand activation of GPCRs results in a conformational alteration in receptor structure, thus allowing the intracellular regions of the receptor to interact with intracellular effector molecules such as heterotrimeric G-proteins, consisting of α, β and γ subunits, and β-arrestins

(Jastrzebska, 2013) (see section 1.3 for a comprehensive review of GPCR structure and function). The activation of specific GPCR-coupled intracellular signalling pathways is dependent on the class of α-subunit that is associated with the heterotrimeric G-protein complex of which there are 4 main classes: Gαs, Gαq, Gαi and Gα12/13. GPCR-mediated effects on insulin secretion vary depending on which α-subunit class is associated with the receptor.

Gαs-coupled GPCRs

GPCRs that couple through Gαs proteins activate membrane bound adenylate cyclase enzymes, which convert intracellular ATP to the second messenger 3',5'-cyclic AMP (cAMP). Elevations in intracellular cAMP result in the activation of protein kinase A (PKA) and exchange proteins activated by cAMP (EPACs), which are involved in the potentiation of insulin secretion by non-nutrients at stimulatory concentrations of glucose. Examples of GPCRs that couple through Gαs to potentiate glucose-induced insulin secretion include the glucagon receptor (GCGR), the glucagon-like peptide 1 receptor (GLP-1R) and the glucose-dependent insulinotropic receptor (GPR119).

Gαi-coupled GPCRs

In contrast to Gαs-coupled GPCRs, GPCRs that couple to Gαi subunits inhibit adenylate cyclase activity, which consequently reduces intracellular cAMP levels and results in inhibition of insulin secretion. Examples of Gαi-coupled GPCRs include the five somatostatin receptors (SSTR1-5), the ghrelin receptor (GHRL), neuropeptide Y receptor 1 (NPYR1) and α2 adrenergic receptors (ADRA2A).

Gαq-coupled GPCRs

Gαq-coupled receptors activate the PLC pathway to generate the intracellular signalling molecules IP_3 and DAG (as described in section 1.1.4.1), resulting in the activation of PKC by DAG in addition to IP_3-mediated mobilisation of calcium from internal stores within the endoplasmic reticulum. Examples of Gαq-coupled receptors include the kisspeptin receptor (KISS1R/GPR54) and the potential T2DM drug targets free fatty acid receptor 1 (FFAR1 or GPR40) and free fatty acid receptor 4 (FFAR4 or GPR120).

1.2 Diabetes mellitus

Diabetes mellitus (DM) is a metabolic disorder characterised by chronically elevated blood glucose levels (hyperglycaemia) resulting from either a complete absence or a relative lack of insulin (Meetoo et al., 2007). The criteria set by the World Health Organisation (WHO) for the diagnosis of diabetes can be defined as glycated haemoglobin (HbA1c) of ≥ 6.5%, fasting plasma glucose concentrations of 7.0mM, plasma glucose levels ≥ 11.1mM for 2 hours following oral consumption of 75g of glucose or random plasma glucose levels of 11.1mM (American Diabetes, 2016). The consequence of chronic hyperglycaemia include microvascular complications, such as retinopathy, nephropathy and neuropathy (Jackson et al., 2014), in addition to macrovascular complications, such as myocardial infarction and stroke.

In addition to the detrimental health implications of diabetes, the economic cost associated with the treatment of diabetes and its comorbidities, both for healthcare services and loss of productivity to society, are large. In the UK alone, approximately 9% of the NHS budget is spent on treating diabetes and its associated complications,

equating to approximately £10 billion per year (Meetoo et al., 2007). Furthermore, according to current trends, the cost of treating diabetes is increasing, which is evidenced by historic figures released by the American Diabetes Association (ADA) revealing that diabetes cost the USA $20.4 billion in 1987, $90 billion 1994 and is estimated to cost $100 billion today (Meetoo et al., 2007). The cost of treating diabetes is certain to rise further, with current projections predicting that global increases in diabetes diagnosis will rise beyond 592 million people by 2035 (da Rocha Fernandes et al., 2016).

The principal causal factors contributing to the increase in incidence of diabetes worldwide include relative over-nutrition and sedentary activity, both of which are a result of a global transition to a more modern westernised lifestyle (Zimmet, 1999). This lifestyle transition promotes the development of the predominant form of diabetes, type 2 diabetes mellitus (T2DM), which accounts for approximately 90% of all diabetes cases (Kharroubi and Darwish, 2015). According to the WHO there are two main types of diabetes: Type 1 DM (T1DM) and Type 2 DM (T2DM) (American Diabetes, 2016). Whilst there are clear overlapping features of both forms of diabetes, in particular the complications associated with both, there are distinct characteristics that exist between the two types.

1.2.1 Type 1 diabetes (T1DM)

T1DM accounts for approximately 10% of all diabetes cases (Daneman, 2006) and occurs as a result of selective autoimmune-mediated destruction of islet β-cells, consequently resulting in complete insulin deficiency (Morgan et al., 2014). Targeted destruction of β-cells is initiated by pancreatic infiltration of immune cells such as macrophages, T cells (CD8+ CD4+) and CD20+ B cells but the exact mechanisms by

which β-cells are specifically targeted remain unclear (Leete et al., 2016). What is clear is that β-cell destruction is progressive and does not occur in a synchronised fashion, a claim that was made following the observation of region-specific islet inflammation within the pancreases of recently diagnosed T1DM patients (Foulis and Stewart, 1984). As a result, early indications of T1DM development tend to go unnoticed until the onset of clinical symptoms become apparent following the destruction of 60-80% of β-cells (Notkins and Lernmark, 2001).

T1DM is a disorder that is typically developed during childhood and early adult life and has been shown to be associated with genetic inheritance. Approximately 40 risk loci are associated with T1DM (Barrett et al., 2009), with the human leukocyte antigen (HLA) gene complex on chromosome 6p21 exhibiting the greatest correlation with T1DM development. The HLA complex is responsible for encoding proteins of the major histocompatibility complex (MHC), which fall into two classes, MHC1 and MHC2. MHC1 proteins present intracellular antigens, whereas MHC2 proteins present cell surface antigens and it is genetic abnormalities in the encoding of MHC2 class antigens which has been shown to correlate with the progression of T1DM. The inheritance of particular HLA alleles account for almost half of the genetic risk associated with T1DM (Todd et al., 1987). Additional susceptibility loci include IDDM2 and CTL4A. The IDDM2 locus is located on chromosome 11p15, contains the insulin gene (INS) and has been shown to contribute approximately 10% towards T1DM susceptibility (Bennett et al., 1995). CLTA4 (cytotoxic T-lymphocyte-associated protein 4) is located on chromosome 2q33 and encodes a molecule that down regulates T-cell activation, thus highlighting the protective role of CLT4A against autoimmunity (Kristiansen et al., 2000).

To compensate for the loss of endogenous insulin secretion, insulin replacement is used as mainstay therapy for the treatment of T1DM (Bacha and Klinepeter Bartz, 2015). The main goals of insulin therapy are to maintain stable blood glucose levels and subsequently HbA1c levels to prevent the development of associated microvascular and macrovascular complications (American Diabetes, 2014). However, due to the requirement for tight regulation of blood glucose levels throughout the day, a range of recombinant insulin analogues have been developed with varying degrees of onset of action (Sanlioglu et al., 2013) e.g. fast-acting and long-acting insulin analogues.

Fast-acting insulin analogues have been designed to be rapidly absorbed following subcutaneous injection (10-15 mins), achieve peak levels within 30-90 mins and have a duration of action of 4-6 hours (Sanlioglu et al., 2013). The overall result is a reduced delay of onset of action which allows for a flexible dosing schedule compared to that of regular insulin, which requires a longer waiting period prior to meal consumption (Sanlioglu et al., 2013). However, hypoglycaemia may be experienced with fast-acting insulin analogues if meals are not consumed within approximately 15mins of administration (Burge et al., 1997). Examples include, insulin-lispro (Humalog) (Zinman et al., 1997), insulin-aspart (Novolog) (Rys et al., 2011) and insulin-glulisine (Apidra) (Lih et al., 2010), which are developed by Eli Lilly, Novo Nordisk and Sanofi-Aventis respectively.

Long-acting insulin analogues are designed to provide basal concentrations of insulin to control fasting hyperglycaemia and pre-prandial blood glucose levels throughout the day (Sanlioglu et al., 2013). The long duration of action is a consequence of formulation design whereby insulin is presented in the form of hexamers which slowly

dissociate to monomers, unlike fast-acting insulin which is presented as a monomeric formulation. Examples include insulin-glargine (Lantus) (Gillies et al., 2000), insulin-detemir (Levemir) (Hermansen et al., 2006) and insulin-degludec (Tresiba) (Zinman et al., 2011) developed by Sanof-Aventis and Novo Nordisk respectively. For almost all T2DM patients starting insulin therapy, long-acting insulin is used alone or in combination with additional anti-diabetic therapies (Sanlioglu et al., 2013), the details of which are described in the following section.

1.2.2 Type 2 diabetes

T2DM is a non-communicable metabolic disorder that accounts for approximately 90% of all diabetes cases. It is characterised by hyperglycaemia, which is a consequence of insufficient insulin secretion, insulin resistance in metabolically active tissues and inadequate suppression of glucagon production (Spellman, 2010). Reduced insulin secretion results in a reduction in the uptake of circulating blood glucose into metabolically active tissues, which is further exacerbated by insulin resistance, both of which collectively contribute to a hyperglycaemic state. The extent of glucose uptake reduction in T2DM was revealed by Groop *et al* who observed that glucose uptake in T2DM patients was reduced by 30% when compared to control patients (Groop et al., 1989). Furthermore, in the same study hepatic glucose production was shown to be significantly greater in T2DM patients compared to control subjects, highlighting the effects of inadequate suppression of glucagon production associated with T2DM (Groop et al., 1989).

It has been well documented that an association between obesity and T2DM exists. Obesity is a state of low grade inflammation and is a key risk factor in the development

of T2DM due to its association with insulin resistance and β-cell dysfunction (Boutens and Stienstra, 2016). Initially, the β-cells compensate for insulin resistance by upregulating insulin secretion and the extent of this upregulation determines whether or not the individual develops T2DM (Bergman, 2005). Eventually, however, the β-cells are unable to meet the demand for insulin production to offset hyperglycaemia.

In addition to promoting insulin resistance, the state of low grade inflammation associated with obesity promotes macrophage infiltration and subsequent release of inflammatory cytokines, which promote islet inflammation and β-cell apoptosis (Stienstra et al., 2007). This contributes to a reduction in β-cell mass that is associated with T2DM but the extent to which β-cell mass is reduced and its role in the etiology of T2DM is not fully understood (Ashcroft and Rorsman, 2012). Butler *et al* reported a 60% reduction β-cell mass in patients with T2DM (Butler et al., 2003), whereas a lower estimation of 39% has also been reported (Rahier et al., 2008). However, Menge *et al* revealed that glucose tolerance was only slightly affected following a partial pancreatectomy in human patients (Menge et al., 2008), suggesting that β-cell mass alone is not the principal factor involved in the development of T2DM.

Genetic factors have also been implicated with T2DM incidence. One of the most important diabetes susceptibility genes is TCF7L2 (transcription factor-7-like-2) located on chromosome 10q, which increases diabetes risk by 45% (Rutter, 2014). TCF7L2 has been shown to be involved in Wnt signalling and it influences insulin secretion but it is unclear whether it is up- or downregulated in T2DM (Lyssenko et al., 2007). In addition, a polymorphism in SLC30A8, a highly expressed β-cell gene which codes for the ZnT8 zinc transporter, has been shown to increase T2DM susceptibility by 20% (Sladek et al., 2007). Variants of the KCNJ11 and ABCC8 genes, which encode the Kir6.2 and SUR1 subunits of the ATP-sensitive K^+ channel,

have been implicated in the development of neonatal diabetes (Bennett et al., 2010, Nessa et al., 2016).

The primary aim of T2DM therapies is to maintain glucose homeostasis for as long as possible following diagnosis, thereby reducing the onset of associated complications (Kahn et al., 2014). There are numerous therapies with varying mechanisms of action that aim to reduce hyperglycaemia associated with T2DM, which are described below.

Biguanides

The first line therapy in treating T2DM is Metformin (Glucophage), which belongs to the biguanide class of compounds. The most prevalent effect of Metformin is a decrease in hepatic glucose production, whilst increased glucose uptake through increased GLUT4 expression and an inhibition of adipocyte lipolysis are the secondary effects of Metformin treatment (Bosi, 2009). The mechanism of action of Metformin centres on the activation of hepatic AMP-activated protein kinase resulting in the inhibition of acetly-coenzyme A carboxylase activity, which leads to reduced fatty acid synthesis, thus relieving the suppression of insulin receptor signalling and subsequent inhibition of hepatic gluconeogenesis (Fullerton et al., 2013). It has therefore essentially been classed as an insulin sensitiser.

Sulphonylureas (SURs) and Glinides

SURs and glinides promote insulin secretion by binding to the SUR1 receptor of β-cells. This leads to closure of ATP-sensitive K^+ channels (K_{ATP}) and the subsequent membrane depolarisation leads to opening of voltage-dependent calcium channels, Ca^{2+} influx and the subsequent triggering of insulin granule exocytosis (Seino et al., 2012). Glinides typically have a quicker onset of action and a shorter half-life than

sulphonylureas and are taken more frequently to reduce postprandial surge in blood glucose concentration. The mechanism by which sulphonylureas and glinides act is not glucose-dependent, unlike some other therapies, and thus their use can lead to undesired hypoglycaemic events (Kelly et al., 2009). Furthermore, weight gain and increased risk of coronary heart disease have also been associated with sulphonylurea use (Seino et al., 2012).

Thiazolidinediones (Glitazones)

The thiazolidinedione (TZD) class of drugs, for example pioglitazone, function by activating the nuclear transcription factor peroxisome proliferator-activated receptor-γ (PPARγ) to stimulate the transcription of anabolic genes such as GLUT4, fatty acid transporter and lipoprotein lipase (Dubois et al., 2002). The resulting effect is enhanced glucose and fatty acid uptake and reduced insulin resistance in adipose tissue, muscle and the liver (Hauner, 2002). However, adverse events such as weight gain (through adipocyte expansion), heart failure, bone fractures and bladder cancer have been associated with TZD use (Takada and Makishima, 2015).

Sodium-glucose co-transporter-2 inhibitors (SGLT2)

SGLT2 inhibitors function by inhibiting the SGLT2 transporter, which is involved in the reabsorption of glucose from the urine back into the circulation (Wright et al., 2011). The resulting effect is lowering of the renal threshold for glucose excretion and subsequently increased excretion of glucose through the urine. This therapeutic approach reduces plasma glucose, body weight and blood pressure, but has been shown to increase the incidence of urinary tract infections by 40% (Vasilakou et al., 2013) and promote unexplained increases in circulating LDL and HDL cholesterol (Lamos et al., 2013).

Alpha-glucosidase inhibitors

The membrane bound intestinal alpha-glucosidase hydrolase enzymes are responsible for the hydrolysis of polysaccharides into monosaccharides, such as glucose, within the brush border of the small intestine (Tran et al., 2015). Inhibitors of α-glucosidase prevent this process thus delaying polysaccharide digestion and uptake of glucose from the lumen of the small intestine. The resulting effect is a reduction in postprandial glucose elevation (Kato and Node, 2014). Dose-dependent adverse events are predominantly gastrointestinal associated and include, flatulence, diarrhoea and abdominal discomfort (Van de Laar et al., 2005).

GLP-1 mimetics

GLP-1 mimetics, such as Exenatide and Liraglutide, are analogues of GLP-1, which is an incretin peptide secreted by intestinal L-cells following food intake (Holst, 1994). GLP-1 stimulates insulin secretion via activation of the β-cell GLP-1 receptors (GLP-1R), which activates adenylate cyclase to promote increases in intracellular cAMP (Ma et al., 2014). GLP-1 has also been shown to preserve β-cell mass by stimulating β-cell proliferation, and it acts centrally to reduce appetite and promote weight loss (Buteau, 2008). Unlike sulphonylureas and glinides, which reduce blood glucose levels irrespective of circulating glucose levels, GLP-1 receptor agonists potentiate glucose-induced insulin secretion, thus reducing the possibility of hypoglycaemic events. However, like most therapies, adverse events exist such as nausea, vomiting (Prasad-Reddy and Isaacs, 2015) and pancreatitis has been involved in some individuals due to acinar cell inflammation (Filippatos et al., 2014). In addition, the method of administration requires daily injections which may result in injection site reactions (Prasad-Reddy and Isaacs, 2015). The identification of orally available

GLP1R agonists with reduced adverse events would be highly attractive and marketable.

Dipeptidyl Peptidase 4 (DPP4) inhibitors

DPP4 is a membrane bound exopeptidase glycoprotein, which is ubiquitously expressed on a variety of cells and is responsible for the N-terminal cleavage of a variety of peptides including growth factors, neuropeptides, cytokines and incretins (Rohrborn et al., 2015). Inhibitors of DPP4 induce 2- to 3-fold increases in endogenous levels of the incretin hormones, GLP-1 and GIP (Tran et al., 2015), which are involved in promoting postprandial release of insulin. Furthermore, DDP4 inhibitors have been shown to promote β-cell mass expansion and improve pancreatic insulin content (van Genugten et al., 2012). However, the effects of DPP4 are relatively modest and associations with acute pancreatitis with Sitagliptin and kidney dysfunction with Vildagliptin have been reported (Scheen, 2015).

1.3 G-protein-coupled receptors

1.3.1 Classification

G-protein-coupled receptors (GPCRs) are a diverse super family of seven transmembrane bound proteins whose primary function is to initiate the activation of intracellular signalling pathways following stimulation by extracellular stimuli, which include photons, amines, lipids, ions, peptides and proteins (Bohme and Beck-Sickinger, 2009). Due to the ubiquitous expression of GPCRs throughout the body, they have been implicated in the regulation of a variety of diverse physiological processes.

In order for a protein to be classified as a GPCR it has to satisfy two main requirements. Firstly, the protein must contain seven stretches of amino acid sequence of approximately 25 to 35 consecutive residues that show a relatively high degree of hydrophobicity. These sequences represent the seven α-helices that form the transmembrane regions of the receptor. The second essential requirement is the ability to interact with a G-protein (Fredriksson et al., 2003). Details on GPCR structure are discussed in detail in section 1.3.2.

GPCRs can be partitioned into two groups: odorant/sensory and non-odorant. The odorant receptors are typically localised to specific cell types and are responsible for detecting external stimuli such as odours, tastes and pheromones and regulate behaviours such as feeding and mating (Regard et al., 2008). Non-odorant GPCRs on the other hand are ubiquitously expressed in a variety of different tissues and interact with a diverse array of endogenous ligands that regulate numerous physiological processes (Regard et al., 2008). According to Bjarnadottir *et al*, the number of genes which encode for GPCRs in both the human and mouse genome totals 791 and 1697

respectively. Of the 791 GPCRs in the human genome, 400 are functional non-odorant GPCRs and the remaining 391 account for odorant GPCRs. As for the mouse, 495 of the 1697 genes are functional non-odorant GPCRs and the remaining odorant GPCRs (Bjarnadottir et al., 2006). Due to the large number of GPCRs in the genome and the multitude of physiological processes that GPCRs regulate, classification systems have been developed over the years to further understand relationships between structure, function, ligand preference and expression patterns.

Attempts to classify GPCRs into groups have been based on various criteria, such as how a ligand binds to its receptor and structural features. The classical model of GPCR classification, the GPCRdb (G-protein-coupled receptor database), was developed by Kolakowski in 1994, which separates GPCRs into clans labelled A, B, C, D, E and F and then further into subclans using Roman numeral nomenclature (Kolakowski, 1994). This system was developed to cover all vertebrate and invertebrate GPCRomes. However, the clans D and E, fungal pheromone and cAMP receptors respectively, are not relevant to the mammalian GPCRome in addition to clan A family IV which contains archaebacterial opsin receptors (Schioth and Fredriksson, 2005). Consequently, a classification system more relevant to the mammalian situation was developed by Fredriksson *et al* in 2002. This newer classification system was generated by analysing a large set of GPCR sequences in the human genome, performing sequence alignment to identify similarities and novel hits using BLAST, and grouping the different GPCR sequences using phylogenetic analysis. This approach resulted in the generation of the GRAFS mammalian classification system consisting of five main groups: Glutamate, Rhodopsin, Adhesion, Frizzled/Taste and Secretin. By using this method, a total of 802 GPCRs were identified in the human genome, accounting for approximately 2% of all human genes (Schioth and

Fredriksson, 2005). According to the GRAFS classification system, human GPCRs are categorised into the following families: Glutamate = 15 (2%); Rhodopsin = 701 (87%); Adhesion = 24 (3%); Frizzled/Taste = 24 (3%); Secretin = 15 (2%); Other = 23 (3%) (Fredriksson et al., 2003).

1.3.2 Structure and function

As previously mentioned, GPCRs are transmembrane bound proteins which initiate the activation of intracellular signalling pathways following activation by extracellular stimuli (Hur and Kim, 2002). Each GPCR contains an extracellular N-terminus, a cytoplasmic C-terminus and seven transmembrane forming hydrophobic α-helices connected by three inter-helical loops in each side of the membrane (See Figure 1.3.1) (Horn et al., 1998).

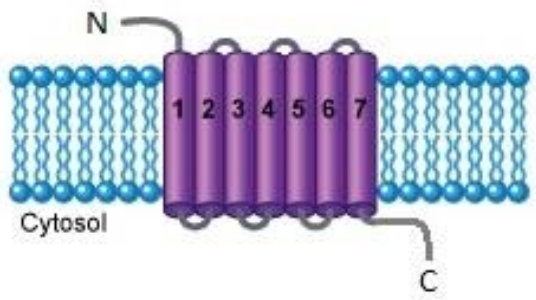

Figure 1.3.1 GPCR structure (adapted from (Wettschureck and Offermanns, 2005). The diagram depicts the seven transmembrane spanning domains (purple), the extracellular N-terminus and the intracellular C-terminus.

The N-terminus and extracellular loops are responsible for recognising extracellular ligands and modulating ligand access. The seven transmembrane region is responsible for ligand binding and transducing the extracellular signals by altering changes in

receptor conformation (Tuteja, 2009). Following a conformational alteration in receptor structure, the intracellular regions are then able to interact with intracellular effector molecules such as G-proteins, β-arrestins, G-protein receptor kinases (GRKs) and other downstream signalling molecules (Zhang et al., 2015).

The ability of a receptor to bind to a G-protein is one of the requirements for a receptor to be classed as a GPCR (Fredriksson et al., 2003). G-proteins are intracellular heterotrimeric proteins composed of α, β and γ subunits with a nucleotide binding pocket located on the α-subunit (Jastrzebska, 2013). In the absence of a suitable agonist the GPCR remains in the inactive/resting state (R), with the G-protein complex bound to GDP. Upon binding of an agonist to the receptor, the receptor undergoes a conformational change, in particular transmembrane helices III and VI (Lohse et al., 2014), which results in the rapid exchange of GDP with GTP for the nucleotide binding site on the α-subunit. This exchange forces the receptor into the active or R* state. Binding of GTP results in the destabilisation of the heterotrimeric complex and the dissociation of the Gα from the βγ subunit (Jastrzebska, 2013). This dissociation allows the Gα-subunit to interact with various effector molecules to initiate downstream signalling events depending on the specific Gα-subunit involved (See Figure 1.3.2). Following effector and subsequent pathway activation, GTP is converted back to GDP by the intrinsic GTPase activity of the α-subunit, which in turn results in the reassembly of the heterotrimeric G-protein complex and the return of the GPCR back to the inactive/resting state (R) (Tuteja, 2009).

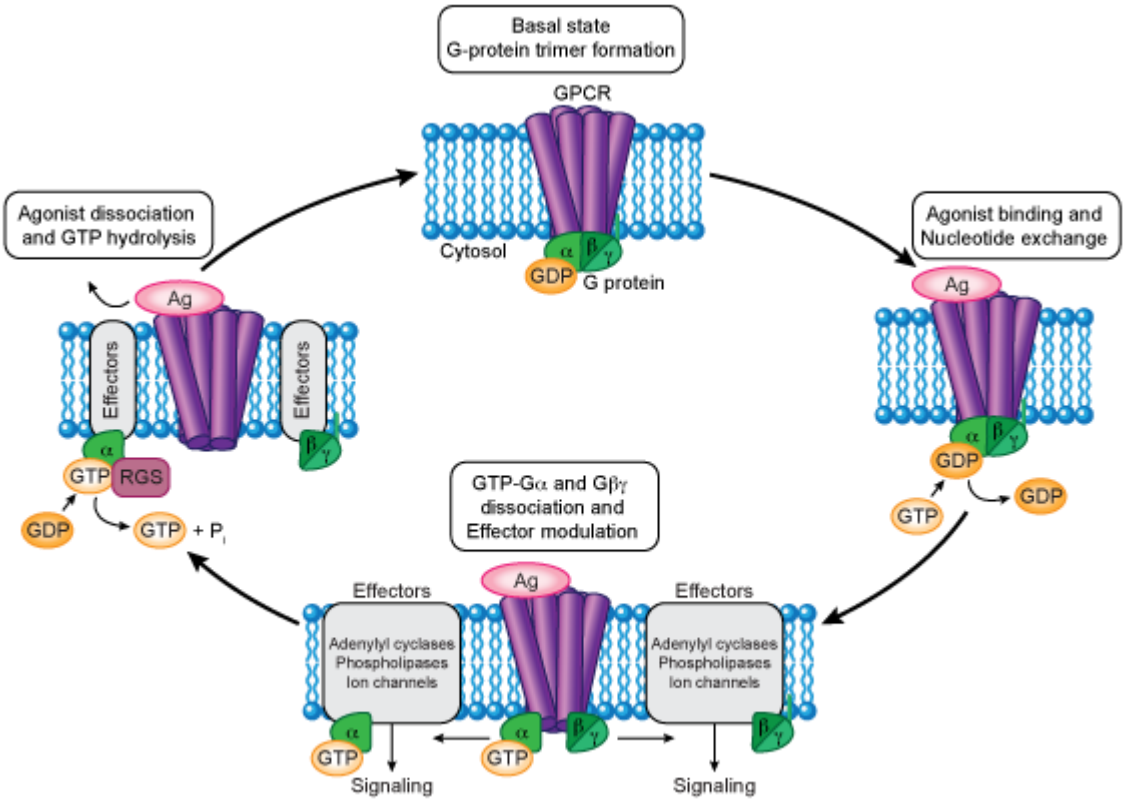

Figure 1.3.2 G-protein interaction following GPCR activation (Wettschureck and Offermanns, 2005). Schematic diagram illustrating the GPCR activation cycle. Ag = agonist, RGS = Regulator of G-protein signalling.

The determining factor in which pathway and subsequent effector molecules are activated following receptor activation depends on the class of Gα-subunit that is associated with the receptor. In humans there are 21 Gα subunits encoded by 16 genes, 6 Gβ subunits (35kDa) and 12 Gγ subunits (8-10kDa) (Moreira, 2014). Heterotrimeric G-proteins are typically grouped into four main classes: Gαs (includes Gαs and Gαolf); Gαi (includes Gαt, Gαi1, Gαi2, Gαi3, Gαo1, Gαo2 and Gαζ); Gαq/11 (includes Gαq, Gα11, Gα14, Gα15 and Gα16); Gα12 (includes Gα12 and Gα13) (Moreira, 2014). GPCRs that couple through Gαs activate the membrane bound adenlyate cyclase enzyme which converts intracellular ATP to the second messenger 3',5'-cyclic AMP. Conversely, Gαi coupled receptors inhibit adenylate cyclase activity thus reducing the

generation of intracellular cAMP from ATP. Gαq coupled receptors activate phospholipase C which hydrolyses PIP_2 to generate diacyclglycerol and inositol 1,4,5 triphosphate, resulting in the mobilisation of calcium from intracellular stores within the endoplasmic reticulum. Finally, Gα12/13 coupled receptors activate the Rho GTPase which is involved in regulating actin cytoskeletal remodelling (Amisten et al., 2013).

In addition to Gα-subunit-mediated activation of particular signalling cascades, GPCRs also have the ability to modify intracellular signalling through Gα-subunit-independent mechanisms such as via the βγ-subunit and β-arrestin. Studies have shown that the βγ-subunit of G-protein complexes has the ability to inhibit calcium channels, in particular the binding of the βγ-subunit to the α1 subunit of Cav2 channels (Currie, 2010), and also activate inward rectifying K+ channels (Dascal, 2001). Arrestins are cytosolic proteins that are typically involved in switching off GPCR activity following ligand binding (Drake et al., 2006). This process involves two steps, the first step being the phosphorylation of a ligand activated receptor by GRKs or second messenger protein kinases. This is then followed by the recruitment of the β-arrestin to the receptor, which results in steric hindrance of further receptor activation and the subsequent initiation of receptor internalisation (Rankovic et al., 2016). In addition to their ability to switch off signalling pathways, arrestins have also been shown to activate signalling effectors such as the mitogen-activated protein kinases ERK1/2, JNK and p38 as well as Akt (DeWire et al., 2007).

1.3.3 GPCRs as drug targets

GPCRs are expressed in various tissue types and are involved in the regulation of many biological processes by controlling a multitude of intracellular signalling cascades. This heterogenous nature of GPCRs has made them an attractive target for therapeutic agents (Garland, 2013). An analysis of the DrugBank database in 2013 revealed that of the 1448 small molecules, 131 biologics and 84 nutraceuticals on the market, 437 (26%) act through GPCRs (Garland, 2013). They also represent the largest number of target class that has achieved market approval since 1982, approximately 17% of all approvals. Furthermore, 6 of the 20 drugs with the highest global sales in 2010 targeted GPCRs (Rask-Andersen et al., 2011).

The success of exploiting the vast potential of GPCRs in the treatment of diseases is dependent on the availability of research tools required to evaluate their suitability as drugable targets. The development of gene expression technologies, such as RNA sequencing, RNA microarray and qPCR, have contributed to the understanding of GPCR expression within specific tissues. Furthermore, tissue expression analysis has allowed for the identification of GPCR targets for therapeutic exploitation in disease states, the assessment of target suitability with regards to off target tissue expression, whilst also contributing to the deorphanisation of orphan GPCRs based on co-expression analysis of both ligand and receptor e.g. the identification of the RDC7 and RDC8 receptors as the adenosine A1 (ADORA1) and A2A (ADORA2A) receptors (Tang et al., 2012). GPCR structural data from X-ray crystallography and STAR technology (Robertson et al., 2011) have promoted the understanding of ligand receptor interactions and when used in combination with *in-silico* computational modelling can be employed to predict potential drug candidate molecules with suitable drug-like moieties from an array of commercially available compound or biologic

libraries (Garland, 2013). Moreover, an array of *in vitro* assay technologies are available for the functional assessment of drug candidates such as, calcium, cAMP, β-arrestin, GTPγS and impedance-based assays. Further assessment of ligand function *in vivo* can be performed using transgenic animal models following receptor knock down or overexpression. The utilisation of such technologies can be used to accelerate target identification, target validation, ligand hit finding, lead optimisation and ligand functional assessment from the early stages of exploratory research through to translational development, thus making GPCRs an attractive tractable target class for therapeutic exploitation.

1.3.4 GPCRs as drug targets for Type 2 diabetes mellitus

One therapeutic approach for treating T2DM centres on promoting insulin secretion in order to compensate for β-cell dysfunction, which is characterised by a decrease in insulin secretion in response to glucose and reduced β-cell mass (Oh da and Olefsky, 2016). However, the ability of a therapeutic target to promote insulin secretion needs to be taken with caution as unnecessary increases in insulin secretion can result in unwanted hypoglycaemia. This type of scenario is dependent on the mechanisms associated with function and therefore, exploiting targets whose associated mechanisms selectively potentiate glucose-induced insulin secretion are more attractive than those that do not e.g. sulphonylureas or insulin therapies (International Hypoglycaemia Study, 2015). One such target class that has been shown to selectively potentiate glucose-induced insulin secretion are GPCRs, in particular GPCRs that couple through the Gαs and Gαq signalling pathways (see section 1.1.4.2). The increase in intracellular cAMP levels through Gαs activation alone is not enough to promote insulin secretion, as cAMP is a poor beta cell secretagogue, but potentiation

of glucose-induced insulin secretion is observed if cytoplasmic calcium is elevated downstream of the glucose-dependent pathway (Tengholm, 2012). Additionally, glucose-dependent stimulation of insulin release is also associated with Gq-coupled GPCRs, which promote PKC activation and release of calcium from intracellular stores.

While promoting insulin secretion, as described above, is the main cornerstone of T2DM therapies, the additional issue of declining β-cell mass with progressive disease state, which in turn exacerbates insulin secretory dysfunction, is also important. This can be overcome therapeutically by either enhancing β-cell proliferation, preventing β-cell apoptosis and/or stimulating β-cell neogenesis. The potential involvement of GPCRs in promoting β-cell mass is exemplified by the role of the GLP-1 receptor. GLP-1 receptor activation promotes β-cell proliferation by activating PI3K and its subsequent downstream effectors Akt, PKCζ and p38 MAPK (Buteau et al., 1999), and it also reduces apoptosis in vitro by preventing peroxide-mediated oxidative stress in a cAMP- and P13K-dependent manner. Additionally, GLP-1 receptor signalling has been shown to reduce ER stress (i.e. overproduction of misfolded proteins that contribute to reduced β-cell survival) through the activation of PKA and translation of AFT4 (Tsunekawa et al., 2007).

However, despite the aim of promoting insulin secretion and maintaining β-cell mass, the association of obesity with T2DM means that there is also an increasing need to target body weight to reduce insulin resistance. This had led to an additional focus on targets that regulate appetite, energy homeostasis and prevent chronic tissue inflammation (Reimann and Gribble, 2016). Whilst this thesis focusses on GPCRs expressed on islets, which are more likely to be targets for regulating islet hormone secretion and β-cell mass, it is also important to acknowledge the role of GPCRs

expressed in alternative tissues to get a holistic view of targeting GPCRs in T2DM. The GPCR targets discussed below cover all aspects of T2DM pathology from insulin secretion, β-cell mass, insulin resistance and appetite regulation.

Glucagon-like peptide 1 receptor (GLP1R)

The GLP-1 receptor is the most well established β-cell GPCR target whose mechanisms and subsequent role as a T2DM target have been extensively explored. In brief, the GLP-1 receptor exerts anti-diabetic effects through four mechanisms: 1) potentiating glucose-induced insulin secretion through the activation of the Gαs signalling pathway, 2) promoting β-cell proliferation and preventing apoptosis (Buteau et al., 2003), 3) inhibiting glucagon secretion (Holst, 2007) and 4) promoting weight loss (Baynes, 2010). As a result of the numerous highly beneficial effects of targeting the GLP-1 receptor for T2DM, a variety of GLP-1 receptor agonists have been developed and approved for clinical use such as Exenatide, Liraglutide, Lixisenatide, Albiglutide and Dulaglutide (Oh da and Olefsky, 2016).

Free fatty acid receptor 1 (FFAR1 or GPR40)

FFAR1 is a Gαq-coupled GPCR that is expressed on β-cells and enteroendocrine cells. Its activation potentiates second-phase insulin secretion (Crespin et al., 1973) and it has also been implicated in promoting GLP-1 secretion (Edfalk et al., 2008). Thus, activation of FFAR1 can promote insulin secretion either directly through activation on β-cells or indirectly through increased GLP-1 release from enteroendocrine cells. Despite clinical interest in this target, a successful drug candidate has yet to be discovered and only a few potential candidates are currently in clinical trials: TAK-875 (Takeda) discontinued at Phase III, AMG-837 (Amgen) discontinued at Phase I,

LY2881835 (Eli Lilly) discontinued at Phase I, JTT-851 (Japan tobacco) currently in Phase II, P11187 (Piramal) currently in Phase I (Oh da and Olefsky, 2016).

Glucose-dependent insulinotropic receptor (GPR119)

Like FFAR1, GPR119 is expressed on both β-cells and gastrointestinal enteroendocrine cells and it potentiates glucose-induced insulin secretion through Gαs-coupled signalling. It also promotes release of GLP-1 and GIP (Chu et al., 2008) in rodent animal models. In contrast to FFAR1, no GPR119 agonists have progressed to later stage clinical trials, the reason of which is attributed to a lack of efficacy in humans (Katz et al., 2012). This apparent species difference highlights the importance of using appropriate translational models in early stage research in order to predict human outcome, an area which is addressed within this thesis.

Free fatty acid receptor 4 (FFAR4 or GPR120)

FFAR4 is expressed on mouse δ-cells (Stone et al., 2014) and mouse gut endocrine cells (Iwasaki et al., 2015) but not on mouse β-cells. The principal transduction pathway associated with FFAR4 receptor activation is Gαq, which is the pathway responsible for promoting GLP-1 secretion from L-cells, but it has also been shown to couple through Gαi to inhibit ghrelin and somatostatin release (Reimann and Gribble, 2016). Interestingly, FFAR4 has been suggested to mediate the anti-inflammatory and insulin-sensitising effects of ω3-FAs, such as DHA and EPA, the effects of which were not observed in Ffar4-KO mice (Oh et al., 2010). However, an area of concern is the differential expression of splice variants between species, where humans express both FFAR4L (long) and FFAR4S (short) whereas other species only express FFAR4S. Stimulation of FFAR4L leads to β-arrestin pathway activation but does not lead to G-protein-dependent calcium signalling whereas FFAR4S does (Watson et al.,

2012). This discrepancy could lead to complications when assessing function in translation models, which could be an explanation for the absence of clinical projects involving FFAR4 receptor agonists.

Despite the appeal of exploiting GPCRs as therapeutic targets for T2DM, the clinical assessment of therapeutic agents that target GPCRs for T2DM has been limited to the receptors highlighted above. Furthermore, clinical success is restricted to the GLP-1 receptor. Such findings are surprising considering that human islets express 293 GPCRs (Amisten et al., 2013). However, despite this large pool of potentially novel targets, the role of most GPCRs in islet function is poorly characterised. A contributing factor which may impede the understanding of GPCR-mediated regulation of islet function is the availability of human tissue required for functional assessment. As a consequence, surrogate tissue, in particular mouse islet tissue, is required to predict the human setting. However, as mentioned previously (section 1.1.1), differences in islet architecture in addition to gene expression (Dai et al., 2012) have been reported, thus questioning the suitability of using mouse islets in predicting human islet function. To date, the quantitative assessment of GPCR expression differences between human and mouse islets has not been performed. Such comparisons would provide further insight into the suitability of using mouse islets as surrogate tissue for studying the role of GPCRs in the regulation of human islet function.

1.4 Islet-expressed GPCR peptide ligands

Previous studies have revealed that approximately 30% of all GPCRs expressed on human islets are activated by peptide ligands and that approximately 50% of all peptide ligands are expressed within islets (Amisten et al., 2013). Such islet GPCR peptide ligands include the 'classic' examples of glucagon and somatostatin, but additional peptides such as peptide YY (PYY) (Persaud and Bewick, 2014), kisspeptin (KISS1) (Hauge-Evans et al., 2006), urocortin3 (UCN3) (van der Meulen et al., 2015) and ghrelin (GHRL) (Dezaki and Yada, 2012) are also expressed within islets and exhibit roles in islet function. Identifying GPCR peptide ligands that play a role in regulating islet function can provide insight into therapeutic opportunities for the treatment of T2DM, an example of which is the development of GLP-1 mimetics. The roles and mechanisms of action of 'classic' and 'non-classic' intraislet expressed GPCR peptide ligands are described below.

Glucagon (GCG)

Glucagon (GCG) is a 29 amino acid peptide that is secreted from islet α-cells and is responsible for opposing the actions of insulin by stimulating hepatic glucose synthesis and glucose mobilisation (Quesada et al., 2008). Glucagon is a derivative of proglucagon, a 160 amino acid precursor polypeptide encoded by the GCG gene, which is converted to glucagon by neuroendocrine convertase 2 expressed in α-cells. In contrast, neuroendocrine convertase enzyme 1, within enteroendocrine cells, is responsible for the conversion of proglucagon into glicentin, oxyntomodulin, GLP-1 and GLP-2 (Campbell and Drucker, 2015). Glucagon functions through the Gαs-coupled glucagon receptor (GCGR), which when activated promotes the activation of membrane bound adenylate cyclases and subsequent intracellular cAMP generation.

The glucagon receptor is expressed on liver, brain, heart, kidney, adipose and gastrointestinal cells in addition to the β-cells, where its activation promotes insulin secretion (Kawai et al., 1995).

Somatostatin (SST)

Somatostatin (SST) is a peptide hormone that is expressed within the hypothalamus, gastrointestinal tract and also by the δ-cells of the endocrine pancreas. Two active forms with lengths of 14 and 28 amino acids exist (SST-14 and SST-28 respectively), both of which exert their function through G-protein-coupled receptors, of which there are five isoforms (SSTR1-5) (Kailey et al., 2012). All five somatostatin receptors couple via Gαi proteins which when activated inhibit membrane bound adenylate cyclases, thus contributing to the general inhibitory actions of somatostatin. SST-14 is the predominant form expressed by the δ-cells within islets, and it is released in response to glucose and amino acids (Ipp et al., 1977). Following its release, SST-14 potently inhibits glucagon and insulin release from α- and β-cells respectively in both humans and rodents, but conflictions regarding which receptor subtypes are involved in somatostatin function exist. Exploring which receptors facilitate SST regulation of islet function is complicated further by reported differences in receptor involvement between human and rodent species. In the mouse, the effects of somatostatin on α- and β-cells are predominantly mediated by SSTR2 and SSTR5 respectively (Strowski et al., 2000), whereas in humans islets conflicting evidence surrounding the involvement of SSTR2 and SSTR5 on β-cell function has been reported (Brunicardi et al., 2003) (Zambre et al., 1999).

Ghrelin (GHRL)

Ghrelin (GHRL) has been implicated in a variety of physiological processes ranging from the promotion of growth-hormone release, appetite regulation and adiposity (Dezaki and Yada, 2012). GHRL cells of the stomach are primarily responsible for the production of circulating levels of ghrelin (Ariyasu et al., 2001) but expression of GHRL and its receptor, growth-hormone secretagogue receptor (GHSR), has also been reported in islets, in particular the α-cells (Date et al., 2002) and β-cells (Volante et al., 2002). Activation of the ghrelin receptor by ghrelin inhibits glucose-induced insulin secretion through the attenuation of intracellular cAMP production and PKA activation in β-cells, and subsequently it has been postulated that the ghrelin-GHSR system could be targeted for the treatment of T2DM (Dezaki and Yada, 2012).

Urocortin3 (UCN3)

Urocortin3 (UCN3) is a peptide hormone that is abundantly expressed within β-cells of both mouse and human islets, but its expression has also been observed within α-cells of human islets (Li et al., 2003). Interestingly, UCN3 expression is down regulated in β-cells of diabetic mouse models and in human diabetic islets (van der Meulen et al., 2015), suggesting it may play a role in the pathophysiology of T2DM. UCN3 promotes both insulin and glucagon secretion, yet increased plasma glucose and increased glucose tolerance observed in these studies contradict the insulinotropic actions of UCN3 (Li et al., 2003) (Li et al., 2007), thus suggesting additional function. It has recently been reported that UCN3 is co-released with insulin and potentiates glucose-stimulated somatostatin secretion via its cognate receptor, the CRF_2 receptor (CRHR2), on δ-cells (van der Meulen et al., 2015). These observations suggest that the paracrine actions of UCN3 activates a negative feedback loop that promotes

somatostatin release to reduce further insulin secretion once plasma glucose levels have normalised.

Peptide YY (PYY)

The gut hormone PYY is expressed in mouse islets, in particular in α- and PP cells (Bottcher et al., 1989), and it has received interest due to its modulation of fuel homeostasis through its central effects on appetite regulation. It also plays a role in islet physiology by modulating β-cell mass, a key feature in the pathophysiology of T2DM, by exhibiting pro-proliferative and anti-apoptotic effects on mouse β-cells through the activation of Y_1 (NPY1R) receptors (Persaud and Bewick, 2014). However, intravenous administration of PYY in mice has been shown to inhibit insulin release in mice (Bottcher et al., 1989), whilst PYY knockout mice are hyperinsulinaemic (Boey et al., 2006), suggesting that while PYY based therapies could treat T2DM, the reduction in insulin secretion may well counteract the beneficial effects of enhanced β-cell mass. Further studies are required to explore whether such observations are translatable to the human setting and to fully understand the involvement of other Y-receptors in PYY-mediated islet function.

Kisspeptin (KISS1)

The kisspeptin peptides (KISS1) are a family of peptides encoded by the KISS1 gene that function through GPR54 (Muir et al., 2001) and are typically involved in controlling the onset of puberty (Messager et al., 2005). Both the KISS1 and GPR54 genes are expressed within the pancreas and further studies have revealed the expression of both genes within both mouse and human islets, in particular the α- and β-cells (Hauge-Evans et al., 2006). Conflicting results exist regarding the role of kisspeptins in islet function, with reports suggesting an inhibitory effect on insulin

secretion from mouse islets below 11.1mM glucose (Vikman and Ahren, 2009), whereas a reversible potentiation of glucose-stimulated (20mM) insulin secretion from pig, mouse and human islets has also been reported (Bowe et al., 2012), which is thought to be mediated by elevations in intracellular calcium (Bowe et al., 2009).

Chemokine (CXC-motif) ligand 14 (CXCL14)

CXCL14, also termed breast and kidney-expressed chemokine (BRAK), is an orphan chemokine ligand that belongs to the CXC-class chemokine family. Abundant expression of CXCL14 mRNA is observed in the lungs, kidneys, brain, skin, small intestine and taste buds (Hara and Tanegashima, 2012), while co-localisation with somatostatin in the δ-cells of mouse islets has also recently been demonstrated (Suzuki and Yamamoto, 2015).

Due to its ubiquitous expression, CXCL14 has been implicated in the involvement of numerous biological processes, including immune cell trafficking, tumour suppression, tumour proliferation, anti-microbial defence and feeding behaviour (Hara and Tanegashima, 2012). Interestingly, CXCL14 has been suggested to participate in the regulation of rodent glucose homeostasis. Studies in mice have shown that a high fat diet markedly upregulates CXCL14 in the serum and white adipose tissue (Takahashi et al., 2007), whilst CXCL14 knock out mice are protected from HFD-induced obesity (Tanegashima et al., 2010), have improved insulin sensitivity and are protected from HFD-induced hyperinsulinemia and hyperglycaemia (Nara et al., 2007). CXCL14 has also been shown to be implicated in modifying insulin-dependent glucose uptake in peripheral tissues, albeit with differing effects, with attenuation observed in monocytes (Hara and Nakayama, 2009) but enhancement observed in adipocytes (Takahashi et al., 2007).

The association of CXCL14 with glucose homeostasis, coupled with its expression within δ-cells suggests that it may play a role in regulating islet function, but, to date, such studies have not been performed. Furthermore, preliminary studies implying a potential role of CXCL14 in islet function have been limited to mouse models and thus the translational relevance of such findings in a human setting are unclear.

Complicating matters further, with regards to revealing the mechanism of action of CXCL14, is the orphan status of CXCL14, i.e. the receptor responsible for its function has not been identified. Typically, chemokines bind to GPCRs of their own chemokine class (Kufareva et al., 2015). Despite this class-specific interaction between chemokine ligands and receptors, a receptor has yet to be identified for CXCL14. It has been proposed that CXCR4 is responsible for mediating CXCL14 function as determined by its ability to bind with high affinity to wild-type and stable CXCR4-overexpressing THP-1 cells in radioligand binding experiments (Tanegashima et al., 2013). In the same study, CXCL14 was also shown to inhibit CXCL12-mediated chemotaxis of THP-1 cells, a process which is facilitated by CXCR4. Conversely, an alternative report revealed conflicting evidence regarding CXCL14-CXCR4 interactions by revealing that CXCL14 did not alter CXCL12-induced CXCR4 phosphorylation, G-protein mediated calcium mobilisation or CXCR4 internalisation in CXCR4 transfected HEK293 and Jurkat T cells (Otte et al., 2014). Current inconsistencies in the literature regarding the involvement of CXCR4, or any other receptor for that matter, in CXCL14-mediated function means CXCL14 retains its orphan ligand status. Whether CXCL14 does in fact bind to a GPCR is also debateable, as CXCL14 homologs in all vertebrates differ structurally from all other chemokines by possessing an uncharacteristically short amino-terminus of only two amino acids

located before the first disulphide bridge, a region which is typically required for triggering GPCR activation (Benarafa and Wolf, 2015).

As discussed in the previous section (1.3.4), understanding the role of GPCRs in human islet function is restricted by the limited availability of human islets required for functional assessment, resulting in a reliance on surrogate tissue. This issue also extends to islet-expressed peptides that function through GPCRs and whose function is yet to be determined. Typically rodent islets, in particular mouse islets, are used to fill the void created by a lack of human tissue, but as previously mentioned (section 1.1.1), concerns over the suitability of using rodent islets to predict the human setting exist due to architectural and gene expression differences. This thesis aims to address such concerns by comparing the mRNA expression profiles of GPCRs (GPCRomes) and GPCR peptide ligands (Secretomes) of human and mouse islets in an attempt to assess the suitability of utilising mouse islets as surrogate tissue for studies exploring the role of GPCRs and GPCR peptide ligands in human islet function. In addition, this thesis also aims to utilise the GPCRome and Secretome data to assess the role of CXCL14 in islet function and to explore the underlying mechanisms involved.

1.5 Thesis aims

- Determine the mRNA expression profiles of GPCRs in human and mouse islets, compare species differences and assess the suitability of using mouse islets for human islet GPCR studies.
- Determine the mRNA expression profiles of GPCR peptide ligands in human and mouse islets, compare species differences and assess the suitability of using mouse islets for predicting the role of islet GPCR peptide ligands in human islet function.
- Explore the effects of CXCL14 on islet function, identify the mechanisms involved in CXCL14-mediated effects and, using the GPCRome and Secretome data, assess which GPCRs may be responsible for CXCL14 action.

CHAPTER 2 – Methods

2.1 Cell culture of pancreatic β-cell lines

The use of primary β-cells in research is limited by the availability of pancreatic endocrine tissue in addition to technical limitations ranging from the isolation of islets, the cell sorting of islet cell populations and the preservation of the innate characteristics of a β-cell (Skelin et al., 2010). In addition, pressures to develop animal free approaches in accordance with the principles of the 3Rs (replacement, reduction, refinement) (Daneshian et al., 2011) has encouraged researchers to seek alternatives. The development of explant derived cell lines with induced proliferation enables the propagation of uniform cells with similar physiological characteristics to the parent tissue, thus avoiding some of the technical issues associated with primary cell culture. Another advantage of using cell lines is the consistency and reproducibility of results obtained from clonal cells, a problem associated with primary cell usage due cellular and hormonal heterogeneity among cellular sources. However, there are disadvantages with using cell lines, such as the change of characteristics over time with continuous culturing, abnormal chromosomal content due to their tumour origin, genetic mutations, altered protein expression, modified metabolism and disruption of cell to cell interaction (Skelin et al., 2010). Despite these concerns, β-cell lines have still been developed and utilise to cautiously predict β-cell function.

MIN6 cells

MIN6 cells originate from an insulinoma of a transgenic C57BL/6 mouse harbouring the insulin promoter-SV40 T antigen hybrid gene (Miyazaki et al., 1990). They exhibit many similar characteristics as primary β-cells, such as GLUT2 expression, glucokinase expression, show glucose-dependent insulin secretion in earlier passages and contain a relatively high insulin content (10% of primary β-cells) (Roderigo-Milne

et al., 2002). However, the loss of glucose-induced insulin secretion can be observed in later passages, which may possibly be due to an outgrowth of cells with a poor response to glucose or a reduced expression of genes responsible for glucose-induced insulin secretion (Miyazaki et al., 1990).

INS-1 cells

INS-1 cells are X-ray induced rat insulinoma derived cells that also display many of the important characteristics of primary β-cells, such as high insulin content (20% of native cells), express GLUT2 and glucokinase and respond to glucose within the physiological range. In addition, glucose-stimulated insulin secretion is maintained over many passages highlighting the robustness of this cell line, in particular the INS1E clone, in comparison to other lines. However, in order for INS-1 cells to propagate and maintain the functional characteristics of β-cells, 2-mercaptoethanol is required within the culture media which can be toxic and denature proteins (Skelin et al., 2010).

Endoc-βH1 cells

Endoc-βH1 cells are a human pancreatic β-cell line derived from human foetal pancreatic buds. Briefly, human foetal pancreatic ducts were transduced with a lenti-viral vector expressing SV40LT under the control of the rat insulin promoter and then transplanted into SCID (severe combined immunodeficiency) mice to allow for the expansion of the transformed β-cells. Following in vivo propagation, resulting insulinomas were removed and transduced with human telomerase reverse transcriptase (hTERT) to promote immortalisation of the cells, before again being transplanted into SCID mice to propagate. The resulting tissue was harvested, cultured in vitro and shown to maintain significant insulin content (10% of native cells) whilst

being able to secrete insulin in response to glucose for over 80 passages (Weir and Bonner-Weir, 2011).

2.1.1 Culture of MIN6 cells

Adherent MIN6 cells were grown as monolayers in tissue culture treated filter capped Nunc flasks within a humidified 37ºC incubator containing a 5% CO_2, 95% air atmosphere. The cells were maintained in culture media comprised of DMEM (containing 25mM glucose) supplemented with 10% FBS, 2mM L-glutamine and 100U/ml penicillin/100µg/ml streptomycin.

MIN6 cells were grown up to 70-80% confluency before subculturing or for experimental use. Subculturing of cells was achieved by aspirating the culture media, washing the cells with PBS (37ºC) to remove residual serum containing media and treating with 0.1% trypsin/0.02% EDTA solution for 3-5 minutes at 37ºC. Following the detachment of cells with trypsin/EDTA treatment, serum containing growth media was added to inhibit trypsin activity. The cells were pelleted at 200 x g for 3 mins, the supernatant removed and the cells resuspended in a suitable volume of growth media. The cells were counted as described in section (2.1.4). The cells were either seeded out into tissue culture flasks for further subculturing or into plates for experimentation.

2.1.2 Culture of INS-1 cells

Adherent INS-1 cells were grown as monolayers in tissue culture treated filter capped Nunc flasks within a humidified 37ºC incubator containing a 5% CO_2, 95% air atmosphere. The cells were maintained in culture media comprised of RPMI (containing 11.1mM glucose) supplemented with 10% FBS, 10mM HEPES, 1mM pyruvate, 100U/ml penicillin/100µg/ml streptomycin and 50µM 2-Mercaptoethanol.

INS-1 cells were grown up to 90% confluency before subculturing or used for experimentation. Subculturing of cells was achieved by aspirating the culture media, washing the cells with PBS (37ºC) to remove residual serum containing media and treating them with 0.1% trypsin/0.02% EDTA solution for 3-5 minutes at 37ºC. Following the detachment of cells with trypsin/EDTA treatment, serum containing growth media was added to inhibit trypsin activity. The cells were pelleted at 200 x g for 3mins, the supernatant removed and the cells resuspended in a suitable volume of growth media. The cells were counted as described in section (2.1.4) and either seeded out into tissue culture flasks for further subculturing or into plates for experimentation.

2.1.3 Culture of Endoc-βH1 cells

The adherent Endoc-βH1 cell line was provided, under MTA to Prof Shanta Persaud, by Dr. Phillipe Ravassard of ICM Biotechnology and Biotherapy, Paris, France.

Endoc-βH1 cells were grown up in monolayers in pre-coated F25cm^2 TPP flasks in culture media comprised of DMEM (5.5mM glucose), 2% BSA fraction V, 50µM 2-Mercaptoethanol, 10mM nicotinamide, 100U/ml penicillin/100µg/ml streptomycin, 6.7ng/ml of sodium selenite and 5.5µg/ml of transferrin. Prior to cell plating or subculturing, plasticware was pre-coated with coating media comprised of 4ºC chilled DMEM (25mM glucose), 100U/ml penicillin/100µg/ml streptomycin, 2µg/ml of fibronectin and 1% ECM. Due to the perishable nature of the coating media constituents it was imperative that the medium was only prepared on day of use and kept at 4ºC. In order to coat an F25cm2 flask, 2.5ml of coating medium was added to an empty flask and placed in a 37ºC incubator for a minimum of 1hr or a maximum of 24 hours. Following incubation, the coating medium was removed immediately before seeding of cells.

Subculturing of cells in F25cm^2 flasks was achieved by removing the medium from the cultured cells, rinsing the cells with 3ml of pre-warmed (37^{o}C) 1X D-PBS followed by the addition of 1ml of 0.1% trypsin/0.02% EDTA solution. The flask was placed into a 37^{o}C incubator for 3 mins to allow for cell detachment before 1ml of neutralising medium (80% 1X D-PBS, 20% heat inactivated FBS) was added to deactivate the trypsin. Detached cells were transferred to a sterile 15ml Falcon tube, pelleted at 700 x g for 5mins, the supernatant removed and then the cells were resuspended in 5ml of growth medium. The cells were counted as described in section (2.1.4). Following cell counting, cells were seeded at a density of 70,000-75,000 cells/cm2 in the pre-coated flasks. The flasks were placed into a humidified 37^{o}C incubator containing a 5% CO_2, 95% air atmosphere.

2.1.4 Cell counting

Cell counting was performed using Invitrogen's Countess Automated Cell Counter. Briefly, cell suspensions were generated prior to counting as described in the cell culture sections above. 10µl of 0.4% Trypan blue solution was added to a 0.6ml Eppendorf tube followed by 10µl of cell suspension. The cells and dye were gently mixed before 10µl was added to a chamber port of a cell counting chamber slide and the cells were counted. Dead cells with disrupted cell membranes show up as blue due to dye uptake, whereas live cells will appear with bright centres.

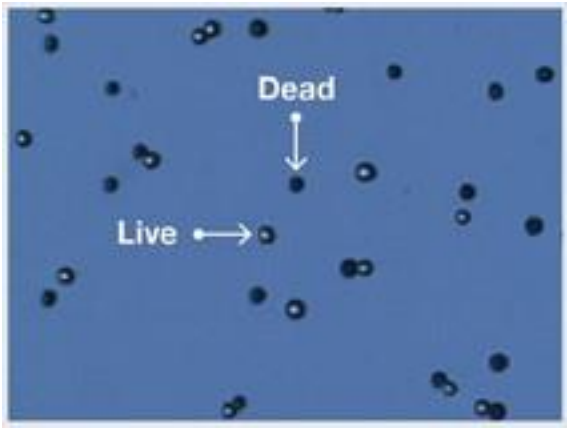

Figure 2.1.1 Cell viability representation using the Countess Automated Cell Counter.

Total cell count, live cell count, dead cell count and percent viability readings were generated.

2.1.5 Freezing down/thawing of cells

In order to maintain a stock of cell lines for long term storage, cells are cryo-preserved in liquid nitrogen at -196^{o}C. Briefly, adherent cells were trypsinised, resuspended in fully complemented growth media, pelleted and resuspended in a volume of cryopreservant (90% fully complemented growth media, 10% DMSO) at a seeding density of 1-3 x 10^{6} cells/ml. 1ml of cell suspension was dispensed into a 2ml cryovial, placed into a Nalgene Mr. Frosty cryo freezing container containing 250ml of isopropyl alcohol and stored for 24 hours at -80^{o}C. The presence of isopropyl alcohol during the freezing process ensures the cells are steadily frozen down at a rate of approximately 1^{o}C/min, thus improving cell survival.

The retrieval of cell lines from liquid nitrogen was achieved by thawing vials of cells in a 37^{o}C water bath before quickly transferring to a 50ml Falcon tube containing 30ml of fully complemented media. The cells were then pelleted at 200 x g for 3 mins, the supernatant removed and the cells resuspended and transferred to a suitably sized culture flask.

2.2 Islet isolation

2.2.1 Isolation of human islets of Langerhans

Human islets were isolated from heart beating donors at the Islet Transplantation Units at King's College Hospital using the Edmonton protocol (Ryan et al., 2001). After islets had been transferred from King's College Hospital to the Guy's campus they were handpicked and transferred to 9cm non-tissue culture treated dishes containing CMRL culture media and maintained at 37ºC, 5% CO_2 for at least 24 hours to allow for recovery.

2.2.2 Isolation of mouse islets of Langerhans

Mouse islet isolation was performed using the collagenase digestion method for both the outbred ICR/CD1 strain and the inbred C57/BL6 strain. Adult males between the ages of 8-12 week old were used.

2.2.2.1 Surgery

Prior to surgery a 1mg/ml collagenase solution was prepared in ice cold MEM and kept on ice. Mice were terminated by the cervical dislocation method and the abdominal cavity was surgically exposed. Under a dissecting microscope the ampulla of Vater was clamped and 2.5ml of ice cold collagenase solution was carefully injected through the common bile duct. The perfused pancreas was then surgically removed and placed into a 50ml Falcon tube on ice.

2.2.2.2 Digestion of the pancreas

Prior to starting, wash media comprised of MEM, 10% NCS, 2mM L-glutamine and 100U/ml penicillin/100µg/ml streptomycin was prepared and placed on ice.

The 50ml Falcon tubes containing pancreatic material were placed into a 37^{o}C water bath for 10mins to allow for collagenase digestion of pancreatic tissue to occur. Following incubation, 25ml of wash media was added to the tubes to deactivate collagenase and halt unwanted digestion of islets. The tubes were shaken vigorously to encourage pancreatic tissue separation and centrifuged at 300 x g for 1.15 mins at 10^{o}C. The supernatant was carefully removed and 25ml of fresh wash media was added, tubes vortexed and centrifuged again. This process was repeated a further two times. After the last wash the resuspended pancreatic tissue was sieved into a funnel and collected in new un-skirted 50ml Falcon tubes. The tubes were centrifuged at 340 x g for 1.5 mins at 10^{o}C. Following centrifugation, the supernatant was removed and tubes inverted onto paper towel to ensure removal of remaining residue. The pellet was resuspended in 15ml of histopaque and vortexed. 10ml of wash media was gently added to the tube so that an interface between media and histopaque was formed. The sample was then centrifuged at 3510 x g for 24 mins at 10^{o}C. Following centrifugation, islets were removed from the interface and placed into a new un-skirted 50ml Falcon tube. The tube was topped up with wash media to the 50ml mark and centrifuged at 300 x g for 1.15 mins at 10^{o}C. Following centrifugation, islets were left to settle for 3mins before 25ml of media was removed from the top, 25ml of fresh media added and islets centrifuged again. This process was repeated 2 more times before the wash steps were repeated with 10ml volumes of replacement media for another three spins. After the final centrifugation step, islets were resuspended in10ml of wash media and added to a 9cm non-tissue culture treated dish. Islets were handpicked into 9cm dishes containing culture media comprised of RPMI supplemented with 10%FBS, 2mM L-glutamine and 100U/ml penicillin/100µg/ml streptomycin and placed into a humidified 37^{o}C incubator containing a 5% CO_2, 95% air atmosphere.

2.3 Gene expression analysis

2.3.1 Total RNA extraction

Total RNA extraction was achieved using a modified version of the TRIzol RNA extraction method. The benefit of this method is that protein and genomic DNA can be extracted alongside total RNA. RNA isolated using this method is then further purified and concentrated using an RNA MiniElute Cleanup kit (Qiagen). The RNeasy MinElute Cleanup Kit columns remove contaminating residual salts and phenol as well as RNAs shorter than 200 base pairs, such as 5.8S rRNA, 5S rRNA, and tRNAs, which together comprise 15–20% of the total RNA, resulting in an enrichment of mRNAs.

Gene expression analysis was performed on both cell lines and islets of Langerhans. For cell lines, media was removed from a confluent 6 well containing the cell line of interest (approximately $1x10^6$ cells/well) and 1ml of TRIzol added. TRIzol was left for 5mins to dissolve cellular material and the sample was transferred to -80^{o}C for storage. For mouse and human islets of Langerhans, each biological replicate contained approximately 150-250 islets. Islets were pelleted at 0.2 x g for 3 mins, the supernatant was completely removed and 1ml of TRIzol was added. The samples were left at room temperature for 5 mins before being stored at -80^{o}C.

Prior to starting the RNA extraction procedure, isopropanol was chilled at -20^{o}C and a centrifuge was pre-chilled to 4^{o}C. TRIzol samples were removed from storage, thawed and left at room temperature for 5 mins. 200µl of chloroform was then added to each sample to create a biphasic mixture where polar single stranded RNA strands migrate to the aqueous phase whilst protein and non-polar double stranded DNA remain in the organic phase (protein) or interphase (DNA). The tubes were manually

shaken 50 times before being centrifuged at 12000 x g for 15 mins at 4°C. During this stage, 0.5µl of 20µg/µl ultra-pure glycogen was added to fresh 1.5ml RNase free tubes. Glycogen is a highly branched carbohydrate which binds to and promotes RNA pellet precipitation. Following centrifugation, the aqueous phase was transferred to the glycogen containing tubes using an RNase free filter tip. 500µl of pre-chilled isopropanol was added to each tube containing the glycogen aqueous phase mix. The sample was mixed by inverting and was stored at -80°C for 1 hour or -20°C overnight.

Next, the samples were centrifuged again at 12,000 x g for 15 mins at 4°C to pellet the RNA. The supernatant was carefully aspirated and 1ml of freshly prepared 75% ethanol was added to the tube. Samples were then centrifuged at 7,500 x g for 10mins at 4°C. The presence of ethanol promotes precipitation allowing for the visualisation of a white RNA pellet. The supernatant was again carefully and completely aspirated and the pellets dried in a heating block set to 37°C for 1-3 mins. The RNA pellet was then dissolved in 100µl of RNase free water, vortexed and stored at -80°C until it was concentrated and purified using the RNEasy MiniElute Cleanup kit (Qiagen).

2.3.2 RNA concentration and purification

Further concentration and purification of total RNA was achieved using Qiagen's RNeasy MiniElute Cleanup kit. No more than 45µg of total RNA in 100µl was added to each column. For each two RNA samples, 1.5ml Eppendorf tubes containing either 800µl of RLT buffer (1% 2-mercaptoethanol), 600µl of 100% ethanol, 1.1ml of RPE buffer or 1.1ml of 80% ethanol were prepared.

Each RNA sample was rapidly defrosted and thoroughly vortexed to ensure that the RNA pellet was completely dissolved in the 100µl of water added at the end of the TRizol purification protocol. 350µl of RLT buffer was then added to each of the 100µl

of RNA sample and vortexed. 250µl of 100% ethanol was then added and mixed by pipetting. The sample was transferred to a MinElute column, placed in a collection tube and centrifuged at 9500 x g for 15 seconds. The flow through was discarded and the column placed into a fresh collection tube. 500µl of RPE buffer was added to the spin column and centrifuged at 9500 x g for 15 seconds. The flow through was decanted from the collection tube, the column and collection tube reassembled and 500µl of 80% ethanol was added to the column. The sample was centrifuged at 9500 x g for 2mins and the collection tube and contents were discarded. The column was placed in a new collection tube with the lid open and spun at 20,000 x g for 5mins to dry the membrane. The collection tube and contents were again discarded and column placed in new collection tube. 14µl of RNase free water was added to the centre of the column membrane and the spin column was centrifuged at 20,000 x g for 1min to elute the RNA. A total elution volume of approximately 12µl was obtained. The RNA concentration was quantified using a Nanodrop instrument and the remaining sample was stored at -80^{o}C.

2.3.3 RNA quantification

Total RNA was quantified using the NanoDrop 2000 spectrophotometer, which is able to detect the concentration and purity of RNA in a 1µl sample. Since nucleotides absorb at 260nm, the concentration of RNA is determined by measuring absorbance at A_{260nm}. Additional ratio readings at 260/280nm and 260/230nm are determined to assess protein, carbohydrate and phenol contamination within the sample. A pure sample of RNA is accepted if the determined 260/280nm ratio is ~2.0 and the 260/230nm measurement is 2.0-2.2. RNA samples classed as pure were stored at -80^{o}C until required for mRNA purification.

2.3.4 cDNA synthesis

Complementary DNA synthesis is the process in which mRNA is transcribed into cDNA by the action of a reverse transcriptase such as the TaqMan Reverse Transcriptase which is a recombinant Murine Leukaemia Vurus reverse transcriptase (MuLVRT). Reverse transcription of RNA to cDNA was performed using the TaqMan Reverse Transcription kit.

A reverse transcription master mix was generated as indicated below and placed on ice.

Table 2.3.1 Reverse transcription master mix preparation.

Reagent	Volume/reaction (µl)
10X TaqMan RT-buffer	2.50
25mM $MgCl_2$	5.50
10mM dNTP	5.00
Random hexamers	1.25
RNase inhibitor	0.50
MultiScribe transcriptase	0.65
Mater mix/tube	15.40
RNA/tube (60-2000ng)	9.60

PCR tubes containing master mix and RNA were placed into a thermal cycler and run under the following settings.

Table 2.3.2. Thermal cycler settings for PCR

Temperature (ºC)	Time (mins)	Cycles
25	10	1
48	30	1
95	5	1
4	eternity	1

Following thermal cycling, the cDNA samples were stored at -20ºC until required for qPCR gene expression analysis.

2.3.5 Quantitative real time polymerase chain reaction

Quantitative real-time polymerase chain reaction (qPCR) is a technique employed to quantify gene expression. It combines the conventional polymerase chain reaction technique with either non-specific fluorescent dyes that bind to double stranded DNA, for example SYBR green, or sequence specific DNA fluorescently labelled probes as is the case with TaqMan probes. The combined effect is the fluorescent quantitative measurement of amplified genes of interest relative to the expression of a suitable housekeeping gene. The Qiagen SYBR green method was employed for the assessment of gene expression analysis.

2.3.5.1 Housekeeping gene normalisation

Due to the fact the concentration of cDNA material cannot be determined by current methods, the expression of genes of interest cannot be quantified per unit of cDNA. Therefore, gene expression is quantified relative to the mRNA expression of a housekeeping gene expression. The quantity of cDNA used for gene expression analysis is initially calculated by determining the Ct value of the chosen housekeeping gene for the cDNA stock. A subsequent dilution of the cDNA stock is then performed to achieve a desired housekeeping gene Ct value to allow for reliable detection of genes of interest. For the purpose of this study the housekeeping gene GAPDH was used and a target Ct value of 18 to 20 for this gene was chosen.

cDNA stocks, Qiagen QuantiTect primer qPCR assays and Qiagen QuantiFast SYBR green mastermix aliquots were all thawed on ice. cDNA stock was diluted tenfold in molecular biology grade water for initial housekeeping gene expression assessment. 5X working substocks of primers were prepared from 10X stocks by diluting in molecular biology grade water. The following reaction mix was prepared for each cDNA sample per well.

Table 2.3.3. qPCR reaction mix preparation per well.

Reagent	Volume (µl)
SYBR green	5
Diluted cDNA	1
Water	2

8µl of reaction mix was added to each well of a 96 well Roche Light Cycler plate and then centrifuged at 1000rpm for 1 min to promote collection of sample at the base of the well. 2µl of 5X primer was then added to each well, the plate sealed with adhesive film and then centrifuged again using the same settings. The plate was then read using the LightCycler 480 RT-PCR System (Roche) using the following settings.

Table 2.3.4. LightCycler run settings.

Step	Target Temp. (ºC)	Acquisition Mode	Time	Ramp Rate (ºC/s)	Acquisitions (per ºC)	Cycles	Analysis Mode
Pre-incubation	95	None	5mins	4.4		1	None
Amplification	95	None	10secs	4.4		40	
	60	Single	30secs	2.2			
Melting Curve	95	None	10secs	4.4		1	
	60	Single	30secs	2.2			
	40	None	30secs	2.2	5		
Cooling	40	None	30secs	2.2			None

Following the plate read, data was extracted using the LightCycler 480 software v1.5. The required volume of cDNA substock required for future gene analysis screens was determined using the following equation, where rCt = required housekeeping gene Ct value and aCt = actual Ct value of housekeeping gene of tenfold diluted cDNA.

$$\text{Volume of cDNA sub-stock required (µl)} = \frac{\text{Volume of cDNA required for screening (µl)}}{2^{(rCt - aCt)}}$$

2.3.5.2 Gene expression profiling

Following the exclusion of all odorant GPCRs, the poorly characterised bitter taste receptor family (TAS2Rs) and GPCRs where no available mouse orthologue existed, the relative quantification of 335 functional GPCRs from a potential ~800 within the human genome were screened in human islets, ICR mouse islets and C57 mouse islets. 145 GPCR peptide ligand genes were also screened in human islets, ICR mouse islets and C57 mouse islets.

Preliminary screening of gene expression was performed in 'single shot' mode using pooled cDNA from biological replicates. Following the exclusion of the negative hits and those with poor melt curve statuses, the qPCR products of the remaining positive hits were run on an agarose gel (section 2.3.6) to assess true amplification of the desired gene and exclude false positive hits. Genes that were known to be expressed from the scientific literature, but whose amplicon bands were incorrect, were re-run with redesigned primers. Genes whose calculated Ct value were ≥30, which had a correct amplicon band size in the gel analysis were labelled as trace expressing genes. Lastly, genes whose amplicon bands were correct and had a Ct value <30 were quantified further by determining expression within each biological replicate.

2.3.5.3 Primer efficiency determination

The amount of amplified cDNA replicated throughout the qPCR thermal cycling process is dependent on intrinsic factors such as the ability of the primer to bind to its specific template region and the ability of the polymerase to amplify the template region of interest. The combination of these factors is referred to as the primer efficiency. In theory, if a primer efficiency value of 100% is observed then a doubling of the amplified product should be observed after each cycle. However, this is often not the case and primers will tend to exhibit slightly different primer efficiency values.

Therefore, in order to correctly compare the expression levels of different genes using qPCR, a primer efficiency value for each primer pair is required. This is achieved by running a cDNA titration experiment and determining the slope of a Ct (cycle threshold) vs log cDNA plot.

Primers selected for primer efficiency analysis have to not only indicate expression within the target tissue of interest but also have to show high enough level of expression (Ct<25) so that reliable detection can be determined over the full cDNA titration range. The assay was performed by titrating stock cDNA by performing a 5 point, 1 in 2 serial dilution in molecular biology grade water. 3µl/well of cDNA was added to Roche LightCycler 480 compatible 96 well plate, followed by 5µl of 2X SYBR green mastermix and 2µl of primer. The plate was run using a Roche LC480 instrument using the same programme as described in Table 2.3.4. Ct values were plotted against Log cDNA dilution and the slope determined. The slope value was then converted to a primer efficiency value using the following equation:

$$E\ (\text{efficiency}) = 10^{(-1/\text{slope})}$$

Figure 2.3.1 Primer efficiency calculation equation

2.3.5.4 Data reduction

Gene expression relative to GAPDH was determined using the ΔΔCt method (Pfaffl, 2001), where E = primer efficiency value; gioCt = Ct value of the gene of interest; hCt = Ct value of the housekeeping gene.

$$\text{Relative expression} = \frac{E^{goiCt}}{E^{hCt}}$$

Figure 2.3.2 Equation for determining relative gene expression

2.3.6 Agarose gel electrophoresis

In order to determine whether the amplified qPCR product is genuine, the product was run on an agarose electrophoresis gel and the amplicon band length was compared to the predicted length supplied by the manufacturer.

Briefly, a 2% agarose gel solution was prepared by dissolving 3g of agarose into 150ml of 1X bionic buffer in a microwave. Once dissolved, 7.5µl of 10mg/ml ethidium bromide was added and poured out into a pre-prepared cast. 2µl of 6X Orange DNA loading dye was added to each well of the qPCR plate containing amplified qPCR product and the plate centrifuged at 200 x g for 1 minute. 12µl/well of dye/qPCR product mix or 7µl/well of OrangeRuler 50bp DNA ladder was added the agarose gel. The gel was then run at 150V for approximately 40 minutes and bands visualised under UV light using a Genius transilluminator.

2.4 Measurement of insulin secretion

The assessment of insulin secretion from cell lines and islets was performed using static incubation measurements. The static method involves incubating islets or cells with ligands of interest in a ‘closed system’ i.e. media is neither removed nor replaced during incubation. In contrast to the dynamic perifusion method, static measurements

improves the chance of observing autocrine and paracrine effects of ligand treatment that may not be observed by the perifusion method.

2.4.1 Static incubation using islets

Cultured handpicked islets were transferred to a 15ml Falcon tube containing Gey and Gey physiological salt solution supplemented with 2mM glucose and centrifuged at 200 x g for 5 mins. The supernatant was removed and 10ml of fresh 2mM glucose Gey and Gey was added to the tube and the islets were incubated in humidified incubator at 37^{o}C for 1 hour. During incubation, 500µl of ligand treatment in Gey and Gey buffer was prepared in 1.5ml Eppendorf tubes and placed on ice. Following incubation the supernatant was removed from the islets, 15ml of 2mM glucose Gey and Gey was added and the islets centrifuged again at 200 x g for 5 mins. The supernatant was removed, the islets resuspended in 15ml of 2mM glucose Gey and Gey buffer and the contents of the tube transferred to a 9cm non-treated Petri dish. Islets were then handpicked under microscope into the prepared 1.5ml Eppendorf tubes and placed back on ice. All tubes were then placed in a water bath at 37^{o}C for 1 hour. The tubes were then centrifuged at 200 x g for 1 min to pellet islets and 250µl of supernatant was carefully harvested and stored at -20^{o}C until required for insulin content assessment by radioimmunoassay.

Table 2.4.1 Preparation of 1 x Gey and Gey buffer (per 2L, pH8.4)

Reagent	Mass (g)	Final Concentration (mM)
NaCl	26	111
KCl	1.48	5
$NaHCO_3$	9.08	27
$MgCl_2.6H_2O$	0.84	1
KH_2PO_4	0.12	0.22
$MgSO_4.7H_2O$	0.28	0.28

Table 2.4.2 preparation of 20mM glucose Gey and Gey buffer.

Reagent	Amount required	Final concentration
G&G buffer	500ml	1X
dH_2O	500ml	-
D-glucose	3.6g	20mM
$CaCl_2$	2ml (of 1M stock)	2mM
BSA	500mg	0.5mg/ml

2.4.2 Static incubation using MIN6 cells

25,000 MIN6 cells per well were plated out in fully complemented growth media in 96 well culture plates and incubated for 24 hours in a humidified 37ºC incubator containing 5% CO_2. The following day the media was replaced with growth media containing low glucose (1g/L) and incubated again for 24 hours. The next day media was removed and 200µl of 2mM glucose Gey and Gey buffer added to each well and the plate incubated at 37ºC for 2 hours. Following incubation, media was removed from the cell plate by tapping and 200µl of ligand buffer was added per well. The plate was incubated for 1 hour in a humidified 37ºC incubator with 5% CO_2. After incubation the plate was spun at 200 x g for 1 minute to pellet floating cells from the supernatant and 100µl of supernatant was transferred to an empty 96 well plate. Samples were stored at -20ºC until required for insulin content assessment by radioimmunoassay.

2.4.3 Static incubation using INS-1 cells

15,000 INS-1 cells per well were plated out in fully complemented growth media in 96 well culture plates and incubated for 24 hours in a humidified 37ºC incubator containing 5% CO_2. The following day the cells were washed with 2.8mM glucose SAB buffer and 150µl/well of fresh 2.8mM glucose SAB buffer was added to the plate. The cells were incubated at in a 37ºC incubator for 2 hours. During incubation ligand treatment was made up in SAB buffer and placed on ice. Following incubation, media

was removed from the cell plate and 200µl of ligand buffer was added per well. The plate was incubated for 1 hour in a humidified 37^{o}C incubator with 5% CO_2. After incubation the plate was spun at 200 x g for 1 minute to pellet floating cells from the supernatant and 100µl of supernatant was transferred to an empty 96 well plate. Samples were stored at -20^{o}C until required for insulin content assessment by radioimmunoassay.

Table 2.4.3 Preparation of 10X SAB buffer.

Reagent	g/500ml	Final concentration
NaCl	33.32	1.14M
KCl	1.73	47mM
KH2PO4	0.82	12mM
MgSO4	0.70	11.6mM

Table 2.4.4 Preparation of 1X SAB buffer.

Reagent	Amount/100ml	Final concentration
10X SAB	90	1X
dH_2O	10	-
HEPES	2ml (of 1M stock)	20mM
$NaHCO_3$	0.214g	25.5mM
$CaCl_2$	0.25ml (of 1M stock)	2.5mM
BSA	0.2g	0.2%

2.4.4 Radioimmunoassay

The insulin radioimmunoassay (RIA) is a competition binding assay which allows for the accurate detection of low concentrations of insulin within a sample. There are three main components of the assay; the insulin antibody (Ab), the radiolabelled insulin (Ag*) and unlabelled insulin (Ag). The assay is based on the competitive and reversible binding of unlabelled insulin and radiolabelled insulin for an anti-insulin antibody binding site:

$$Ab + Ag + Ag^* \leftrightarrow Ab{:}Ag + Ab{:}Ag + Ag + Ag^*$$

The assay is performed by incubating a fixed concentration of antibody with ^{125}I-insulin and non-radiolabelled insulin (either samples or standards) at 4^{o}C for 48 hours. Following incubation, the antibody:antigen bound complex is then separated from free antigen by precipitation and insulin content of the sample quantified by the displacement of radioactive antigen. Insulin content is determined by extrapolating sample cpm counts from standard curve cpm counts.

Prior to starting, samples for testing were thawed out at room temperature and both borate buffer and 30% PEG solutions were prepared as described below.

Table 2.4.5. Borate buffer preparation.

Reagent	Required conc.	Amount for 2L
Boric Acid	133mM	16.5g
EDTA	10mM	7.4g
NaOH	67.5mM	5.4g
BSA	1g/L	2g

Table 2.4.6. 30% PEG solution preparation

Reagent	Amount
dH_2O	2L
PEG	600g

Sample conditions were assayed in duplicate and diluted 5X in 80µl of borate buffer, whilst standard curve samples and reference samples (total, NSB and maximum binding) were performed in triplicate. A nine point insulin standard curve was prepared by performing a one in two serial dilution in borate buffer of a 10ng/ml stock and 100µl transferred to each standard tube. Antibody stock was diluted tenfold in borate buffer and 100µl added to each tube with the exception of NSB and total tubes. Insulin tracer (^{125}I-insulin) was prepared in borate buffer at a concentration giving 10,000cpm. 100µl of tracer was added to each tube, tubes covered with Parafilm and

incubated at 4ºC for 48 hours. A summary table of reagent addition for each condition can be found below.

Table 2.4.7. Summary table of test condition preparations for RIA

Condition	Buffer	Antibody	Tracer	Standard	Sample
Totals			100µl		
NSB	200µl		100µl		
Max	100µl	100µl	100µl		
Standards		100µl	100µl	100µl	
Samples		100µl	100µl		100µl

Following the 48 hour incubation period, a 15% PEG precipitation buffer was prepared as follows.

Table 2.4.8. Preparation of RIA precipitation solution

Reagent	Amount/500ml
30% PEG stock solution	250ml
PBS	250ml
γ-globulins	500mg
Tween-20	250µl

With the exception of the total condition, 1ml of precipitation solution was added to each tube and then centrifuged at 1500 x g for 15 mins at 4ºC using a Jouan Cool Spin centrifuge. Following centrifugation, the supernatant was carefully aspirated leaving a pellet containing antibody:antigen bound complexes. Radioactive content was measured on a Perkin Elmer WIZARD2 gamma counter.

2.5 Measurement of apoptosis

Apoptosis is an energy dependent process that involves the activation of a group of cysteine proteases called “caspases” which mediate a multitude of apoptotic events such as DNA fragmentation, degradation of cytoskeletal and nuclear proteins, expression of ligands for phagocytic receptors and uptake by phagocytic cells (Elmore, 2007). Cellular apoptosis was assessed using Promega’s Caspase-Glo 3/7 assay. The assay is based on a luminescent readout which is directly proportional to the activity of the apoptotic enzymes, caspase-3/7, within the cell.

In brief, 100µl of cells per well were plated out in white 96 well plates for 24hours before the cells were challenged with 50µl of ligand treatment in the absence or presence of 50µl of cytokines (1U/µl TNFα, 1U/µl IFNγ, 0.01U/µl IL1β) for 18hours at 37ºC, 5% CO_2. Following ligand/cytokine challenge, 75µl of media was removed and cells were lysed by the addition of 25µl of Caspase-Glo 3/7 reagent containing a lysing agent, proluminescent caspase-3/7 DEVD-aminolucoferin substrate and a proprietary thermostable luciferase. Lysis of the cell releases intracellular endogenous caspase-3/7 enzymes which convert the pro-aminoluciferin substrate into free aminoluciferin, which is then metabolised by the luciferase in the presence of ATP and O_2 to generate a luminescent signal. Luminescent signal was captured on a Veritas luminometer.

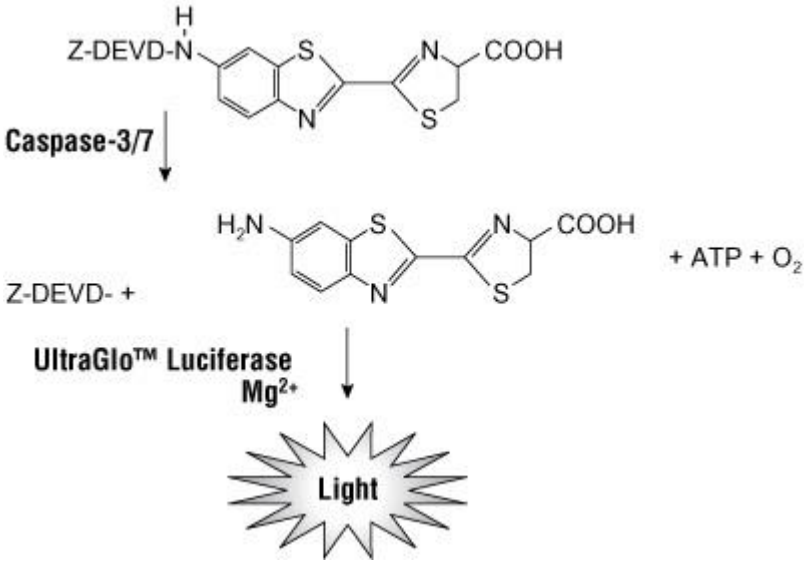

Figure 2.5.1. Caspase-3/7 assay principle.

2.6 Measurement of cell proliferation

Cell proliferation was indirectly assessed by measuring 5-bromo2'-deoxyuridine (BrdU) incorporation into newly synthesised genomic DNA of replicated cells. The extent of BrdU uptake was then quantified by combining ELISA and chemiluminescence technologies.

Briefly, cells were plated out in 96 well plates and incubated overnight in fully complemented growth media. The next day, cell media was changed to serum free media containing 2mM glucose, to ensure that the cells reached a quiescent state prior to ligand treatment, and the cells once again incubated overnight. Following overnight incubation, the cells were treated with ligand in the presence or absence of serum and incubated at 37ºC for 2 days. On day five, the cell media was spiked with 10µl of 1:100 BrdU labelling solution and incubated for 4 hours at 37ºC before the cell media was removed. 200µl of FixDenat solution was then added to each well and the plate

incubated for 30 mins at room temperature. The contents of the wells was aspirated, 100µl/well of anti-BrdU-POD working solution added and the plate incubated for 90 mins at room temperature. Following the incubation, the cells were washed three times with 200µl/well of wash solution before 100µl/well of substrate solution was added. The plate was then incubated at room temperature until blue staining developed. 25µl/well of 1M H_2SO_4 was then added to halt the intensity of further staining and the absorbance was read at 450nm.

2.7 Measurement of intracellular cAMP

The effects of test ligands on intracellular cAMP levels was measured using Cisbio's HTRF cAMP assay. An HTRF assay is an assay which utilises the combination of FRET technology and time resolved (TR) fluorescence. FRET is the process by which a fluorescent signal is generated following energy transfer from an excited fluorophore donor molecule to an acceptor fluorophore molecule when in close proximity to each other. A fluorescent measurement is recorded over a time to create a fluorescent spectrum also known as a time resolved fluorescent readout. The incorporation of a dual emission readout minimises the background interference of media and buffer quenching and allows for normalisation of readout signal to cell number.

The cAMP HTRF assay is based on the competition between endogenously produced cAMP with a donor fluorophore (d2) conjugated cAMP molecule for an acceptor fluorophore (cryptate) conjugated anti-cAMP antibody. Production of endogenous intracellular cAMP results in the competitive displacement of d2-cAMP from the anti-cAMP antibody resulting in a decrease in FRET signal. The introduction of a cAMP

standard curves allows for the direct measurement of intracellular cAMP production by extrapolating FRET values from the standard curve.

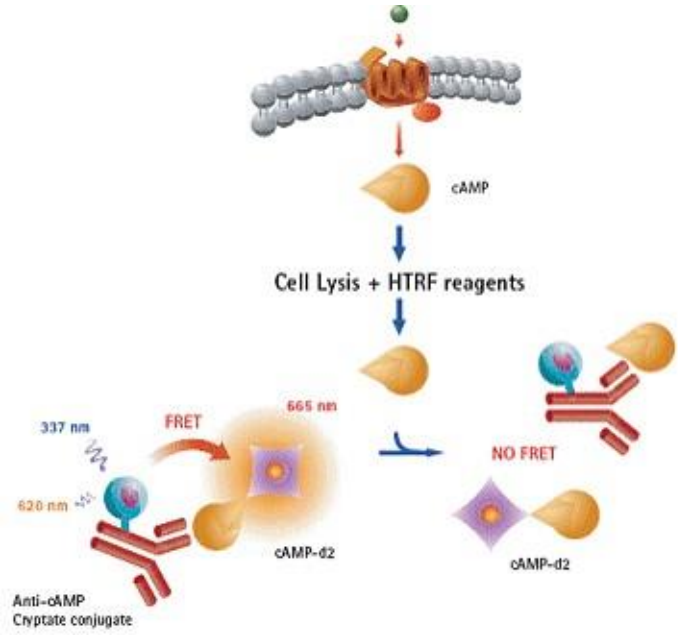

Figure 2.7.1. cAMP HTRF assay principle

In brief, MIN6 cells were detached from a T75 flask using 5ml of enzyme free cell dissociation buffer. Enzyme free dissociation buffer was used rather than trypsin so that cell surface receptors would not be digested during the detachment process. Following detachment, 5ml of full complemented growth media was added to the cell suspension and centrifuged at 200 x g for 3 mins. The supernatant was removed and the cell pellet resuspended in a volume non-complemented DMEM to create the required cell density per well per 5µl. 5µl/well of cells were plated out in a white 384 well round bottomed plate followed by 5µl of ligand treatment prepared in HBSS supplemented with 10mM HEPES, 0.2% BSA and 2mM IBMX with a pH of 7.4 (pH adjusted with HCl). The plate was incubated at room temperature for 1 hour. Following incubation 5µl of d2-cAMP prepared in lysis buffer was added to each well followed by the addition of 5µl/well of cryptate-Ab prepared in lysis buffer. The plate

was again incubated at room temperature for 1 hour before being read on a Pherastar FS plate reader (BMG LabTech) under the following settings (Table 2.7.1).

Table 2.7.1. Pherastar HTRF plate read settings

Parameter	Setting
Delay time	100µs
Integration time	100µs
No. flashes	50

2.7.1.1 Data reduction

The dual emission readout allows for the normalisation of the 665nm wavelength to background fluorescence at 620nm. This allows for the correction of signal interference caused by the potential quenching of media, quenching by coloured compounds and variations in cell number. Ratio values for each well are calculated as described below where A_{665nm} is the 665nm wavelength and B_{620nm} is the 620nm wavelength.

$$\text{Ratio} = \left(\frac{A_{665nm}}{B_{620nm}} \right) \times 10^4$$

2.8 ATP assay

Intracellular ATP levels were measured using Promega's CellTiter-Glo Luminescent Cell Viability assay. This particular assay is typically used to assess cell viability following chronic ligand treatment but for the purposes of the experiments described in this thesis the procedure was modified to assess acute ligand treatment.

The principle of the CellTiter-Glo assay is based on the conversion of luciferin into oxyluciferin, AMP, PP_i, CO_2 and light by Ultra-Glo Luciferase which requires both Mg^{2+}, O_2 and ATP. The reliance of luciferase enzyme activity on ATP means luminescent output is altered by intracellular ATP levels. Therefore, an indirect quantification of intracellular ATP levels can be determined following extrapolation from a standard curve.

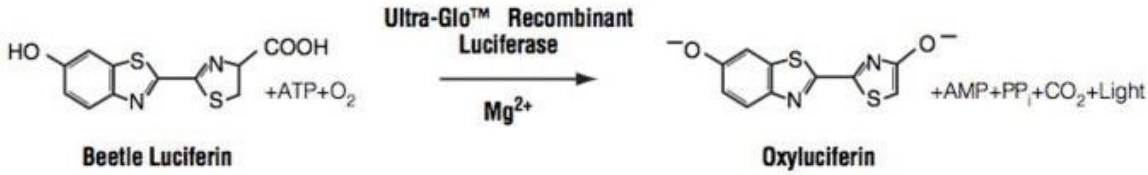

Figure 2.8.1 CellTiter-Glo Cell Viability assay principle.

For the purpose of studies assessing the effects of acute ligand treatment on intracellular ATP levels, MIN6 cells were used. Cells were plated out in white walled, clear bottomed 96 well plates and incubated overnight in a humidified incubator at 37ºC supplemented with 5% CO_2. The following day, the media was changed to low glucose media to allow cells to reach a more glucose responsive state the following day. The next day media was removed from the plate and replaced with 50µl/well of ligand made up in Gey and Gey buffer. The plate was then incubated for 1 hour at 37ºC. Following incubation, 50µl/well of CellTiter-Glo reagent was added to the plate, the contents mixed on a plate shaker for 1 minute and the plate incubated at room temperature for 10 mins. The plate was then read on a Veritas luminometer using the pre-installed CellTiter protocol.

2.9 Glucose uptake assay

One of the main functions of β-cells is to sense increases in circulating glucose concentrations and subsequently secrete insulin in response. Insulin secretion from β-cells is mediated by glucose uptake via the GLUT2 and subsequent phosphorylation by glucokinase (Thorens, 2001).

In order to assess the effects of exogenous CXCL14 on glucose uptake in the MIN6 cell line a glucose uptake assay from Promega was developed. Glucose uptake and glucokinase activity is indirectly assessed by replacing glucose within the assay buffer with 2DG and measuring the accumulation of the cell impermeable metabolite 2DG6P, a process catalysed by intracellular glucokinase. After incubation with 2DG in the presence of test ligand, the cells are lysed with STOP buffer to terminate uptake and destroy endogenous levels of NADPH within the cells. A high pH buffer solution (Go buffer) is added to neutralise the acid and a detection reagent is added that includes NAD+, G6PDH, a reductase, pro-luciferin, and luciferase. The result is the generation of NADPH from 2DG6P, luciferin from NADPH and luminescence from the metabolism of luciferin by luciferase. The luminescent signal is proportional to the accumulation of 2DG6P.

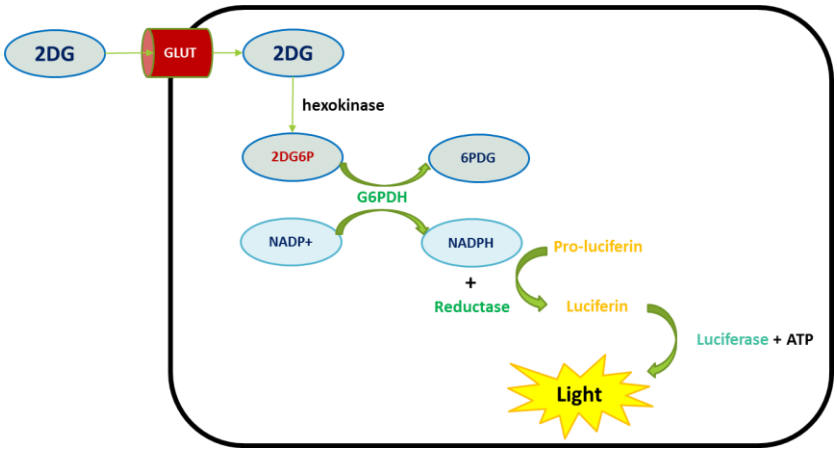

Figure 2.9.1 Promega glucose uptake assay principle.

2.10 β-arrestin assays

β-arrestin technology exploits the mechanism of intracellular β-arrestin recruitment at agonist-activated receptors, allowing for the functional measurement of ligand-receptor interactions irrespective of the G-protein-coupled pathways involved. The experiments described in this thesis utilise the PathHunter β-arrestin assays developed by DiscoveRx. Briefy, PathHunter technology involves fusing GPCRs with ProLink enzymes that are co-expressed in cell lines expressing a fusion protein of β-arrestin and an N-terminal deletion mutant of β-galactosidase. Activation of the GPCR results in recruitment of the fusion β-arresin protein to the ProLinked-tagged GPCR forcing the complementation of the two enzyme fragments resulting in the formation of an active β-galactosidase enzyme. The active form of the β-galactosidase enzyme catalyses the conversion of a chemiluminescent detection reagent into a luminescent signal which is directly proportional to receptor activation.

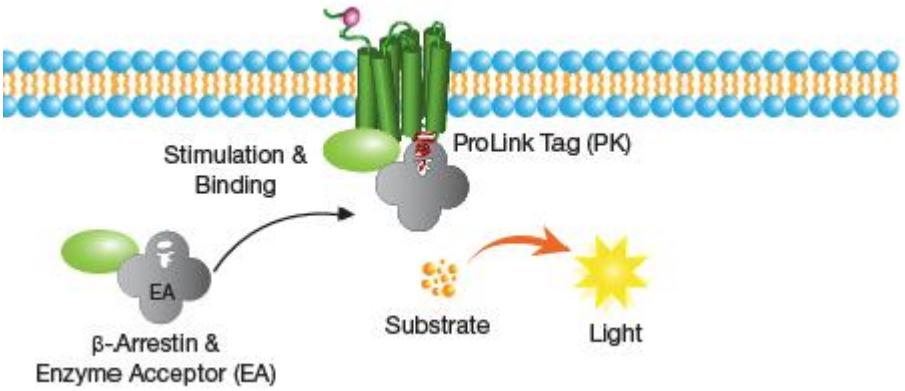

Figure 2.10.1 PathHunter β-arrestin assay principle.

The β-arrestin assays were performed as follows. A frozen vial containing 1.25 x 10^6 of PathHunter eXpress β-arrestin GPCR U2OS cells in 0.1ml of cryopreservant was thawed out in a water bath at 37°C. 0.5ml of pre-warmed CP (cell plating) reagent was

then added to the vial and the contents transferred to a 15ml Falcon tube containing 11.5ml of pre-warmed CP reagent. 100µl/well of cell suspension (10,000 cells/well) was then plated out into a white walled, clear bottomed 96 well plate and the cells were cultured for 48 hours in a 37ºC humidified incubator supplemented with 5% CO_2. 48 hours later, the media was carefully removed from the plate and 50µl/well of vehicle (ligand diluent in assay buffer) or 2X antagonist prepared in assay buffer (HBSS, 10mM HEPES, 0.1% BSA) was added to each well. Immediately after, 50µl/well of 2X agonist prepared in assay buffer was added and the plate was incubated at 37ºC for 90 mins. During incubation, 5.5ml of detection reagent was prepared by adding 1.25ml of substrate reagent 1 and 0.25ml of substrate reagent 2 to 4.75ml of cell assay buffer (all supplied within the kit). After the 90 minute incubation, 55µl of detection reagent was added to each well and the plate was incubated at room temperature for 60 mins. Luminescence was captured on a Veritas luminometer.

CHAPTER 3 – GPCRome comparison

3.1 Background

G protein-coupled receptors (GPCRs) are a diverse super family of seven transmembrane bound proteins whose primary function is to initiate the activation of intracellular signalling pathways following stimulation by extracellular stimuli, which include photons, amines, lipids, ions, peptides and proteins (Kroeze et al., 2003). Due to the ubiquitous expression of GPCRs throughout various tissues, they are implicated in the regulation of a variety of diverse physiological processes (Moller et al., 2001), such as the regulation of the secretion of the blood glucose controlling hormones insulin, glucagon and somatostatin from islets (Amisten et al., 2013). As a result, GPCRs are being identified as therapeutic targets for the treatment of T2DM (Reimann and Gribble, 2016).

To date, the success of GPCRs as targets for the treatment of T2DM is limited to the GLP-1 receptor (GLP1R), which mediates the function of the GLP-1 peptide to regulate insulin and glucagon secretion from the pancreas. Drugs that target the GLP1R have been shown to enhance glucose-stimulated insulin release, reduce elevated levels of glucagon, inhibit gastric emptying and suppress appetite, but adverse effects such as pancreatitis, nausea, vomiting and gastrointestinal complaints are associated with such therapeutics (Trujillo and Nuffer, 2014). In addition, current GLP1R agonist therapeutics require injectable dosing thus negatively impacting patient compliance (Tomkin, 2014). As a result, there are continuing efforts to identify alternative GPCR targets for the treatment of diabetes.

According to Amisten *et al* (Amisten et al., 2013), human islets express 293 non-odorant GPCRs, but despite this large pool of potential targets only 2 GPCR targets, other than GLP1R, are currently under clinical investigation, GPR119 and GPR40

(FFAR1) (Reimann and Gribble, 2016). Part of the issue contributing the limited success of targeting GPCRs for T2DM is the poor functional characterisation of the majority of islet expressed GPCRs. This issue is further exacerbated by the limited availability of human islets required to study GPCR function, and as a result rodent islets, particularly mouse islets, are relied upon as translational models.

Whilst the issue of islet availability is resolved by using rodent models, the suitability of rodent islets as translational models to predict human islet function is unclear. Differences in the proportion of islet endocrine cell populations (Steiner et al., 2010) and islet architecture between human and mouse islets have been documented (Cabrera et al., 2006), and the fact that the mouse genome contains a total of 1697 GPCRs whereas the human genome contains approximately 791 GPCRs (Bjarnadottir et al., 2006) gives rise to questions regarding the suitability of using mouse islets for human islet GPCR studies.

The experiments described in this chapter aim to compare human and mouse islet GPCR mRNA expression profiles (GPCRomes). Mouse islets from both the outbred ICR mouse strain and the inbred C57/BL6 (C57) mouse strain are compared to human islets with the aim of identifying similarities and differences in GPCR mRNA expression between the two species and to determine the suitability of using mouse islets as translational models for the study of human islet GPCRs.

3.2 Aims

- Quantify the mRNA expression of 376 human non-olfactory GPCRs in human islets and their orthologue counterparts in mouse islets.
- Compare the GPCR mRNA expression profiles of human and mouse islets and highlight species differences and similarities.
- Determine the suitability of using mouse islets as translational models to assess the function of newly identified GPCR targets for the treatment of T2DM.

3.3 Methods

3.3.1 Gene expression analysis

Human and mouse islet GPCRomes were determined by qPCR using Qiagen's QuantiTect primers and QuantiFast SYBR green mastermix. 376 human non-odorant GPCRs and 335 mouse orthologues were included in this study. 41 human GPCRs had no known mouse orthologues. The human bitter taste receptors were excluded from the inter-species comparative analysis due to the poor annotation of mouse orthologue bitter taste receptors.

3.3.1.1 Isolation of human and mouse islets for GPCR mRNA quantification

As described in section 2.2.1, human islets were obtained from four heart beating donors (2 male, 2 female) at the Islet Transplantation Units at King's College London using a revised version (Huang et al., 2004) of the Edmonton protocol. The donors were between the ages of 43-59, were non-diabetic and had a BMI of 22-33kg/m^2.

Mouse islets were isolated *in-house* as described in section 2.2.2. Two strains of mice were used for the purpose of this study, the outbred ICR strain and the inbred C57/BL6 (C57) strain, so that strain differences as well as species differences could be compared. All islets were obtained from adult male mice aged 8-12 weeks.

Following the isolation of human and mouse islets, approximately 200 islets per biological replicate were handpicked and added to 1ml of TRIzol for 5mins before being stored at -80^{o}C awaiting RNA extraction and cDNA generation.

3.3.1.2 cDNA generation

Quantitative real time polymerase chain reaction was performed using the two step approach which requires the generation of cDNA prior to performing the qPCR reaction. Firstly, total RNA was extracted from previously TRIzol harvested tissue as described in detail in section 2.3.1 and quantified as described in section 2.3.3. Following quantification, mRNA was purified from the total RNA sample using Qiagen's RNeasy MiniElute Cleanup kit (section 2.3.2). Finally, cDNA was reversed transcribed from purified mRNA using the TaqMan Reverse Transcription kit (section 2.3.4).

3.3.1.3 Quantitative real time polymerase chain reaction

qPCR was performed using Qiagen's QuantiTect primers, QuantiFast SYBR green master mix and the Roche LightCycler 480 under the settings described in section 2.3.5. Gene expression was represented as expression relative to GAPDH expression from four biological replicates.

3.4 Results

3.4.1 Confirmation of islet endocrine cell presence

In order to confirm the presence of α-, β-, δ-, PP- and ε- endocrine cell populations within the islet groups, mRNA quantification of glucagon (GCG), insulin (INS), somatostatin (SST), pancreatic polypeptide (PPY) and ghrelin (GHRL) was performed (Figure 3.4.1). All aforementioned peptides were expressed at the mRNA level within each islet population, thus confirming the presence of the endocrine cell populations within each islet group.

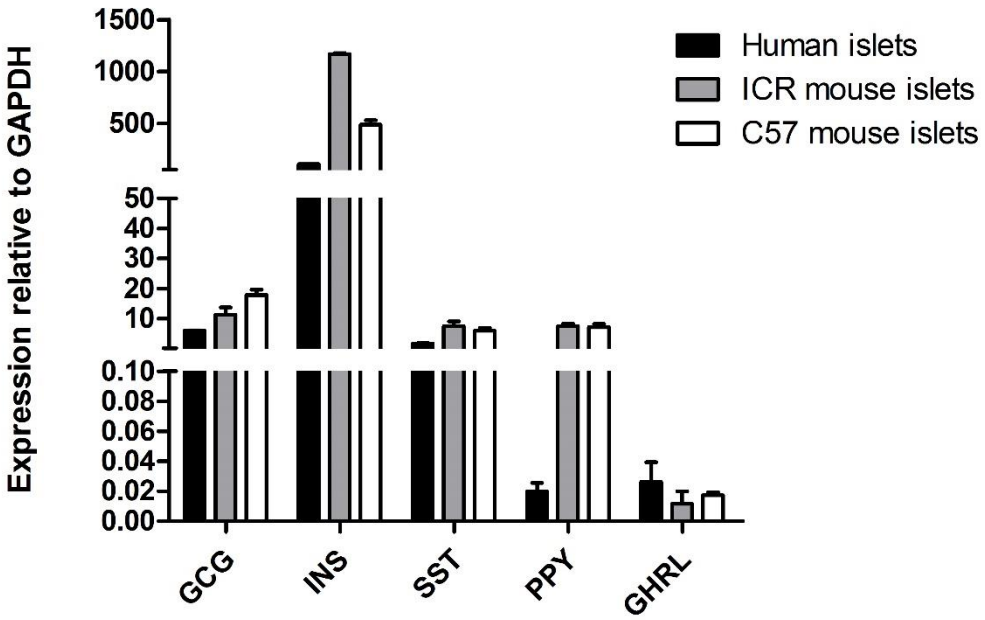

Figure 3.4.1 mRNA confirmation of endocrine cell presence within islet groups. The presence of α-, β-, δ-, PP- and ε-cells endocrine cells were confirmed by the detection of GCG, INS, SST, PPY and GHRL mRNA expression respectively. Data expressed as mean + SEM relative to GAPDH expression, from four biological replicates.

3.4.2 GPCR mRNA expression analysis in human and mouse islets

Expression of 376 human GPCR mRNAs and 335 mouse orthologous counterparts relative to the house keeping gene GAPDH in both human and mouse islets has been organised alphabetically into receptor families as illustrated below.

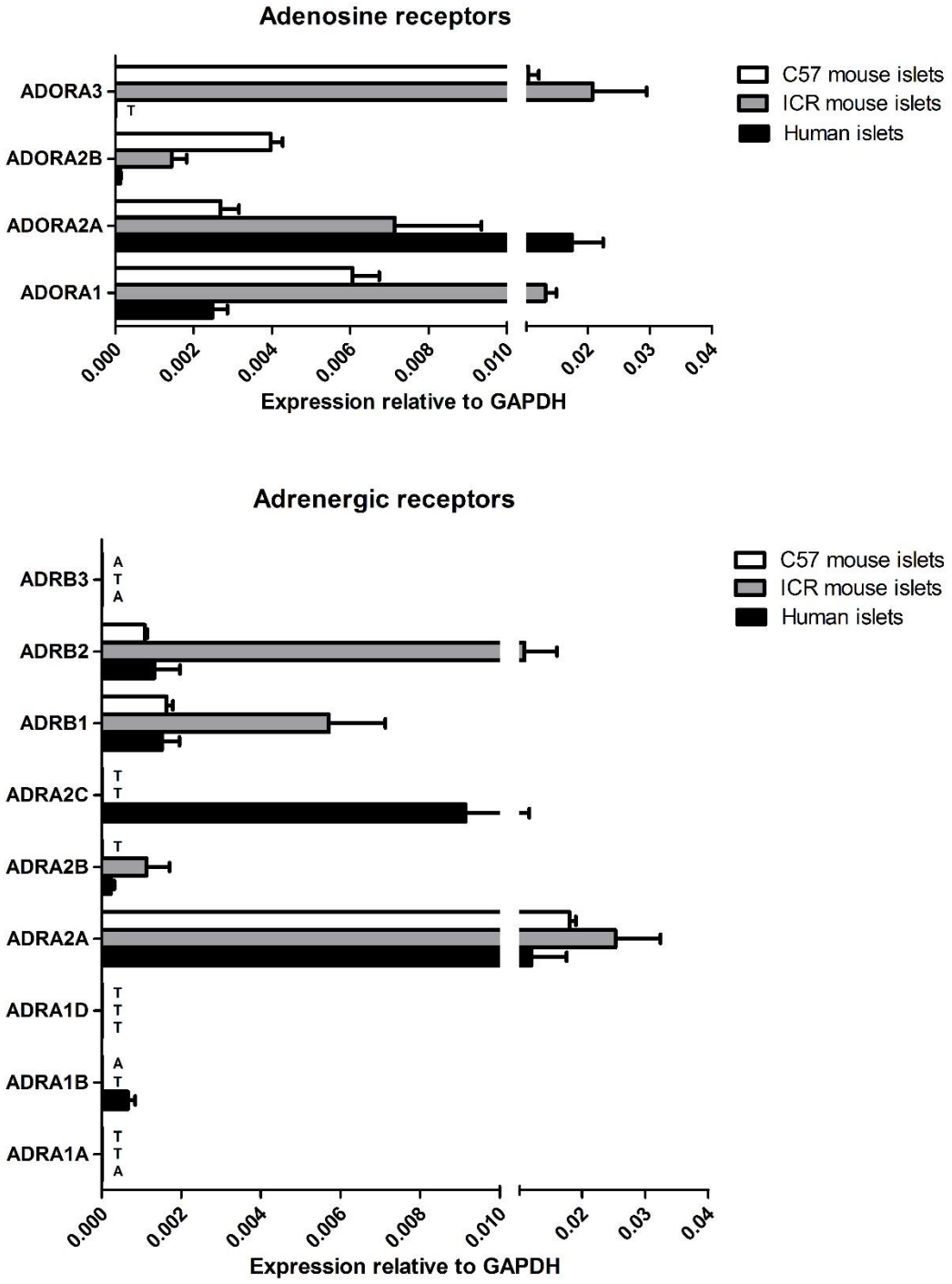

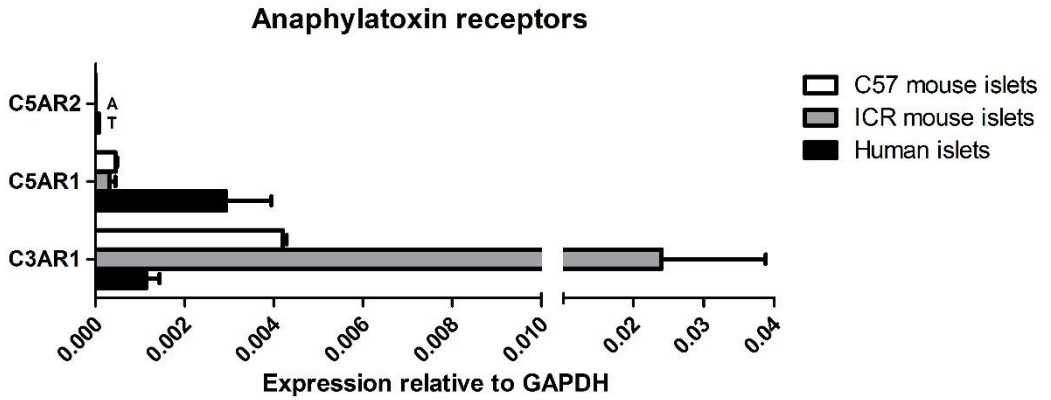
Anaphylatoxin receptors
C5AR2
C5AR1
C3AR1
A
T
C57 mouse islets
ICR mouse islets
Human islets
0.000
0.002
0.004
0.006
0.008
0.010
0.02
0.03
0.04
Expression relative to GAPDH

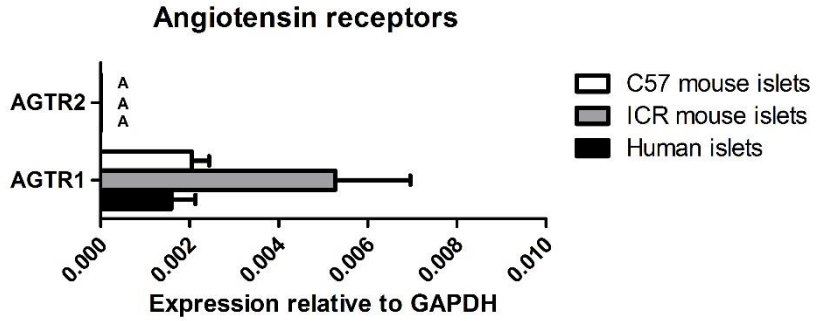
Angiotensin receptors
AGTR2
AGTR1
A
A
A
C57 mouse islets
ICR mouse islets
Human islets
0.000
0.002
0.004
0.006
0.008
0.010
Expression relative to GAPDH

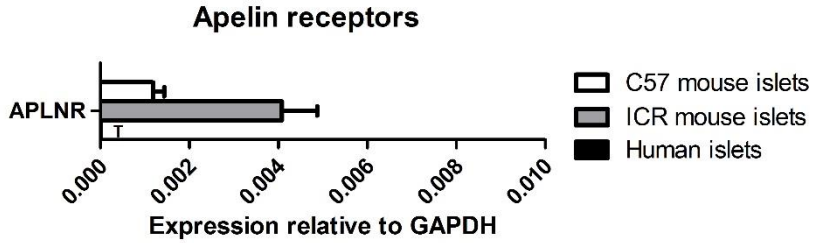
Apelin receptors
APLNR
T
C57 mouse islets
ICR mouse islets
Human islets
0.000
0.002
0.004
0.006
0.008
0.010
Expression relative to GAPDH

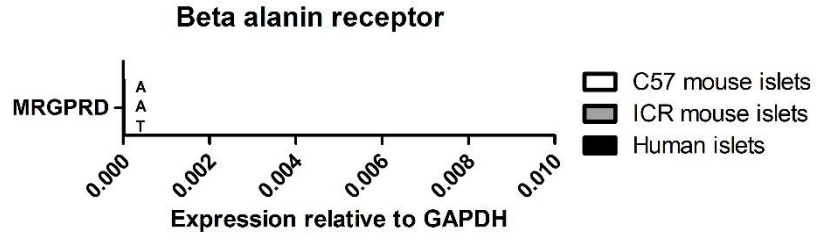
Beta alanin receptor
MRGPRD
A
A
T
C57 mouse islets
ICR mouse islets
Human islets
0.000
0.002
0.004
0.006
0.008
0.010
Expression relative to GAPDH

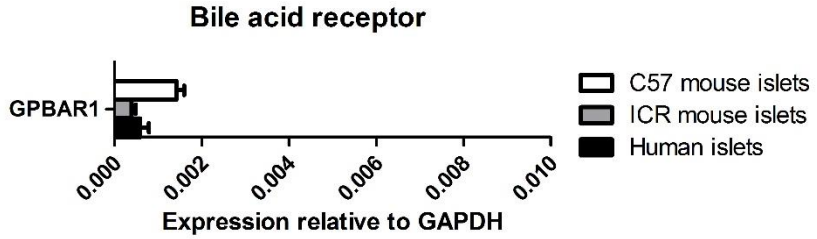
Bile acid receptor
GPBAR1
C57 mouse islets
ICR mouse islets
Human islets
0.000
0.002
0.004
0.006
0.008
0.010
Expression relative to GAPDH

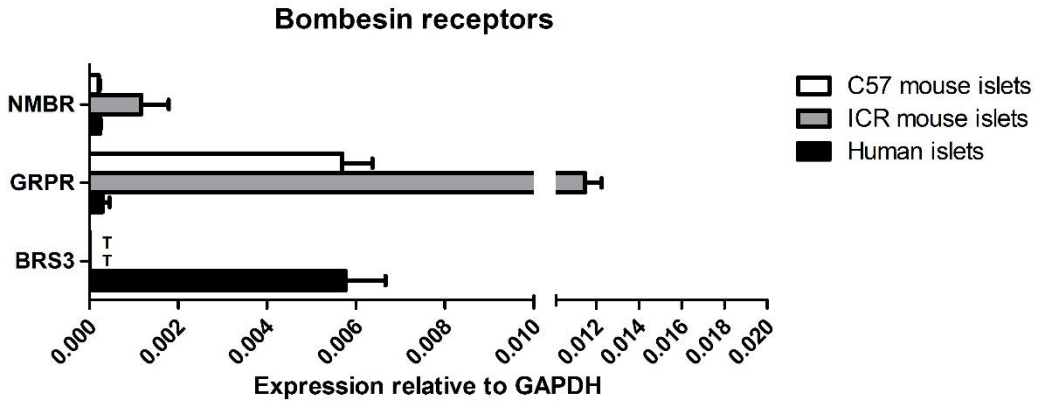
Bombesin receptors
NMBR
GRPR
BRS3
T
T
C57 mouse islets
ICR mouse islets
Human islets
0.000
0.002
0.004
0.006
0.008
0.010
0.012
0.014
0.016
0.018
0.020
Expression relative to GAPDH

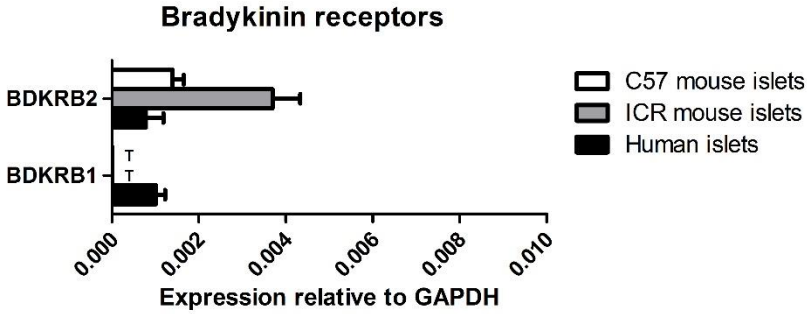
Bradykinin receptors
BDKRB2
BDKRB1
T
T
C57 mouse islets
ICR mouse islets
Human islets
0.000
0.002
0.004
0.006
0.008
0.010
Expression relative to GAPDH

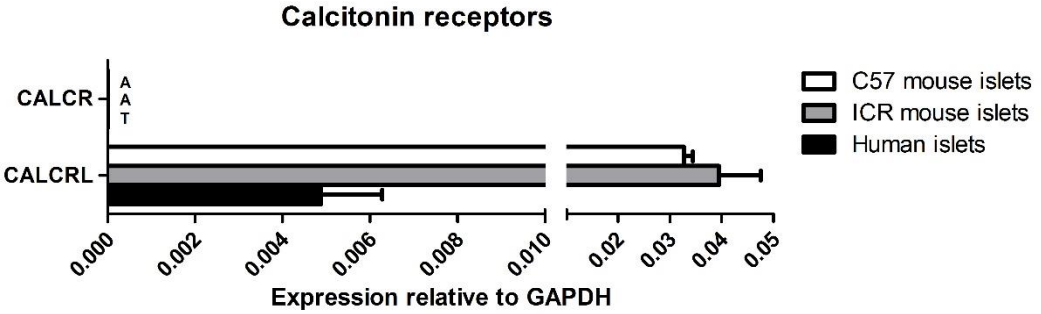
Calcitonin receptors
CALCR
CALCRL
A
A
T
C57 mouse islets
ICR mouse islets
Human islets
0.000
0.002
0.004
0.006
0.008
0.010
0.02
0.03
0.04
0.05
Expression relative to GAPDH

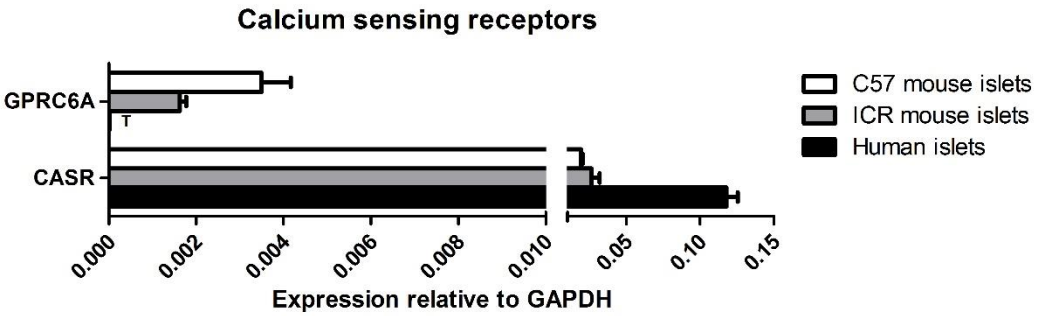
Calcium sensing receptors
GPRC6A
CASR
T
C57 mouse islets
ICR mouse islets
Human islets
0.000
0.002
0.004
0.006
0.008
0.010
0.05
0.10
0.15
Expression relative to GAPDH

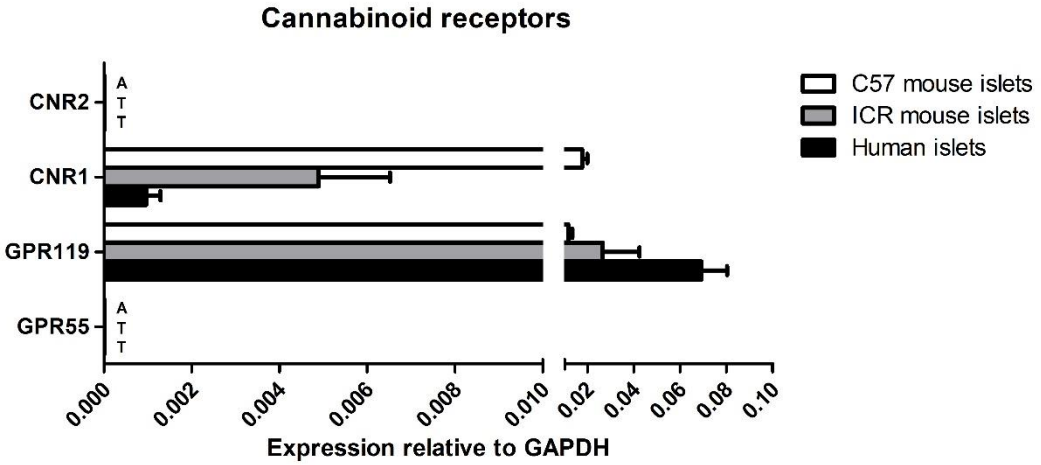
Cannabinoid receptors
C57 mouse islets
ICR mouse islets
Human islets
CNR2
CNR1
GPR119
GPR55
A
T
T
A
T
T
0.000
0.002
0.004
0.006
0.008
0.010
0.02
0.04
0.06
0.08
0.10
Expression relative to GAPDH

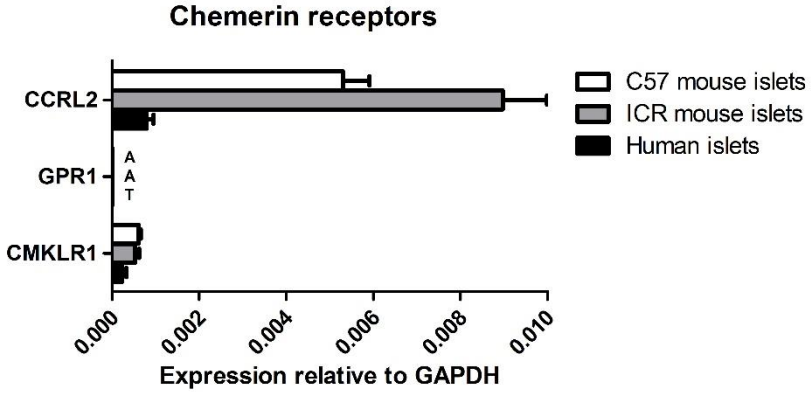
Chemerin receptors
C57 mouse islets
ICR mouse islets
Human islets
CCRL2
GPR1
CMKLR1
A
A
T
0.000
0.002
0.004
0.006
0.008
0.010
Expression relative to GAPDH

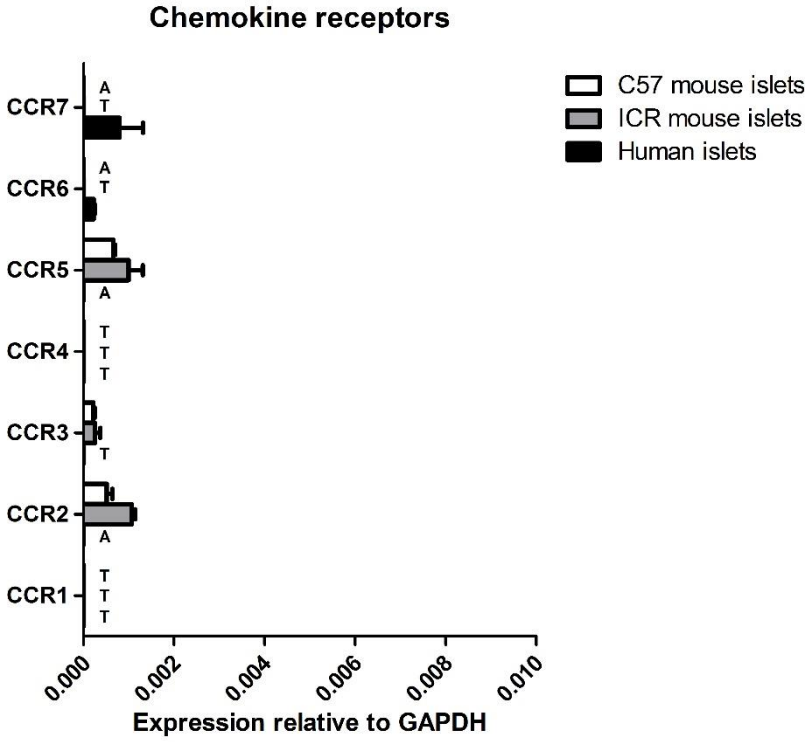
Chemokine receptors
C57 mouse islets
ICR mouse islets
Human islets
CCR7
CCR6
CCR5
CCR4
CCR3
CCR2
CCR1
A
T
A
T
A
T
T
T
T
T
A
T
T
T
T
0.000
0.002
0.004
0.006
0.008
0.010
Expression relative to GAPDH

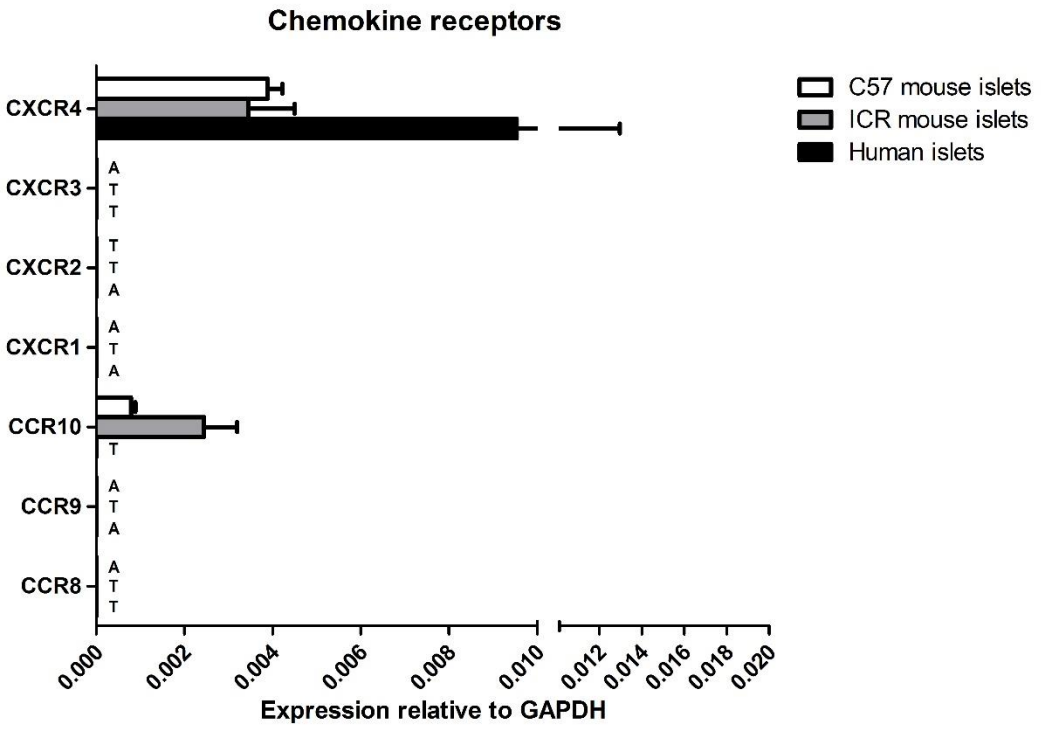
Chemokine receptors
C57 mouse islets
ICR mouse islets
Human islets
CXCR4
CXCR3
CXCR2
CXCR1
CCR10
CCR9
CCR8
A T T
T T A
A T A
T
A T A
A T T
0.000
0.002
0.004
0.006
0.008
0.010
0.012
0.014
0.016
0.018
0.020
Expression relative to GAPDH

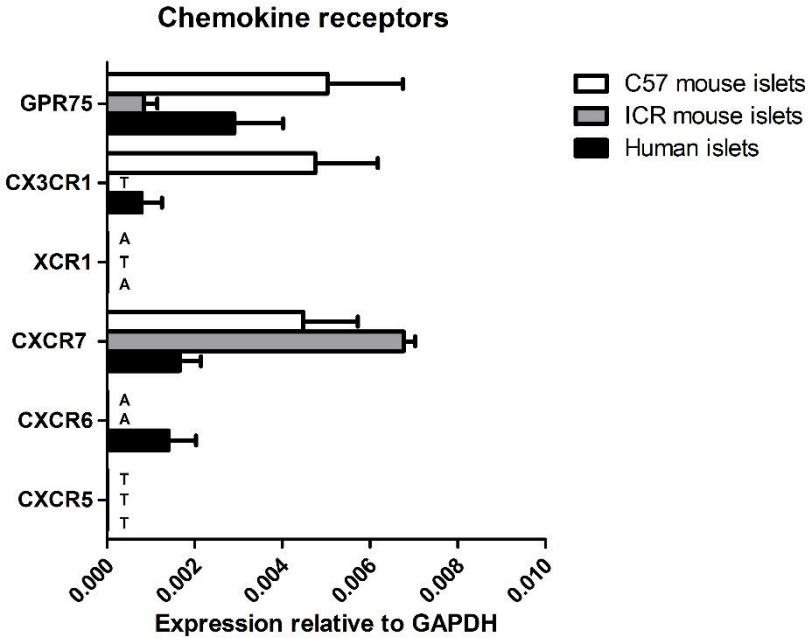
Chemokine receptors
C57 mouse islets
ICR mouse islets
Human islets
GPR75
CX3CR1
XCR1
CXCR7
CXCR6
CXCR5
T
A T A
A A
T T T
0.000
0.002
0.004
0.006
0.008
0.010
Expression relative to GAPDH

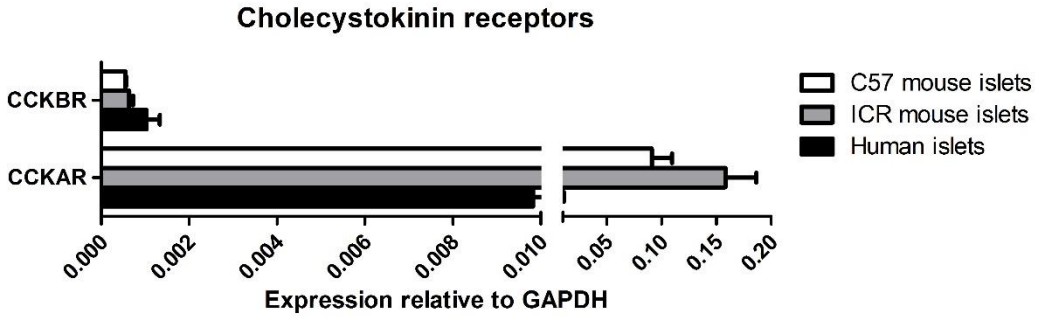
Cholecystokinin receptors
CCKBR
CCKAR
C57 mouse islets
ICR mouse islets
Human islets
0.000
0.002
0.004
0.006
0.008
0.010
0.05
0.10
0.15
0.20
Expression relative to GAPDH

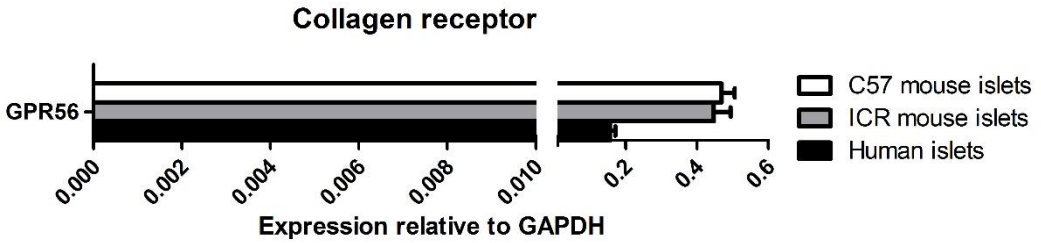
Collagen receptor
GPR56
C57 mouse islets
ICR mouse islets
Human islets
0.000
0.002
0.004
0.006
0.008
0.010
0.2
0.4
0.6
Expression relative to GAPDH

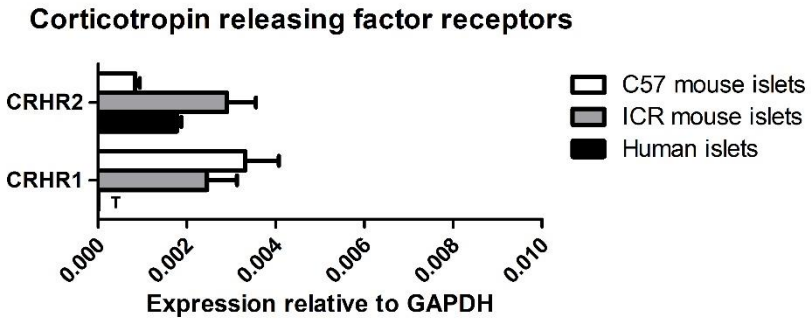
Corticotropin releasing factor receptors
CRHR2
CRHR1
C57 mouse islets
ICR mouse islets
Human islets
0.000
0.002
0.004
0.006
0.008
0.010
Expression relative to GAPDH

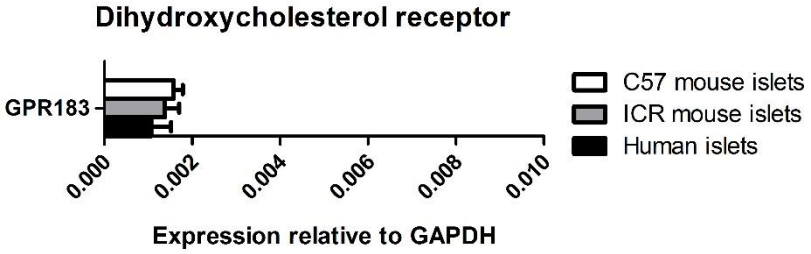
Dihydroxycholesterol receptor
GPR183
C57 mouse islets
ICR mouse islets
Human islets
0.000
0.002
0.004
0.006
0.008
0.010
Expression relative to GAPDH

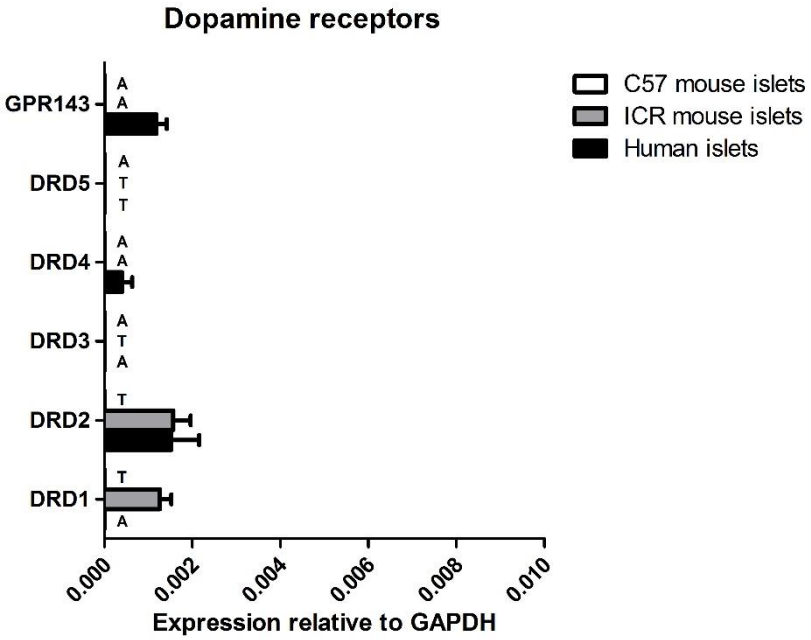
Dopamine receptors
GPR143
DRD5
DRD4
DRD3
DRD2
DRD1
C57 mouse islets
ICR mouse islets
Human islets
0.000
0.002
0.004
0.006
0.008
0.010
Expression relative to GAPDH

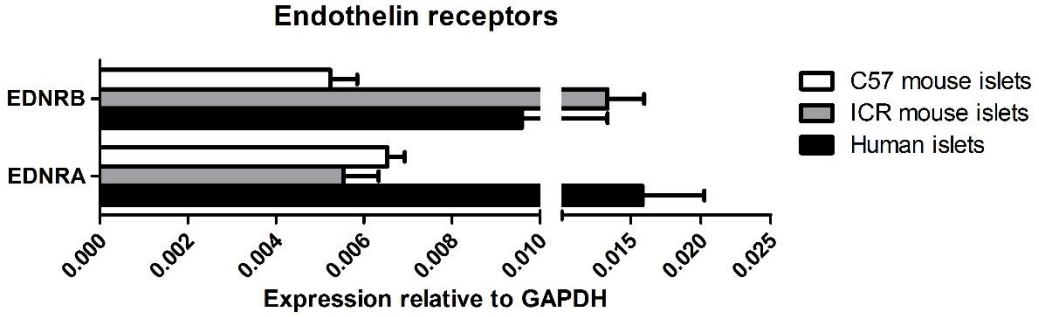
Endothelin receptors
EDNRB
EDNRA
C57 mouse islets
ICR mouse islets
Human islets
0.000
0.002
0.004
0.006
0.008
0.010
0.015
0.020
0.025
Expression relative to GAPDH

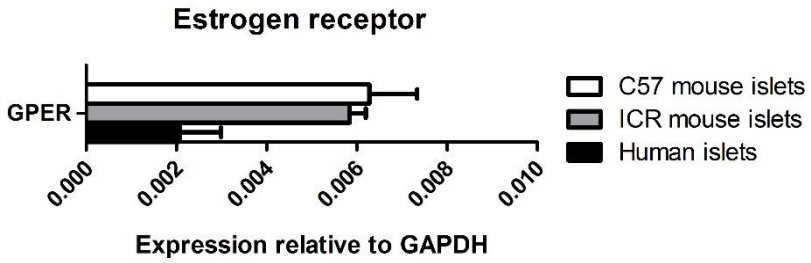
Estrogen receptor
GPER
C57 mouse islets
ICR mouse islets
Human islets
0.000
0.002
0.004
0.006
0.008
0.010
Expression relative to GAPDH

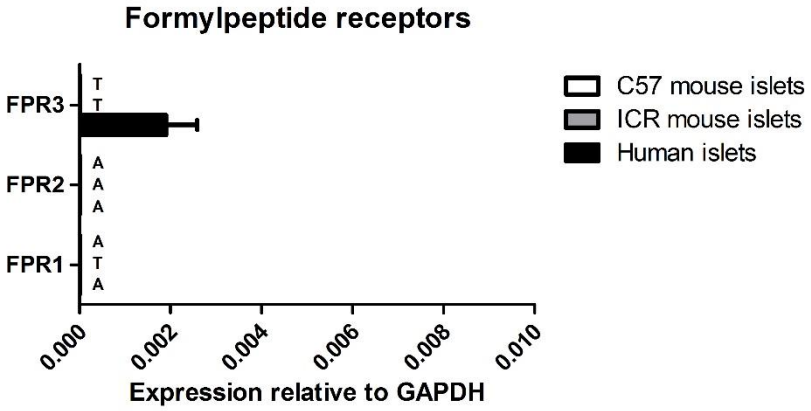
Formylpeptide receptors
FPR3
FPR2
FPR1
C57 mouse islets
ICR mouse islets
Human islets
0.000
0.002
0.004
0.006
0.008
0.010
Expression relative to GAPDH

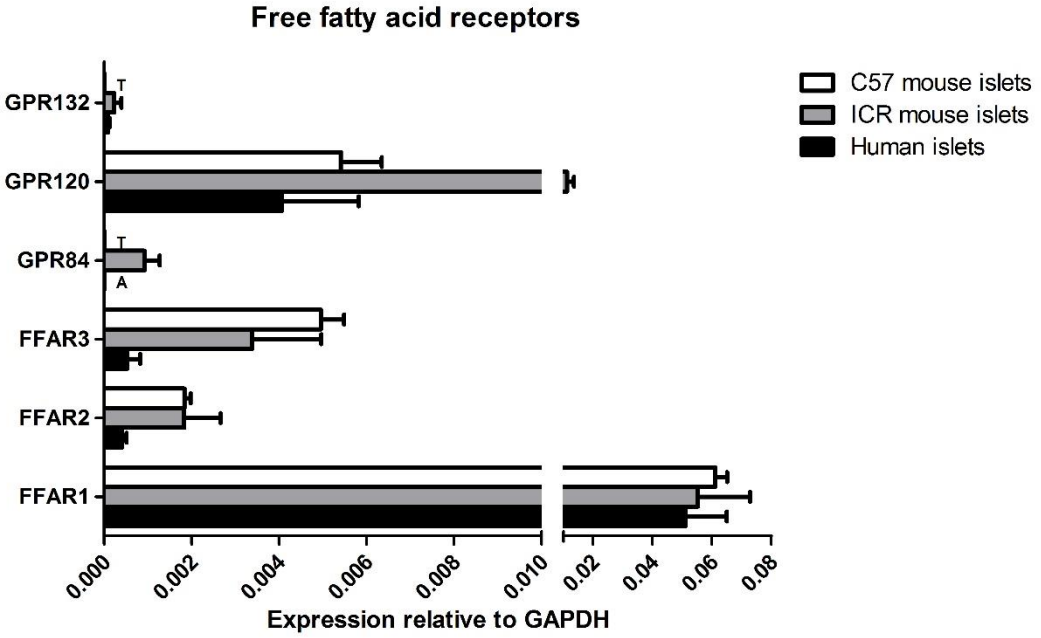
Free fatty acid receptors
GPR132
GPR120
GPR84
FFAR3
FFAR2
FFAR1
C57 mouse islets
ICR mouse islets
Human islets
0.000
0.002
0.004
0.006
0.008
0.010
0.02
0.04
0.06
0.08
Expression relative to GAPDH

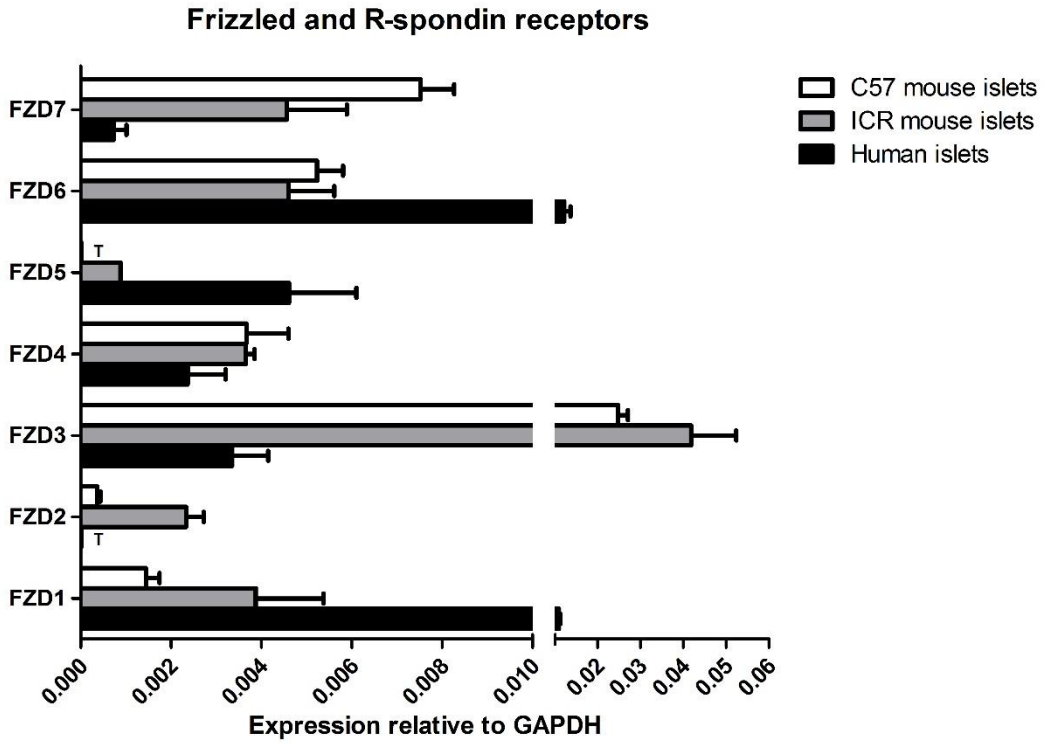
Frizzled and R-spondin receptors
C57 mouse islets
ICR mouse islets
Human islets
FZD7
FZD6
FZD5
FZD4
FZD3
FZD2
FZD1
T
T
0.000
0.002
0.004
0.006
0.008
0.010
0.02
0.03
0.04
0.05
0.06
Expression relative to GAPDH

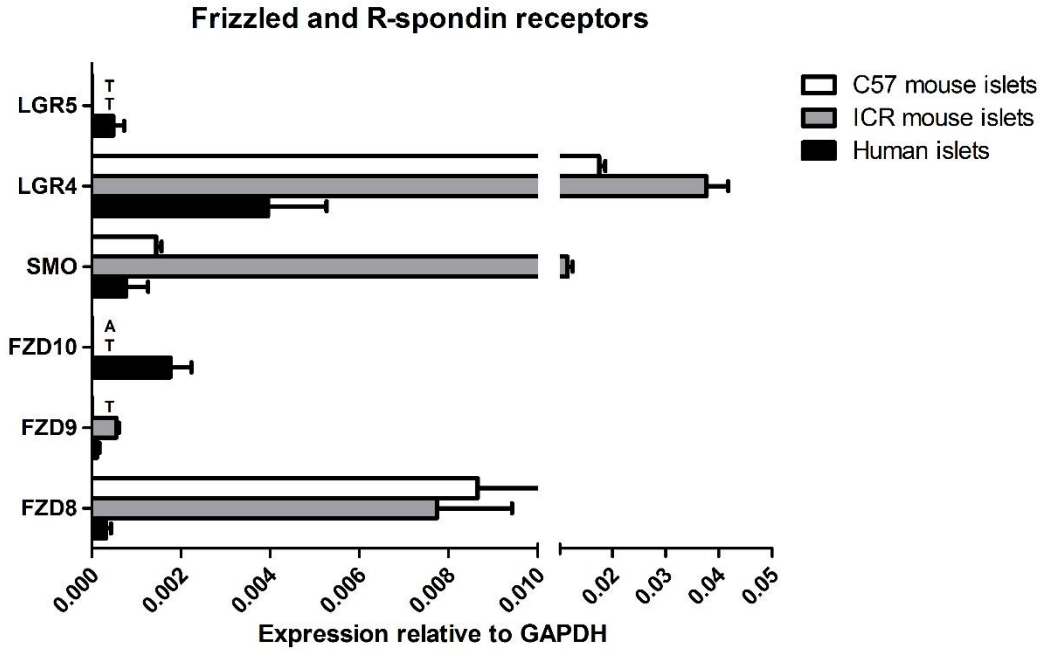
Frizzled and R-spondin receptors
C57 mouse islets
ICR mouse islets
Human islets
LGR5
LGR4
SMO
FZD10
FZD9
FZD8
T
T
T
A
T
T
0.000
0.002
0.004
0.006
0.008
0.010
0.02
0.03
0.04
0.05
Expression relative to GAPDH

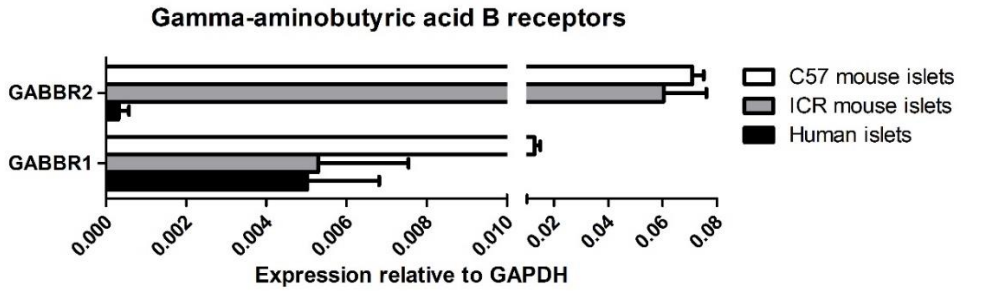
Gamma-aminobutyric acid B receptors
GABBR2
GABBR1
C57 mouse islets
ICR mouse islets
Human islets
0.000
0.002
0.004
0.006
0.008
0.010
0.02
0.04
0.06
0.08
Expression relative to GAPDH

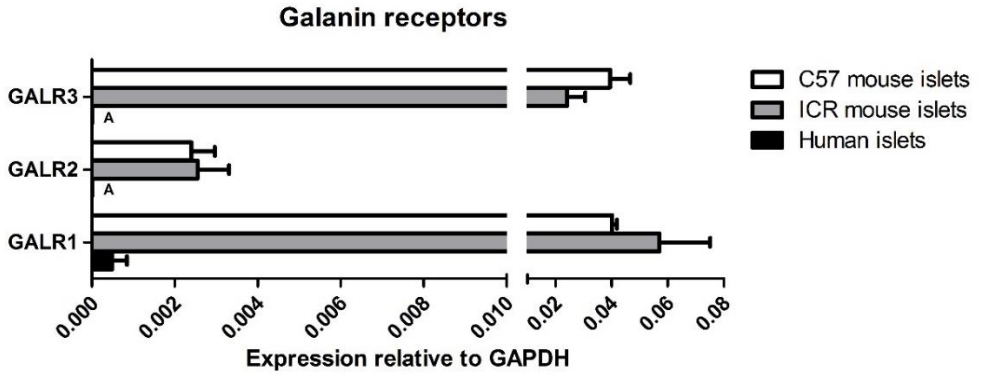
Galanin receptors
GALR3
GALR2
GALR1
A
A
C57 mouse islets
ICR mouse islets
Human islets
0.000
0.002
0.004
0.006
0.008
0.010
0.02
0.04
0.06
0.08
Expression relative to GAPDH

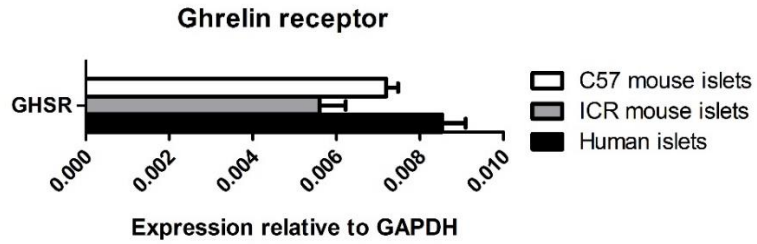
Ghrelin receptor
GHSR
C57 mouse islets
ICR mouse islets
Human islets
0.000
0.002
0.004
0.006
0.008
0.010
Expression relative to GAPDH

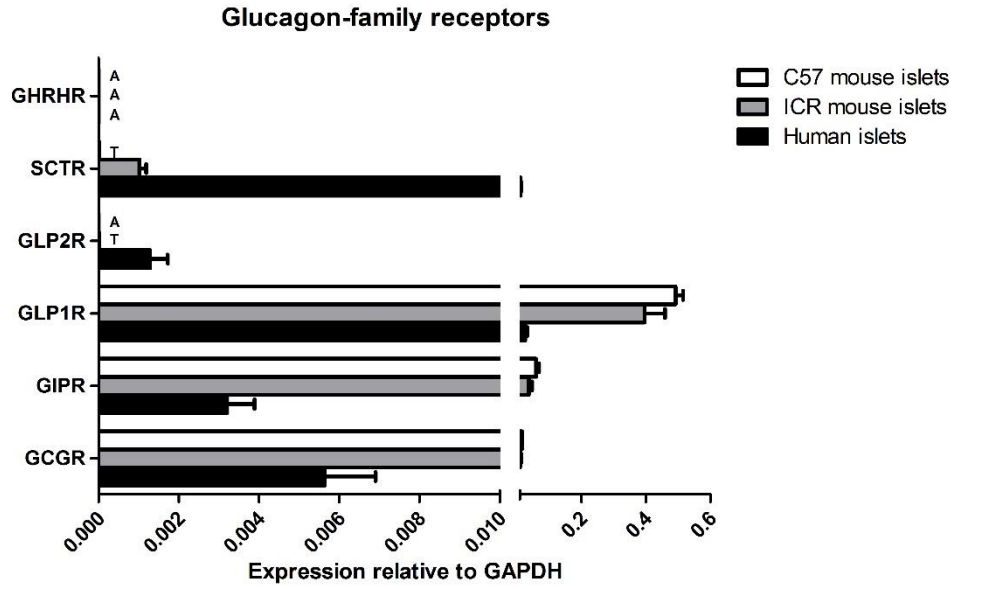
Glucagon-family receptors
GHRHR
SCTR
GLP2R
GLP1R
GIPR
GCGR
A
A
A
T
A
T
C57 mouse islets
ICR mouse islets
Human islets
0.000
0.002
0.004
0.006
0.008
0.010
0.2
0.4
0.6
Expression relative to GAPDH

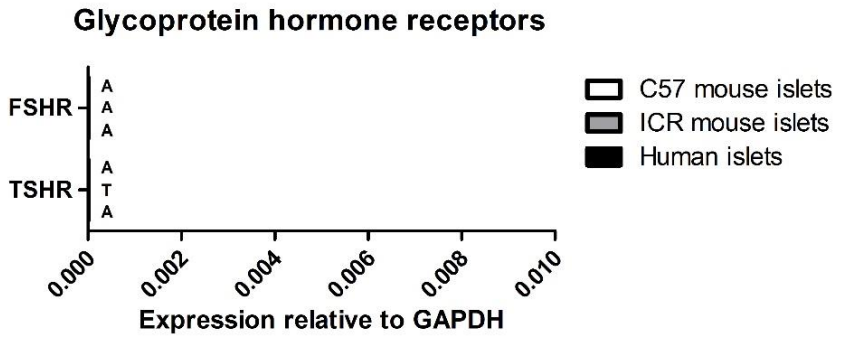
Glycoprotein hormone receptors
FSHR
TSHR
A
A
A
A
T
A
0.000
0.002
0.004
0.006
0.008
0.010
Expression relative to GAPDH
C57 mouse islets
ICR mouse islets
Human islets

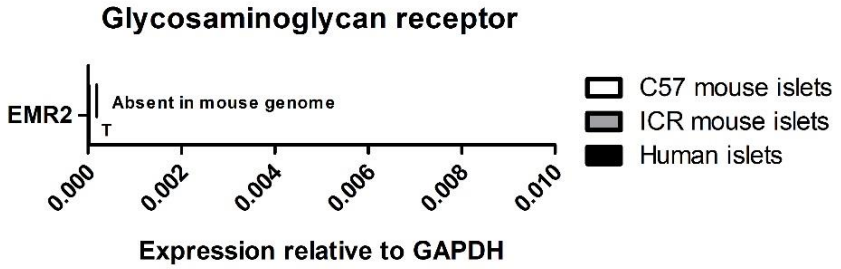
Glycosaminoglycan receptor
EMR2
Absent in mouse genome
T
0.000
0.002
0.004
0.006
0.008
0.010
Expression relative to GAPDH
C57 mouse islets
ICR mouse islets
Human islets

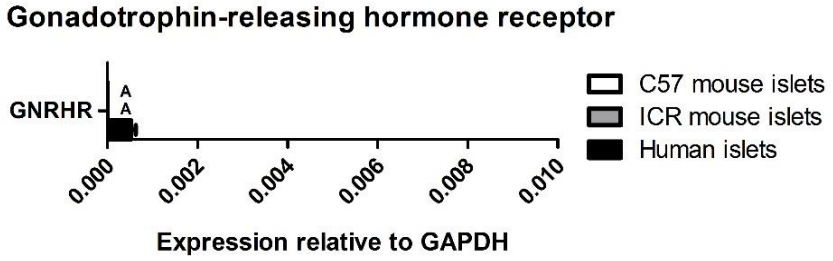
Gonadotrophin-releasing hormone receptor
GNRHR
A
A
0.000
0.002
0.004
0.006
0.008
0.010
Expression relative to GAPDH
C57 mouse islets
ICR mouse islets
Human islets

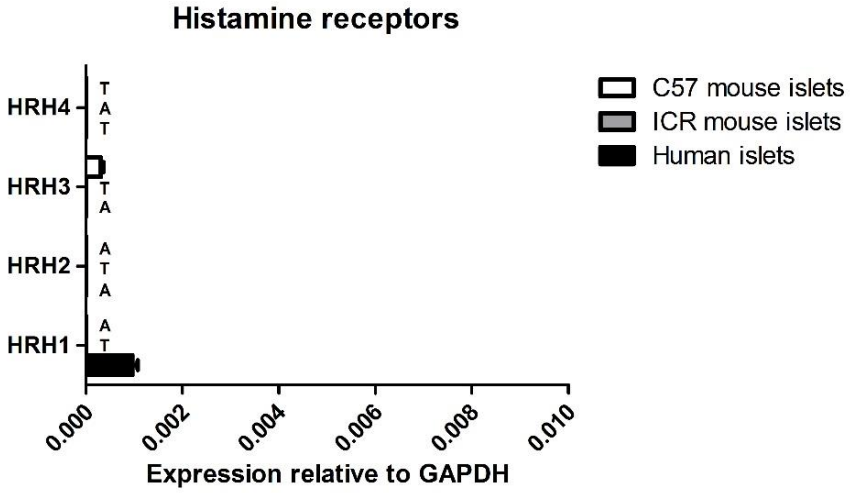
Histamine receptors
HRH4
HRH3
HRH2
HRH1
T
A
T
T
A
A
T
A
A
T
0.000
0.002
0.004
0.006
0.008
0.010
Expression relative to GAPDH
C57 mouse islets
ICR mouse islets
Human islets

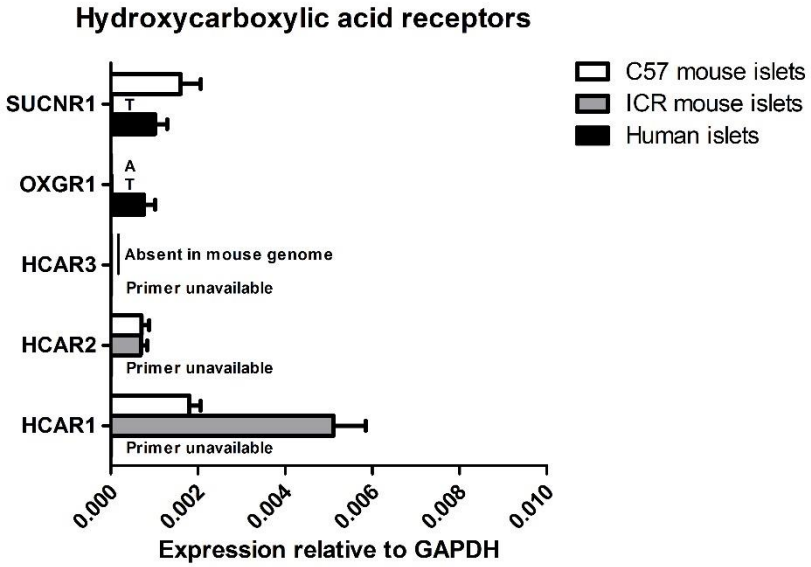
Hydroxycarboxylic acid receptors
C57 mouse islets
ICR mouse islets
Human islets
SUCNR1
T
OXGR1
A
T
HCAR3
Absent in mouse genome
Primer unavailable
HCAR2
Primer unavailable
HCAR1
Primer unavailable
0.000
0.002
0.004
0.006
0.008
0.010
Expression relative to GAPDH

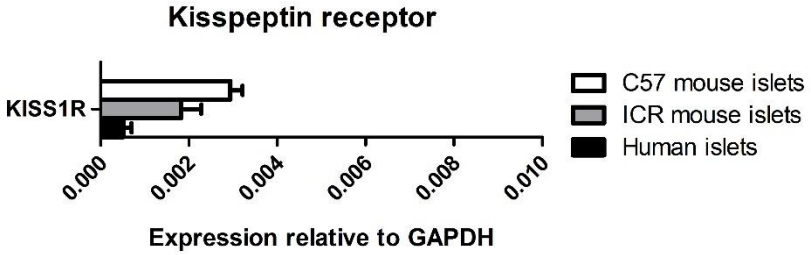
Kisspeptin receptor
C57 mouse islets
ICR mouse islets
Human islets
KISS1R
0.000
0.002
0.004
0.006
0.008
0.010
Expression relative to GAPDH

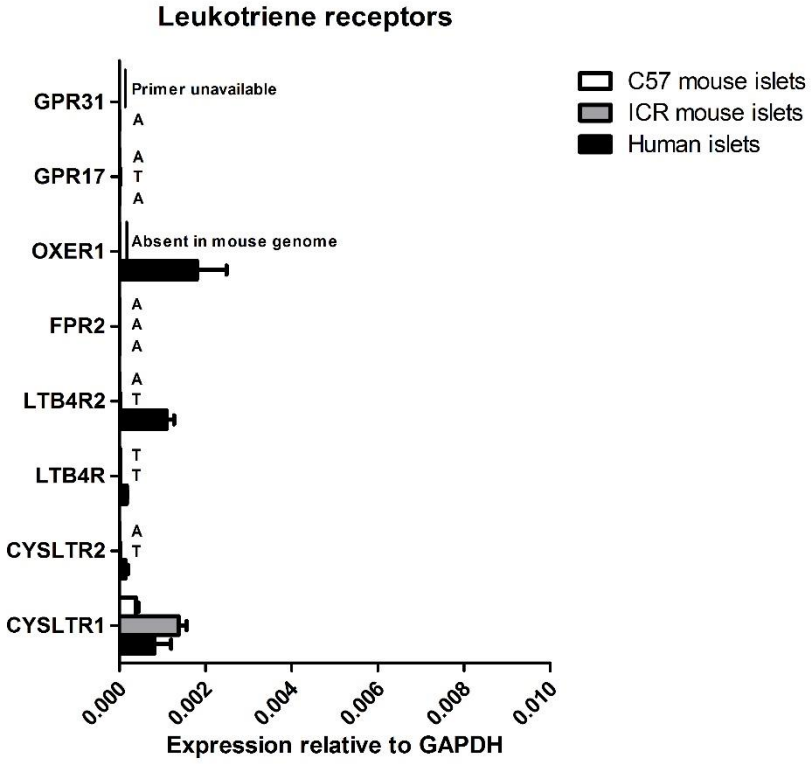
Leukotriene receptors
C57 mouse islets
ICR mouse islets
Human islets
GPR31
Primer unavailable
A
GPR17
A
T
A
OXER1
Absent in mouse genome
FPR2
A
A
A
LTB4R2
A
T
LTB4R
T
T
CYSLTR2
A
T
CYSLTR1
0.000
0.002
0.004
0.006
0.008
0.010
Expression relative to GAPDH

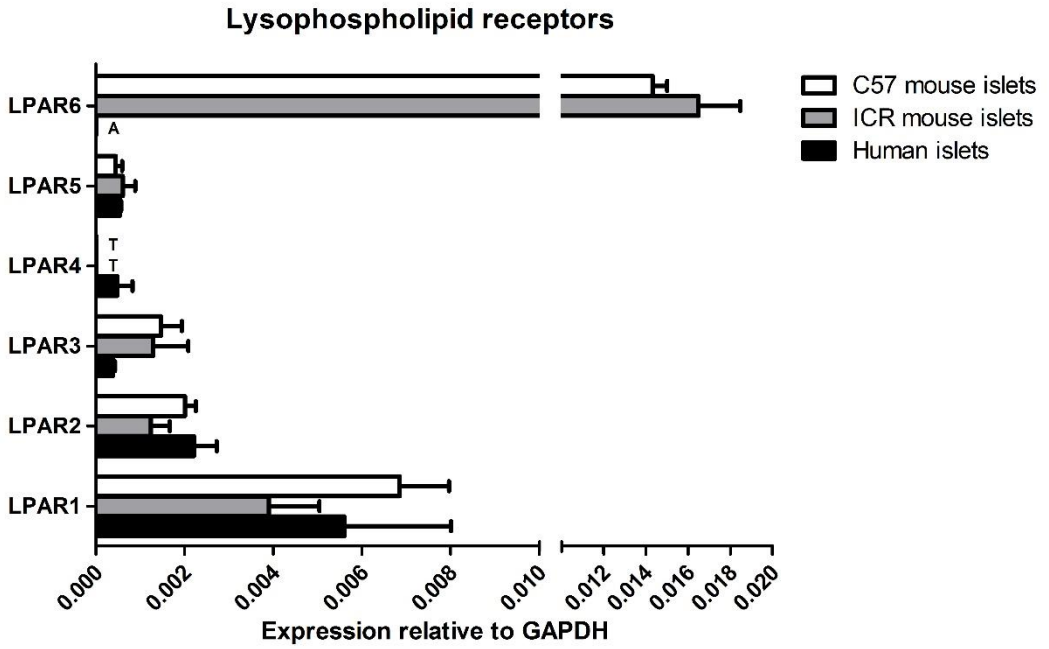
Lysophospholipid receptors
C57 mouse islets
ICR mouse islets
Human islets
LPAR6
LPAR5
LPAR4
LPAR3
LPAR2
LPAR1
0.000
0.002
0.004
0.006
0.008
0.010
0.012
0.014
0.016
0.018
0.020
Expression relative to GAPDH

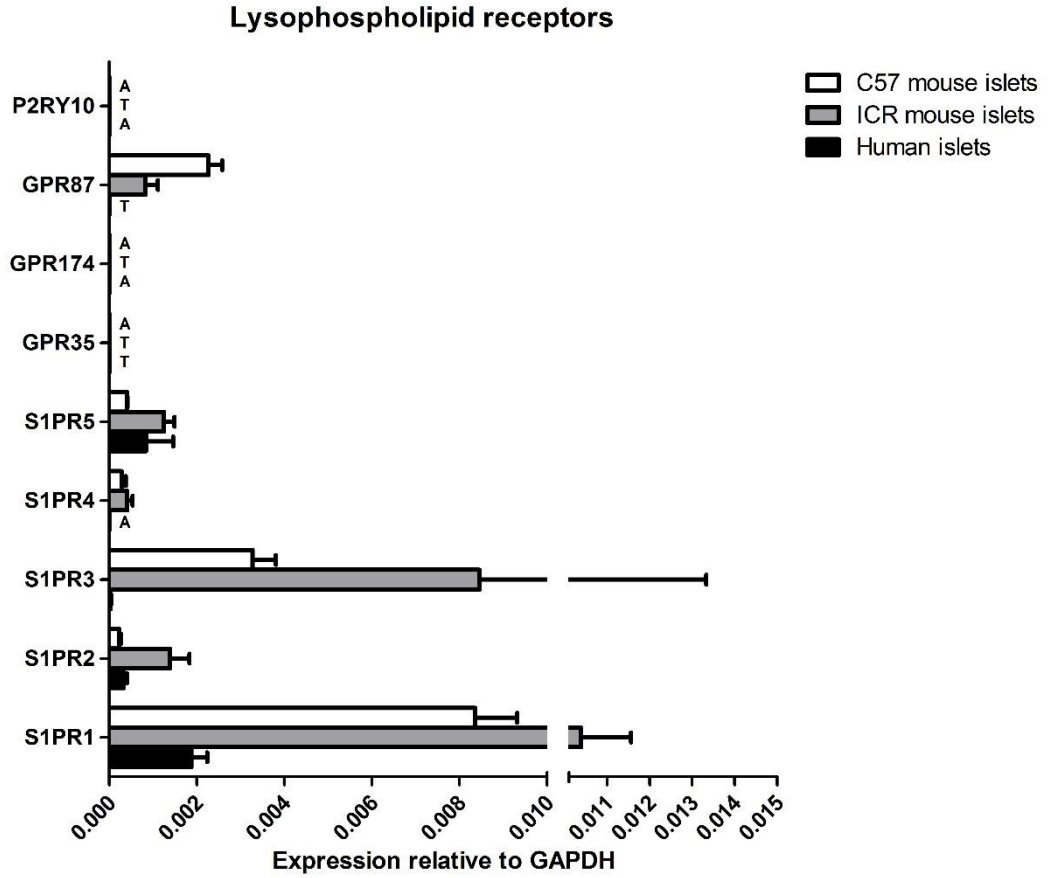
Lysophospholipid receptors
C57 mouse islets
ICR mouse islets
Human islets
P2RY10
GPR87
GPR174
GPR35
S1PR5
S1PR4
S1PR3
S1PR2
S1PR1
0.000
0.002
0.004
0.006
0.008
0.010
0.011
0.012
0.013
0.014
0.015
Expression relative to GAPDH

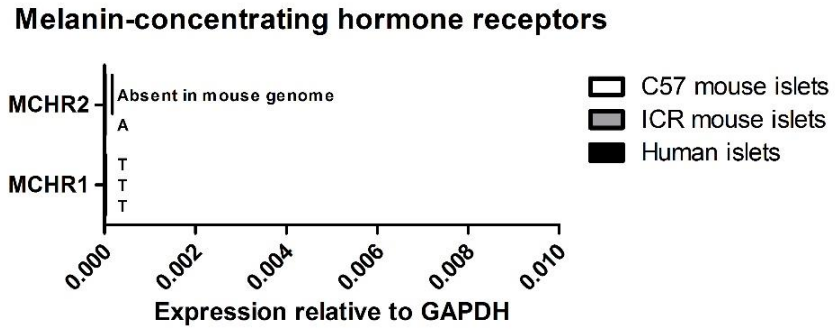
Melanin-concentrating hormone receptors
MCHR2
Absent in mouse genome
A
MCHR1
T
T
T
0.000
0.002
0.004
0.006
0.008
0.010
Expression relative to GAPDH
C57 mouse islets
ICR mouse islets
Human islets

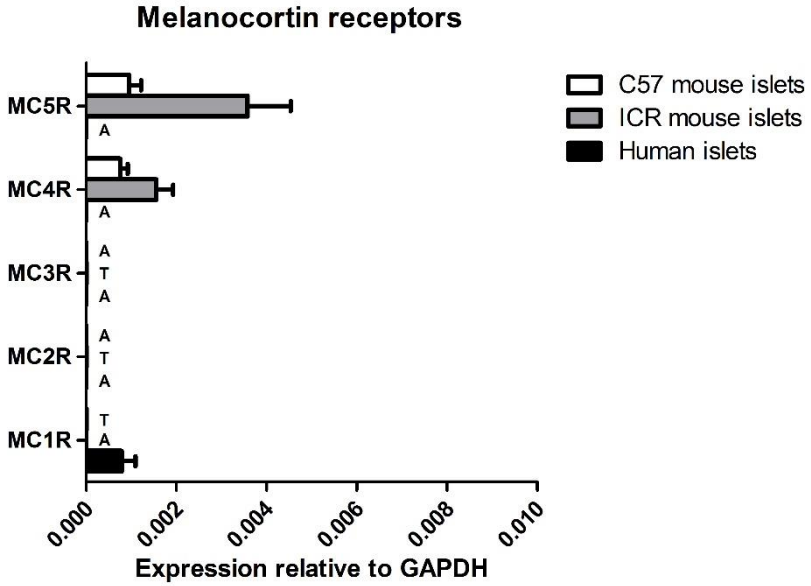
Melanocortin receptors
MC5R
A
MC4R
A
MC3R
A
T
A
MC2R
A
T
A
MC1R
T
A
0.000
0.002
0.004
0.006
0.008
0.010
Expression relative to GAPDH
C57 mouse islets
ICR mouse islets
Human islets

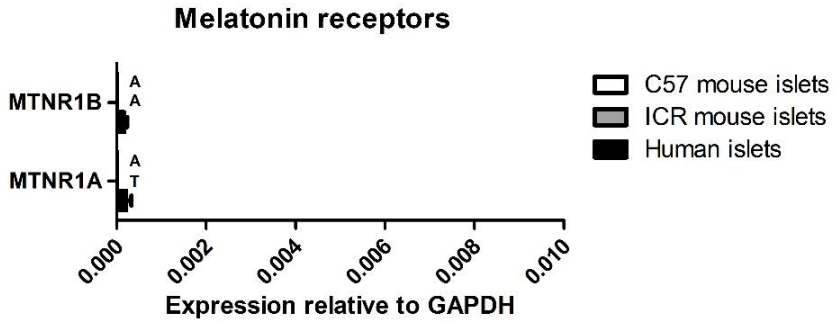
Melatonin receptors
MTNR1B
A
A
MTNR1A
A
T
0.000
0.002
0.004
0.006
0.008
0.010
Expression relative to GAPDH
C57 mouse islets
ICR mouse islets
Human islets

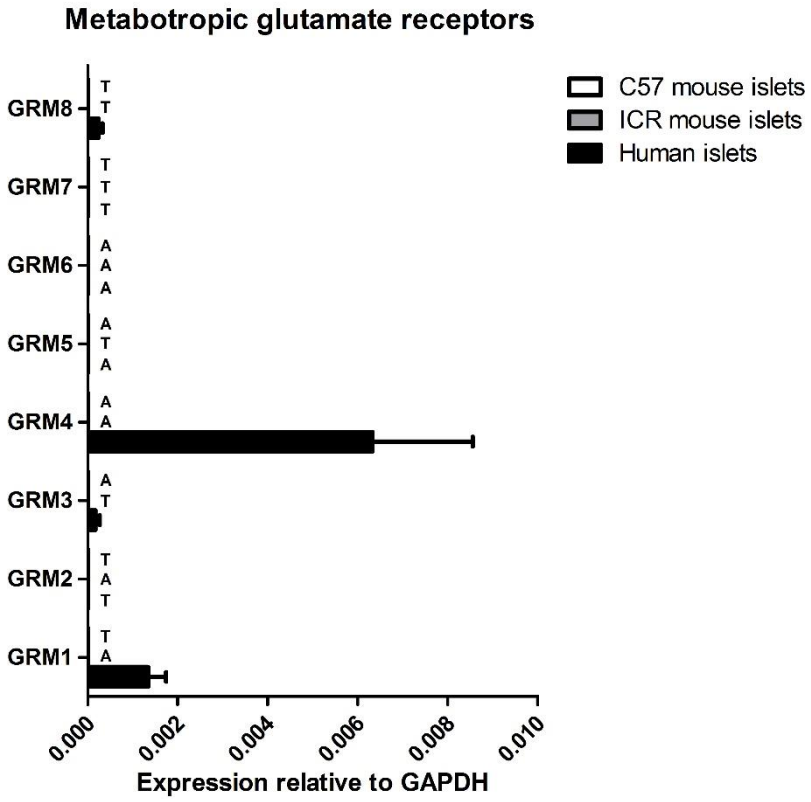
Metabotropic glutamate receptors
C57 mouse islets
ICR mouse islets
Human islets
GRM8
GRM7
GRM6
GRM5
GRM4
GRM3
GRM2
GRM1
0.000
0.002
0.004
0.006
0.008
0.010
Expression relative to GAPDH

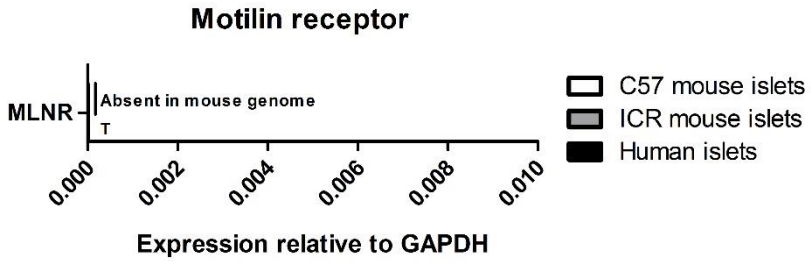
Motilin receptor
C57 mouse islets
ICR mouse islets
Human islets
MLNR
Absent in mouse genome
0.000
0.002
0.004
0.006
0.008
0.010
Expression relative to GAPDH

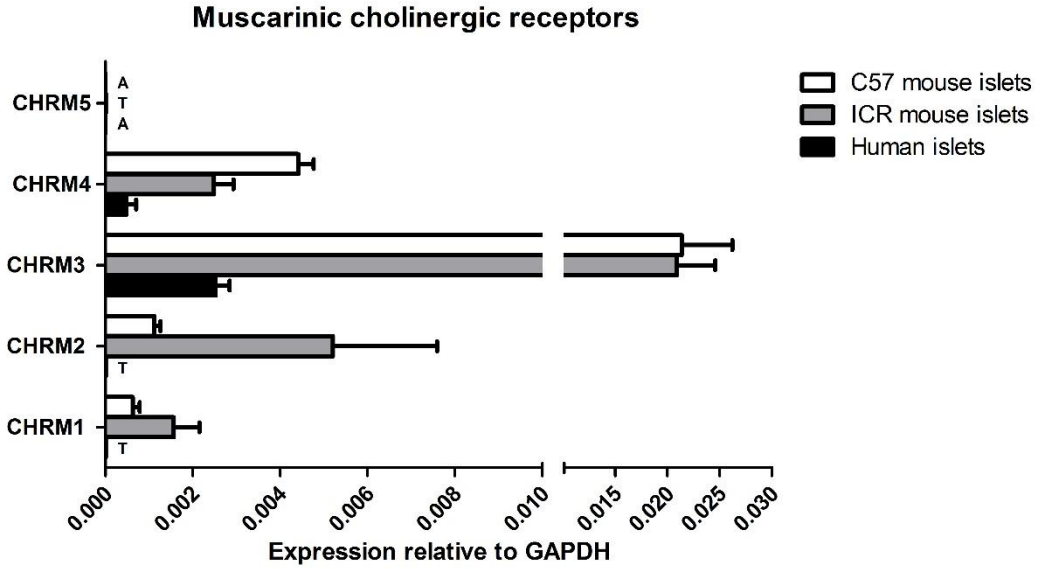
Muscarinic cholinergic receptors
C57 mouse islets
ICR mouse islets
Human islets
CHRM5
CHRM4
CHRM3
CHRM2
CHRM1
0.000
0.002
0.004
0.006
0.008
0.010
0.015
0.020
0.025
0.030
Expression relative to GAPDH

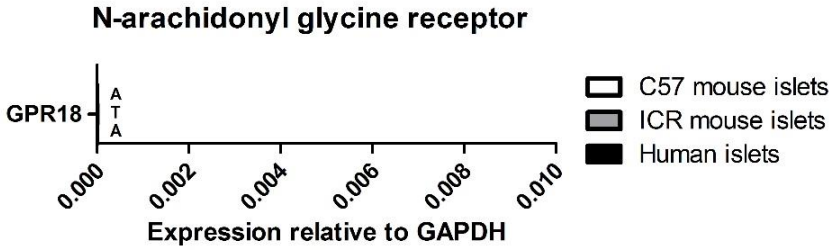
N-arachidonyl glycine receptor
GPR18
A
T
A
0.000
0.002
0.004
0.006
0.008
0.010
Expression relative to GAPDH
C57 mouse islets
ICR mouse islets
Human islets

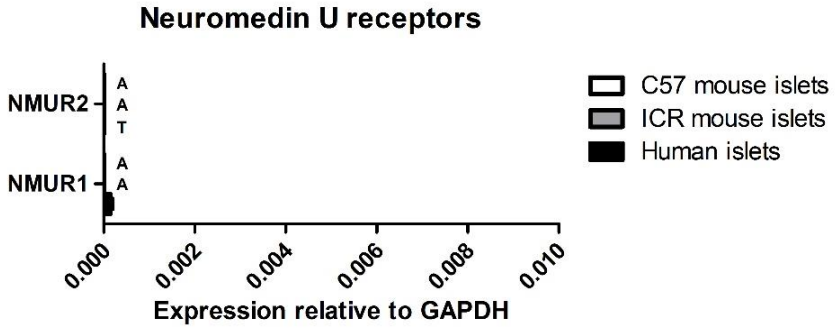
Neuromedin U receptors
NMUR2
A
A
T
NMUR1
A
A
0.000
0.002
0.004
0.006
0.008
0.010
Expression relative to GAPDH
C57 mouse islets
ICR mouse islets
Human islets

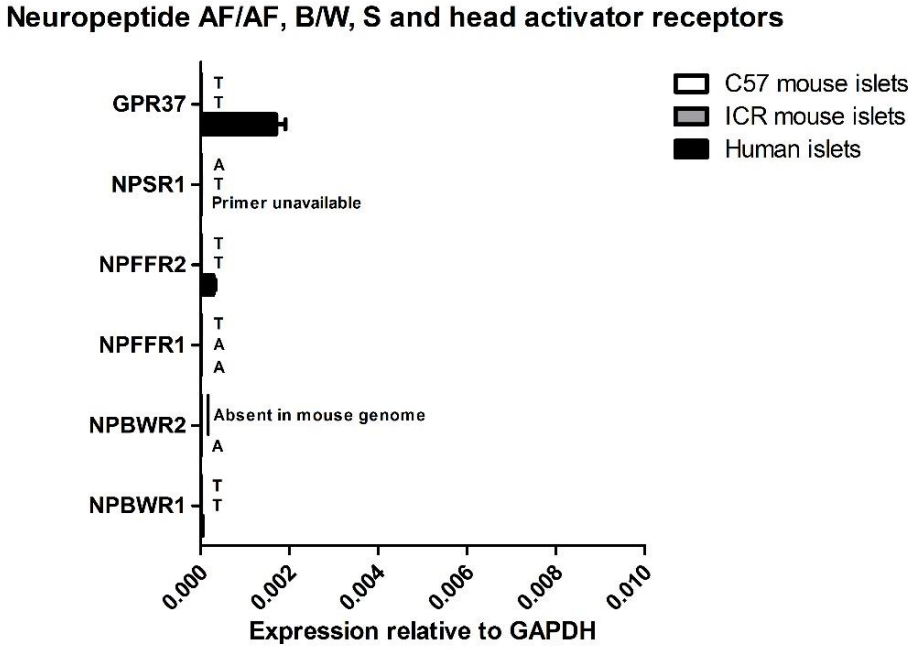
Neuropeptide AF/AF, B/W, S and head activator receptors
GPR37
T
T
NPSR1
A
T
Primer unavailable
NPFFR2
T
T
NPFFR1
T
A
A
NPBWR2
Absent in mouse genome
A
NPBWR1
T
T
0.000
0.002
0.004
0.006
0.008
0.010
Expression relative to GAPDH
C57 mouse islets
ICR mouse islets
Human islets

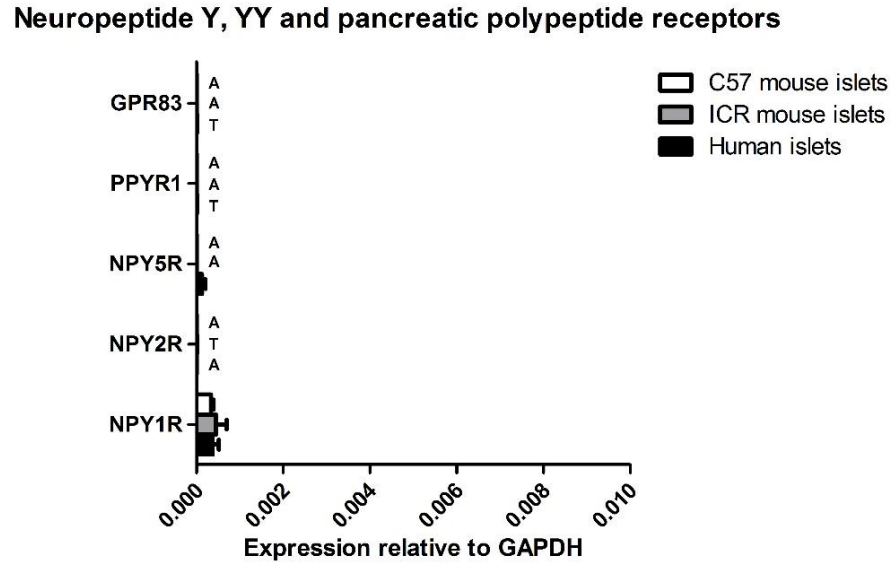
Neuropeptide Y, YY and pancreatic polypeptide receptors
C57 mouse islets
ICR mouse islets
Human islets
GPR83
PPYR1
NPY5R
NPY2R
NPY1R
A
A
T
A
A
T
A
A
A
T
A
0.000
0.002
0.004
0.006
0.008
0.010
Expression relative to GAPDH

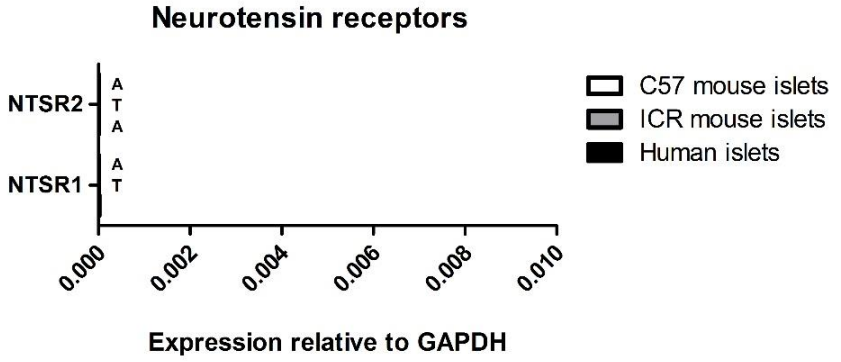
Neurotensin receptors
C57 mouse islets
ICR mouse islets
Human islets
NTSR2
NTSR1
A
T
A
A
T
0.000
0.002
0.004
0.006
0.008
0.010
Expression relative to GAPDH

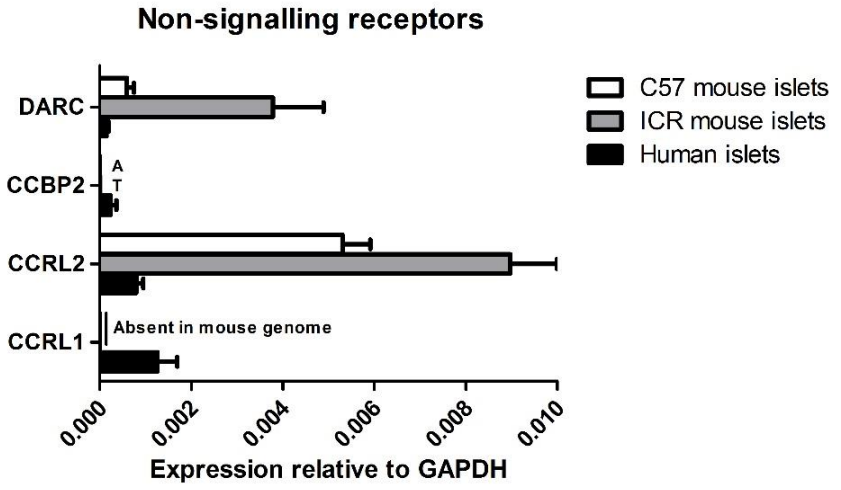
Non-signalling receptors
C57 mouse islets
ICR mouse islets
Human islets
DARC
CCBP2
CCRL2
CCRL1
A
T
Absent in mouse genome
0.000
0.002
0.004
0.006
0.008
0.010
Expression relative to GAPDH

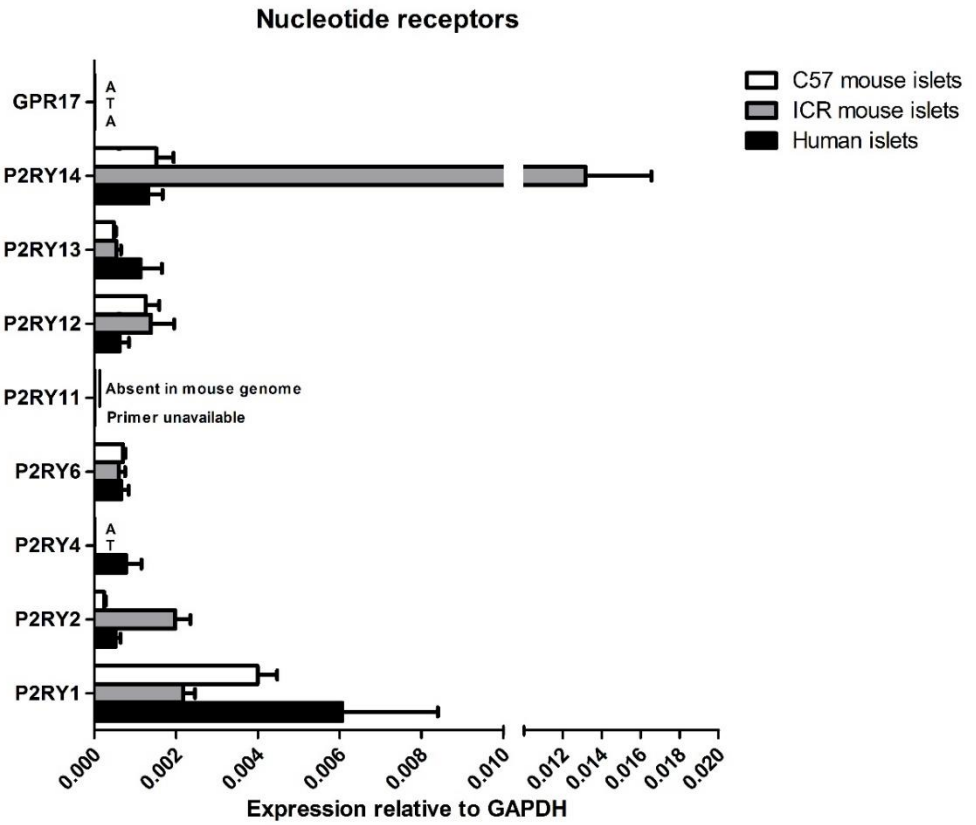
Nucleotide receptors
C57 mouse islets
ICR mouse islets
Human islets
GPR17
P2RY14
P2RY13
P2RY12
P2RY11
Absent in mouse genome
Primer unavailable
P2RY6
P2RY4
P2RY2
P2RY1
0.000
0.002
0.004
0.006
0.008
0.010
0.012
0.014
0.016
0.018
0.020
Expression relative to GAPDH

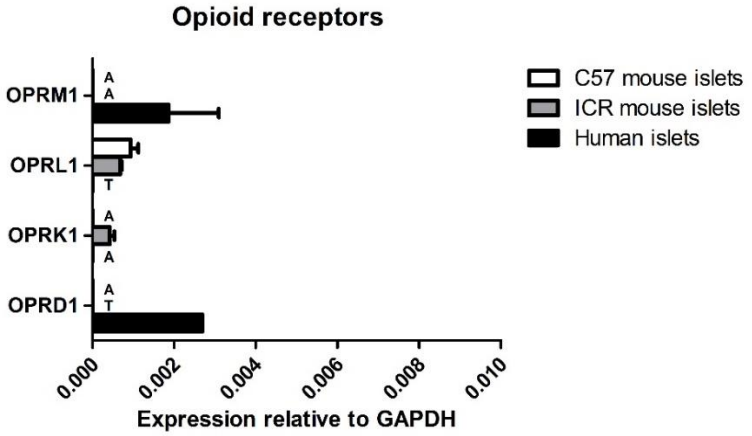
Opioid receptors
C57 mouse islets
ICR mouse islets
Human islets
OPRM1
OPRL1
OPRK1
OPRD1
0.000
0.002
0.004
0.006
0.008
0.010
Expression relative to GAPDH

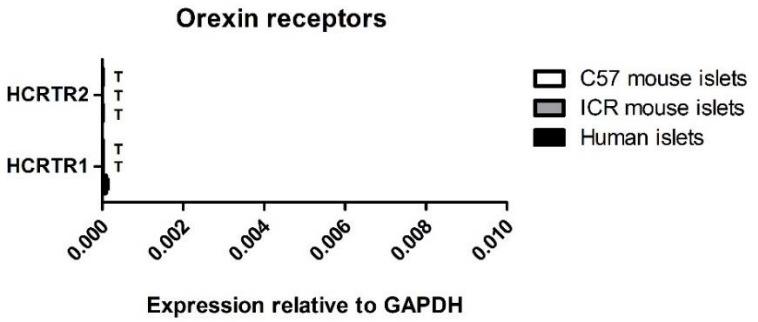
Orexin receptors
C57 mouse islets
ICR mouse islets
Human islets
HCRTR2
HCRTR1
0.000
0.002
0.004
0.006
0.008
0.010
Expression relative to GAPDH

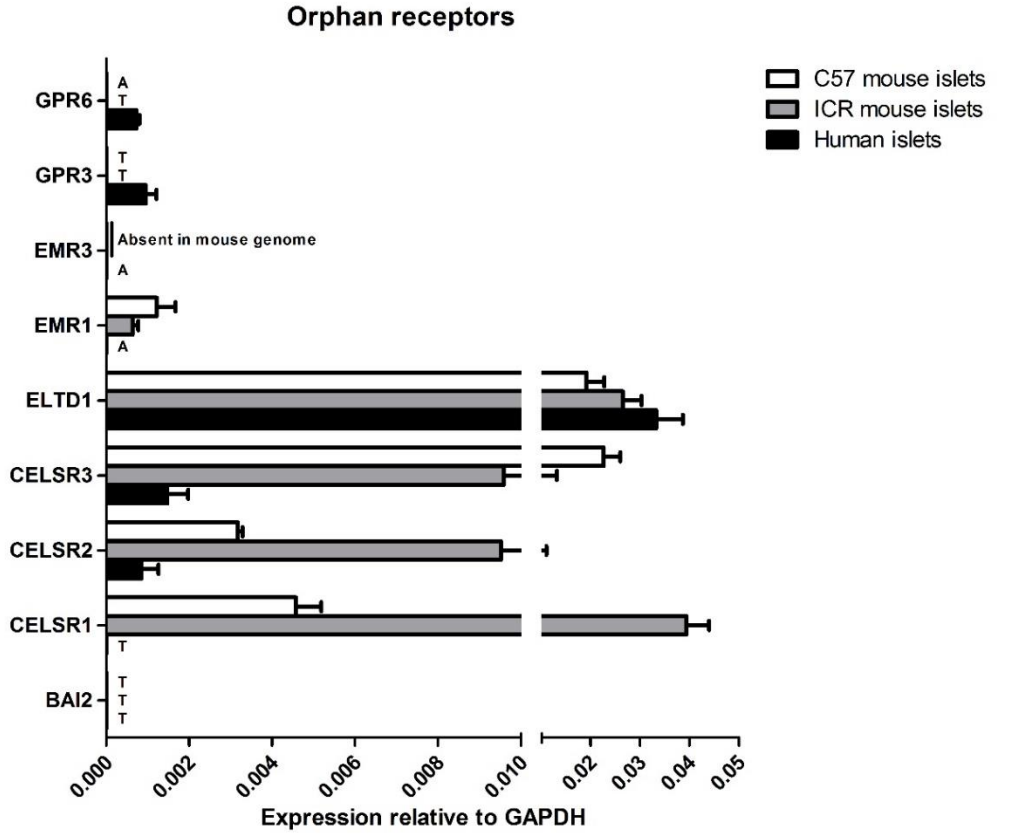
Orphan receptors
C57 mouse islets
ICR mouse islets
Human islets
GPR6
GPR3
EMR3
Absent in mouse genome
EMR1
ELTD1
CELSR3
CELSR2
CELSR1
BAI2
0.000
0.002
0.004
0.006
0.008
0.010
0.02
0.03
0.04
0.05
Expression relative to GAPDH

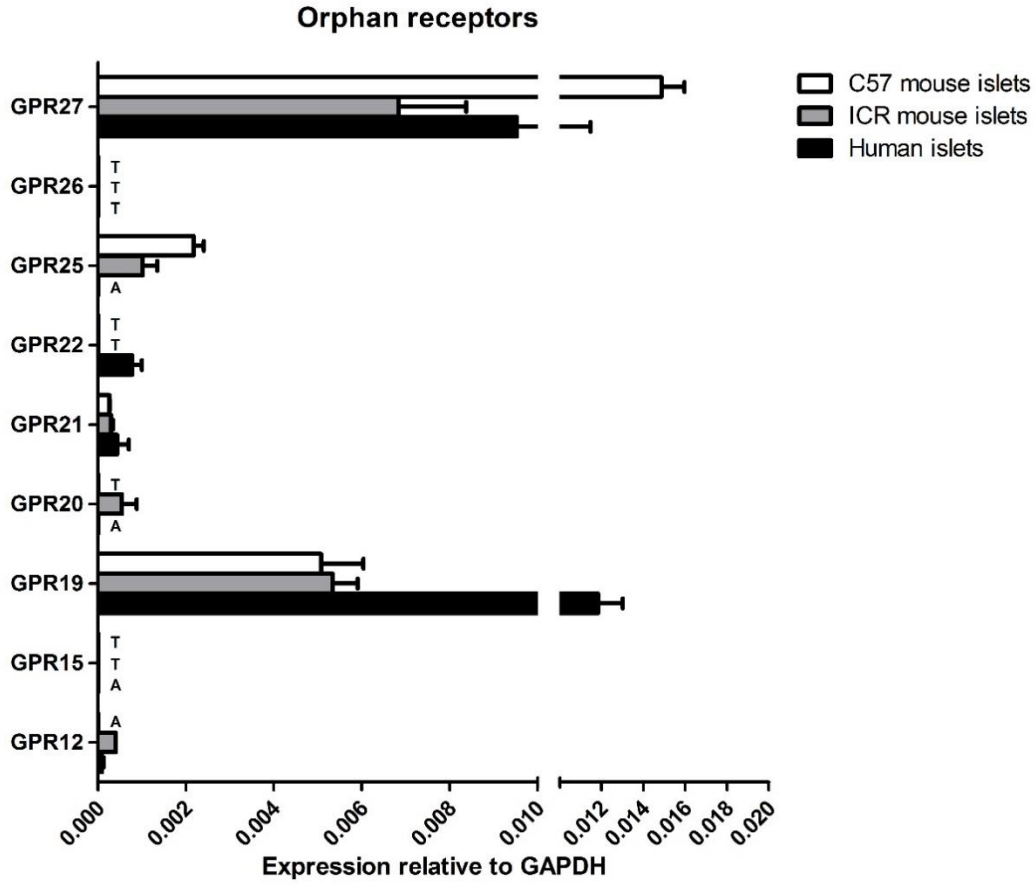
Orphan receptors
C57 mouse islets
ICR mouse islets
Human islets
GPR27
GPR26
GPR25
GPR22
GPR21
GPR20
GPR19
GPR15
GPR12
0.000
0.002
0.004
0.006
0.008
0.010
0.012
0.014
0.016
0.018
0.020
Expression relative to GAPDH

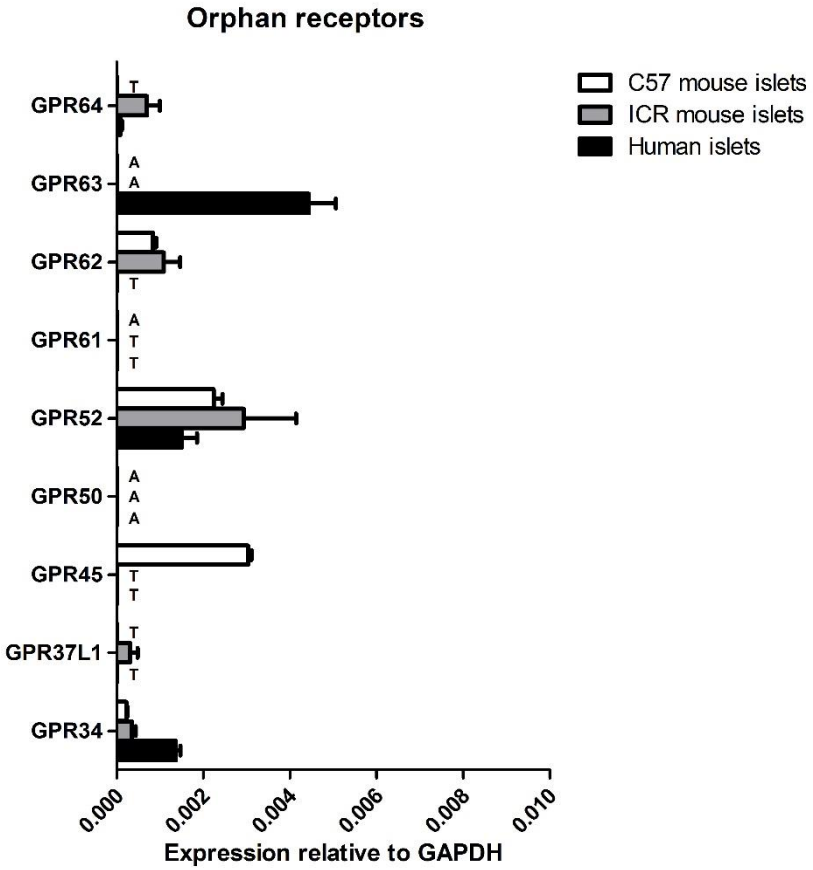
Orphan receptors
C57 mouse islets
ICR mouse islets
Human islets
GPR64
GPR63
GPR62
GPR61
GPR52
GPR50
GPR45
GPR37L1
GPR34
0.000
0.002
0.004
0.006
0.008
0.010
Expression relative to GAPDH

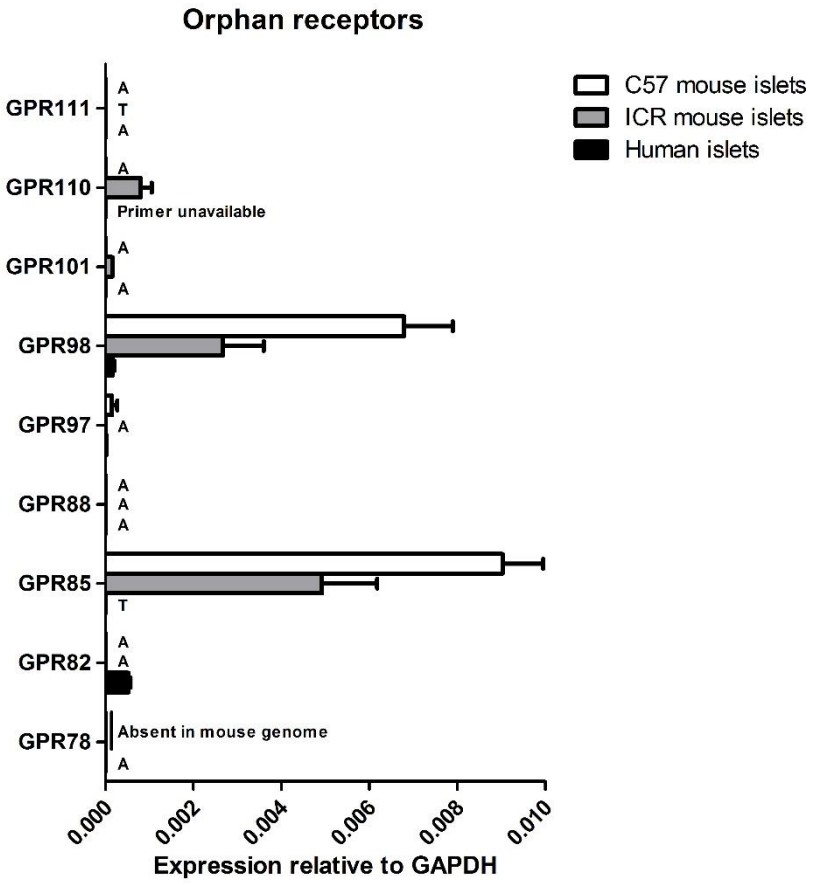
Orphan receptors
C57 mouse islets
ICR mouse islets
Human islets
GPR111
GPR110
Primer unavailable
GPR101
GPR98
GPR97
GPR88
GPR85
GPR82
GPR78
Absent in mouse genome
0.000
0.002
0.004
0.006
0.008
0.010
Expression relative to GAPDH

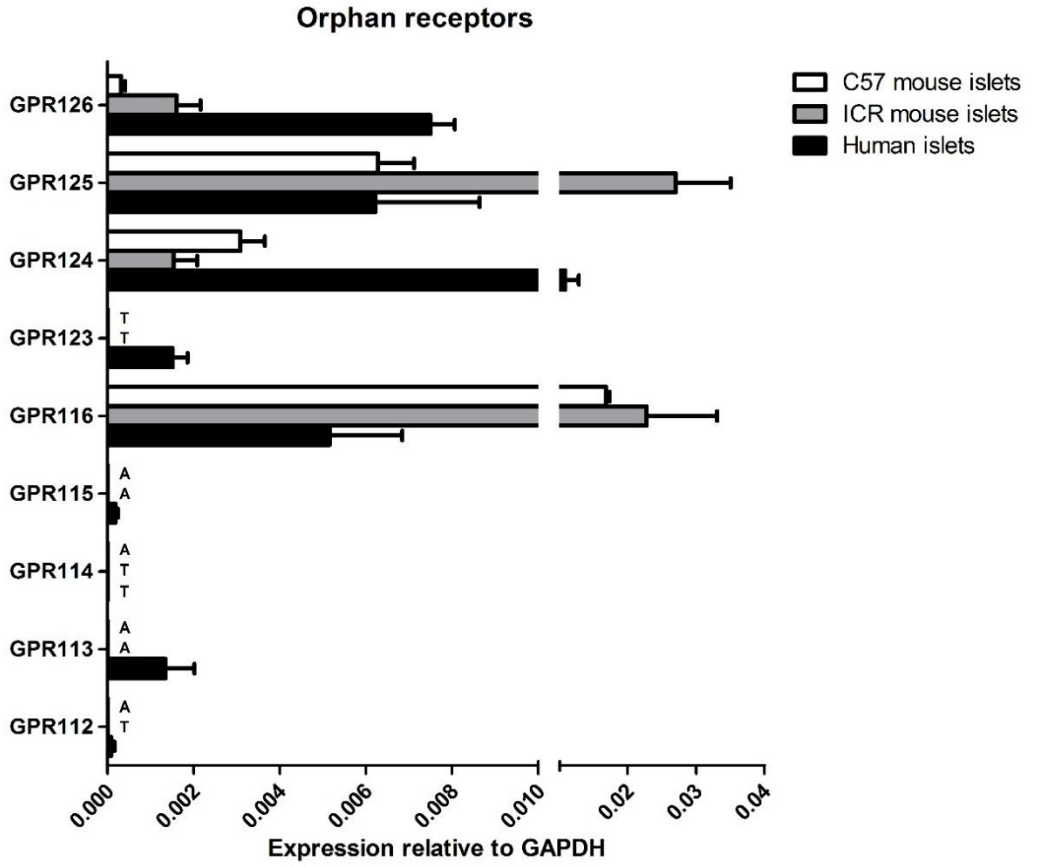
Orphan receptors
C57 mouse islets
ICR mouse islets
Human islets
GPR126
GPR125
GPR124
GPR123
GPR116
GPR115
GPR114
GPR113
GPR112
T
T
A
A
A
T
T
A
A
A
T
0.000
0.002
0.004
0.006
0.008
0.010
0.02
0.03
0.04
Expression relative to GAPDH

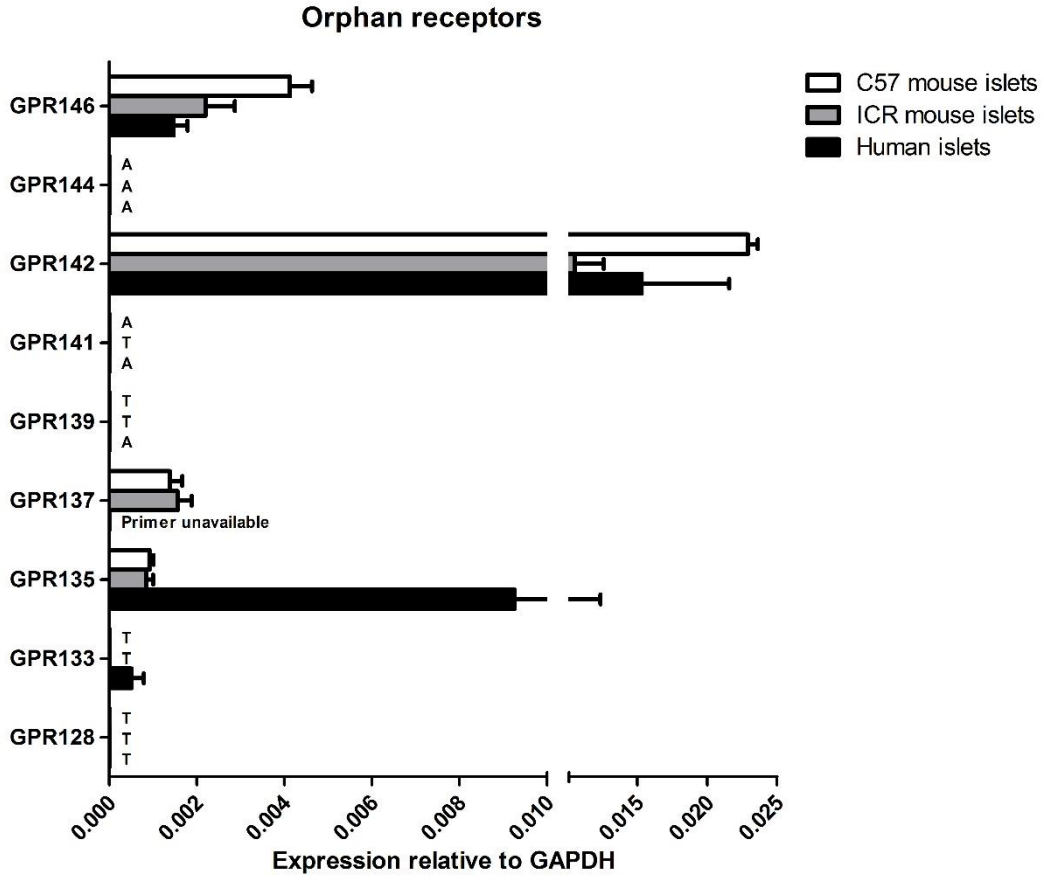
Orphan receptors
C57 mouse islets
ICR mouse islets
Human islets
GPR146
GPR144
GPR142
GPR141
GPR139
GPR137
GPR135
GPR133
GPR128
A
A
A
A
T
A
T
T
A
Primer unavailable
T
T
T
T
0.000
0.002
0.004
0.006
0.008
0.010
0.015
0.020
0.025
Expression relative to GAPDH

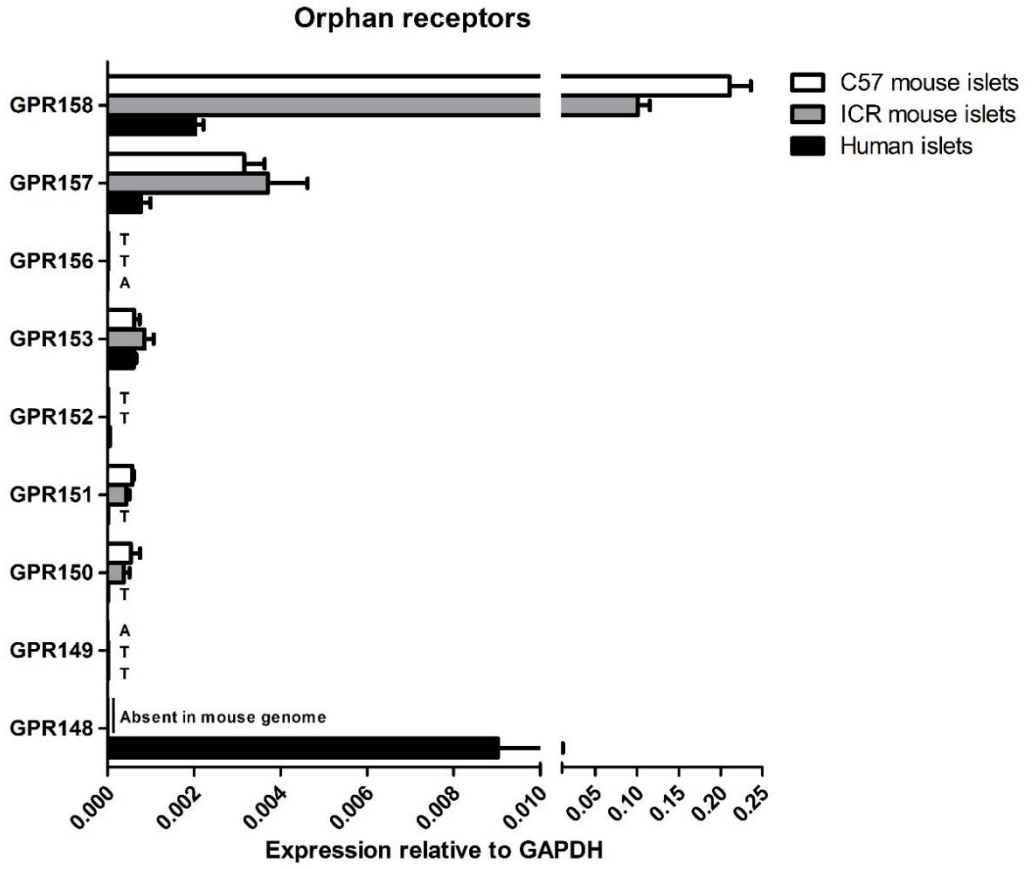
Orphan receptors
C57 mouse islets
ICR mouse islets
Human islets
GPR158
GPR157
GPR156
GPR153
GPR152
GPR151
GPR150
GPR149
GPR148
Absent in mouse genome
0.000
0.002
0.004
0.006
0.008
0.010
0.05
0.10
0.15
0.20
0.25
Expression relative to GAPDH

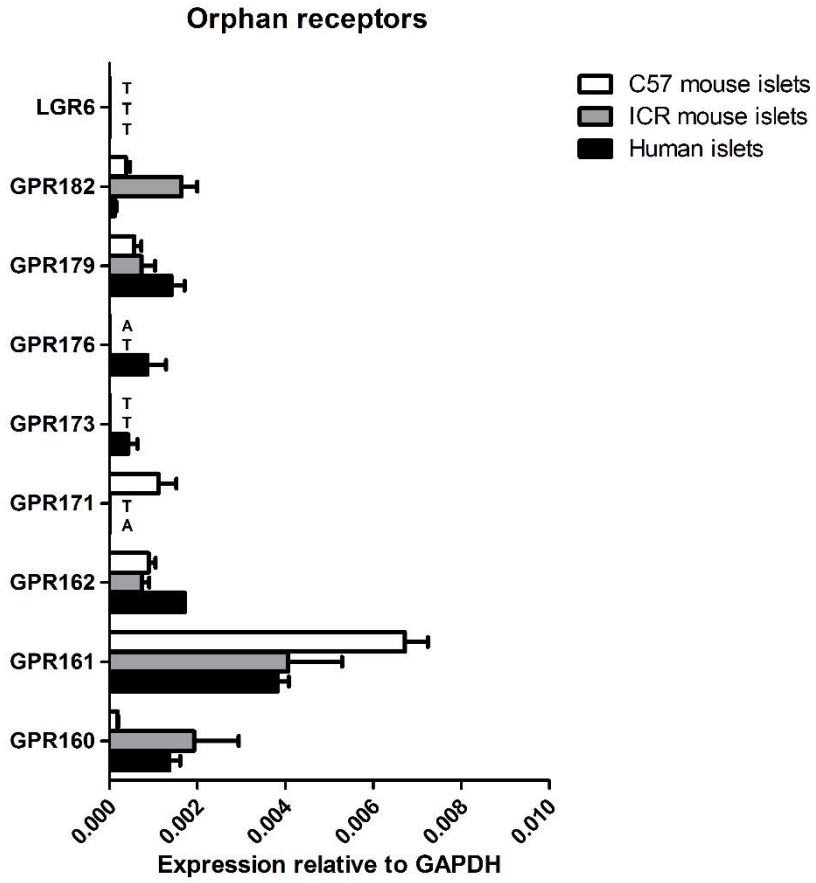
Orphan receptors
C57 mouse islets
ICR mouse islets
Human islets
LGR6
GPR182
GPR179
GPR176
GPR173
GPR171
GPR162
GPR161
GPR160
0.000
0.002
0.004
0.006
0.008
0.010
Expression relative to GAPDH

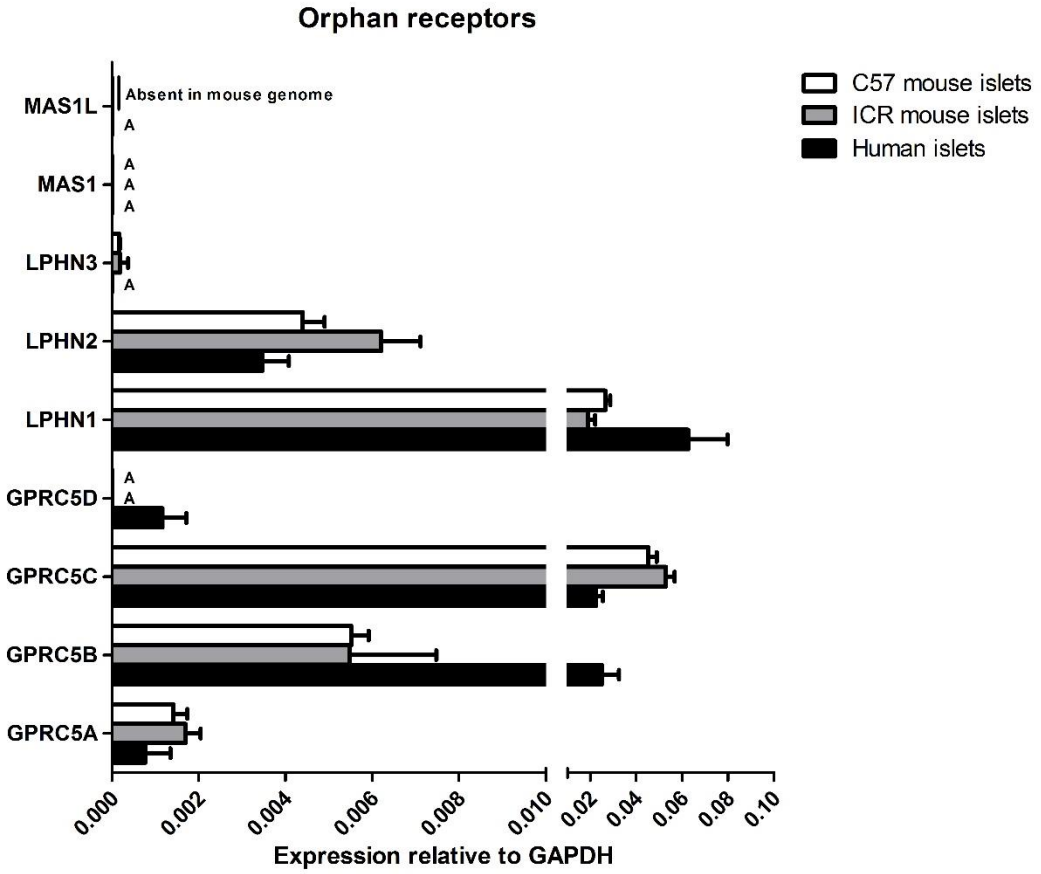
Orphan receptors
C57 mouse islets
ICR mouse islets
Human islets
MAS1L
Absent in mouse genome
A
MAS1
A
A
A
LPHN3
A
LPHN2
LPHN1
GPRC5D
A
A
GPRC5C
GPRC5B
GPRC5A
0.000
0.002
0.004
0.006
0.008
0.010
0.02
0.04
0.06
0.08
0.10
Expression relative to GAPDH

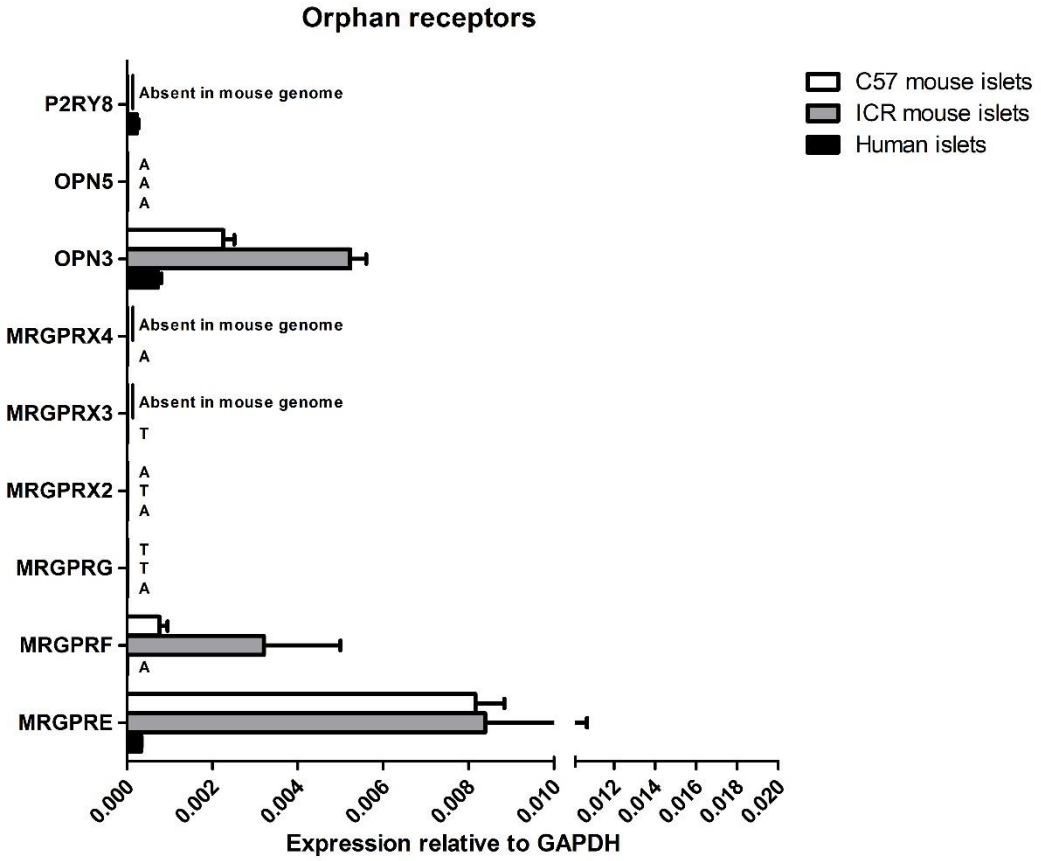
Orphan receptors
C57 mouse islets
ICR mouse islets
Human islets
P2RY8
Absent in mouse genome
OPN5
A
A
A
OPN3
MRGPRX4
Absent in mouse genome
A
MRGPRX3
Absent in mouse genome
T
MRGPRX2
A
T
A
MRGPRG
T
T
A
MRGPRF
A
MRGPRE
0.000
0.002
0.004
0.006
0.008
0.010
0.012
0.014
0.016
0.018
0.020
Expression relative to GAPDH

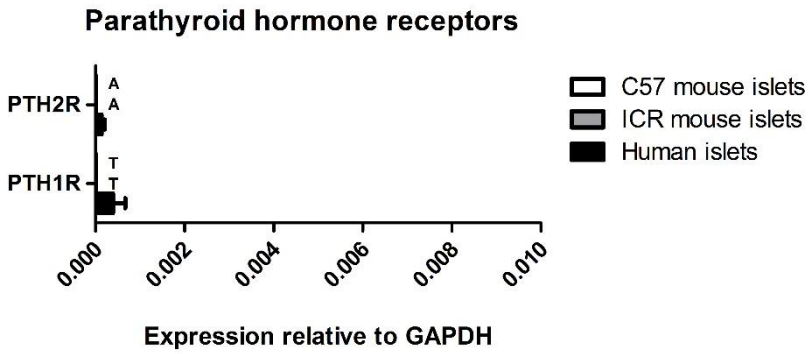
Parathyroid hormone receptors
PTH2R
PTH1R
A
A
T
T
0.000
0.002
0.004
0.006
0.008
0.010
Expression relative to GAPDH
C57 mouse islets
ICR mouse islets
Human islets

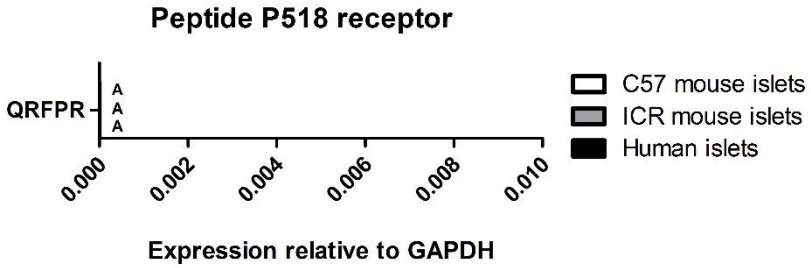
Peptide P518 receptor
QRFPR
A
A
A
0.000
0.002
0.004
0.006
0.008
0.010
Expression relative to GAPDH
C57 mouse islets
ICR mouse islets
Human islets

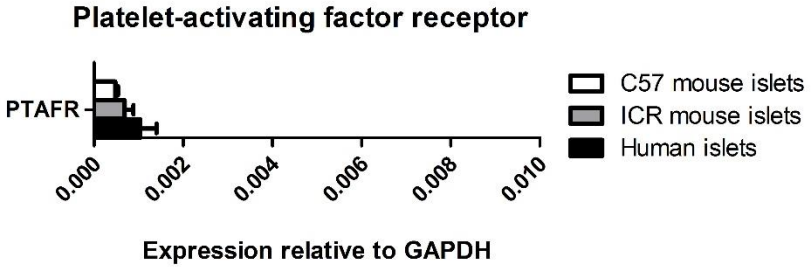
Platelet-activating factor receptor
PTAFR
0.000
0.002
0.004
0.006
0.008
0.010
Expression relative to GAPDH
C57 mouse islets
ICR mouse islets
Human islets

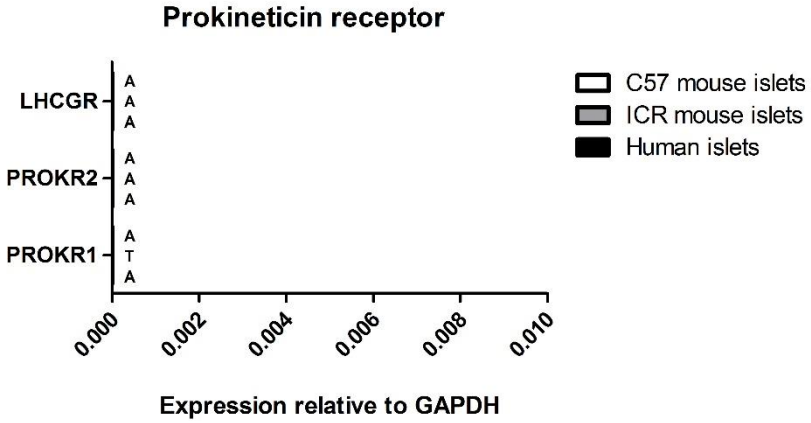
Prokineticin receptor
LHCGR
PROKR2
PROKR1
A
A
A
A
A
A
A
T
A
0.000
0.002
0.004
0.006
0.008
0.010
Expression relative to GAPDH
C57 mouse islets
ICR mouse islets
Human islets

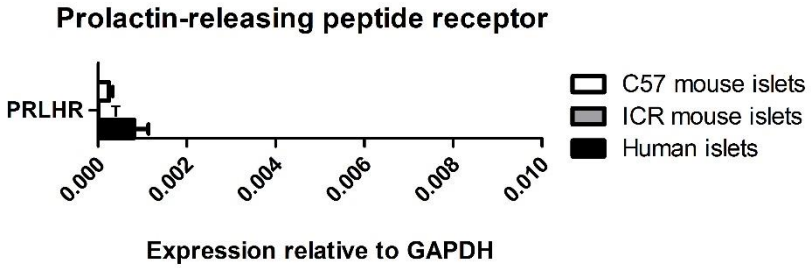
Prolactin-releasing peptide receptor
PRLHR
T
C57 mouse islets
ICR mouse islets
Human islets
0.000
0.002
0.004
0.006
0.008
0.010
Expression relative to GAPDH

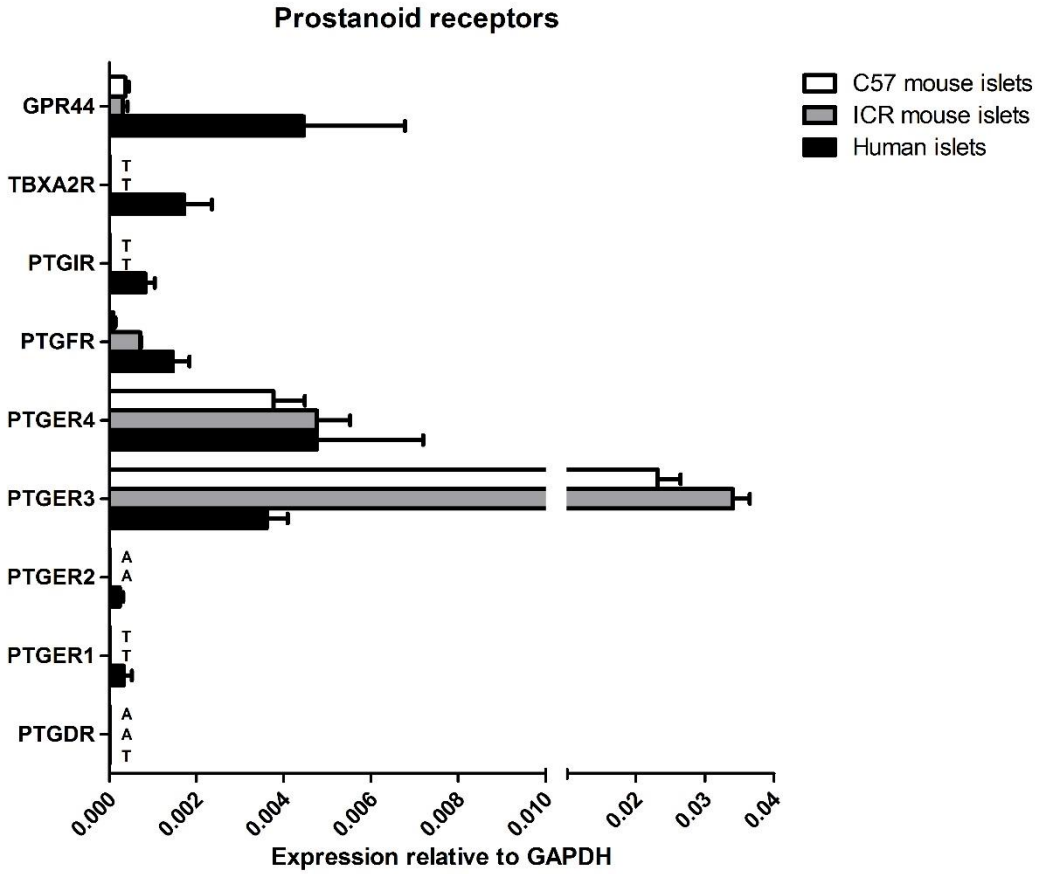
Prostanoid receptors
GPR44
TBXA2R
T
T
PTGIR
T
T
PTGFR
PTGER4
PTGER3
PTGER2
A
A
PTGER1
T
T
PTGDR
A
A
T
C57 mouse islets
ICR mouse islets
Human islets
0.000
0.002
0.004
0.006
0.008
0.010
0.02
0.03
0.04
Expression relative to GAPDH

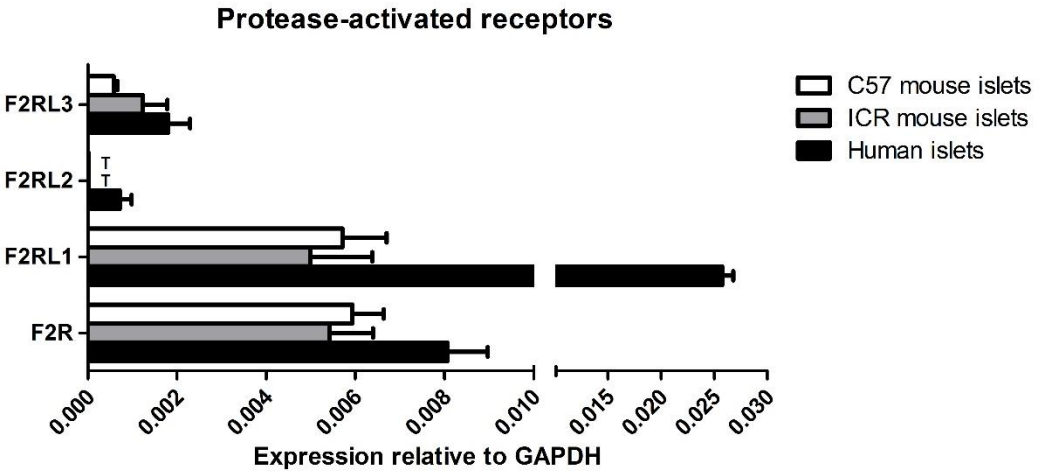
Protease-activated receptors
F2RL3
F2RL2
T
T
F2RL1
F2R
C57 mouse islets
ICR mouse islets
Human islets
0.000
0.002
0.004
0.006
0.008
0.010
0.015
0.020
0.025
0.030
Expression relative to GAPDH

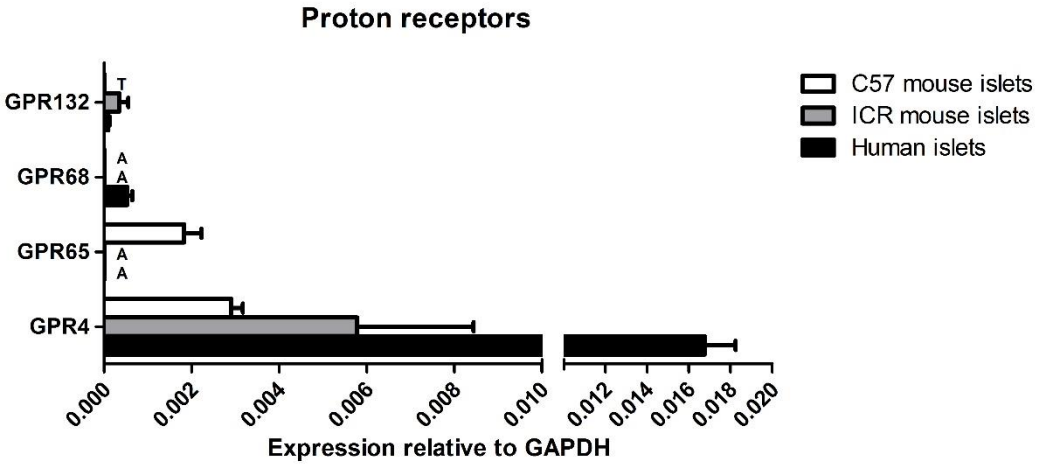
Proton receptors
C57 mouse islets
ICR mouse islets
Human islets
GPR132
GPR68
GPR65
GPR4
T
A
A
A
A
0.000
0.002
0.004
0.006
0.008
0.010
0.012
0.014
0.016
0.018
0.020
Expression relative to GAPDH

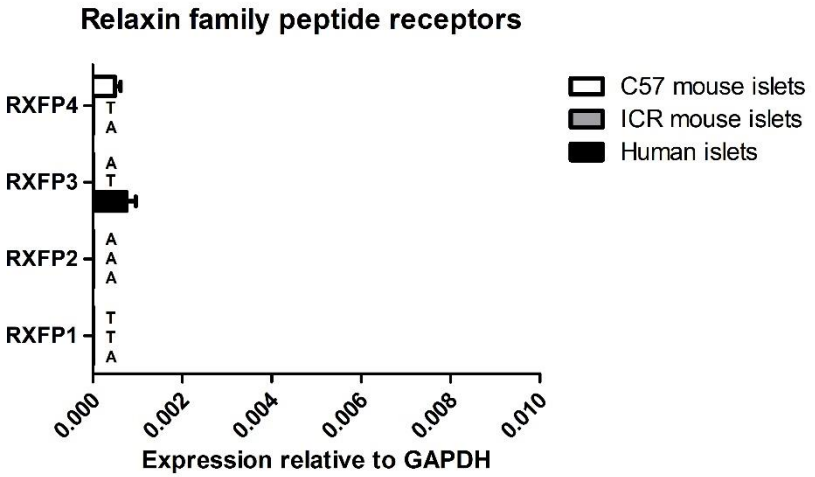
Relaxin family peptide receptors
C57 mouse islets
ICR mouse islets
Human islets
RXFP4
RXFP3
RXFP2
RXFP1
T
A
A
T
A
A
A
T
T
A
0.000
0.002
0.004
0.006
0.008
0.010
Expression relative to GAPDH

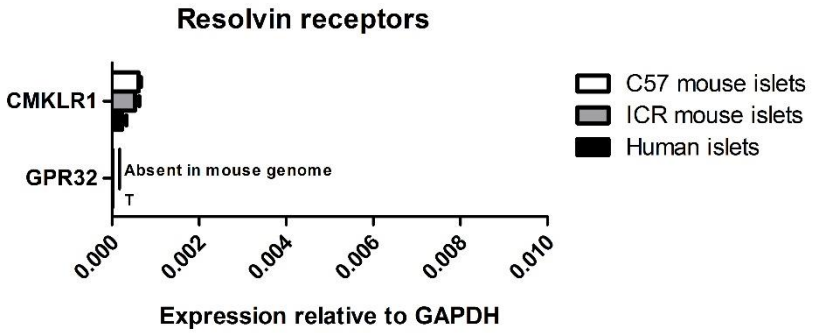
Resolvin receptors
C57 mouse islets
ICR mouse islets
Human islets
CMKLR1
GPR32
Absent in mouse genome
T
0.000
0.002
0.004
0.006
0.008
0.010
Expression relative to GAPDH

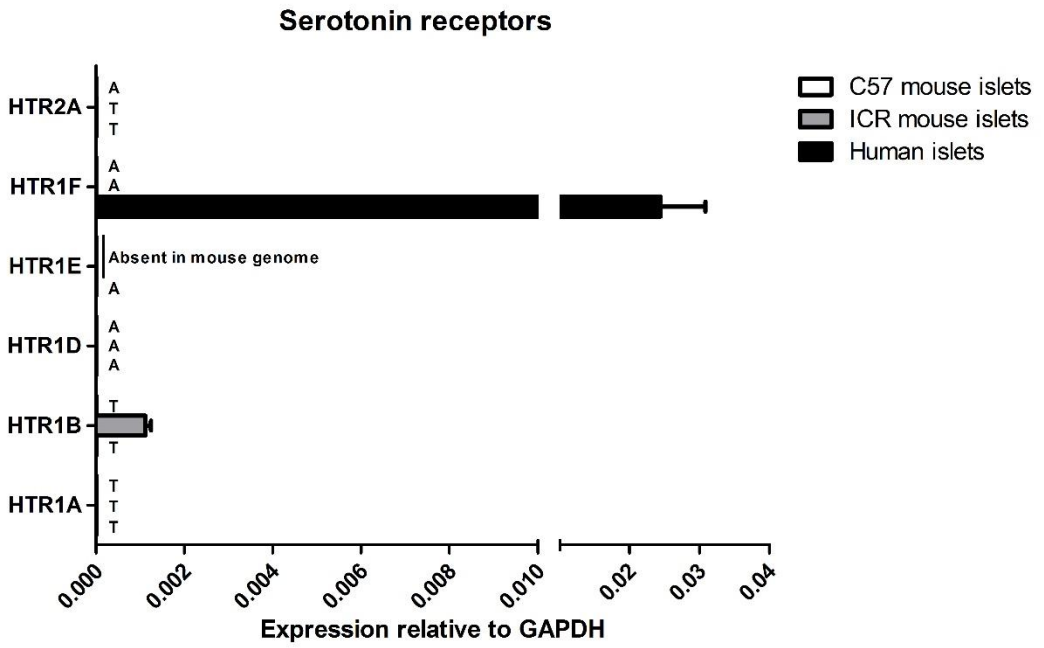
Serotonin receptors
C57 mouse islets
ICR mouse islets
Human islets
HTR2A
HTR1F
HTR1E
Absent in mouse genome
HTR1D
HTR1B
HTR1A
0.000
0.002
0.004
0.006
0.008
0.010
0.02
0.03
0.04
Expression relative to GAPDH

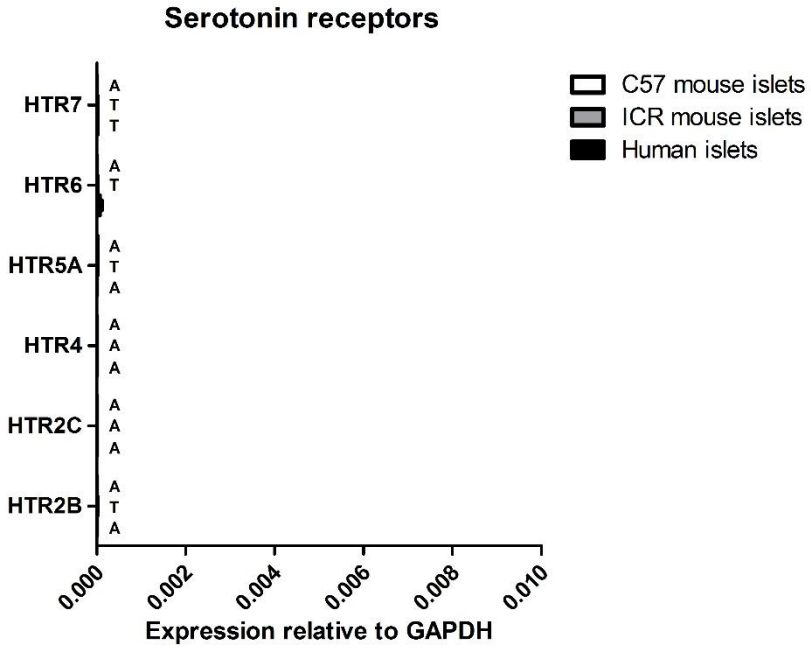
Serotonin receptors
C57 mouse islets
ICR mouse islets
Human islets
HTR7
HTR6
HTR5A
HTR4
HTR2C
HTR2B
0.000
0.002
0.004
0.006
0.008
0.010
Expression relative to GAPDH

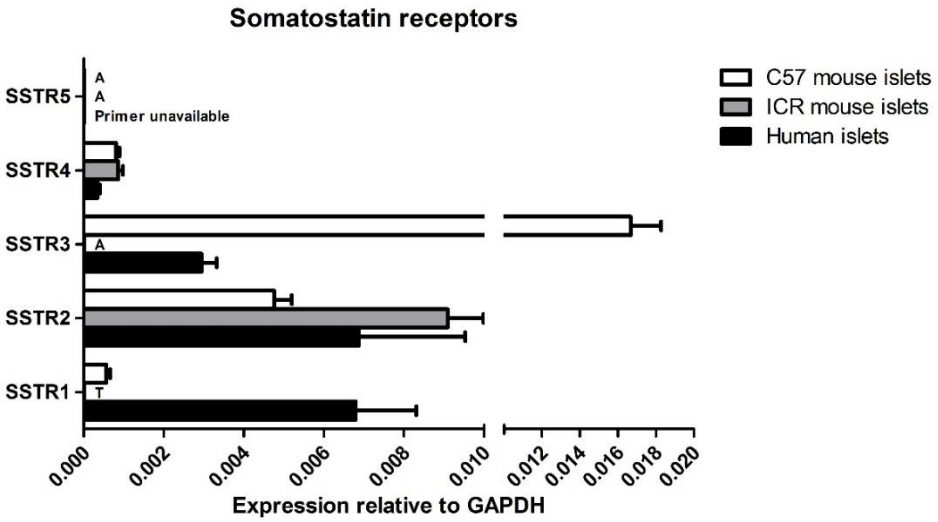
Somatostatin receptors
C57 mouse islets
ICR mouse islets
Human islets
SSTR5
A
A
Primer unavailable
SSTR4
SSTR3
A
SSTR2
SSTR1
T
0.000
0.002
0.004
0.006
0.008
0.010
0.012
0.014
0.016
0.018
0.020
Expression relative to GAPDH

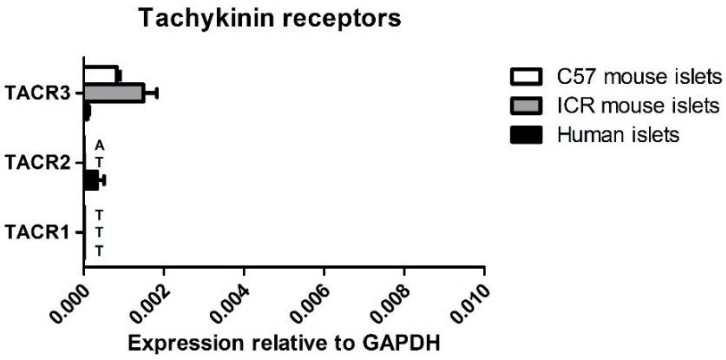
Tachykinin receptors
C57 mouse islets
ICR mouse islets
Human islets
TACR3
TACR2
A
T
TACR1
T
T
T
0.000
0.002
0.004
0.006
0.008
0.010
Expression relative to GAPDH

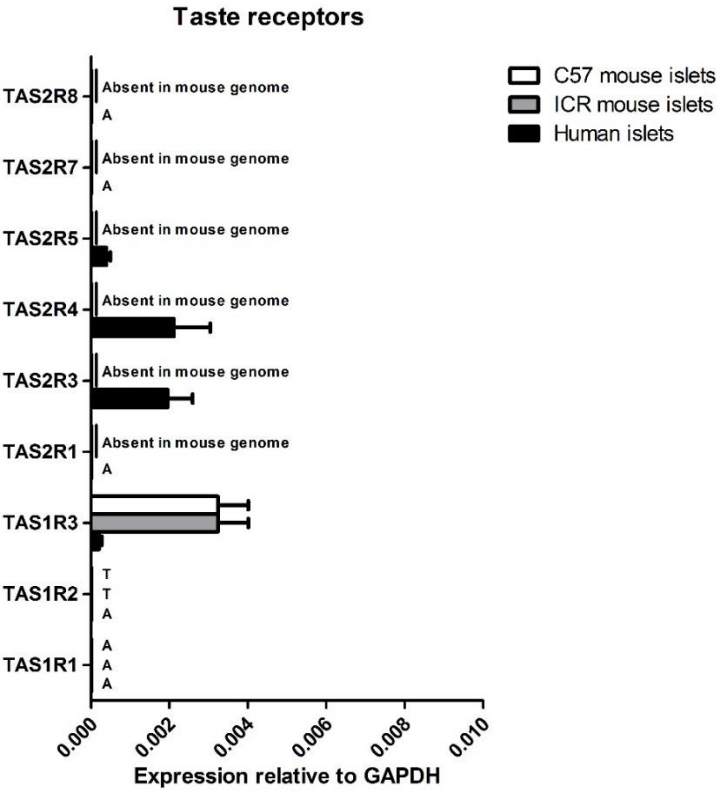
Taste receptors
C57 mouse islets
ICR mouse islets
Human islets
TAS2R8
Absent in mouse genome
A
TAS2R7
Absent in mouse genome
A
TAS2R5
Absent in mouse genome
TAS2R4
Absent in mouse genome
TAS2R3
Absent in mouse genome
TAS2R1
Absent in mouse genome
A
TAS1R3
TAS1R2
T
T
A
TAS1R1
A
A
A
0.000
0.002
0.004
0.006
0.008
0.010
Expression relative to GAPDH

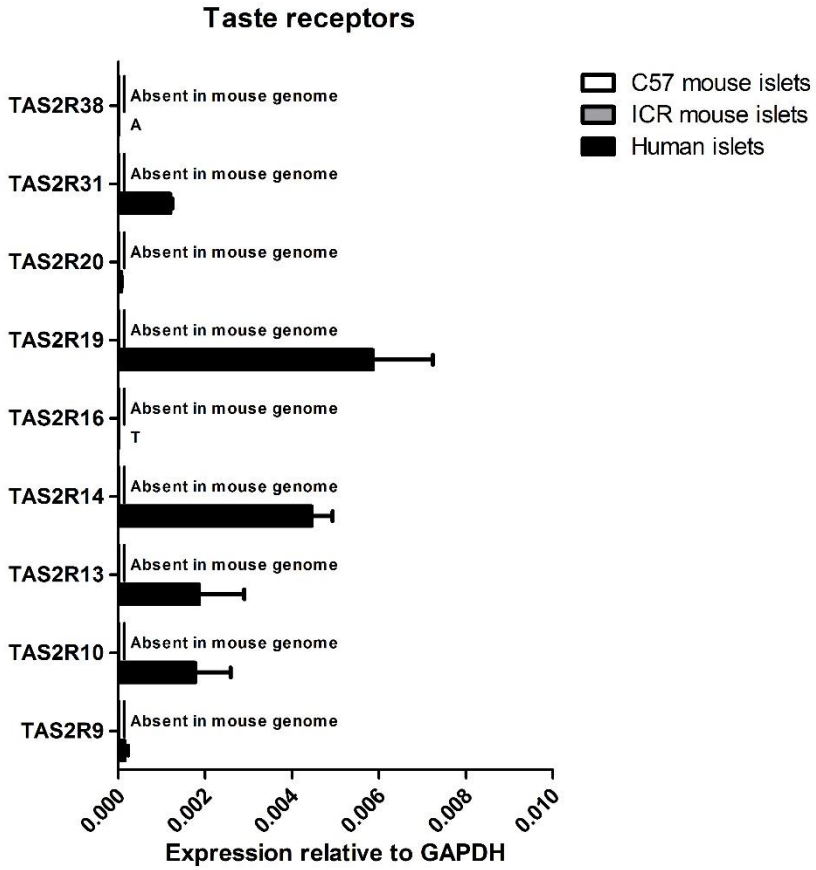
Taste receptors
C57 mouse islets
ICR mouse islets
Human islets
TAS2R38
TAS2R31
TAS2R20
TAS2R19
TAS2R16
TAS2R14
TAS2R13
TAS2R10
TAS2R9
Absent in mouse genome
A
T
0.000
0.002
0.004
0.006
0.008
0.010
Expression relative to GAPDH

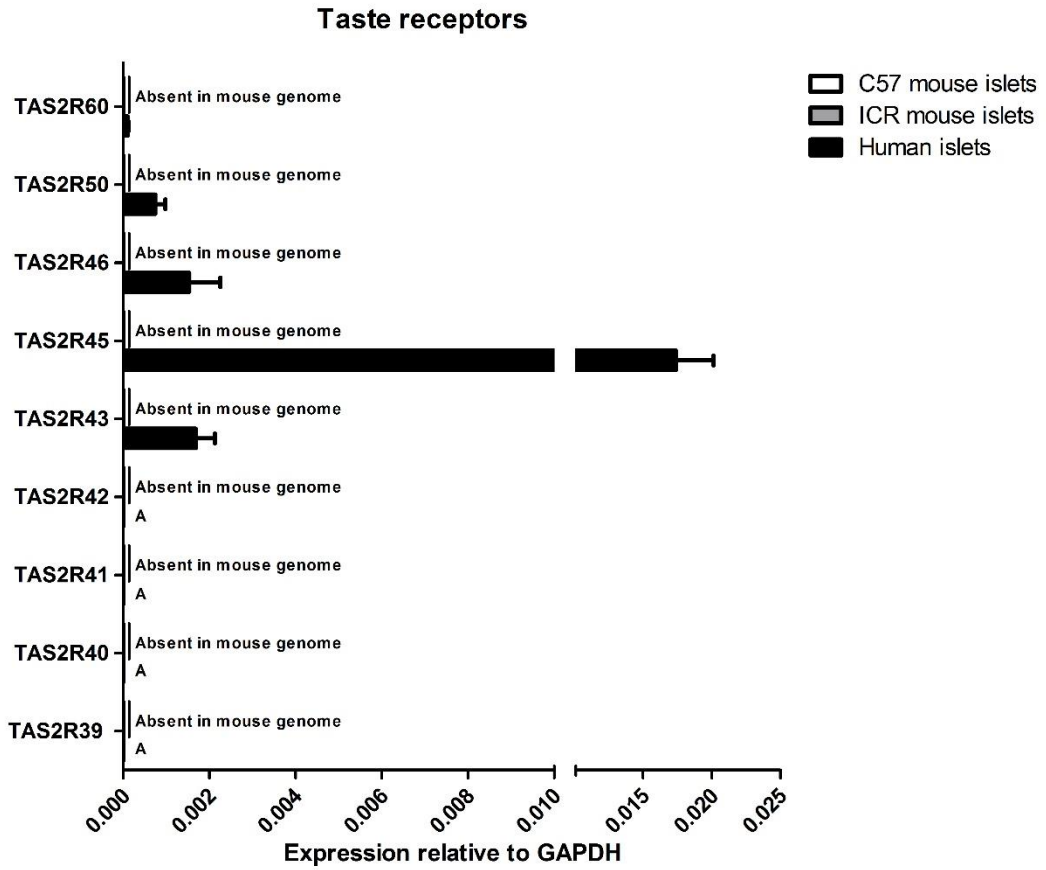
Taste receptors
C57 mouse islets
ICR mouse islets
Human islets
TAS2R60
TAS2R50
TAS2R46
TAS2R45
TAS2R43
TAS2R42
TAS2R41
TAS2R40
TAS2R39
Absent in mouse genome
A
0.000
0.002
0.004
0.006
0.008
0.010
0.015
0.020
0.025
Expression relative to GAPDH

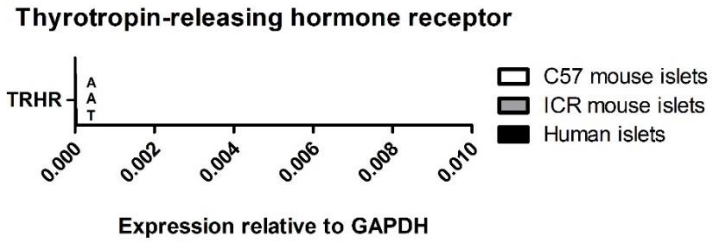
Thyrotropin-releasing hormone receptor
TRHR
A
A
T
C57 mouse islets
ICR mouse islets
Human islets
0.000
0.002
0.004
0.006
0.008
0.010
Expression relative to GAPDH

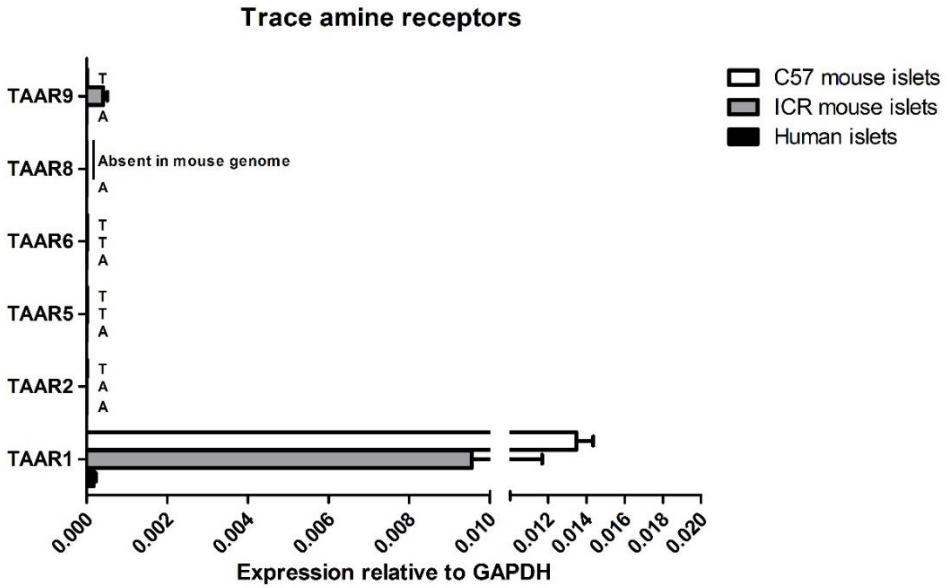
Trace amine receptors
TAAR9
T
A
TAAR8
Absent in mouse genome
A
TAAR6
T
T
A
TAAR5
T
T
A
TAAR2
T
A
A
TAAR1
C57 mouse islets
ICR mouse islets
Human islets
0.000
0.002
0.004
0.006
0.008
0.010
0.012
0.014
0.016
0.018
0.020
Expression relative to GAPDH

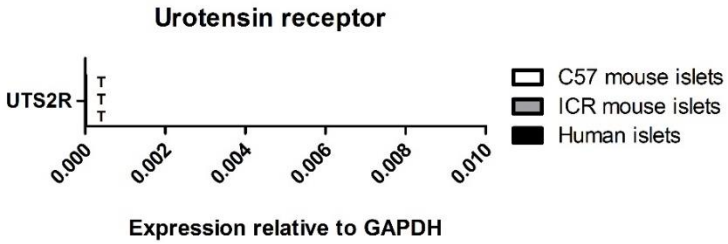
Urotensin receptor
UTS2R
T
T
T
C57 mouse islets
ICR mouse islets
Human islets
0.000
0.002
0.004
0.006
0.008
0.010
Expression relative to GAPDH

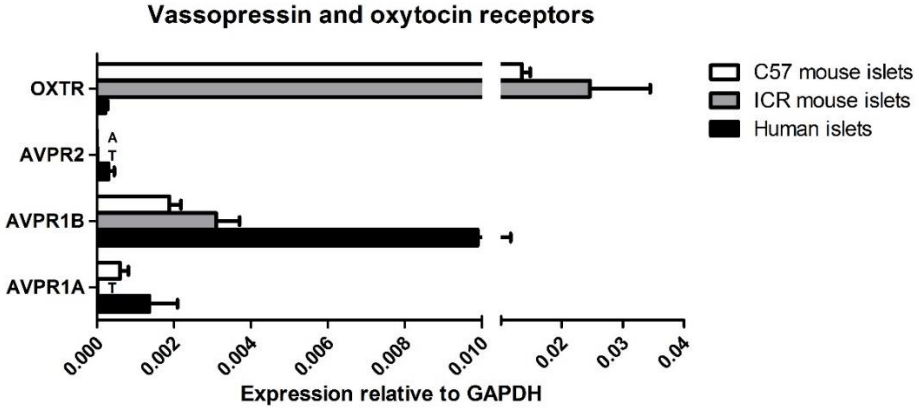
Vassopressin and oxytocin receptors
OXTR
AVPR2
A
T
AVPR1B
AVPR1A
T
C57 mouse islets
ICR mouse islets
Human islets
0.000
0.002
0.004
0.006
0.008
0.010
0.02
0.03
0.04
Expression relative to GAPDH

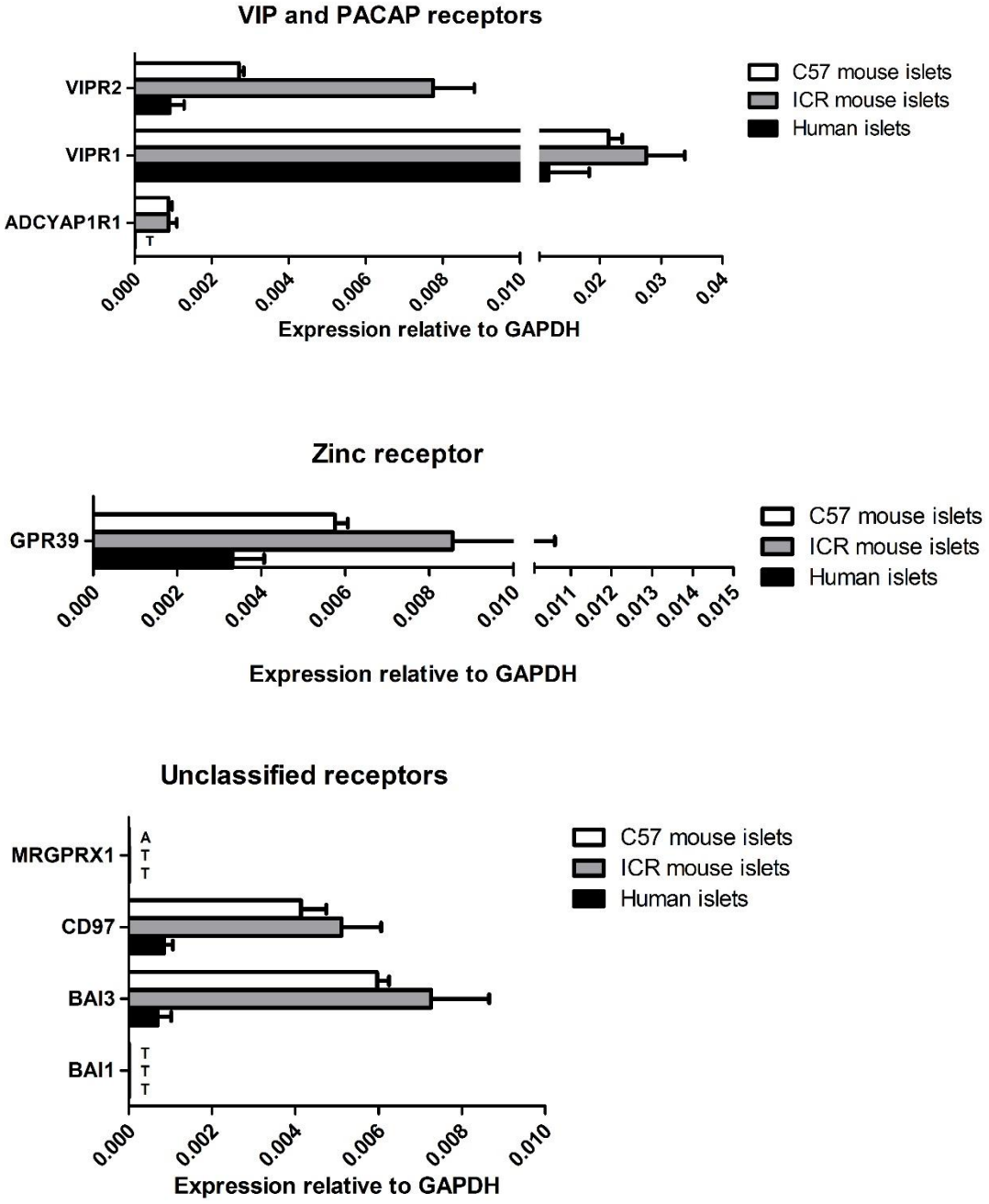

Figure 3.4.2 Column plots of GPCR mRNA expression in human and mouse islets. Receptor mRNA expression data are grouped within GPCR subfamilies and arranged in alphabetical order. Data are expressed as mean + SEM relative to GAPDH expression, from four biological replicates for all islet groups. T = trace expression, A = absent expression.

qPCR analyses revealed that of the 376 human GPCR mRNAs screened for expression in human islets, 221 (59%) were expressed and quantified, 63 (17%) were present at non-quantifiable trace levels and 92 (24%) were absent (Figure 3.4.3).

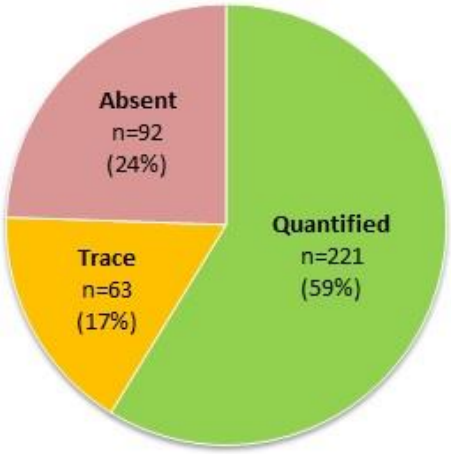

Figure 3.4.3 Proportional analysis of GPCR mRNA expression in human islets

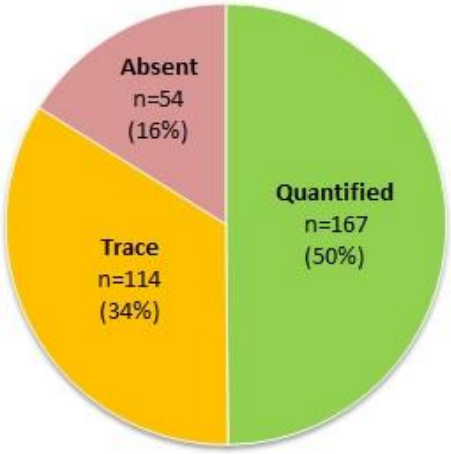

Figure 3.4.4 Proportional analysis of GPCR mRNA expression in ICR mouse islets

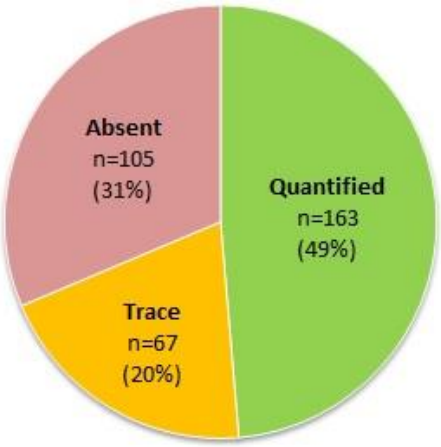

Figure 3.4.5 Proportional analysis of GPCR mRNA expression in C57 mouse islets

Of the 335 mouse GPCR orthologues screened for expression in ICR mouse islets, 167 (50%) were expressed and quantified, 114 (34%) were expressed at non-quantifiable trace levels and 54 (16%) were absent (Figure 3.4.4). This compares similarly with the C57 mouse islets where 163 (49%) were expressed and quantified, 67 (20%) expressed at non-quantifiable levels and 105 (31%) that were not detected (Figure 3.4.5).

The mRNA expression data for each islet group were re-plotted as dot plots and tabulated to create a rank order of GPCR expression. This revealed that within human islets, the top ten highest expressed GPCRs were GPR56, CASR, GPR119, LPNH1, FFAR1 (GPR40), ELTD1, GLP1R, GPRC5B, HTR1F and GPRC5C (Figure 3.4.6). The top ten highest expressed GPCRs in ICR mouse islets were revealed as Gpr56, Glp1r, Cckar, Gpr158, Gabbr2, Galr1, Ffar1 (Gpr40), Gprc5c, Fzd3 and Calcrl (Figure 3.4.7). Within C57 mouse islets Glp1r, Gpr56, Gpr158, Cckar, Gabbr2, Ffar1 (Gpr40), Gipr, Gprc5c, Galr1 and Galr3 were ranked as the top ten highest expressed GPCRs (Figure 3.4.8).

Table 3.4.1 Rank order of the top highest expressed GPCRs in human and mouse islets. GPCRs ranked in order of expression with expression compared to the total GPCR expression within each islet group.

Rank	**Human**		**ICR**		**C57**	
	GPCR	*% total GPCR mRNA expression*	*GPCR*	*% total GPCR mRNA expression*	*GPCR*	*% total GPCR mRNA expression*
1	GPR56	13.9	Gpr56	18.7	Glp1r	21.0
2	CASR	10.5	Glp1R	16.6	Gpr56	20.1
3	GPR119	6.2	Cckar	6.6	Gpr158	9.0
4	LPHN1	5.6	Gpr158	4.2	Cckar	3.9
5	FFAR1	4.5	Gabbr2	2.5	Gabbr2	3.0
6	ELTD1	3.0	Galr1	2.4	Ffar1	2.6
7	GLP1R	2.3	Ffar1	2.3	Gipr	2.6
8	GPRC5B	2.2	Gprc5c	2.2	Gprc5c	1.9
9	HTR1F	2.2	Fzd3	1.8	Galr1	1.7
10	GPRC5C	2.0	Calcrl	1.7	Galr3	1.7

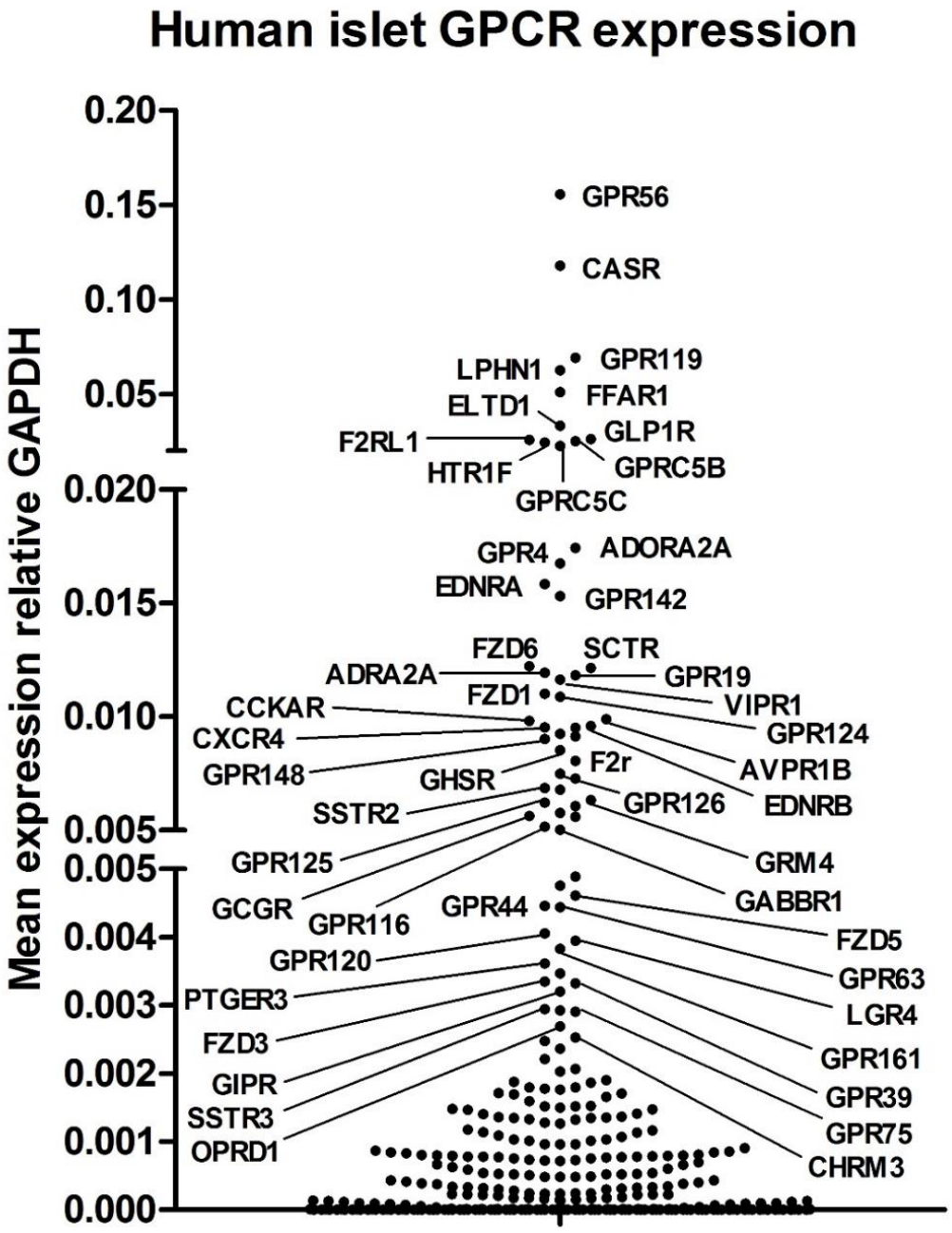

Figure 3.4.6 A dot plot representing the mRNA expression of 376 GPCRs in human islets. Data expressed as mean expression relative to GAPDH from four biological replicates.

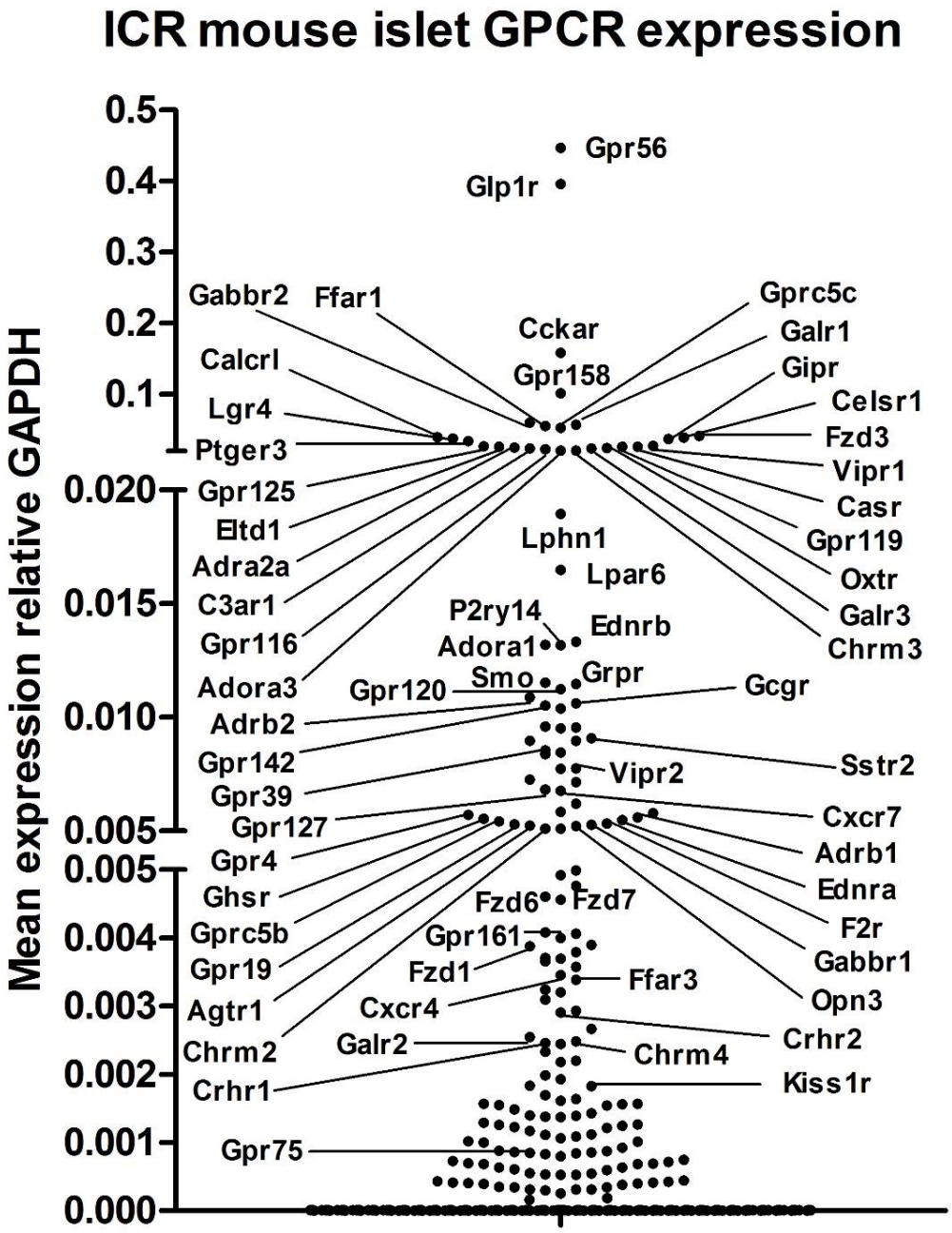

Figure 3.4.7 A dot plot representing the mRNA expression of 335 mouse orthologue GPCRs in ICR mouse islets. Data expressed as mean expression relative to Gapdh from four biological replicates.

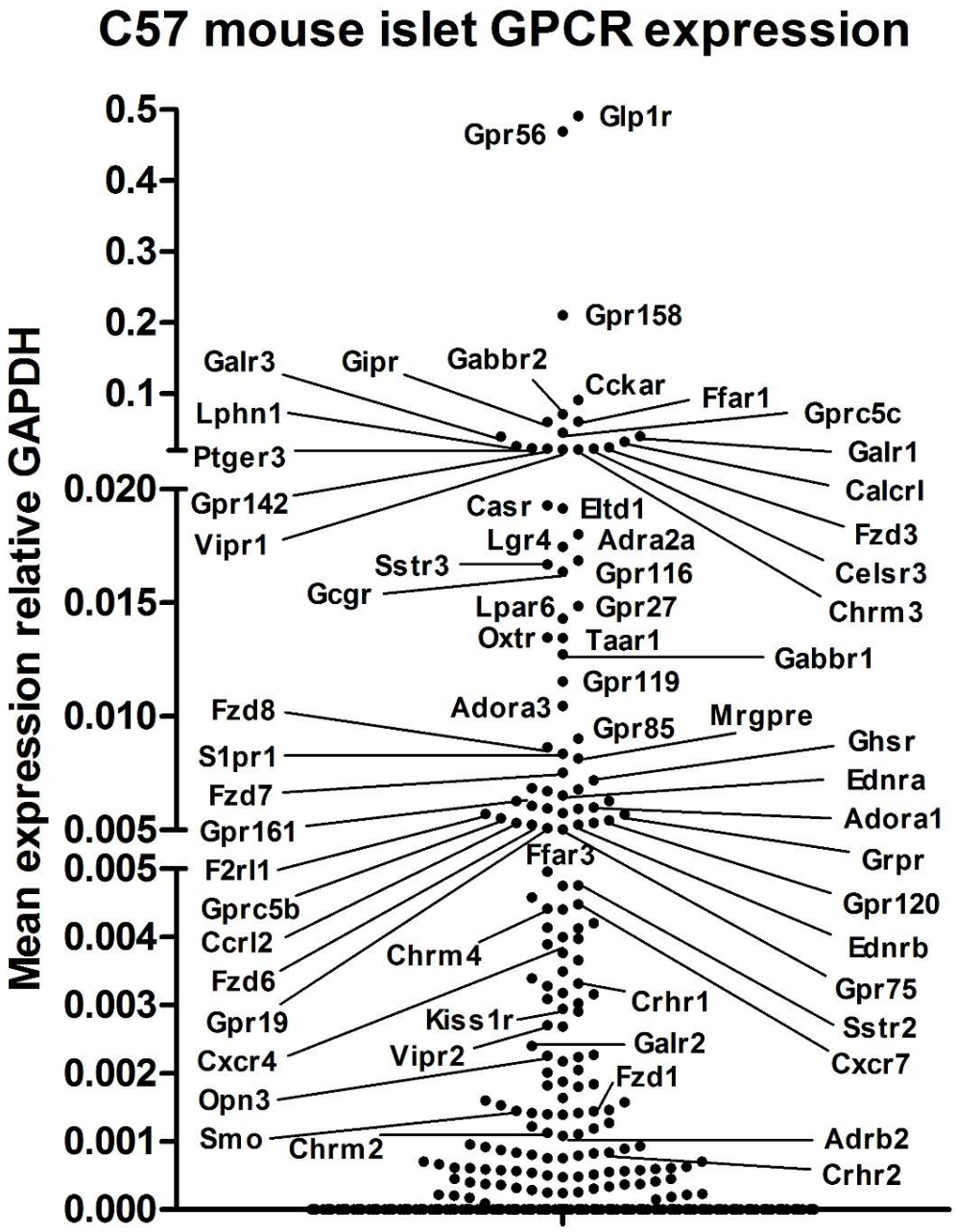

Figure 3.4.8 A dot plot representing the mRNA expression of 335 mouse orthologue GPCRs in C57 mouse islets. Data expressed as mean expression relative to Gapdh from four biological replicates.

3.4.3 A comparison of human and mouse islet GPCR expression profiles

A comparison of orthologue GPCR expression between the islets groups was performed using regression analysis and quantified by defining a coefficient of determination (r^2). In order to incorporate the absent and trace expressed GPCRs, which could not be reliably quantified relative to the housekeeping gene GAPDH, into the r^2 calculation, the trace and absent expressed GPCRs were assigned an expression value of 0.00001 and 0.000001 relative to GAPDH respectively.

A comparison of GPCR expression between human islets and mouse ICR islets revealed a reasonable degree of similarity with an r^2 value of 0.360 determined (Figure 3.4.9). Similarly, an r^2 value of 0.304 was determined when comparing GPCR expression between human and C57 mouse islets (Figure 3.4.10). A high degree of similarity was observed between both the inbred and outbred mouse strains as indicated by an r^2 value of 0.946 (Figure 3.4.11).

Further analysis of the GPCR expression profiles within human and mouse islets revealed that of the 335 GPCR orthologues screened, 190 GPCRs were commonly expressed in human and both strains of mouse islets (Figure 3.4.12), a list of which can be found in Table 3.4.2. Species and mouse strain specific differences in GPCR expression were also observed within the islet groups, with 26, 24 and 3 GPCRs exclusively expressed within human, ICR and C57 islets respectively (Table 3.4.3).

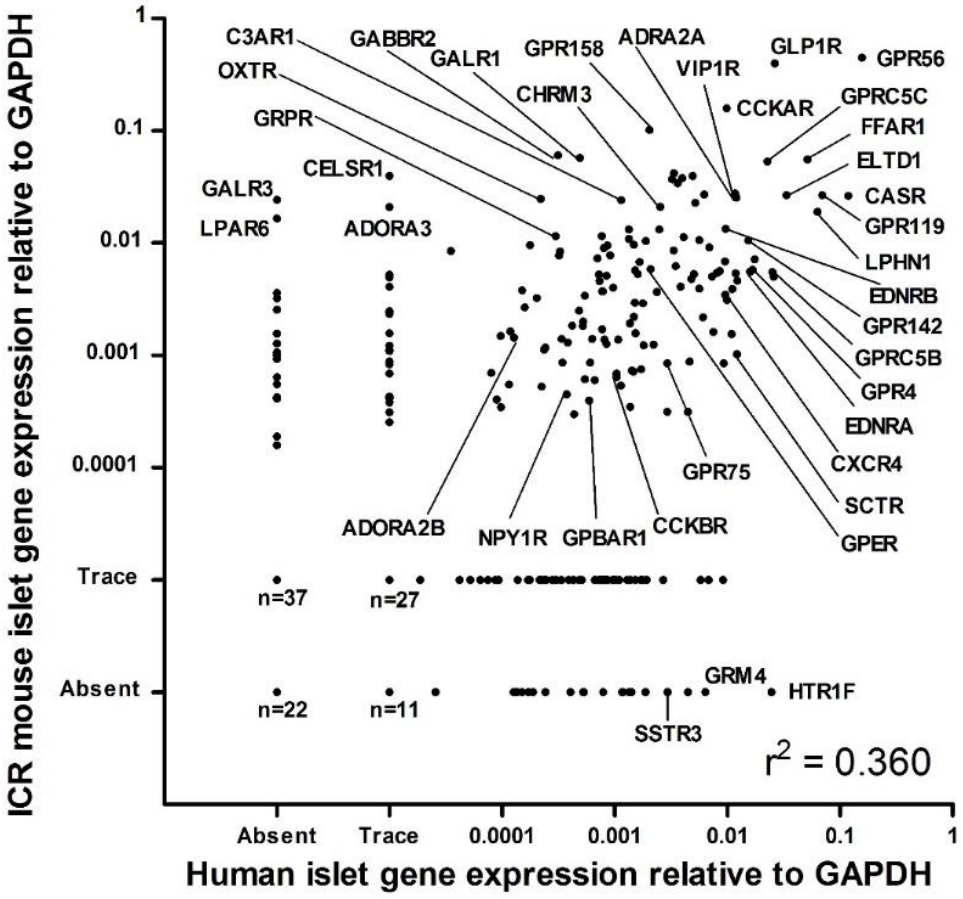

Figure 3.4.9 Regression analysis of orthologue GPCR expression between human and ICR mouse islets. A coefficient of determination (r^2) of 0.360 was determined. Data expressed as mean expression relative to GAPDH from four biological replicates.

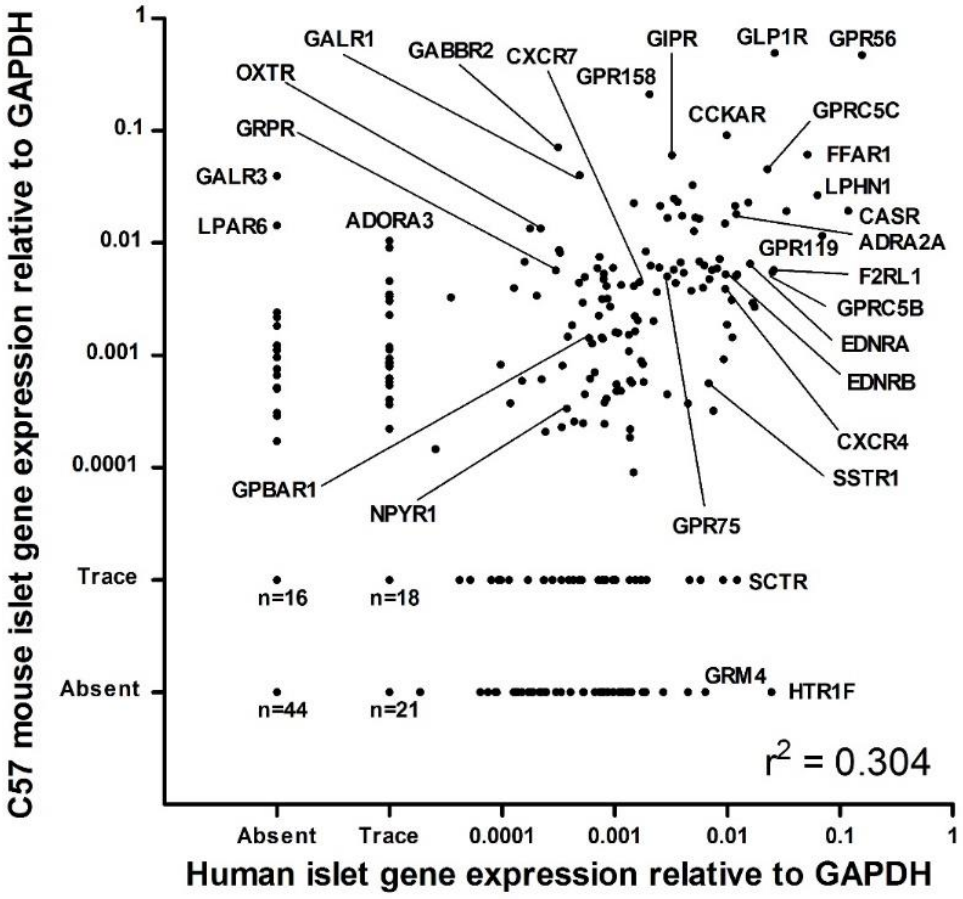

Figure 3.4.10 Regression analysis of orthologue GPCR expression between human and C57 mouse islets. A coefficient of determination (r^2) of 0.304 was determined. Data expressed as mean expression relative to GAPDH from four biological replicates.

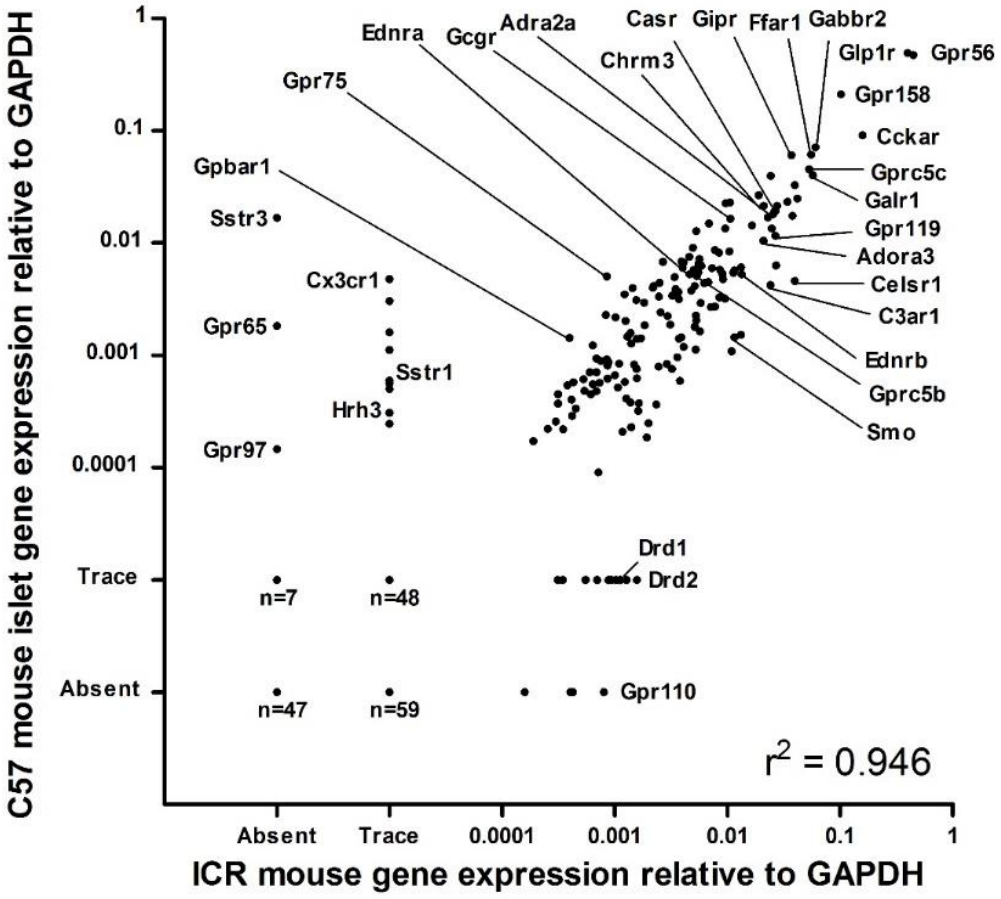

Figure 3.4.11 Regression analysis of orthologue GPCR expression between ICR and C57 mouse islets. A coefficient of determination (r^2) of 0.946 was determined. Data expressed as mean expression relative to GAPDH from four biological replicates.

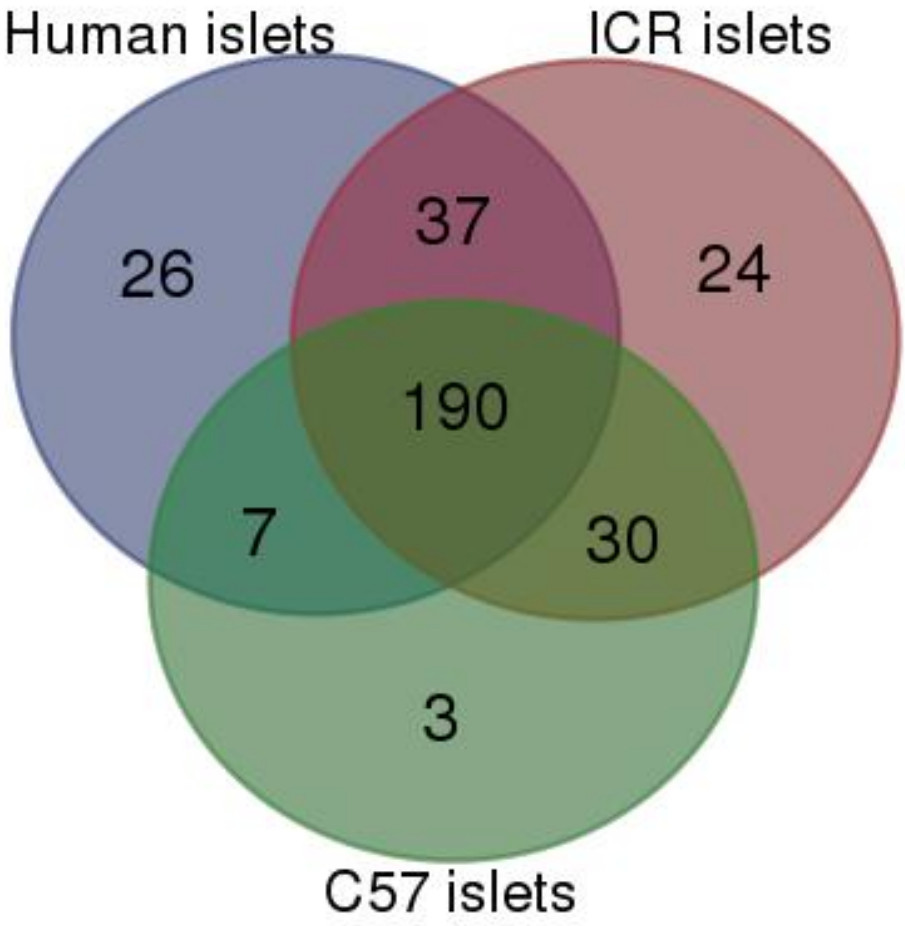

Figure 3.4.12 Venn diagram of orthologue GPCR expression in human and mouse islets. Data includes GPCRs expressed at trace level and above.

Table 3.4.2 A table of 190 commonly expressed GPCRs in human and mouse islets. Data arranged in rank order of expression within human islets.

Rank		Rank		Rank		Rank	
1	GPR56	**49**	LPHN2	**97**	CYSLTR1	**145**	GPR98
2	CASR	**50**	FZD3	**98**	PRLHR	**146**	ACKR1
3	GPR119	**51**	GPR39	**99**	CCRL2	**147**	ADORA2B
4	LPHN1	**52**	GIPR	**100**	CX3CR1	**148**	GPR182
5	FFAR1	**53**	C5AR1	**101**	BDKRB2	**149**	FZD9
6	ELTD1	**54**	GPR75	**102**	GPR22	**150**	GPR132
7	GLP1R	**55**	CHRM3	**103**	GPRC5A	**151**	TACR3
8	GPRC5B	**56**	ADORA1	**104**	GPR157	**152**	HCRTR1
9	GPRC5C	**57**	FZD4	**105**	SMO	**153**	GPR64
10	ADORA2A	**58**	LPAR2	**106**	FZD7	**154**	GPR152
11	GPR4	**59**	GPER	**107**	OPN3	**155**	NPBWR1
12	EDNRA	**60**	GPR158	**108**	F2RL2	**156**	S1PR3
13	GPR142	**61**	FPR3	**109**	BAI3	**157**	ADORA3
14	FZD6	**62**	S1PR1	**110**	P2RY6	**158**	GPR85
15	SCTR	**63**	F2RL3	**111**	P2RY12	**159**	CELSR1
16	ADRA2A	**64**	CRHR2	**112**	GPR153	**160**	GPRC6A
17	GPR19	**65**	TBXA2R	**113**	GPBAR1	**161**	CRHR1
18	VIPR1	**66**	GPR162	**114**	LPAR5	**162**	GPR45
19	FZD1	**67**	GPR37	**115**	FFAR3	**163**	GPR87
20	GPR124	**68**	CXCR7	**116**	P2RY2	**164**	APLNR
21	AVPR1B	**69**	AGTR1	**117**	KISS1R	**165**	CHRM2
22	CCKAR	**70**	DRD2	**118**	GPR133	**166**	OPRL1
23	EDNRB	**71**	ADRB1	**119**	GALR1	**167**	ADCYAP1R1
24	CXCR4	**72**	GPR123	**120**	LGR5	**168**	GPR62
25	GPR27	**73**	GPR52	**121**	LPAR4	**169**	CCR10
26	GPR135	**74**	CELSR3	**122**	CHRM4	**170**	CHRM1
27	ADRA2C	**75**	GPR146	**123**	GPR21	**171**	GPR151
28	GHSR	**76**	PTGFR	**124**	GPR173	**172**	GPR150
29	F2R	**77**	GPR179	**125**	FFAR2	**173**	XCR1
30	GPR126	**78**	GPR34	**126**	PTH1R	**174**	FZD2
31	F2RL1	**79**	AVPR1A	**127**	LPAR3	**175**	CCR3
32	SSTR2	**80**	GPR160	**128**	NPY1R	**176**	HTR1B
33	SSTR1	**81**	P2RY14	**129**	SSTR4	**177**	GPR37L1
34	GPR125	**82**	ADRB2	**130**	S1PR2	**178**	ADRA1D
35	P2RY1	**83**	C3AR1	**131**	PTGER1	**179**	BAI1
36	BRS3	**84**	P2RY13	**132**	MRGPRE	**180**	BAI2
37	GCGR	**85**	GPR183	**133**	FZD8	**181**	CCR1
38	LPAR1	**86**	PTAFR	**134**	GABBR2	**182**	CCR4
39	GPR116	**87**	CCKBR	**135**	GRPR	**183**	CXCR5
40	GABBR1	**88**	SUCNR1	**136**	NPFFR2	**184**	GPR26
41	CALCRL	**89**	BDKRB1	**137**	NMBR	**185**	GRM7
42	PTGER4	**90**	CNR1	**138**	ADRA2B	**186**	HTR1A
43	FZD5	**91**	GPR3	**139**	GRM8	**187**	LGR6
44	GPR44	**92**	VIPR2	**140**	CMKLR1	**188**	MCHR1
45	GPR120	**93**	CELSR2	**141**	OXTR	**189**	TACR1
46	LGR4	**94**	CD97	**142**	TAS1R3	**190**	UTS2R
47	GPR161	**95**	S1PR5	**143**	TAAR1		
48	PTGER3	**96**	PTGIR	**144**	LTB4R		

Table 3.4.3 A table of tissue specific GPCR expression in human and mouse islets. Data depicted represents orthologue GPCRs expressed at trace (*italics*) levels and above and arranged in rank order of expression level.

Expression rank	**Human islets**	**ICR islets**	**C57 islets**
1	HTR1F	Oprk1	Gpr65
2	GRM4	Gpr101	*Npffr1*
3	GPR63	*Ackr2*	*Taar2*
4	OPRM1	*Adrb3*	
5	CXCR6	*Chrm5*	
6	GPR113	*Ccxr11*	
7	GPR143	*Drd3*	
8	GPRC5D	*Fpr1*	
9	GPR68	*Gpr111*	
10	GNRHR	*Gpr141*	
11	GPR82	*Gpr17*	
12	DRD4	*Gpr174*	
13	PTGER2	*Gpr18*	
14	GPR115	*Grm5*	
15	MTNR1B	*Hrh2*	
16	NMUR1	*Htr2b*	
17	PTH2R	*Mc2r*	
18	NPY5R	*Mc3r*	
19	*CALCR*	*Mrgprx2*	
20	*GPR1*	*Npy2r*	
21	*GPR83*	*Ntsr2*	
22	*MRGPRD*	*P2ry10*	
23	*NMUR2*	*Prokr1*	
24	*PPYR1*	*Tshr*	
25	*PTGDR*		
26	*TRHR*		

3.4.4 Targets

In order to highlight GPCRs that have been proposed to be of interest as therapeutic targets for the treatment of T2DM and to assess the suitability of using mouse islets to study such targets, a regression analysis plot comparing GPCR mRNA expression between human and ICR mouse islets was generated (Figure 3.4.13). These data indicate that of the 284 GPCRs that are expressed within human islets at trace level and above, only 1 GPCR (GLP1R), which is also highly expressed within mouse islets, has had clinical success. Only 2 other GPCRs, FFAR1 and GPR119, have undergone clinical investigation and like in human islets are also expressed highly in mouse islets. The data provided here allow the identification of 14 GPCRs that have suitable characteristics as potential targets for T2DM therapy and are highlighted by red dots in Figure 3.4.13: GPR56, GIPR, GPR120, GCGR, GPRC5B, CNR1, FFAR3, FFAR2, KISS1R, GPR75, NPY1R, GPBAR1, GPR55 and CNR2. It is interesting to note that these potential GPCR targets are expressed in both mouse and human islets at similar levels ($r^2 = 0.531$). Table 3.4.4 summarises the functional relevance of the 14 GPCRs as targets for T2DM.

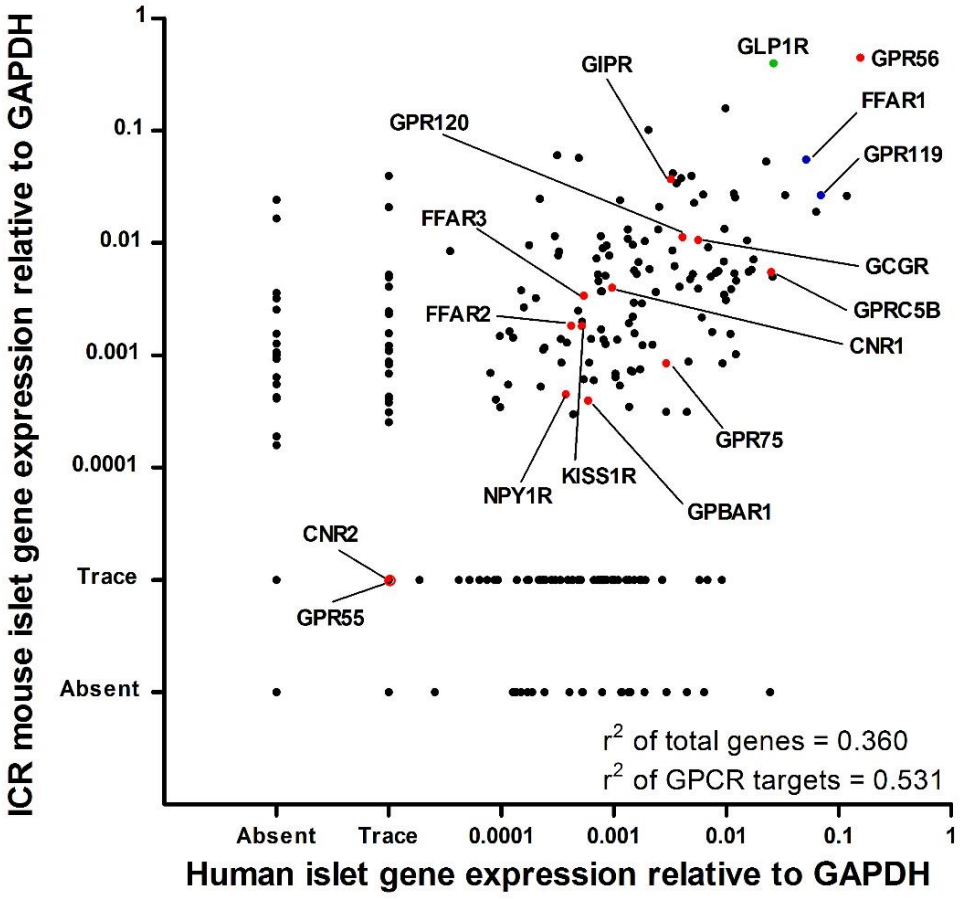

Figure 3.4.13 Identification of GPCR targets of interest for the treatment of T2DM. Green dots indicate clinically successful targets, blue dots indicate GPCRs currently under clinical investigation and red dots are GPCRs proposed to have clinical relevance. Data expressed as mean expression relative to GAPDH.

Table 3.4.4 A table GPCR targets with potential therapeutic benefit for T2DM.

Receptor	Natural Ligand/s	Tissue expression	Effects (receptor activation)	Reference
GPR56	Collagen III, transglutaminase	Islet vasculature, thyroid, testis, heart, brain, placenta, lung	↑ insulin	Unpublished data
GIPR	GIP	α, β and σ cells, adipose tissue	↑ insulin, ↑ glucagon, ↑ fat storage	(Irwin and Flatt, 2009)
FFAR4 (GPR120)	Long-chain NEFA	Enteroendocrine cells, β- and σ-cells	↑ GLP-1, ↑ GIP, ↓somatostatin, ↓ ghrelin	(Stone et al., 2014)
GCGR	Glucagon, oxyntomodulin	β-cells, liver, adipose, brain	↑ insulin, ↑ energy expenditure, ↓ food intake	(Reimann and Gribble, 2016)
GPRC5B	Unknown	High expression in islets, adipose tissue, kidney and testis	Receptor knock down: ↑ insulin, ↓ β-cell apoptosis	(Soni et al., 2013)
CNR1	Anandamide, 2-arachidonoylglycerol	CNS, β-cells	↑ insulin	(Li et al., 2010)
FFAR3	Short chain fatty acids	β-cells, spleen, lymph node, bone marrow, adipose tissue	↓ insulin	(Tang et al., 2015)
FFAR2	Short chain fatty acids	β-cells, monocytes, adipose tissue	↓ insulin	(Tang et al., 2015)
KISS1R (GPR54)	Kisspeptin cleaved peptides	β-cells, pituitary, placenta, brain, lymphocytes	↑ insulin	(Bowe et al., 2012)
GPR75	CCL5	α- and β-cells, brain	↑ insulin, ↓ β-cell apoptosis, ↑ β-cell proliferation	(Liu et al., 2013)
NPY1R	NPY, PYY, PPY	β-cells, colon, heart, kidney, adrenal gland, placenta	↓ β-cell apoptosis, ↑ β-cell proliferation	(Persaud and Bewick, 2014)
GPBAR1	Bile acids	Enteroendocrine cells, adipose tissue	↑ GLP-1, ↑ energy expenditure	(Duan et al., 2015)
GPR55	lysophosphatidylinositol	β-cells, CNS, GI tract, skeletal muscle, adipose tissue	↑ insulin secretion	(Romero-Zerbo et al., 2011)
CNR2	Anandamide, 2-arachidonoylglycerol	β-cells, spleen, tonsils, bone marrow, leukocytes.	↑ insulin	(Li et al., 2010)

3.5 Discussion

G-protein coupled receptors play an important role in regulating islet function by mediating the actions of various stimuli such as nutrients, bile acids, gut hormones and neurotransmitters (Reimann and Gribble, 2016) and as a result have been targeted by therapeutics for the treatment of T2DM. However, despite the expression of nearly 300 GPCRs within islets (Amisten et al., 2013), only the GLP-1 receptor (GLP1R) has been clinically successful, whilst only two other GPCRs have undergone clinical assessment, FFAR1 and GLP119 (Oh da and Olefsky, 2016). Part of the reason for this limited success could be due to the restricted availability of human islets required to assess GPCR-mediated islet function, thus subsequently resulting in the reliance on cell lines and animal tissue to predict human islet physiology. The most common tissue used for predicting human islet function are mouse islets, but studies have identified gene expression differences between mouse and human islets (Kutlu et al., 2009), (Dai et al., 2012), (Benner et al., 2014), which raises questions as to the suitability of using mouse islets in predicting the human islet setting.

The experiments described within this chapter were designed to compare the GPCR mRNA expression profiles between human islets and islets isolated from two strains of mice to assess the suitability of using mouse islets as surrogate models for human islet GPCR studies. Due to the large volume of data that is included within this chapter, results will be discussed in sections with respect to the aims of the study; 1) Reveal the GPCR expression profiles within human and mouse islets, 2) Compare the GPCR expression profiles between mouse and human islets and 3) Assess the suitability of using mouse islets to assess the function of newly identified GPCR targets for the treatment of T2DM.

Reveal the human and mouse islet GPCRomes

Gene expression analysis revealed that a high proportion of total non-odorant GPCRs are expressed within the islets of Langerhans in both human and mouse islets. Of the 376 GPCRs assessed for expression within human islets, 284 GPCR mRNAs (75%) were shown to be expressed by human islets, whereas of the 335 mouse orthologue GPCR genes screened in mouse islets, 281 (84%) GPCRs were identified in ICR mouse islets and 230 (67%) were expressed in C57 mouse islets. It is well documented that GPCRs play an important role in regulating biological processes by mediating the activation of intracellular signalling pathways following stimulation by extracellular stimuli, and thus the revelation that both human and mouse islets express a high proportion non-odorant GPCRs highlights the complexity and variety of ways by which islet function is regulated. For example, islet function is regulated by neural input from the CNS, by gastrointestinal peptides, bile acids and also circulating nutrients, fatty acids and amino acids, all of which have the ability to regulate islet function through GPCR-mediated mechanisms (Reimann and Gribble, 2016). It is therefore unsurprising that a large number and variety of GPCRs are required to respond to this diverse array of physiological inputs.

However, what is particularly interesting is that whilst islets express a high percentage of non-odorant GPCRs that are available within the genome, the number of potential intracellular signalling pathways through which GPCRs couple is limited. Whilst the abundance of islet receptor expression compared to the limited number of pathways that could potentially be activated may seem excessive, it does highlight the variety of scenarios in which islets may be stimulated in order to maintain the primary function of regulating glucose homeostasis. For example, not only do islets respond to inputs during food intake, but also in situations of stress, pregnancy and during development.

Furthermore, the islet is a multicellular micro-organ comprised of a variety of different cell populations, such as the endocrine α-, β-, δ-cells, and cells of the intra-islet vasculature. Each cell population is responsible for mediating numerous unique functions that are regulated by specific GPCR mechanisms, thus contributing to the variety and abundance of receptor expression observed within the islet.

Compare GPCRomes between human and mouse islets

In addition to revealing the GPCR expression profiles within human and mouse islets, a principle aim of this chapter was to compare GPCR mRNA expression profiles between species. Before undertaking such studies, it was postulated that a certain degree of difference in GPCR gene expression would be observed between mouse and human islets due to the already documented differences in the number of non-odorant GPCRs that exists in the mouse compared to the human genome, 495 compared to 400 respectively (Bjarnadottir et al., 2006). In addition, it has been revealed that the islet architecture also differs between the species, with mouse islets being comprised of β-cells that are arranged in a central core surrounded by a mantle of α-cells and δ-cells, whereas the arrangement of such cells within human islets is less defined and found to be more interspersed with each other (Cabrera et al., 2006). Furthermore, the proportions of endocrine cells that reside within islets also differs between the two species. The proportion of α-, β-, δ-cells within the human islet is approximately 40, 50, 10% respectively, whereas in mouse islets the proportions are approximately 15-20, 60-80, 10% respectively (Steiner et al., 2010). However, whilst it can be postulated that differences in islet GPCR gene expression may exist between species, a

quantitative assessment of such GPCR expression differences between species, as well as between islets from different mouse strains, has not been revealed.

For the purpose of comparing and quantifying the GPCR mRNA expression between islet groups, regression analysis was performed. A comparison of the GPCR expression profiles between the two mouse strains revealed a high degree of similarity, with an r^2 value of 0.946 (Figure 3.4.11), despite C57 mice expressing 52 fewer GPCRs than their outbred counterpart (Figure 3.4.5). A comparison of the GPCR expression profiles between human islets and islets from the ICR and C57 mouse strains revealed a greater degree of difference, with r^2 values of 0.360 and 0.304 determined respectively (Figure 3.4.10, Figure 3.4.11). This observation was further emphasised by the revelation that human islets express 26 GPCRs that are not expressed by either mouse strains (Table 3.4.3). The observation that the degree of similarity in overall GPCR expression in human islets is more similar to that of the ICR strain than the C57 strain is likely to be due to the fact that human and ICR mouse islets share 227 commonly expressed GPCRs whereas human islets only share 197 with C57 mouse islets. An additional contributing factor is likely to be the degree of genetic variability between the two mouse strains, as one would presume that a greater degree of gene expression variability is likely to be observed within the outbred ICR strain. This degree of genetic variability between biological replicates of the ICR strain could result in a greater degree of inconsistency in expression compared to the C57 strain, thus preferentially skewing the data in favour of using ICR islets as suitable surrogate models for human islet studies. Furthermore, the use of outbred models is likely to introduce a degree of genetic variability consistent with the human situation and thus more translationally relevant.

With regards to species- and mouse strain-specific receptor expression, 26 orthologue GPCRs were shown to be specifically expressed in human islets, 24 specifically expressed in ICR mouse islets and 3 in C57 mouse islets (Figure 3.4.12). Of the 26 GPCRs that are exclusively expressed in human islets, HTR1F was identified as the most abundantly expressed. In recent years, serotonin has received interest with regards to the functional adaptation of β-cells during pregnancy, in particular the ability of mouse β-cells to secrete serotonin during pregnancy (Goyvaerts et al., 2016), (Ohara-Imaizumi et al., 2013). However, the use of mouse islets to predict the functional effects of serotonin in human islets ought to consider the disparity in expression of the HTR1F receptor between human and mouse islets, as the full functional effects of serotonin may not be revealed when using mouse islets should the HTR1F receptor modulate islet function. In addition to HTR1F, further examples of GPCRs that are exclusively expressed in human islets include DRD4, GRM4, GPR143 and OPRM1. Besides the effects of receptor expression exclusivity, a degree of enrichment of GPCR expression within human islets compared to mouse islets may also have contributed to the low correlation values determined by regression analysis. Examples of receptors with enriched expression in human islets include BRS3, FPR3, FZD1, SCTR and OPRD1. Interestingly though, whilst BRS3 mRNA expression is enriched in human islets by a factor of >500, functional studies have demonstrated that pharmacological agonism of BRS3 promotes glucose-induced insulin secretion from both isolated mouse and human islets (Feng et al., 2011). These findings suggest that while mRNA expression is an indicator of receptor involvement in tissue function, follow up functional studies are still required to fully confirm such predictions.

Further to human islet-specific expression, examples of mouse islet-specific GPCR expression was also observed and include, Galr2, Galr3 and Crhr1. Galr2, Galr3 were

shown to be exclusively expressed within mouse islets whereas, Crhr1 was shown to be enriched in mouse islets. Increased plasma levels of galanin and reduced galanin receptor expression have been reported in T2DM, and this state of galanin resistance has been shown to positively correlate with insulin resistance (Fang et al., 2016). However, the difference in galanin receptor mRNA expression between mouse and human islets may require the use of a more suitable surrogate model in order to fully understand the involvement of galanin in the pathophysiology of T2DM in humans. The corticotropin-releasing hormone (CRH) system has also received attention with regards to islet function following the revelation that UCN3 is expressed by β-cells and activates a negative feedback loop that promotes somatostatin release to inhibit glucose-induced insulin secretion upon normalisation of blood glucose (van der Meulen et al., 2015). Additionally, CRH promotes glucose-induced insulin secretion and proliferation of rat β-cells through the activation of the CRH1 receptor (Huising et al., 2010). However, only trace level expression of the CRH1 receptor was observed in human islets suggesting that CRH-mediated increases in glucose-stimulated insulin secretion via the CRH1 receptor in rat islets may not be observed in human islets.

Differences in GPCR mRNA expression were also observed between the mouse strains. Of particular interest is the SSTR3 receptor, which was revealed to be exclusively expressed in the islets of the C57 mouse strain. Evidence of disparities in somatostatin receptor subtype expression between rodent species have been reported previously. Interestingly however, in the same study, both absence and presence of the SSTR3 receptor was observed between islets of individual mice from the same population of C57 mice (Ludvigsen et al., 2004). Reasons for such differences are unlikely to be due to genetic background due to the fact that such intra-species differences are observed in the genetically stable inbred C57 strain, thus suggesting

that SSTR3 receptor expression may be regulated. The regulation of SSTR3 expression has previously been reported in neuronal cilia, whereby agonist treatment with somatostatin decreases SSTR3 expression via a β-arrestin-dependent mechanism (Green et al., 2016). Interestingly, the expression of SSTR3 is suggested to be restricted to the primary cilia within islets (Iwanaga et al., 2011) and therefore, like within neuronal cilia, its expression may also be regulated by somatostatin. This dynamic expression of SSTR3 may account for the expression differences observed between islets. Based on our findings and published studies, understanding the role of the poorly characterised SSTR3 in islet function may be impeded not only by inter-species variabilities but also intra-species variabilities in SSTR3 islet expression.

Whilst exclusivity in GPCR expression was observed between islet groups, a large proportion of GPCR mRNAs were commonly expressed by both human islets and both strains of mouse islets, 190 (57%) in total (Figure 3.4.12). Of the 190 commonly expressed GPCRs, genes encoding the 'classic' T2DM receptor targets GLP1R, FFAR1 and GPR119 were shown to be highly expressed, highlighting the suitability of using mouse islets to further evaluate the pharmacological properties of novel therapeutics for these receptors. In addition to the 'classic' T2DM receptors, a number of proposed novel targets were also shown to be commonly expressed as indicated in (Table 3.4.4). These receptors will be discussed further in the following section.

The suitability of using mouse islets as surrogate models to assess the function of novel T2DM GPCR targets in human islet function

The final aim of this chapter was to assess the suitability of using mouse islets to further explore the role of potential T2DM GPCR targets in human islet function. The

expression levels of 14 GPCR targets (Table 3.4.4) were compared in human and ICR mouse islets using a correlation plot (Figure 3.4.13). The data revealed a coefficient of determination of $r^2 = 0.531$, signifying a reasonable degree of similarity in expression between both human and mouse islets, suggesting that mouse islets may well be suited to predict the function of such GPCRs in human islets. However, it is important to note that expression comparisons should be performed for each GPCR to give a true indication of whether mouse islets are suitable for the prediction of GPCR function for the particular target of interest, as global regression analysis of multiple targets can mask the suitability of using mouse islets for specific targets of interest. It is also possible that although mRNA expression within the whole islet may be similar between species, differences in cell specific expression between islets of different species may exist, which may be of importance when assessing the suitability of assessing the functional role of GPCRs when using translation models.

Summary and future perspectives

In summary, the experiments and analyses described in this chapter reveal 1) the mRNA expression profiles of most non-odorant GPCRs in human and mouse islets, 2) compare GPCR expression profiles to highlight similarities and differences in GPCR expression between human and mouse islets and 3) assess whether mouse islets are suitable for assessing the function of novel GPCR targets in human islets based on expression levels.

The data generated in this chapter provides a comprehensive insight into the suitability of using mouse islets as surrogate tissue for human islet GPCR studies based on mRNA expression. However, there are limitations to this form of assessment that need to be considered. Firstly, the data presented does not include non-orthologue receptors

which may be present but were not screened. The mouse genome contains 95 extra non-odorant GPCRs which were not quantified and thus the degree of tissue-specific differences are likely to be underestimated. Furthermore, GPCR expression comparisons were based on mRNA expression and not protein, and thus does not take into account whether actual functional protein is expressed. Factors such as whether the actual protein is synthesised, undergoes post-translational modification, localises to the plasma membrane or whether cellular machinery required for protein function is present, cannot be determined by mRNA expression analysis. In addition, gene expression analysis is performed on whole islets which are comprised of multiple cells types and thus further analysis, such as single cell PCR, FACS purification of endocrine cell populations or immunohistochemistry is required to determine the cells in which the GPCRs are expressed. An added complication to performing such comparative analyses with whole islets is that the cell population proportions differ between both human and mouse islets. For example, the proportion of β-cells in human islets is less than that observed in mouse islets and therefore the expression levels of GPCRs by the β-cells of human islets are automatically likely to show reduced expression compared to mouse islets.

Thus, whilst there are limitations to this form of analysis, the data generated provide a substantial amount of information that can be utilised as a foundation for further enhancing our knowledge of the role of GPCRs in human islet function using mouse islets as translational models.

CHAPTER 4 – Secretome comparison

4.1 Background

G-protein coupled receptors are important regulators of islet function and they do so by mediating the actions of a variety of ligand classes, such as neurotransmitters, nutrients, bile acids, divalent cations and peptide ligands (Reimann and Gribble, 2016). Previous studies have revealed that approximately 30% of all GPCRs expressed on human islets are activated by peptide ligands and that approximately 50% of all peptide ligands are expressed within islets (Amisten et al., 2013). Such intra-islet GPCR peptide ligands include the 'classic' examples of glucagon and somatostatin but additional peptides such as PYY (Persaud and Bewick, 2014), KISS1 (Hauge-Evans et al., 2006), and UCN3 (van der Meulen et al., 2015) have also been shown to be expressed and exhibit a role in islet function.

Since the emergence of gene expression analysis techniques such as RNA sequencing, microarray and qPCR, increasing information has been gathered on tissue specific gene expression and such data have been utilised to identify genes encoding proteins which may play key roles in tissue function. However, understanding the function of such proteins in human tissues is highly dependent on tissue availability, and in the event of limited supply of human tissue, surrogate tissue from model animals is required. However, differences in islet gene expression (Dai et al., 2012) and islet architecture (Cabrera et al., 2006) between human and rodent islets have been documented, thus questioning the suitability of such translational models.

The experiments described in this chapter aim to compare the mRNA expression profiles of GPCR-peptide ligands ('Secretomes') in human islets with those of islets from the outbred ICR and the inbred C57/BL/6 (C57) mouse strains in order to assess whether mouse islets can be used as a suitable translational model to evaluate GPCR

peptide ligand function in human islets. In addition, the data generated within this chapter will form the basis for novel exploratory projects aimed at assessing the role of GPCR peptide ligands in islet function.

4.2 Aims

- Quantify the mRNA expression of GPCR peptide ligands in human islets and their orthologue counterparts in islets isolated from the outbred ICR and the inbred C57/BL6 mouse strains.
- Compare the GPCR peptide ligand expression profiles of human and mouse islets and highlight species differences and similarities.
- Identify GPCR peptide ligands of interest for future projects aimed at assessing their role in islet function.

4.3 Methods

4.3.1 Gene expression analysis

Human and mouse islet 'Secretomes' were determined by qPCR using Qiagen's QuantiTect primers and QuantiFast SYBR green mastermix. 159 GPCR peptide ligands and 145 mouse orthologues were screened for expression. The mRNA expression of 14 genes could not be determined due to primer unavailability or because mouse orthologues of human GPCR peptide ligand genes do not exist.

4.3.1.1 Isolation of human and mouse islets for mRNA quantification

As described in section 2.2.1, human islets were isolated from pancreases retrieved from four heart beating donors (2 male, 2 female) at the Islet Transplantation Units at King's College London, using a revised version of (Huang et al., 2004) the Edmonton protocol. The donors were between the ages of 43-59, were non-diabetic and had a BMI of 22-33kg/m^2.

Mouse islets were isolated *in-house* from male adult ICR and C57/BL6 mice aged 8-12 weeks as described in section 2.2.2. Approximately 200 isolated mouse and human islets per biological replicate were handpicked, dissolved in 1ml of TRIzol for 5mins before being stored at -80^{o}C awaiting RNA extraction and cDNA generation.

4.3.1.2 cDNA generation

Quantitative real time polymerase chain reaction (qPCR) was performed using the two step approach which requires the generation of cDNA prior to performing the qPCR. Firstly, total RNA was extracted from previously TRIzol harvested tissue as described in detail in section 2.3.1 and further purified and concentrated using Qiagen's RNeasy MiniElute Cleanup kit (section 2.3.2). The purified mRNA was then quantified as

described in section 2.3.3 and reversed transcribed into cDNA using the TaqMan Reverse Transcription kit (section 2.3.4).

4.3.1.3 Quantitative real time polymerase chain reaction

qPCR was performed using Qiagen's QuantiTect primers, Quantifast SYBR green master mix and the Roche LightCycler 480 using the settings described in section 2.3.5. GPCR peptide ligand expression data are represented as expression relative to the mRNA expression of the house keeping gene GAPDH.

4.4 Results

4.4.1 mRNA expression analysis of GPCR peptide ligands in human and mouse islets

The mRNA expression of 159 human GPCR peptide ligands and their mouse orthologous counterparts (145 in total) relative to the house keeping gene GAPDH in both human and mouse islets was quantified. Expression of islet peptide ligand family mRNAs have been presented alphabetically below.

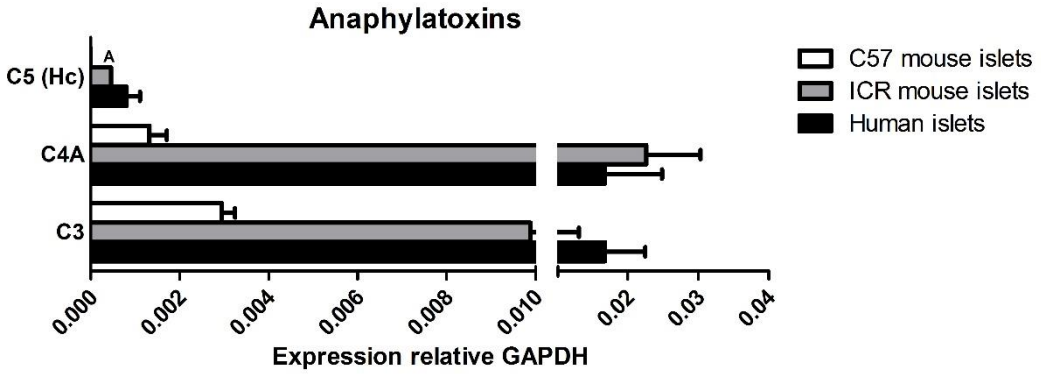

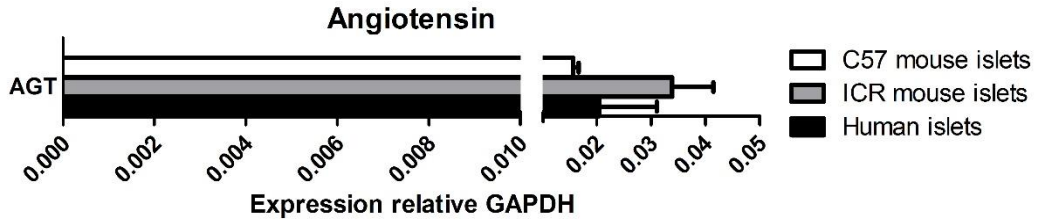

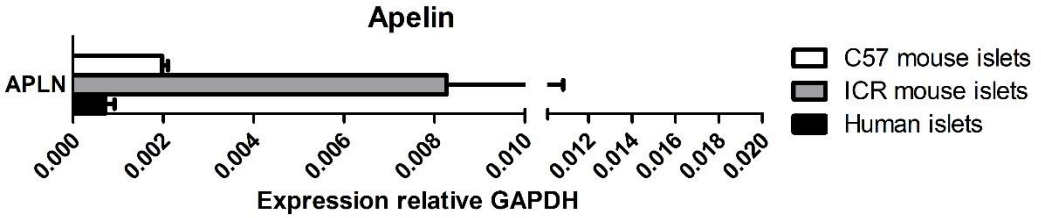

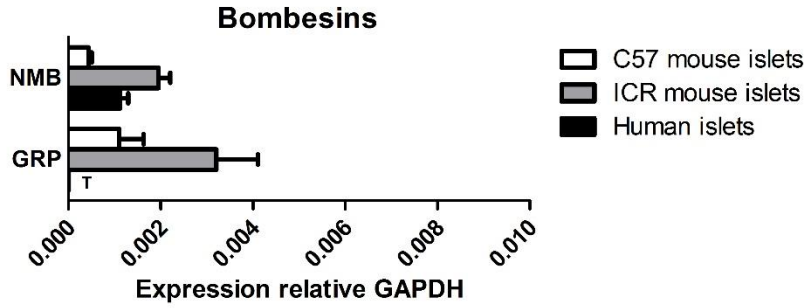
Bombesins
NMB
GRP
T
C57 mouse islets
ICR mouse islets
Human islets
0.000
0.002
0.004
0.006
0.008
0.010
Expression relative GAPDH

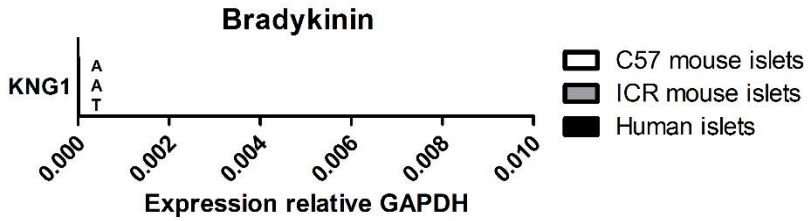
Bradykinin
KNG1
A
A
T
C57 mouse islets
ICR mouse islets
Human islets
0.000
0.002
0.004
0.006
0.008
0.010
Expression relative GAPDH

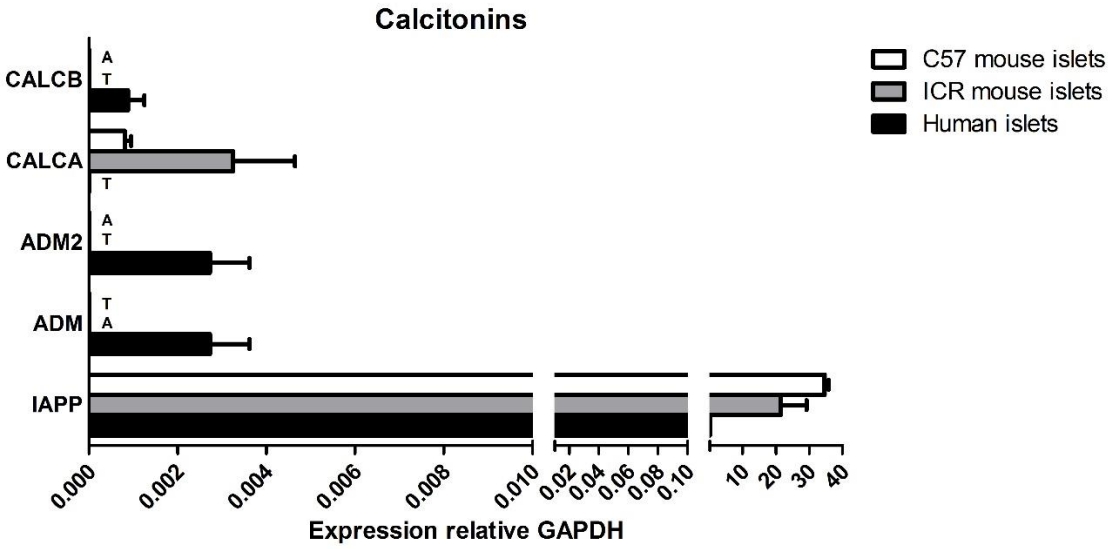
Calcitonins
CALCB
A
T
CALCA
T
ADM2
A
T
ADM
T
A
IAPP
C57 mouse islets
ICR mouse islets
Human islets
0.000
0.002
0.004
0.006
0.008
0.010
0.02
0.04
0.06
0.08
0.10
10
20
30
40
Expression relative GAPDH

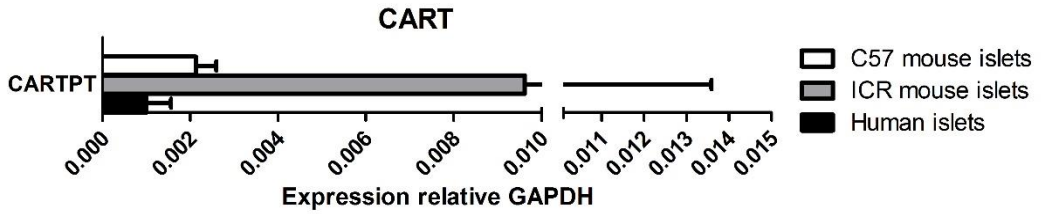
CART
CARTPT
C57 mouse islets
ICR mouse islets
Human islets
0.000
0.002
0.004
0.006
0.008
0.010
0.011
0.012
0.013
0.014
0.015
Expression relative GAPDH

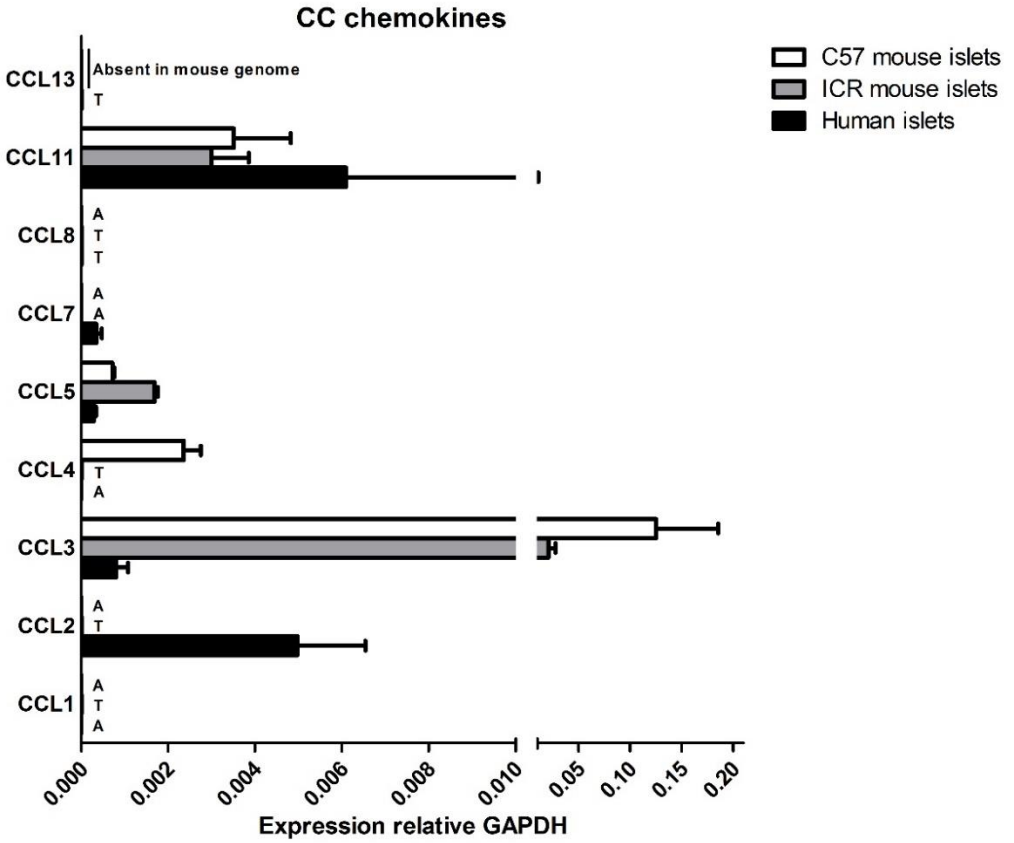
CC chemokines
C57 mouse islets
ICR mouse islets
Human islets
CCL13
Absent in mouse genome
T
CCL11
CCL8
A
T
T
CCL7
A
A
CCL5
CCL4
T
A
CCL3
CCL2
A
T
CCL1
A
T
A
0.000
0.002
0.004
0.006
0.008
0.010
0.05
0.10
0.15
0.20
Expression relative GAPDH

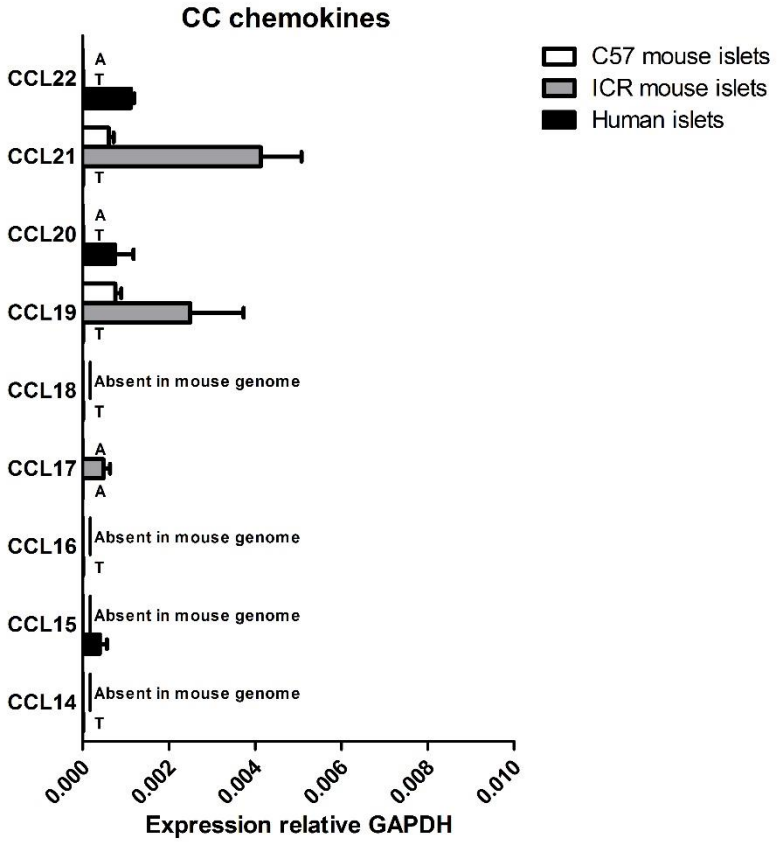
CC chemokines
C57 mouse islets
ICR mouse islets
Human islets
CCL22
A
T
CCL21
T
CCL20
A
T
CCL19
T
CCL18
Absent in mouse genome
T
CCL17
A
A
CCL16
Absent in mouse genome
T
CCL15
Absent in mouse genome
CCL14
Absent in mouse genome
T
0.000
0.002
0.004
0.006
0.008
0.010
Expression relative GAPDH

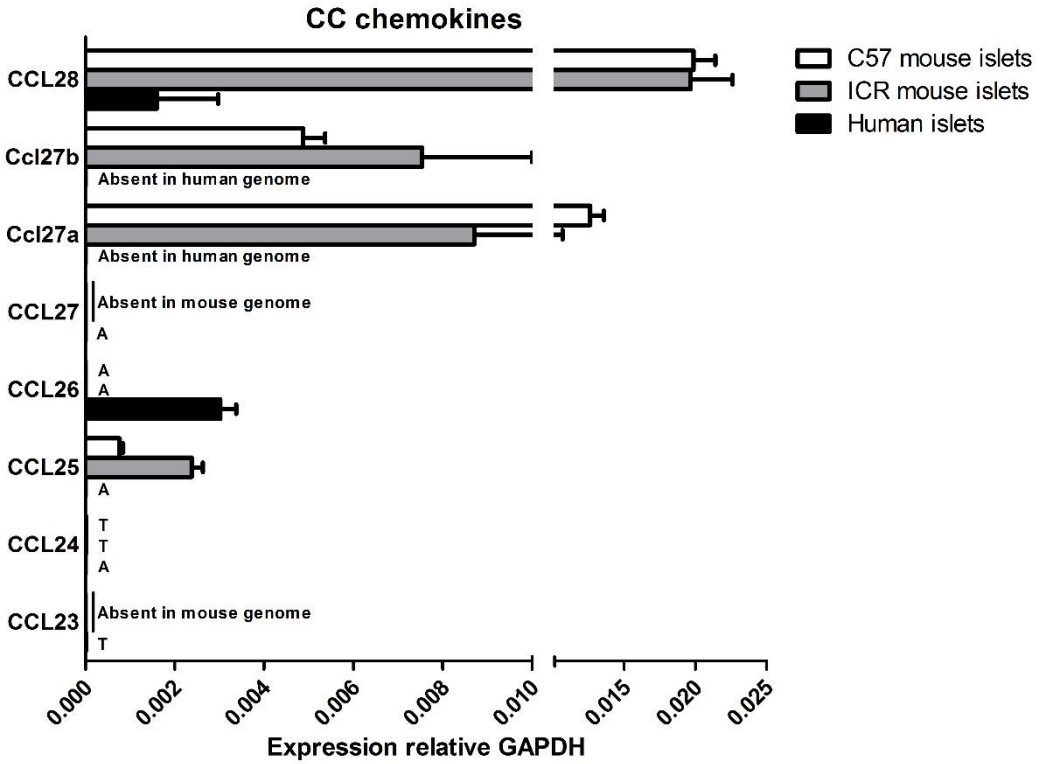
CC chemokines
CCL28
Ccl27b
Absent in human genome
Ccl27a
Absent in human genome
CCL27
Absent in mouse genome
A
CCL26
A
A
CCL25
A
CCL24
T
T
A
CCL23
Absent in mouse genome
T
0.000
0.002
0.004
0.006
0.008
0.010
0.015
0.020
0.025
Expression relative GAPDH
C57 mouse islets
ICR mouse islets
Human islets

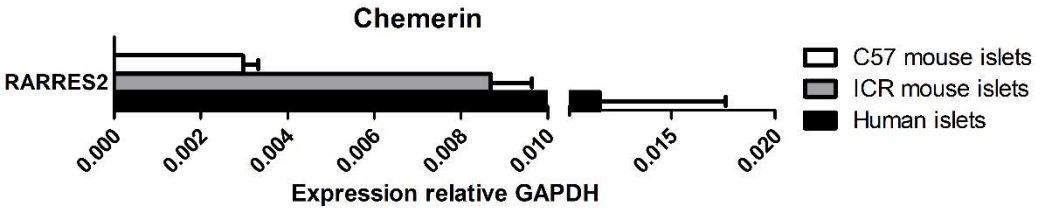
Chemerin
RARRES2
0.000
0.002
0.004
0.006
0.008
0.010
0.015
0.020
Expression relative GAPDH
C57 mouse islets
ICR mouse islets
Human islets

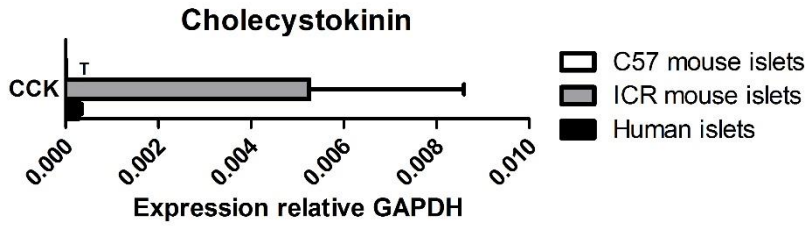
Cholecystokinin
CCK
T
0.000
0.002
0.004
0.006
0.008
0.010
Expression relative GAPDH
C57 mouse islets
ICR mouse islets
Human islets

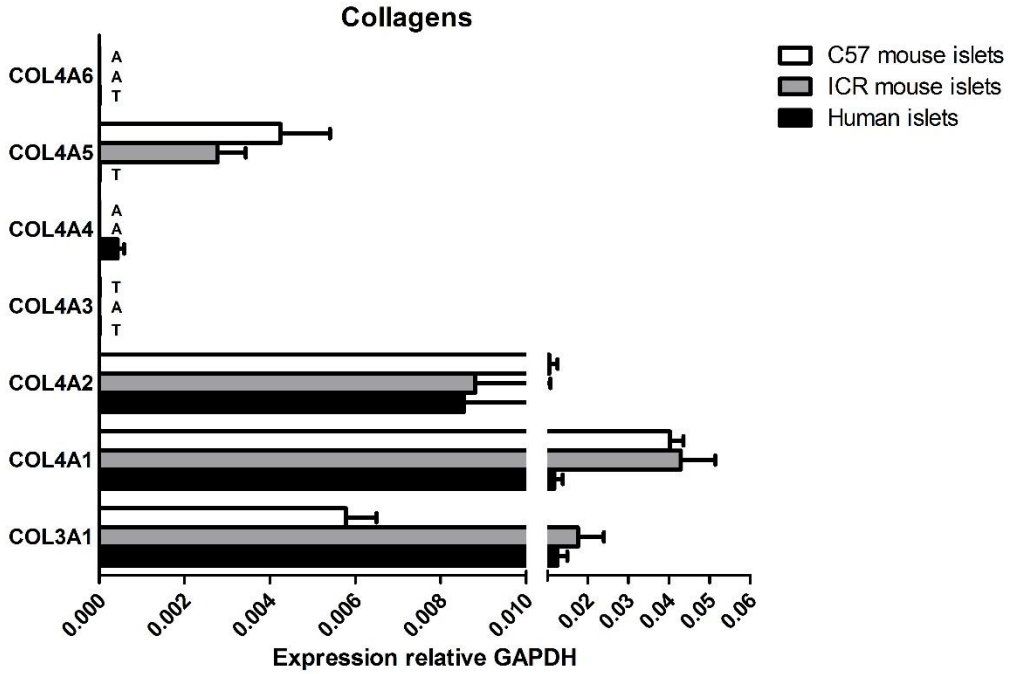
Collagens
C57 mouse islets
ICR mouse islets
Human islets
COL4A6
COL4A5
COL4A4
COL4A3
COL4A2
COL4A1
COL3A1
A A T
T
A A
T A T
0.000 0.002 0.004 0.006 0.008 0.010 0.02 0.03 0.04 0.05 0.06
Expression relative GAPDH

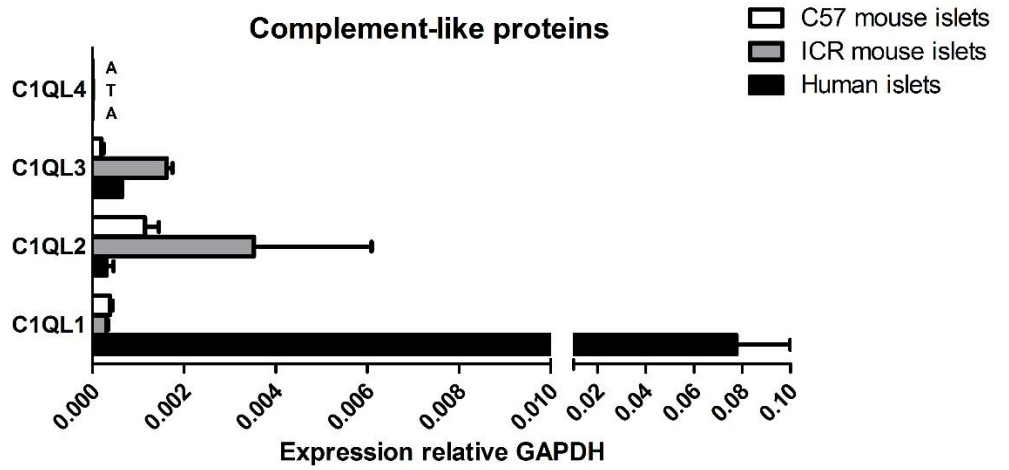
Complement-like proteins
C57 mouse islets
ICR mouse islets
Human islets
C1QL4
C1QL3
C1QL2
C1QL1
A T A
0.000 0.002 0.004 0.006 0.008 0.010 0.02 0.04 0.06 0.08 0.10
Expression relative GAPDH

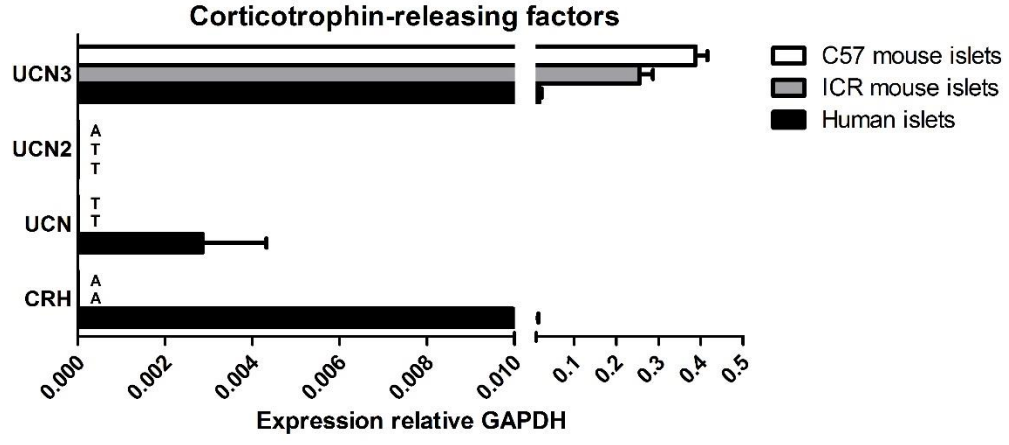
Corticotrophin-releasing factors
C57 mouse islets
ICR mouse islets
Human islets
UCN3
UCN2
UCN
CRH
A T T
T T
A A
0.000 0.002 0.004 0.006 0.008 0.010 0.1 0.2 0.3 0.4 0.5
Expression relative GAPDH

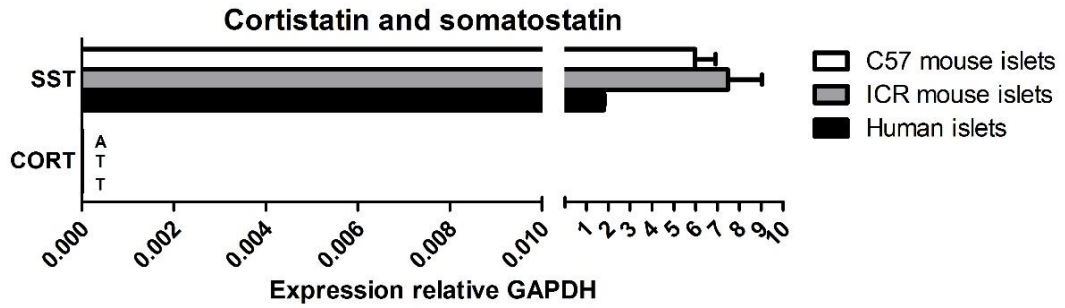
Cortistatin and somatostatin
SST
CORT
A
T
T
0.000
0.002
0.004
0.006
0.008
0.010
1
2
3
4
5
6
7
8
9
10
Expression relative GAPDH
C57 mouse islets
ICR mouse islets
Human islets

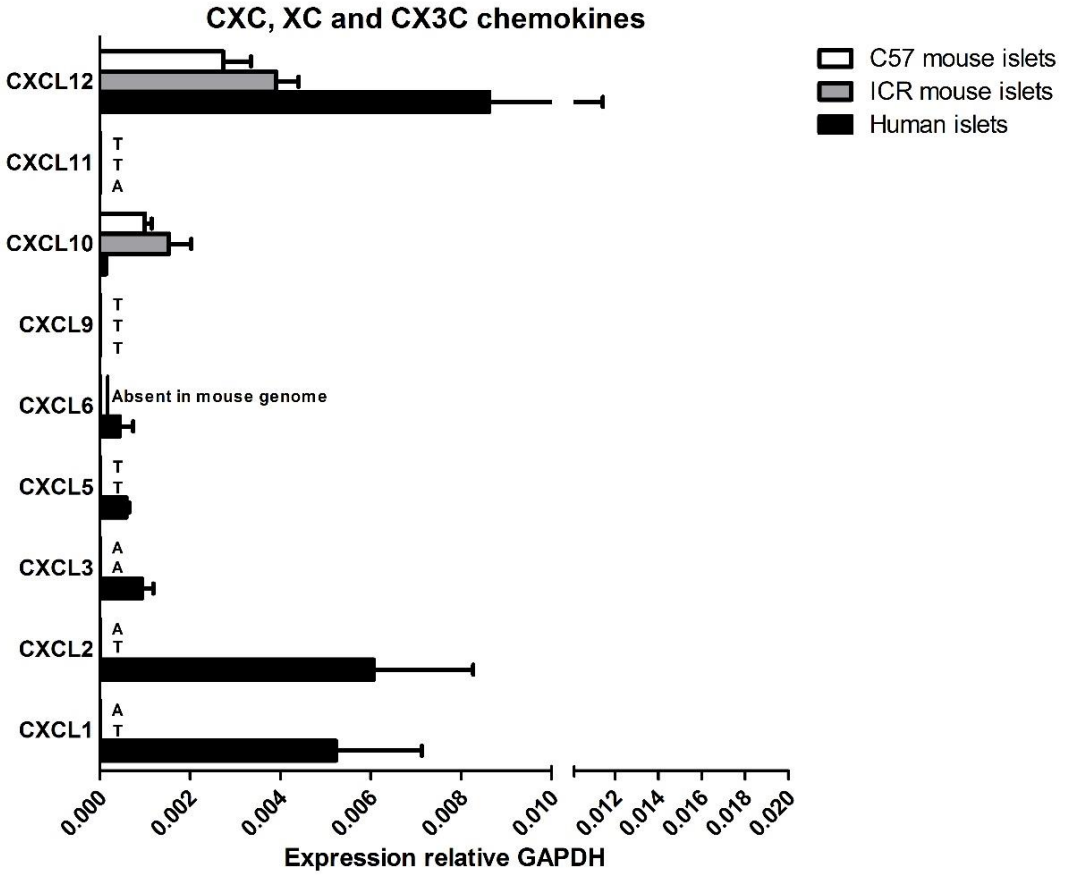
CXC, XC and CX3C chemokines
CXCL12
CXCL11
T
T
A
CXCL10
CXCL9
T
T
T
CXCL6
Absent in mouse genome
CXCL5
T
T
CXCL3
A
A
CXCL2
A
T
CXCL1
A
T
0.000
0.002
0.004
0.006
0.008
0.010
0.012
0.014
0.016
0.018
0.020
Expression relative GAPDH
C57 mouse islets
ICR mouse islets
Human islets

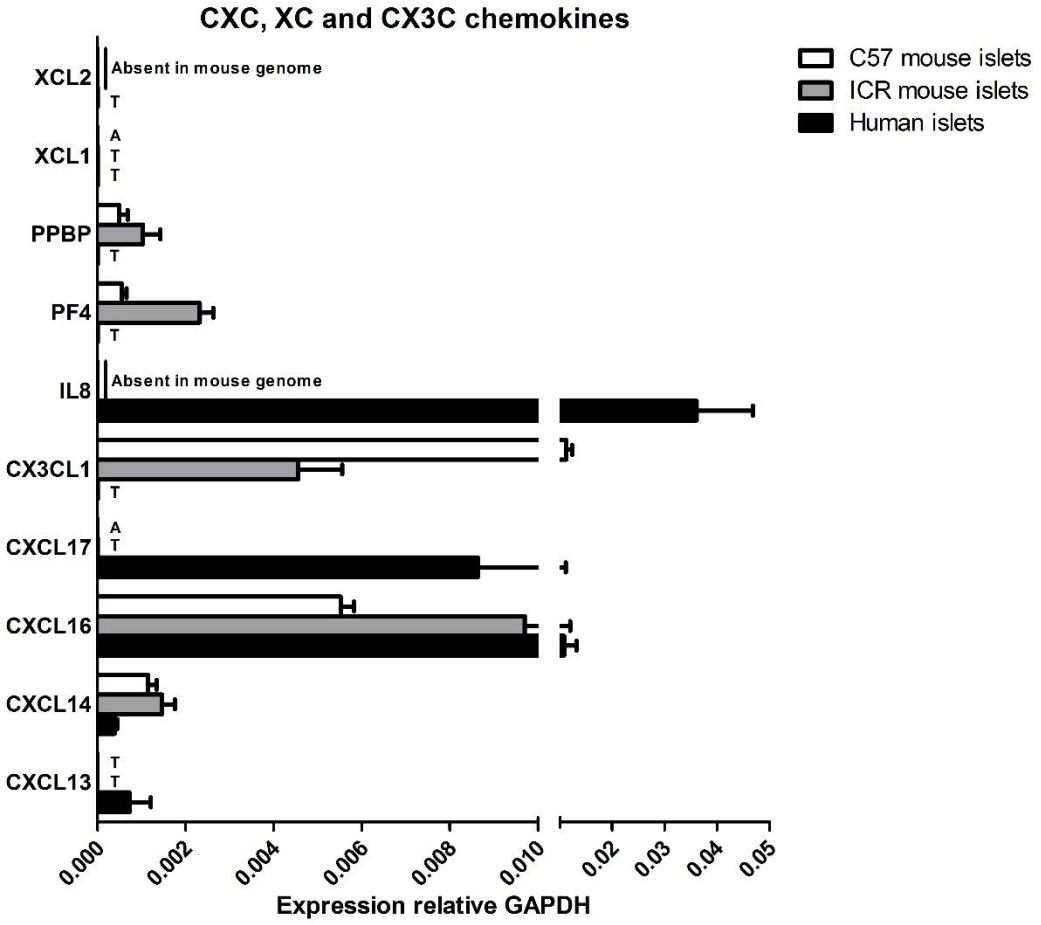
CXC, XC and CX3C chemokines
C57 mouse islets
ICR mouse islets
Human islets
XCL2
Absent in mouse genome
T
XCL1
A
T
T
PPBP
T
PF4
T
IL8
Absent in mouse genome
CX3CL1
T
CXCL17
A
T
CXCL16
CXCL14
CXCL13
T
T
0.000
0.002
0.004
0.006
0.008
0.010
0.02
0.03
0.04
0.05
Expression relative GAPDH

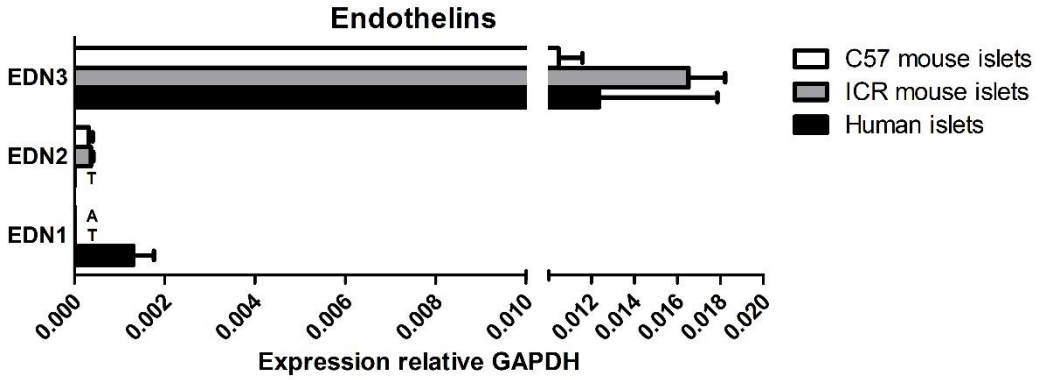
Endothelins
C57 mouse islets
ICR mouse islets
Human islets
EDN3
EDN2
T
EDN1
A
T
0.000
0.002
0.004
0.006
0.008
0.010
0.012
0.014
0.016
0.018
0.020
Expression relative GAPDH

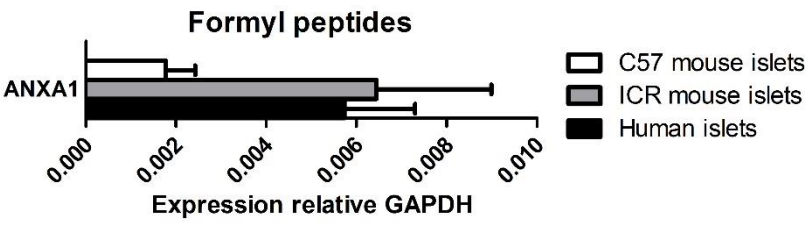
Formyl peptides
C57 mouse islets
ICR mouse islets
Human islets
ANXA1
0.000
0.002
0.004
0.006
0.008
0.010
Expression relative GAPDH

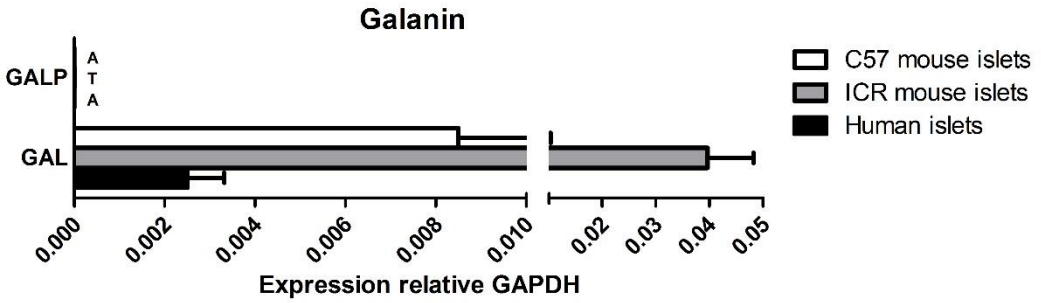
Galanin
GALP
A
T
A
GAL
C57 mouse islets
ICR mouse islets
Human islets
0.000
0.002
0.004
0.006
0.008
0.010
0.02
0.03
0.04
0.05
Expression relative GAPDH

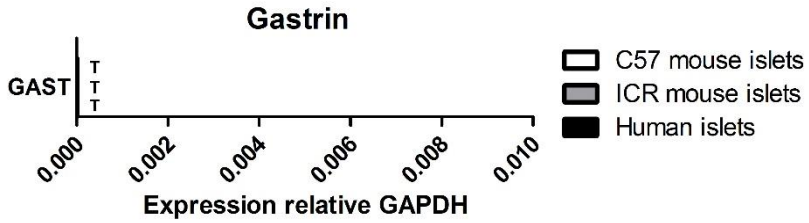
Gastrin
GAST
T
T
T
C57 mouse islets
ICR mouse islets
Human islets
0.000
0.002
0.004
0.006
0.008
0.010
Expression relative GAPDH

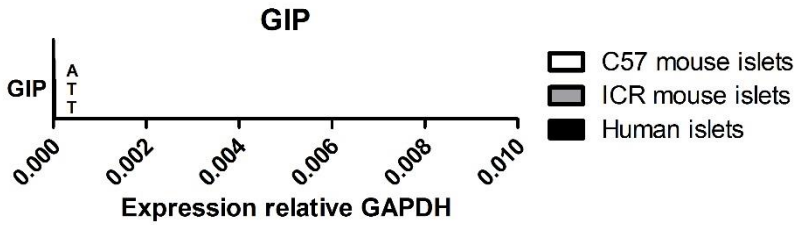
GIP
GIP
A
T
T
C57 mouse islets
ICR mouse islets
Human islets
0.000
0.002
0.004
0.006
0.008
0.010
Expression relative GAPDH

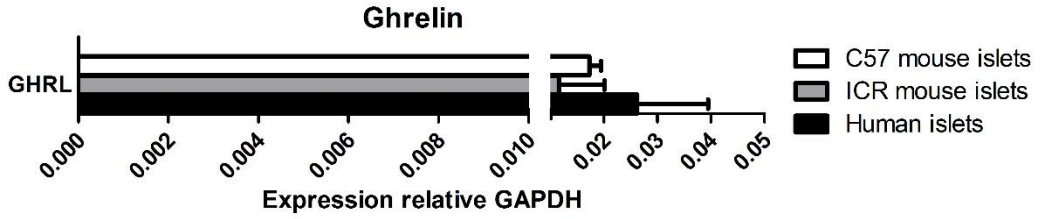
Ghrelin
GHRL
C57 mouse islets
ICR mouse islets
Human islets
0.000
0.002
0.004
0.006
0.008
0.010
0.02
0.03
0.04
0.05
Expression relative GAPDH

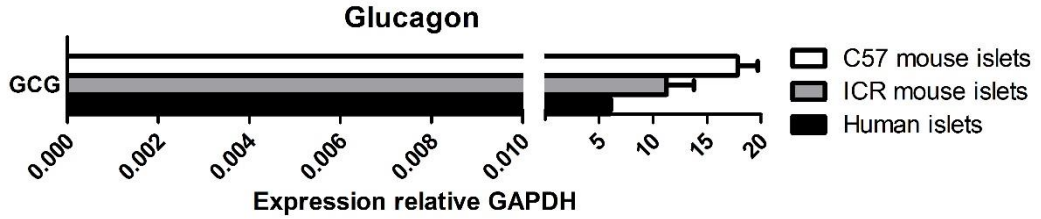
Glucagon
GCG
C57 mouse islets
ICR mouse islets
Human islets
0.000
0.002
0.004
0.006
0.008
0.010
5
10
15
20
Expression relative GAPDH

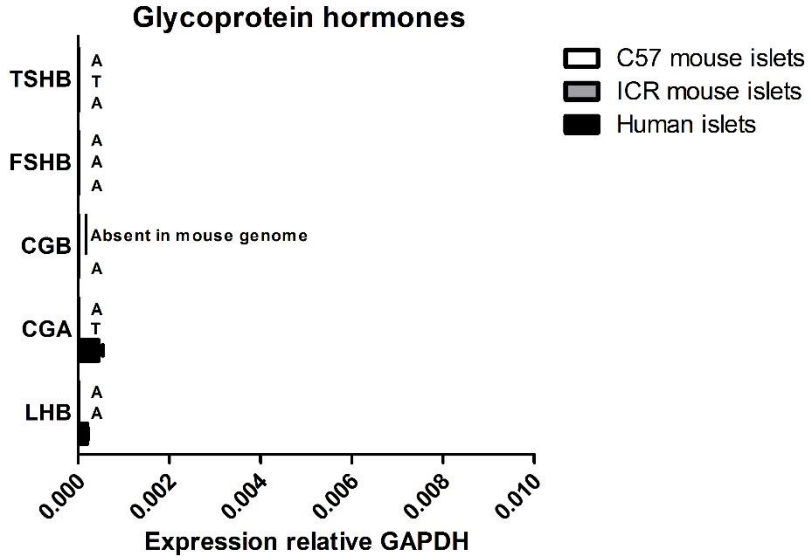
Glycoprotein hormones
TSHB
FSHB
CGB
CGA
LHB
Absent in mouse genome
C57 mouse islets
ICR mouse islets
Human islets
0.000
0.002
0.004
0.006
0.008
0.010
Expression relative GAPDH

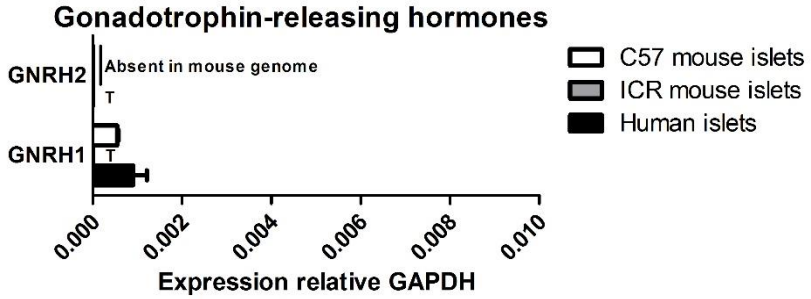
Gonadotrophin-releasing hormones
GNRH2
GNRH1
Absent in mouse genome
C57 mouse islets
ICR mouse islets
Human islets
0.000
0.002
0.004
0.006
0.008
0.010
Expression relative GAPDH

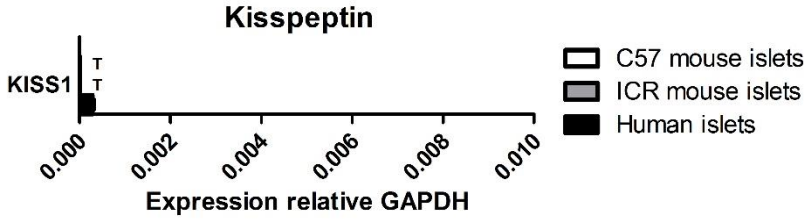
Kisspeptin
KISS1
C57 mouse islets
ICR mouse islets
Human islets
0.000
0.002
0.004
0.006
0.008
0.010
Expression relative GAPDH

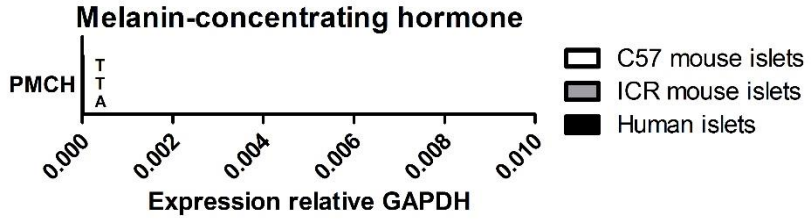
Melanin-concentrating hormone
PMCH
C57 mouse islets
ICR mouse islets
Human islets
0.000
0.002
0.004
0.006
0.008
0.010
Expression relative GAPDH

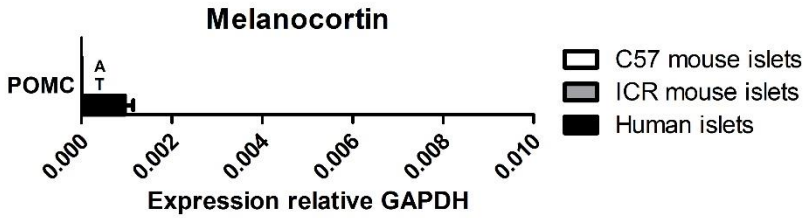
Melanocortin
POMC
A
T
C57 mouse islets
ICR mouse islets
Human islets
0.000
0.002
0.004
0.006
0.008
0.010
Expression relative GAPDH

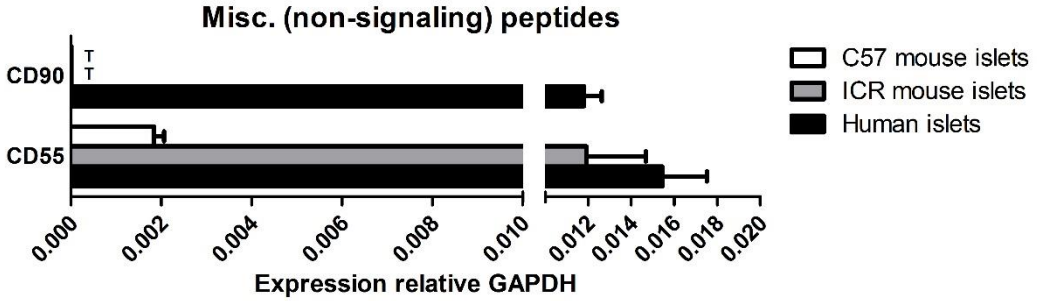
Misc. (non-signaling) peptides
CD90
CD55
T
T
C57 mouse islets
ICR mouse islets
Human islets
0.000
0.002
0.004
0.006
0.008
0.010
0.012
0.014
0.016
0.018
0.020
Expression relative GAPDH

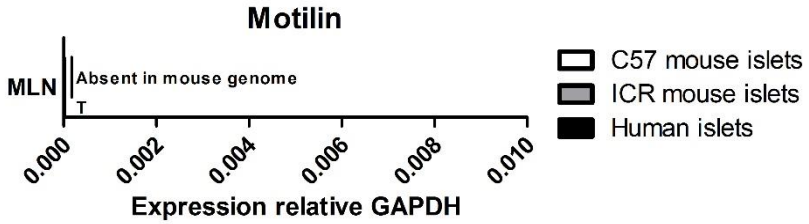
Motilin
MLN
Absent in mouse genome
T
C57 mouse islets
ICR mouse islets
Human islets
0.000
0.002
0.004
0.006
0.008
0.010
Expression relative GAPDH

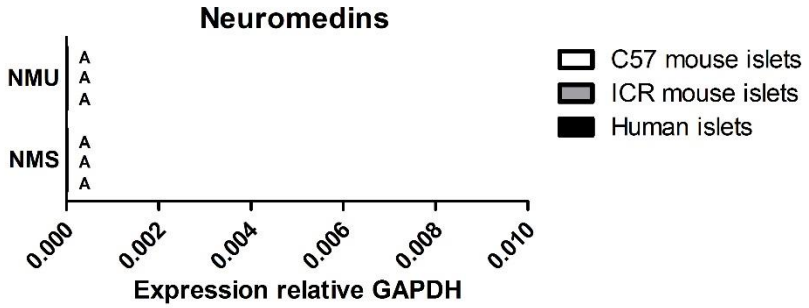
Neuromedins
NMU
NMS
A
A
A
C57 mouse islets
ICR mouse islets
Human islets
0.000
0.002
0.004
0.006
0.008
0.010
Expression relative GAPDH

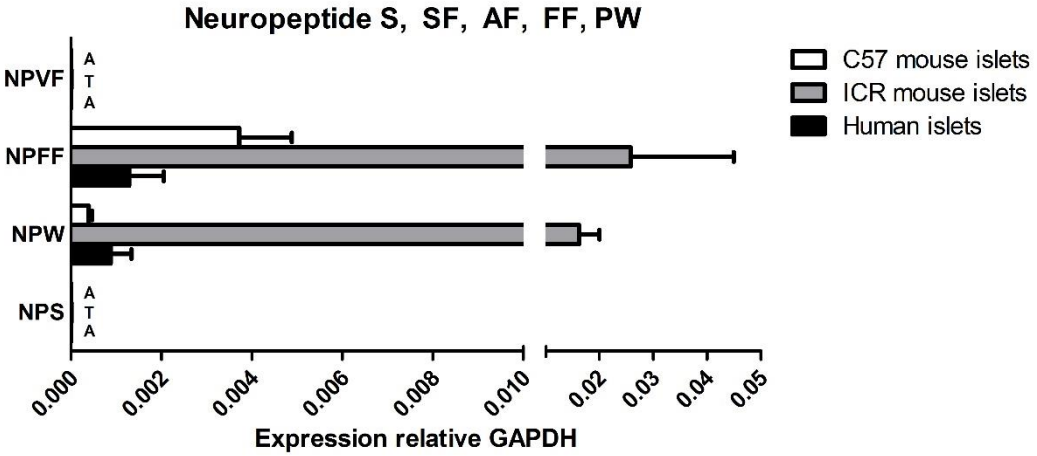
Neuropeptide S, SF, AF, FF, PW
NPVF
NPFF
NPW
NPS
C57 mouse islets
ICR mouse islets
Human islets
0.000
0.002
0.004
0.006
0.008
0.010
0.02
0.03
0.04
0.05
Expression relative GAPDH

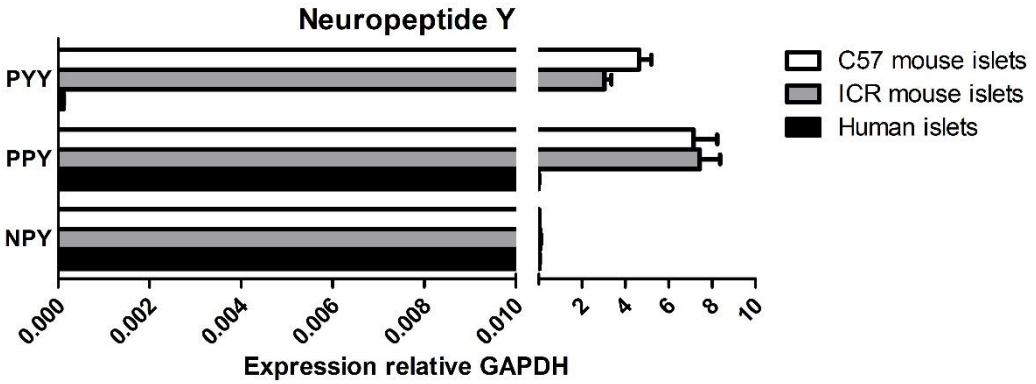
Neuropeptide Y
PYY
PPY
NPY
0.000
0.002
0.004
0.006
0.008
0.010
2
4
6
8
10
Expression relative GAPDH
C57 mouse islets
ICR mouse islets
Human islets

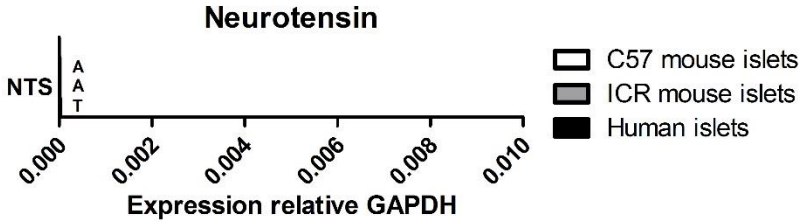
Neurotensin
NTS
A
A
T
0.000
0.002
0.004
0.006
0.008
0.010
Expression relative GAPDH
C57 mouse islets
ICR mouse islets
Human islets

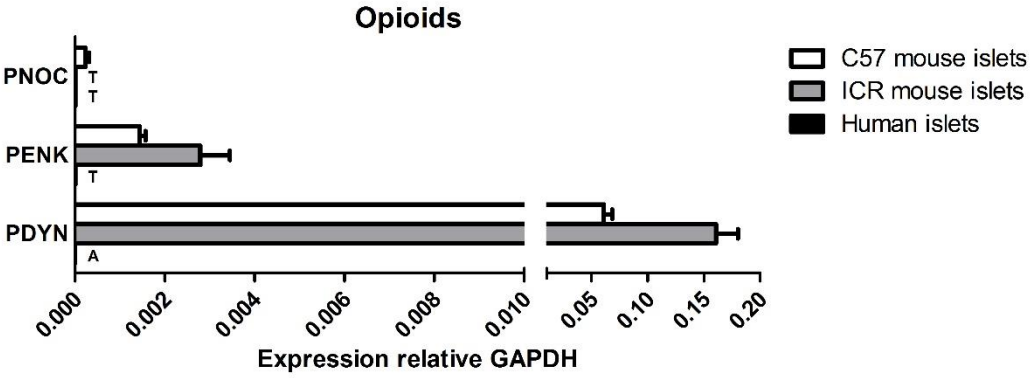
Opioids
PNOC
T
T
PENK
T
PDYN
A
0.000
0.002
0.004
0.006
0.008
0.010
0.05
0.10
0.15
0.20
Expression relative GAPDH
C57 mouse islets
ICR mouse islets
Human islets

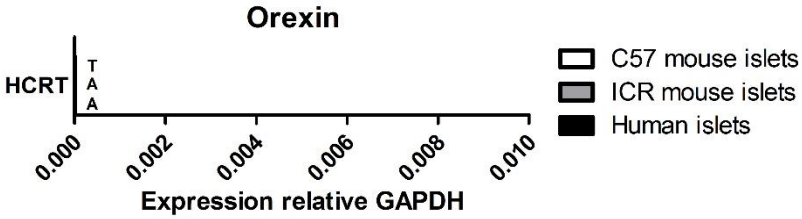
Orexin
HCRT
T
A
A
0.000
0.002
0.004
0.006
0.008
0.010
Expression relative GAPDH
C57 mouse islets
ICR mouse islets
Human islets

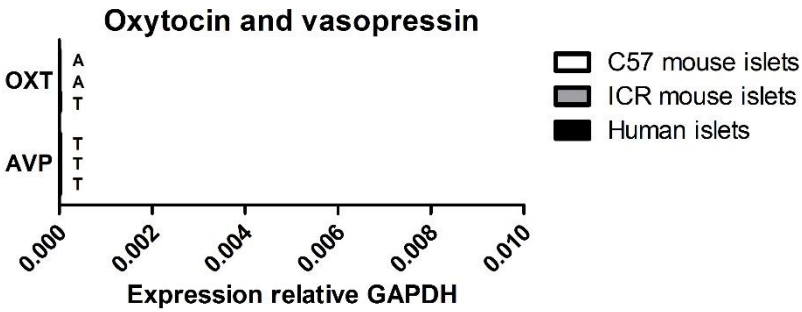
Oxytocin and vasopressin
OXT
A
A
T
AVP
T
T
T
0.000
0.002
0.004
0.006
0.008
0.010
Expression relative GAPDH
C57 mouse islets
ICR mouse islets
Human islets

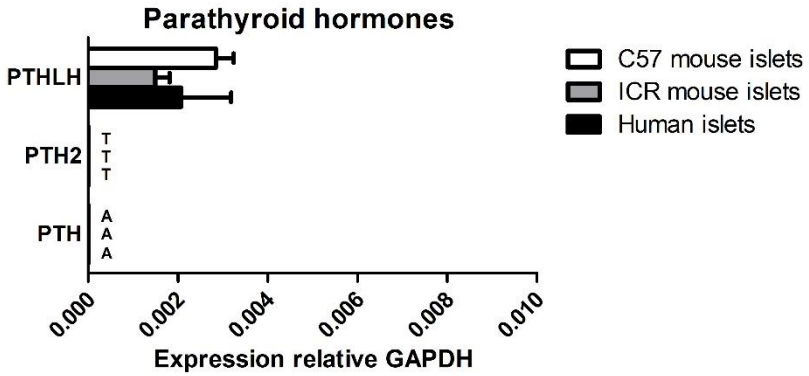
Parathyroid hormones
PTHLH
PTH2
PTH
T T T
A A A
0.000
0.002
0.004
0.006
0.008
0.010
Expression relative GAPDH
C57 mouse islets
ICR mouse islets
Human islets

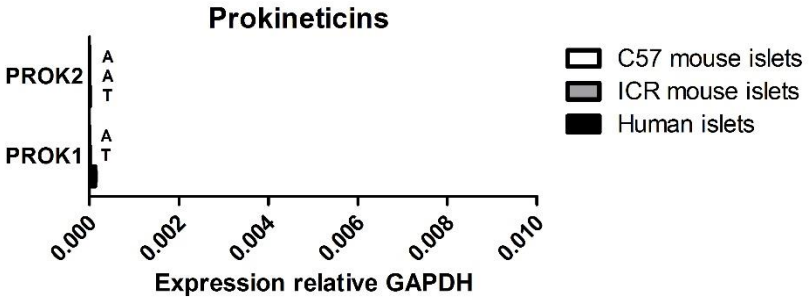
Prokineticins
PROK2
PROK1
A A T
A T
0.000
0.002
0.004
0.006
0.008
0.010
Expression relative GAPDH
C57 mouse islets
ICR mouse islets
Human islets

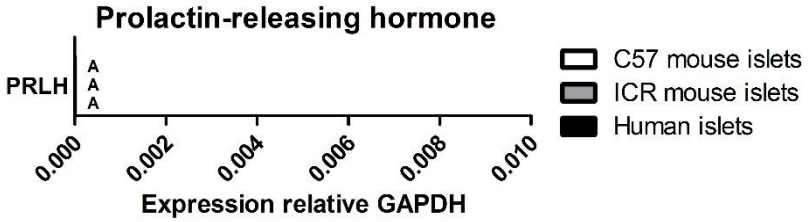
Prolactin-releasing hormone
PRLH
A A A
0.000
0.002
0.004
0.006
0.008
0.010
Expression relative GAPDH
C57 mouse islets
ICR mouse islets
Human islets

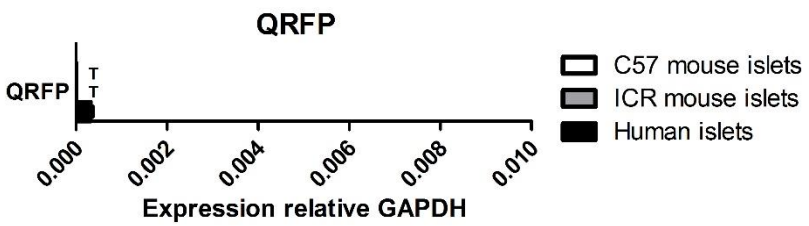
QRFP
QRFP
T T
0.000
0.002
0.004
0.006
0.008
0.010
Expression relative GAPDH
C57 mouse islets
ICR mouse islets
Human islets

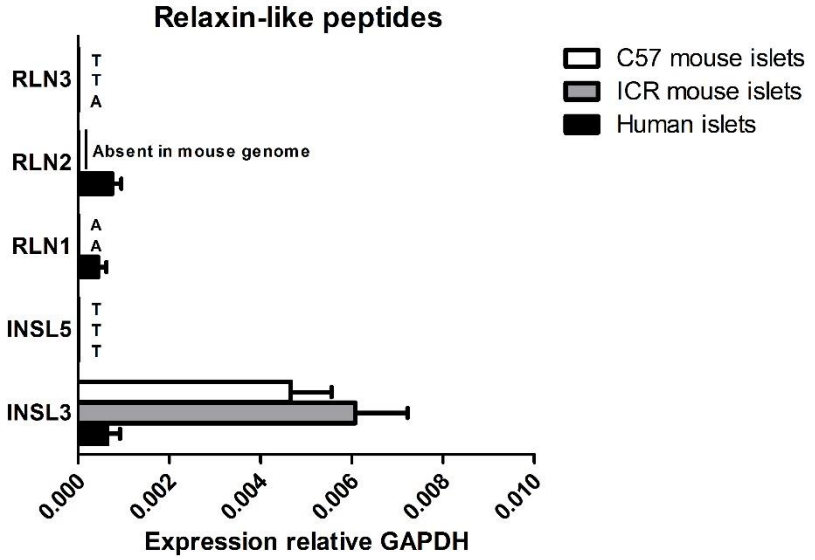
Relaxin-like peptides
C57 mouse islets
ICR mouse islets
Human islets
RLN3
T
T
A
RLN2
Absent in mouse genome
RLN1
A
A
INSL5
T
T
T
INSL3
0.000
0.002
0.004
0.006
0.008
0.010
Expression relative GAPDH

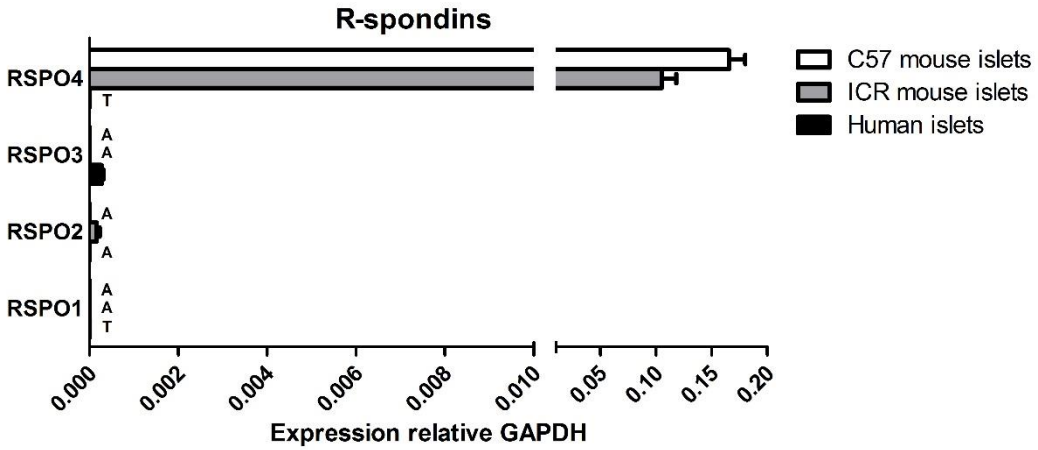
R-spondins
C57 mouse islets
ICR mouse islets
Human islets
RSPO4
T
RSPO3
A
A
RSPO2
A
A
RSPO1
A
A
T
0.000
0.002
0.004
0.006
0.008
0.010
0.05
0.10
0.15
0.20
Expression relative GAPDH

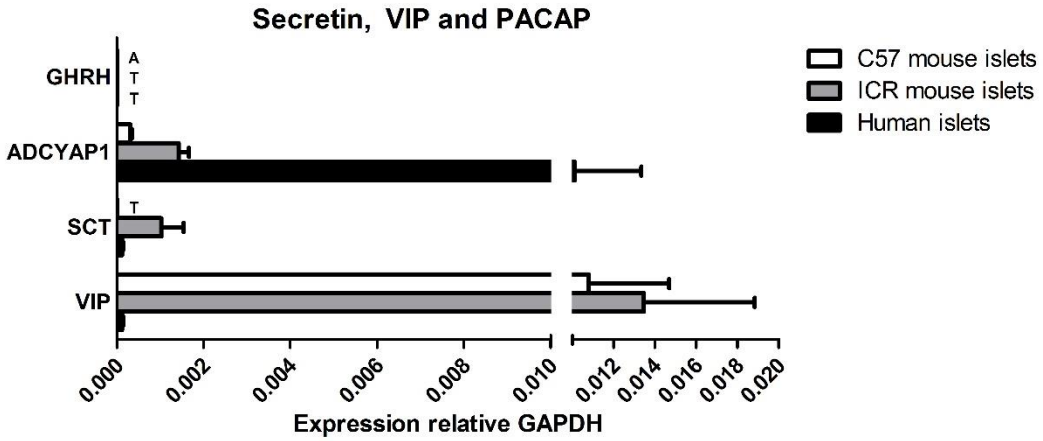
Secretin, VIP and PACAP
C57 mouse islets
ICR mouse islets
Human islets
GHRH
A
T
T
ADCYAP1
SCT
T
VIP
0.000
0.002
0.004
0.006
0.008
0.010
0.012
0.014
0.016
0.018
0.020
Expression relative GAPDH

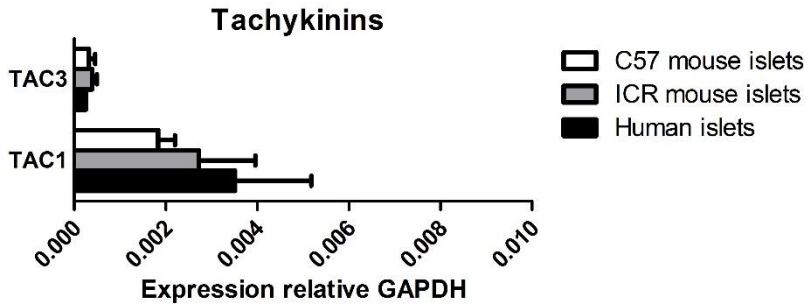
Tachykinins
TAC3
TAC1
C57 mouse islets
ICR mouse islets
Human islets
0.000
0.002
0.004
0.006
0.008
0.010
Expression relative GAPDH

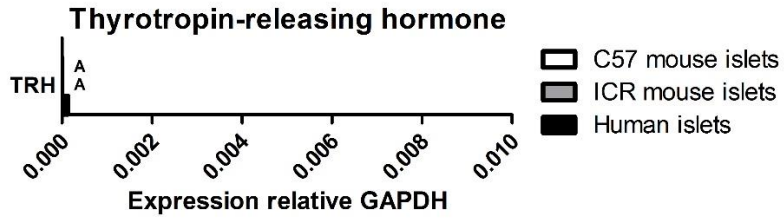
Thyrotropin-releasing hormone
TRH
A
A
C57 mouse islets
ICR mouse islets
Human islets
0.000
0.002
0.004
0.006
0.008
0.010
Expression relative GAPDH

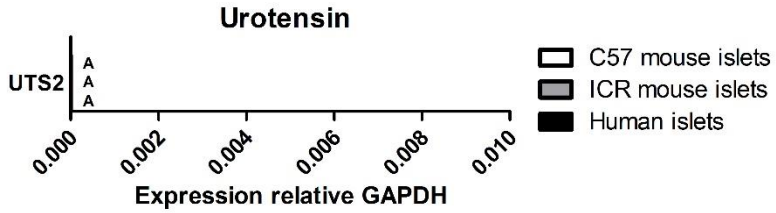
Urotensin
UTS2
A
A
A
C57 mouse islets
ICR mouse islets
Human islets
0.000
0.002
0.004
0.006
0.008
0.010
Expression relative GAPDH

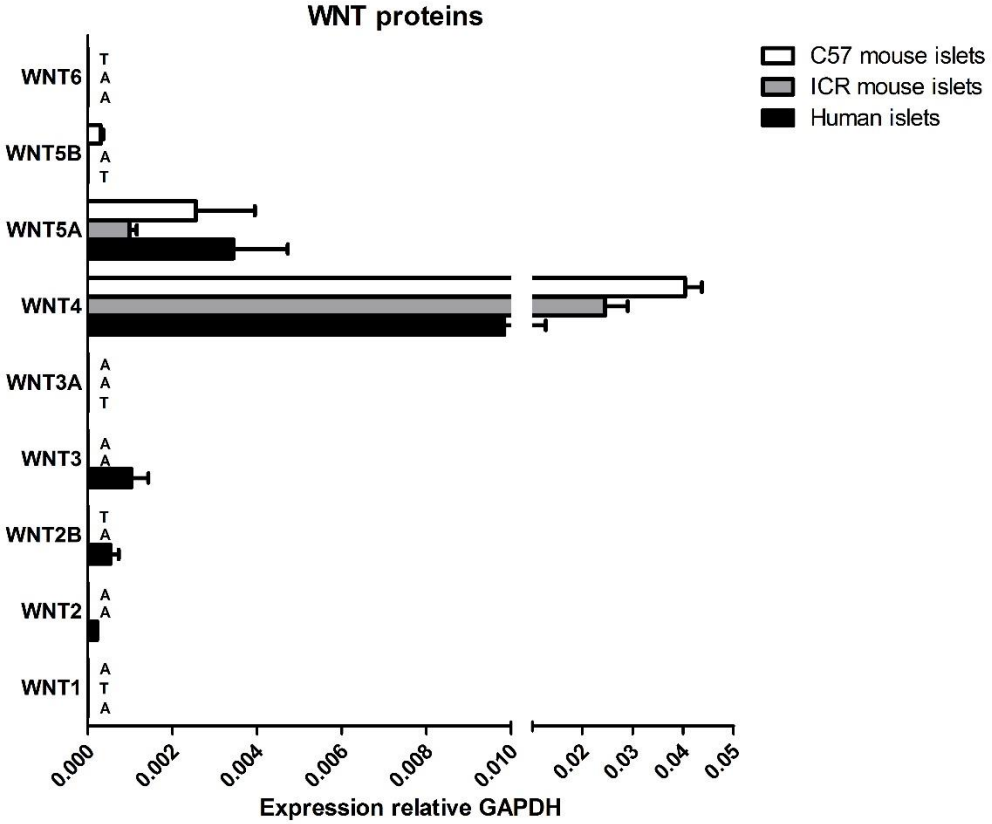
WNT proteins
WNT6
T
A
A
WNT5B
A
T
WNT5A
WNT4
WNT3A
A
A
T
WNT3
A
A
WNT2B
T
A
WNT2
A
A
WNT1
A
T
A
C57 mouse islets
ICR mouse islets
Human islets
0.000
0.002
0.004
0.006
0.008
0.010
0.02
0.03
0.04
0.05
Expression relative GAPDH

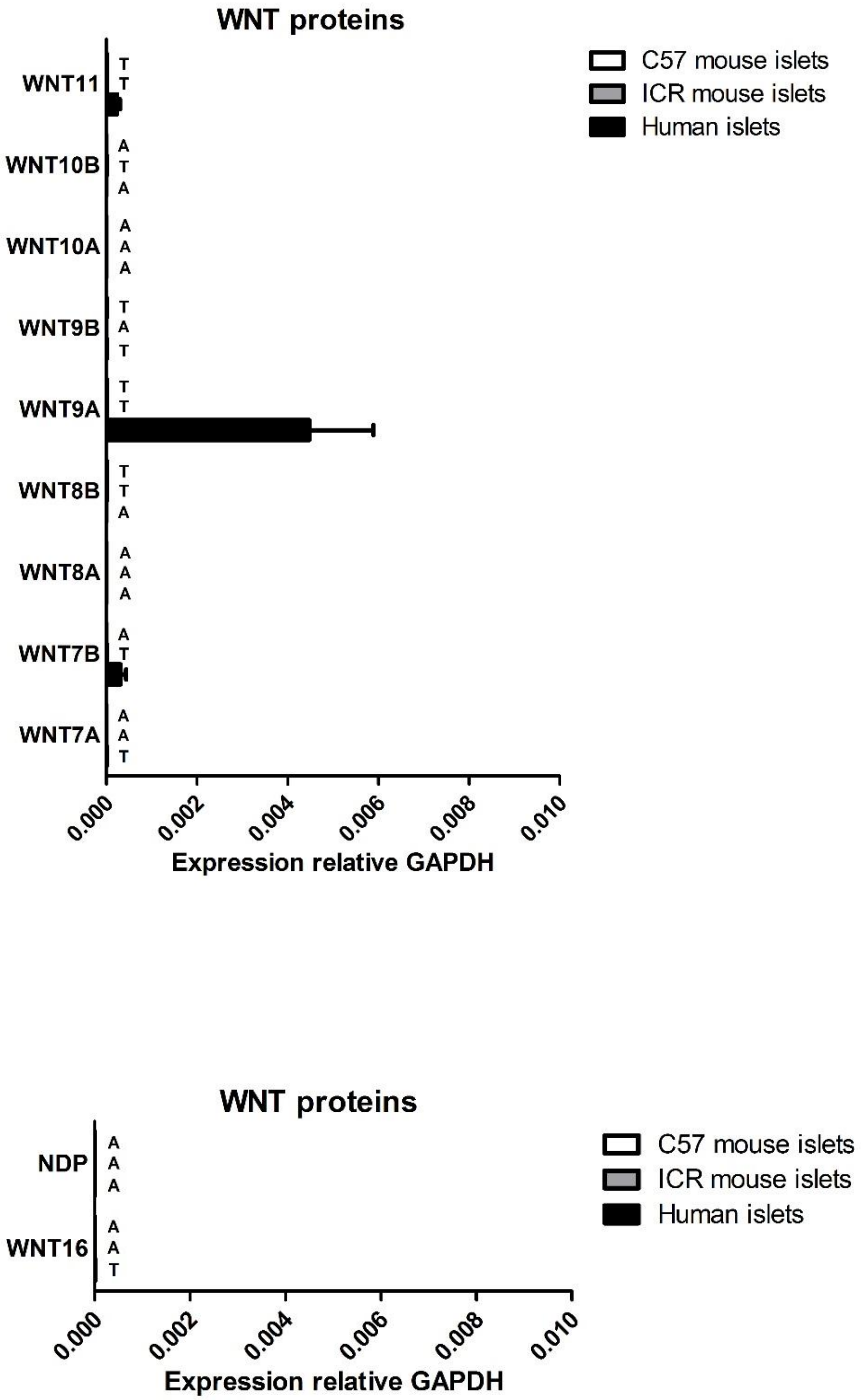

Figure 4.4.1 Column plots of GPCR peptide ligand mRNA expression in human and mouse islets. Expression data are grouped into peptide families and arranged in alphabetical order. Data are expressed as mean + SEM relative to the mRNA expression of GAPDH, from four biological replicates for each islet group. T = trace expression, A = absent expression.

Analysis of GPCR peptide ligand mRNA expression revealed that of the 159 genes screened in human islets, 85 (53%) genes were expressed and quantified, 43 (27%) were present at non-quantifiable trace levels (i.e <0.001% of the mRNA expression of GAPDH) and 31 (20%) were absent (Figure 4.4.2). Of the 145 mouse GPCR peptide ligand orthologues screened for expression in ICR mouse islets, 61 (42%) were expressed and quantified, 48 (33%) were expressed at trace level and 36 (25%) were absent (Figure 4.4.3). In C57 mouse islets, 61 (42%) peptide ligands were expressed and quantified, 25 (17%) were expressed at trace level whilst 59 (41%) were absent (Figure 4.4.4).

To highlight the rank order of GPCR peptide ligand expression, mRNA expression dot plots were generated for each islet group. Within human islets, the top ten highest expressed GPCR peptide ligands were GCG, SST, IAPP, C1QL1, NPY, IL8, GHRL, AGT, PPY and UCN3 (Figure 4.4.5). In ICR mouse islets, the ten highest expressed peptide ligands were Iapp, Gcg, Sst, Ppy, Pyy, Ucn3, Pdyn, Rspo4, Npy and Col4a (Figure 4.4.6), whereas in C57 mouse islets the ten highest expressing peptide ligands were Iapp, Gcg, Ppy, Sst, Pyy, Ucn3, Rspo4, Pdyn, Wnt4 and Col4a (Figure 4.4.7). A summary of this information can be found in Table 4.4.1.

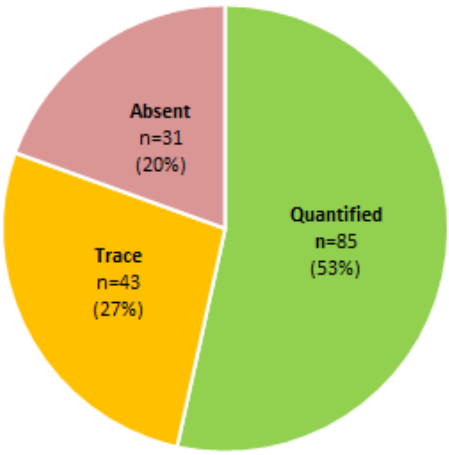

Figure 4.4.2 Proportional analysis of GPCR peptide ligand mRNA expression in human islets.

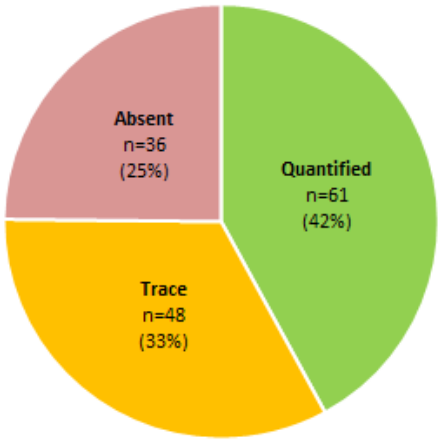

Figure 4.4.3 Proportional analysis of orthologue GPCR peptide ligand mRNA expression in ICR mouse islets.

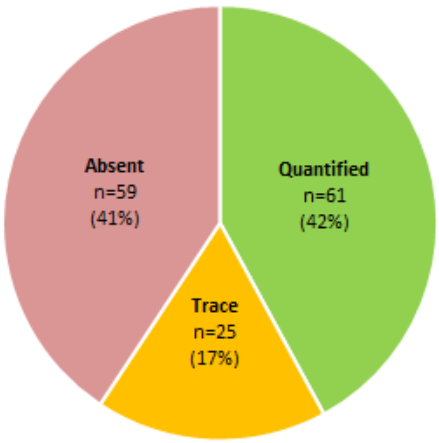

Figure 4.4.4 Proportional analysis of orthologue GPCR peptide ligand mRNA expression in C57 mouse islets.

Table 4.4.1 Rank order of the top ten highest expressed orthologue GPCR peptide ligand mRNAs in human and mouse islets. % total indicates expression as a percent of total GPCR peptide ligand expression relative to GAPDH mRNA.

	Human		**ICR**		**C57**	
Rank	*Ligand*	*% of total ligand mRNA expression*	*Ligand*	*% of total ligand mRNA expression*	*Ligand*	*% of total ligand mRNA expression*
1	GCG	71.28	Iapp	41.42	Iapp	48.73
2	SST	21.28	Gcg	21.78	Gcg	25.05
3	IAPP	1.47	Sst	14.46	Ppy	10.04
4	C1QL1	0.92	Ppy	14.40	Sst	8.38
5	NPY	0.57	Pyy	5.89	Pyy	6.51
6	IL8	0.43	Ucn3	0.49	Ucn3	0.55
7	GHRL	0.31	Pdyn	0.31	Rspo4	0.23
8	AGT	0.24	Rspo4	0.20	Pdyn	0.09
9	PPY	0.23	Npy	0.17	Wnt4	0.06
10	UCN3	0.21	Col4a1	0.08	Col4a1	0.06

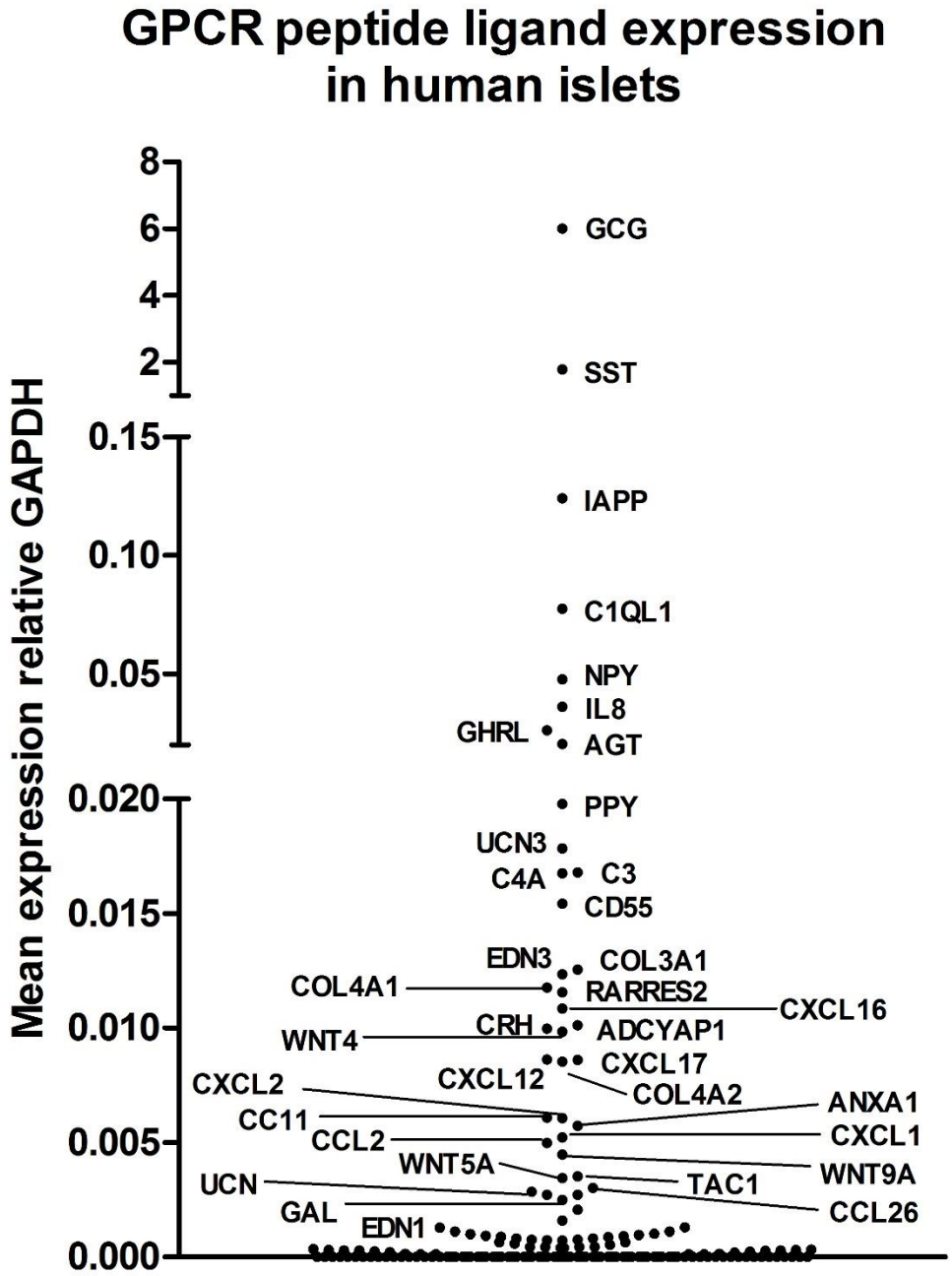

Figure 4.4.5 A dot plot representing the mRNA expression of 159 GPCR peptide ligands in human islets. Data are expressed as mean expression relative to GAPDH from four biological replicates.

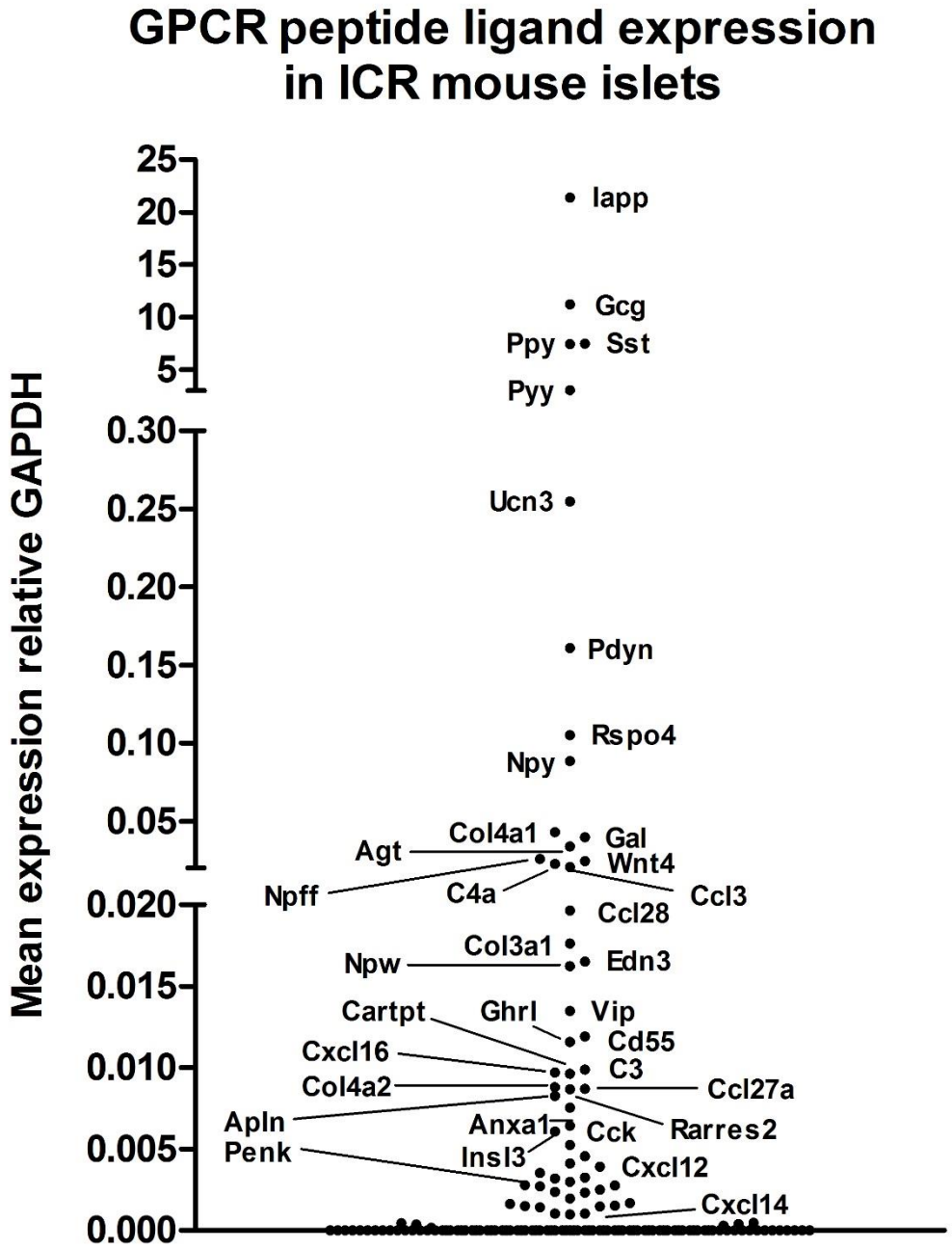

Figure 4.4.6 A dot plot representing the mRNA expression of 145 orthologue GPCR peptide ligands in ICR mouse islets. Data are expressed as mean expression relative to Gapdh from four biological replicates.

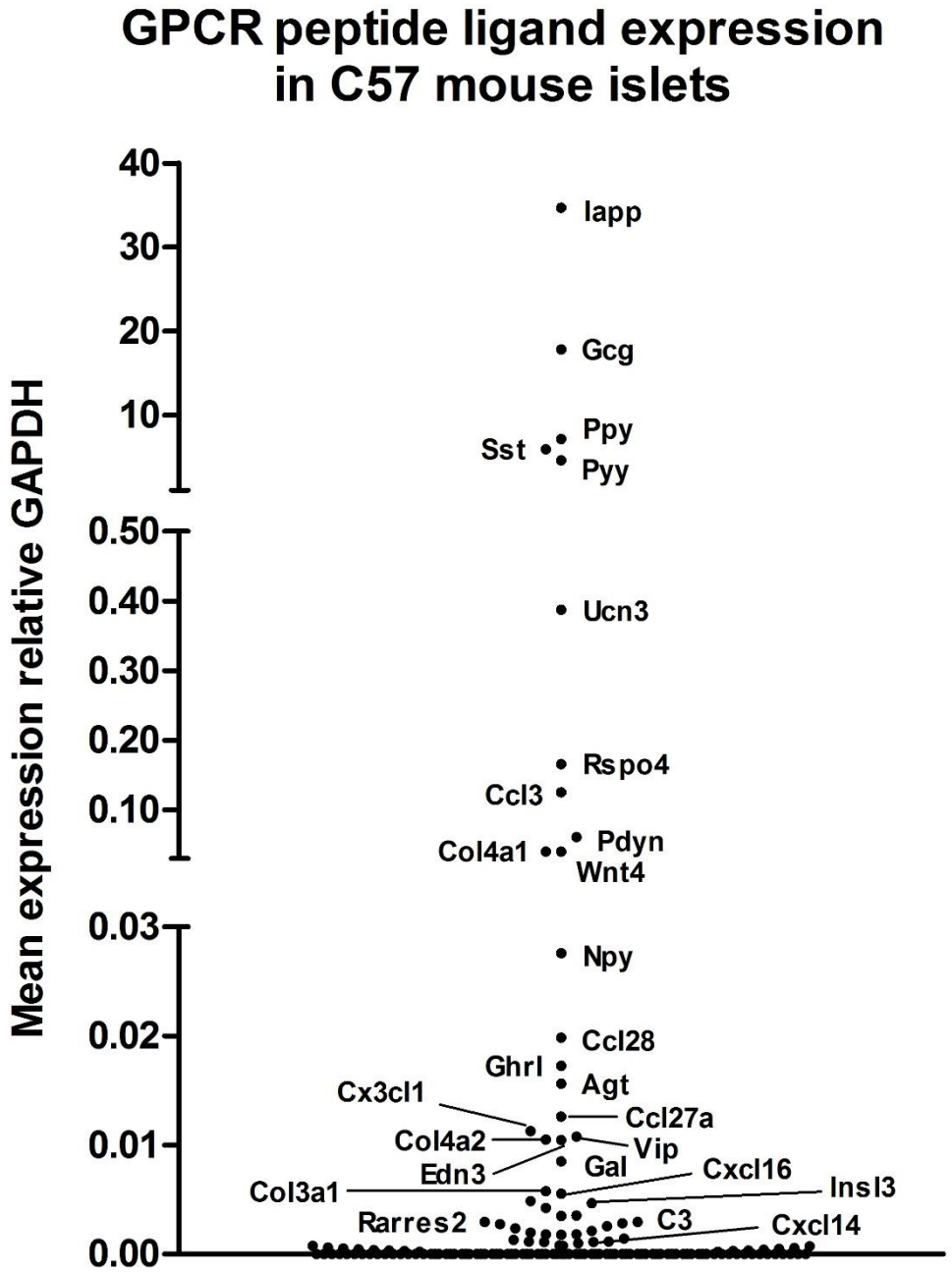

Figure 4.4.7 A dot plot representing the mRNA expression of 145 orthologue GPCR peptide ligands in C57 mouse islets. Data are expressed as mean expression relative to Gapdh from four biological replicates.

4.4.2 A comparison of GPCR peptide ligand expression profiles between human and mouse islets.

A comparison of orthologue GPCR peptide ligand mRNA expression profiles between the islets groups was performed using regression analysis and quantified by defining a coefficient of determination (r^2). In order to incorporate the absent and trace expressed peptides, which could not be reliably quantified relative to the house keeping gene GAPDH, into the r^2 calculation, the trace and absent expressed peptides were assigned expression values of 0.00001 and 0.000001 relative to GAPDH respectively.

A linear regression comparison of GPCR peptide ligand expression between human and the mouse ICR islets revealed a low degree of similarity with an r^2 value of 0.245 (Figure 4.4.8). Similarly, an r^2 value of 0.225 was determined when comparing GPCR peptide ligand expression between human and C57 mouse islets (Figure 4.4.9). A high degree of similarity in GPCR peptide ligand expression was observed between the inbred and outbred mouse strains as indicated by an r^2 value of 0.968 (Figure 4.4.10).

In order to further quantify the extent of orthologue GPCR peptide ligand expression overlap, as well as highlight distinct expression differences between the islet groups, Venn analysis was performed (Figure 4.4.11). Of the 145 GPCR peptide ligand orthologues screened, 71 GPCR ligands expressed above trace levels were commonly expressed in human islets and both strains of mouse islets, a list of which can be found in Table 4.4.2. Species and strain specific GPCR peptide ligand mRNA expression was also observed within the islet groups with 20, 10 and 2 ligands only expressed within human, ICR and C57 islets respectively (Table 4.4.3).

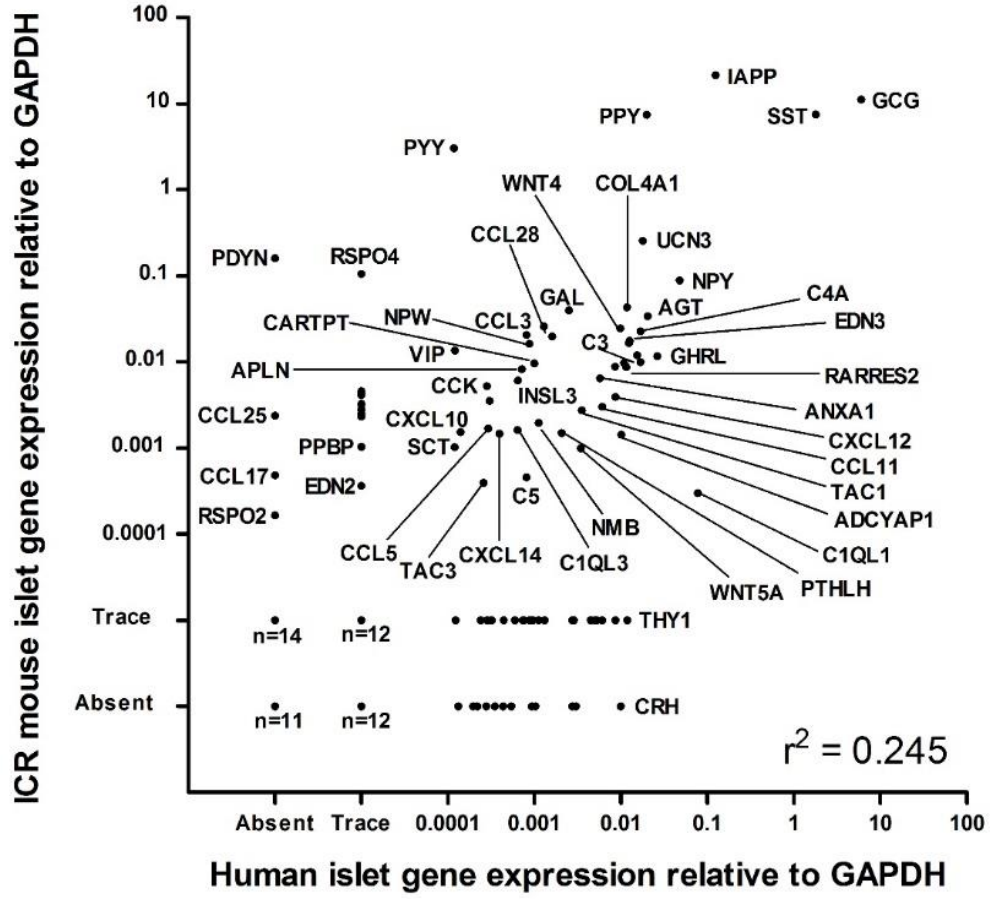

Figure 4.4.8 Regression analysis of GPCR peptide ligand mRNA expression between human and ICR mouse islets. A coefficient of determination (r^2) of 0.245 was determined. Data are expressed as mean expression relative to GAPDH from four biological replicates.

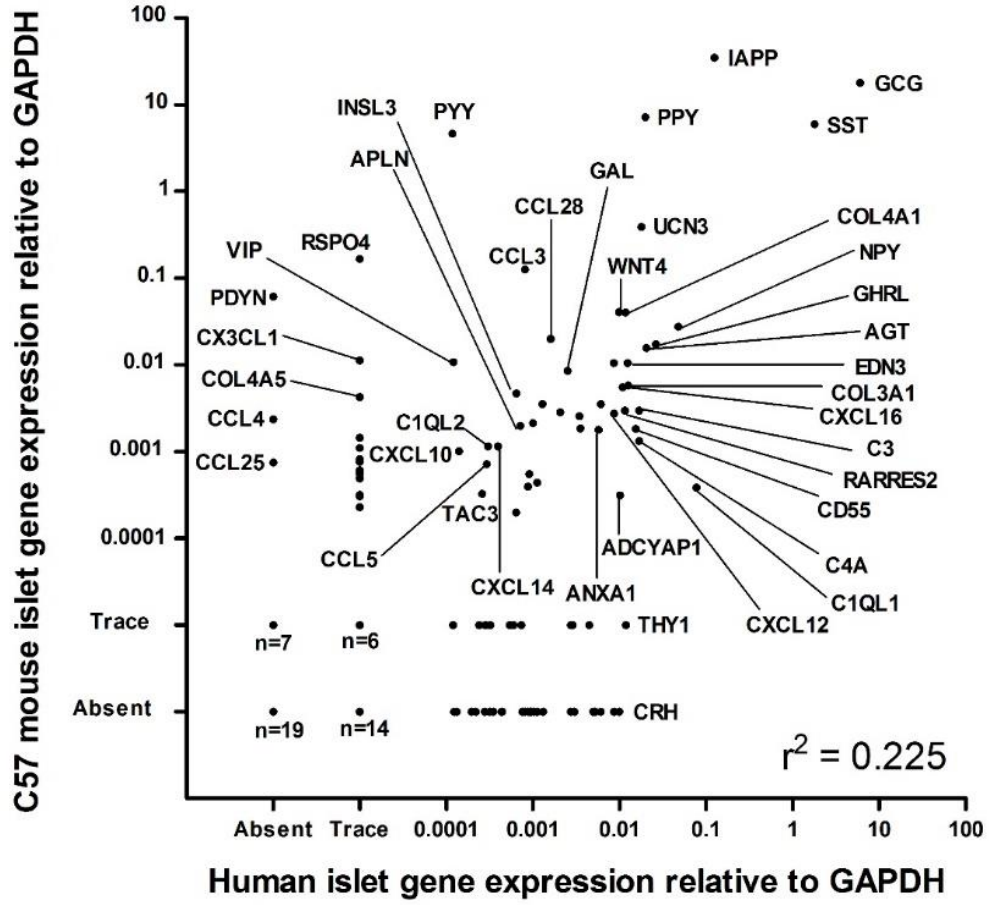

Figure 4.4.9 Regression analysis of GPCR peptide ligand mRNA expression between human and C57 mouse islets. A coefficient of determination (r^2) of 0.225 was determined. Data are expressed as mean expression relative to GAPDH from four biological replicates.

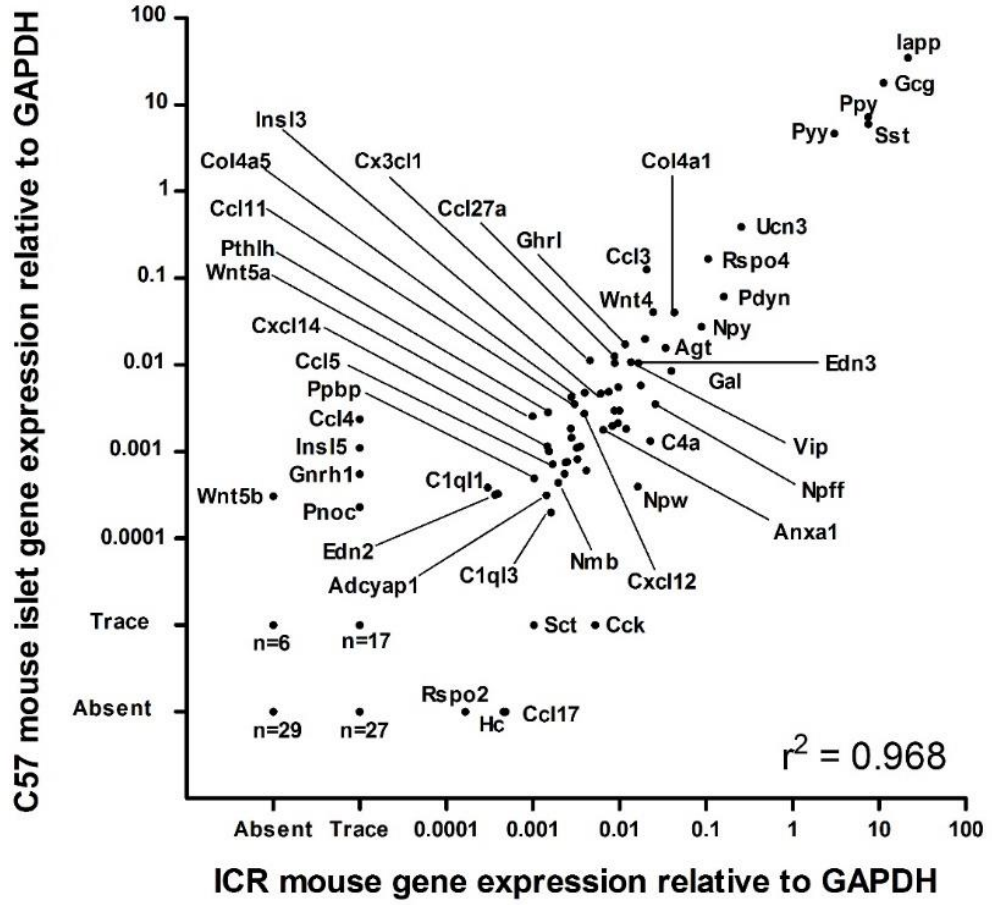

Figure 4.4.10 Regression analysis of GPCR peptide ligand mRNA expression between ICR mouse islets and C57 mouse islets. A coefficient of determination (r^2) of 0.968 was determined. Data are expressed as mean expression relative to GAPDH from four biological replicates.

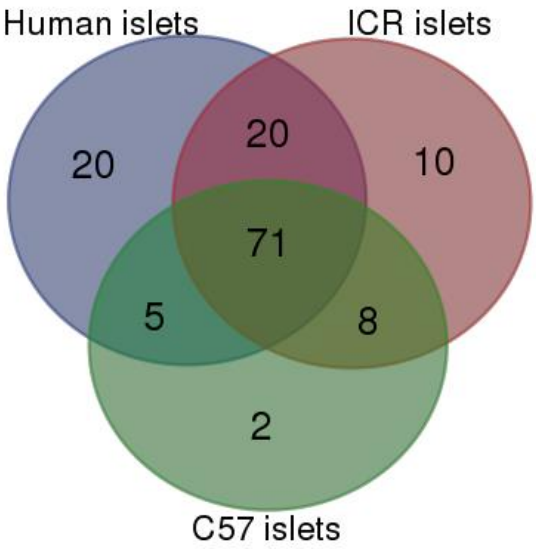

Figure 4.4.11 Venn diagram of orthologue GPCR peptide ligand mRNA expression in human and mouse islets. The data depicts GPCR peptide ligand orthologues expressed at trace level and above.

Table 4.4.2 Commonly expressed GPCR peptide ligand mRNAs in human and mouse islets. Data are arranged in rank order of expression within human islets.

Rank		Rank		Rank	
1	GCG	**26**	TAC1	**51**	CXCL10
2	SST	**27**	WNT5A	**52**	VIP
3	IAPP	**28**	UCN	**53**	SCT
4	C1QL1	**29**	GAL	**54**	PYY
5	NPY	**30**	PTHLH	**55**	RSPO4
6	GHRL	**31**	CCL28	**56**	CX3CL1
7	AGT	**32**	NPFF	**57**	COL4A5
8	PPY	**33**	NMB	**58**	PENK
9	UCN3	**34**	CARTPT	**59**	INSL5
10	C3	**35**	GNRH1	**60**	GRP
11	C4A	**36**	NPW	**61**	CALCA
12	CD55	**37**	CCL3	**62**	CCL19
13	COL3A1	**38**	CXCL13	**63**	CCL21
14	EDN3	**39**	APLN	**64**	CXCL4
15	THY1	**40**	INSL3	**65**	PPBP
16	COL4A1	**41**	C1QL3	**66**	EDN2
17	RARRES2	**42**	CXCL5	**67**	PNOC
18	CXCL16	**43**	CXCL14	**68**	AVP
19	ADCYAP1	**44**	QRFP	**69**	CXCL9
20	WNT4	**45**	C1QL2	**70**	GAST
21	CXCL12	**46**	CCL5	**71**	PTH2
22	COL4A2	**47**	KISS1		
23	CCL11	**48**	CCK		
24	ANXA1	**49**	TAC3		
25	WNT9A	**50**	WNT11		

Table 4.4.3 Species- and strain-specific GPCR peptide ligand mRNA expression in human and mouse islets. Data depicted include othologue GPCR peptide ligands expressed at trace level (*italics*) and above.

Rank	Human islets	ICR islets	C57 islets
1	CRH	Ccl17	*Hcrt*
2	CCL26	Rspo2	*Wnt6*
3	WNT3	*C1ql4*	
4	CXCL3	*Ccl1*	
5	RLN1	*Galp*	
6	COL4A4	*Nps*	
7	CCL7	*Npvf*	
8	RSPO3	*Tshb*	
9	WNT2	*Wnt1*	
10	LHB	*Wnt10b*	
11	TRH		
12	*COL4A6*		
13	*KNG1*		
14	*NTS*		
15	*OXT*		
16	*PROK2*		
17	*RSPO1*		
18	*WNT16*		
19	*WNT3A*		
20	*WNT7A*		

4.5 Discussion

G-protein-coupled receptors are responsible for regulating islet function by mediating the actions of a variety of ligands, which include intra-islet peptides, such as PACAP and VIP, and peptides delivered via the systemic circulation following secretion from alternative tissues, such as incretins (Ahren, 2000). Due to the importance of peptide ligand-mediated GPCR signalling in the regulation of islet function, exploration into the role of peptide ligands, in particular incretins, has received much attention with regards to identifying novel therapeutic approaches to improve islet function in T2DM (Gribble, 2012). The classic example of such an approach is the development of GLP-1 peptide mimetics, which enhance glucose-stimulated insulin release, reduce elevated levels of glucagon, promote β-cell proliferation, reduce β-cell apoptosis, inhibit gastric emptying and suppress appetite (Drucker, 2015). However, despite the success of the GLP-1 mimetics in the treatment of T2DM, it is the only peptide-GPCR-mediated approach that has proven to be clinically successful. Therefore, efforts to identify the role of GPCR peptide ligands in islet function and to exploit such novel peptide-GPCR-mediated mechanisms as potential therapies for T2DM are under investigation (Irwin and Flatt, 2015).

Examples of intra-islet expressed GPCR peptide ligands that are under investigation include urocortin-3 (UCN3), ghrelin (GHRL), peptide tyrosine tyrosine (PYY) and kisspeptin (KISS1). Urocortin-3 has recently been shown to be abundantly expressed in β-cells, is co-released with insulin and causes a reduction in glucose-induced insulin secretion by promoting somatostatin release from δ-cells. It is thought that the paracrine effects of urocortin-3 activate a negative feedback loop that promotes somatostatin release to inhibit glucose-induced insulin secretion (van der Meulen et al., 2015). Ghrelin is another peptide ligand that inhibits glucose-induced insulin

secretion through a GPCR-mediated mechanism by attenuating intracellular cAMP production and PKA activation in β-cells (Dezaki and Yada, 2012). Finally, the gut hormone PYY has been shown to be expressed in mouse islets, in particular in α- and PP cells (Bottcher et al., 1989), and has received interest due to its regulation of appetite, inhibition of glucose-stimulated insulin secretion, whilst exhibiting pro-proliferative and anti-apoptotic effects on mouse β-cells mediated through the activation of NPY1R receptors (Persaud and Bewick, 2014). However, some of the studies investigating the role of the aforementioned peptides in islet function have only been performed in animal models and thus a knowledge gap exists in the role of such peptides in human islet function.

Understanding the role of GPCR peptide ligands in human islet function is restricted by the limited availability of human islets, thus resulting in the reliance on using animal islets to predict the human situation. However, it is well documented that mouse islets, the typical surrogate tissue, exhibit a different islet architecture (Cabrera et al., 2006) and contain different proportions of endocrine cells (Steiner et al., 2010). Furthermore, species differences in human and mouse islet gene expression have been well documented (Kutlu et al., 2009) (Dai et al., 2012) (Benner et al., 2014), a claim that can be supported by the GPCR expression results obtained in the previous chapter. Such reported dissimilarities raise questions over the suitability of utilising mouse islets as surrogate models for assessing human islet function.

The aims of the experiments described in this chapter were to 1) quantify the mRNA expression of GPCR peptide ligands in human islets and the islets of outbred ICR and inbred C57 mouse strains, 2) compare the mRNA expression profiles to assess the suitability of using mouse islets as surrogate models for human islet GPCR peptide

ligand studies and 3) identify islet expressed GPCR peptide ligands whose role in islet function is yet to be determined and thus should be investigated.

Quantify human and mouse islet GPCR peptide ligand mRNA expression profiles

Gene expression analysis revealed that a high proportion of GPCR peptide ligands are expressed by both human and mouse islets. Of the 159 GPCR peptide ligands screened for expression in human islets, 128 (81%) were shown to be expressed, whilst of the 145 mouse orthologues screened, 109 (75%) and 86 (59%) were shown to be expressed in ICR and C57 mouse islets respectively. This extent of abundant expression is expected of endocrine cells whose primary function is to secrete a multitude of factors which regulate not only processes within the islet microenvironment but also the processes of other tissues through delivery via the systemic circulation (Brereton et al., 2015). Interestingly, the number of peptide mRNAs expressed by C57 mouse islets was less compared to ICR mouse islets, a trend that was observed also with GPCR expression (Figure 3.4.4, Figure 3.4.5), as discussed in the previous chapter. This trend is likely to be attributed to the greater genetic variability of the outbred ICR strain compared to the more homogeneous inbred C57 mouse strain, where expression between biological replicates is more consistent.

High expression of the classic intra-islet GPCR peptide ligands, SST, GCG, IAPP, was observed for all of the islet groups along with intra-islet peptide ligands PPY, UCN3, NPY and GHRL (Figure 4.4.5, Figure 4.4.6, Figure 4.4.7), thus confirming the suitability of our approach in reliably revealing GPCR peptide ligand mRNA expression. However, while the expression values of these ‘classic’ islet peptides was

revealed to be similar between islet groups, it did not conclusively confirm whether mouse islets are suitable for assessing the function of the numerous additional peptides expressed in human islets. Therefore, comparative analyses were performed to reveal the similarities and differences in GPCR peptide ligand mRNA expression between human and mouse islets.

Comparison of islet GPCR peptide ligand expression profiles

For the purpose of comparing and quantifying the GPCR peptide ligand mRNA expression profiles between islet groups, regression analysis was performed. As previously observed with GPCR expression (Figure 3.4.11), a remarkable degree of similarity in islet GPCR peptide ligand gene expression was observed between both mouse strains, $r^2 = 0.968$. Conversely, linear regression analysis revealed that there was weaker correlation between GPCR peptide gene expression in human and mouse islets, with r^2 values of 0.245 and 0.225 determined versus the ICR mouse strain and C57 strain respectively. A factor that could influence such dissimilarities could be the differences in islet endocrine cell proportions between human and rodent species (Steiner et al., 2010), whereby β-cell specific peptide ligands are likely to be perceived to be expressed at lower levels in human compared to mouse islets due to the higher proportion of β-cells within mouse islets. It is interesting to note that, similarly with GPCR expression, ICR mouse islets appear to resemble human islets more than the C57 counterpart, which as mentioned previously is likely to be due the similarity in genetic variability of biological replicate samples for both human and outbred ICR mice, unlike the inbred C57 mouse strain. Whilst a degree of genetic variability may result in inconsistent results between biological replicates when using ICR mouse

islets, the fact that this degree of variability is also likely to be observed between human islet samples, suggests that ICR mice may well be a more suitable translational murine model system for human islets than islets from C57 mice.

Despite the fact that a large degree of overlap in gene expression was observed between the three islet groups, species- and strain-specific expression was also observed (Table 4.4.3). Examples of human islet-specific or human islet-enriched peptide mRNAs include CRH, UCN, C1QL1 and ADCYAP1. Corticotrophin-releasing factor (CRH) was shown to be exclusively expressed within human islets and is ranked #21 with regards to expression of the 128 peptide ligands expressed in human islets. The receptors responsible for CRH function are CRHR1 and CRHR2 (Fekete and Zorrilla, 2007), both of which are expressed by human islets and also by both strains of mouse islets (Figure 3.4.2). CRH has been shown to promote glucose-induced insulin secretion in isolated rat β-cells through the activation of the CRH1 receptor and subsequent generation of increased intracellular cAMP. In the same study, CRH also promoted proliferation of primary rat neonatal β-cells through ERK1/2 phosphorylation, a mechanism which was further promoted under elevated glucose conditions (Huising et al., 2010). Another study revealed that intravenous infusion of CRH through the superior mesenteric artery increased whole pancreatic and islet blood flow in rat but in contrast did not influence insulin secretion (Carlsson et al., 1995). Whilst it appears that CRH may promote glucose-induced insulin secretion, β-cell mass and islet blood flow in rodent models, the lack of endogenous islet expression of CRH in mouse islets suggests that such effects could only be mediated through systemic delivery of CRH, rather than by local activation as may be the case with human islets. Furthermore, the CRH1 receptor is only expressed at trace levels in human islets but it is expressed approximately 250 times more in mouse islets

(Figure 3.4.2), suggesting that the observed effects of CRH in islet function in rodents may not in fact translate to humans. It is also interesting to note that urocortin1 (UCN1), another CRH1 ligand, is also predominantly expressed in human islets. Such results indicate that mouse islets may not be suitable for assessing the role of CRH1 ligands, CRH and UCN, in human islets.

Examples of mouse islet-specific or mouse islet-enriched peptide ligand mRNA expression include Pyy, Vip, Ccl3, Grp, Penk and Pdyn. PYY mRNA was shown to be expressed at very low levels in human islets but was expressed at levels approximately 26,000 times higher in islets from both mouse strains, and it was ranked as the fifth highest expressed peptide ligand in mouse islets from a total of 145 peptide ligands screened. The role of PYY in islet function has been explored in mouse models and it has been demonstrated to promote cell proliferation and protect from cytokine-induced apoptosis in mouse β-cells (Persaud and Bewick, 2014). With regards to insulin secretion, PYY inhibits glucose- and carbachol induced insulin secretion from mouse islets (Bottcher et al., 1989), but has no effect on glucose-induced insulin secretion in humans following i.v administration (Ahren and Larsson, 1996), thus clearly highlighting a species-specific effect. Interestingly though, the expression profiles of the receptors for PYY between human and mouse islets are similar (Figure 3.4.2). Whilst PYY appears to exhibit effects on islet function in mouse models, the absence of effect in humans in addition to the discrepancy in expression of PYY between mouse and human islets questions the relevance of studying PYY as an intraislet regulator of human islet function.

It is clear that consistencies in GPCR peptide ligand mRNA expression exist between human and mouse islets, as exemplified by the highly expressed SST, GCG, IAPP,

UCN3, PPY, NPY and GHRL peptides, but a certain degree of specificity is also observed between species e.g. CRH and PYY in particular. Whilst similarities in peptide expression may be observed within the islets of different species, the expression profiles of the receptors responsible for function also needs to be taken into consideration before an assumption on using mouse islets to predict human islet function can be declared. For example, whilst SST is highly expressed within human, ICR and C57 islets, the SST receptor family mRNA expression profiles differ between human and ICR mouse islets; where SSTR3 is absent and SSTR1 is only expressed at trace levels in ICR mice (Figure 3.4.2). In this scenario it would be more appropriate to use islets from C57 mice as a translational model to study SST signalling that would be relevant to the situation in human islets. A further complication is the fact that islets are made up of several different cell types. It is therefore possible that even though the expression of a particular gene may be found at similar levels in human and mouse islets, the cell type-specific expression may be different in the two species, which may have significant consequences for the functional role of specific GPCRs or GPCR peptide ligands.

Identify peptides for further islet function studies

Complement component 1, q subcomponent-like 1 (C1QL1)

CIQL1 is the fourth highest expressed GPCR peptide ligand mRNA in human islets (Figure 4.4.5), accounting for 0.92% of total ligand expression (Table 4.4.1). While the mRNA expression of CIQL1 in human islets is approximately 260 times greater in human islets compared to mouse islets, its cognate receptor, BAI3 (Bolliger et al., 2011), is expressed in both human and mouse islets (Figure 3.4.2), suggesting that

mouse islets could be utilised to assess C1QL1 function. To date, no studies assessing the role of C1QL1 on islet function have been performed, but the high expression of this ligand in human islets makes it a potentially interesting candidate for further studies.

Endothelin-3 (EDN3)

Endothelin-3 (EDN3) is the 14th, 18th and 19th most abundantly expressed peptide ligand in human islets, ICR mouse islets and C57 mouse islets respectively (Figure 4.4.5, Figure 4.4.6 and Figure 4.4.7). The endothelin peptide family (endothelin-1, -2 and -3, encoded by genes EDN1, EDN2 and EDN3) are vasoactive peptides that are released from vascular endothelium and function via the endothelin-A (EDNA) and endothelin-B (ENDB) receptors. Increased serum protein levels of endothelin-1 are observed in diabetes patients (Takahashi et al., 1990) and whilst endothelin-1 has been shown to promote insulin release from isolated rat and mouse islets via the endothelin-A receptor (De Carlo et al., 2000), (Gregersen et al., 2000), it has consequently been shown to exacerbate cardiovascular complications in T2DM and contribute to elevated blood pressure through vasoconstriction (Ergul, 2011). Unlike endothelin-1, endothelin-3 acts only on the endothelin-B receptor, which is primarily involved in promoting vasodilation and thus opposes the vasoconstrictive effects of endothelin-1. Studies assessing the role of endothelin-3 in islet function are limited, but due to the relationship between the endothelin system and cardiovascular effects in T2DM, further investigation into the role of endothelin-3 in islet function ought to be considered.

Chemokine-ligand (CXC-motif)-14 (CXCL14)

CXCL14 is a chemokine ligand belonging the CXC-class of chemokines. CXCL14 is currently being investigated by several research groups for its role in regulating metabolism. Studies in mice have demonstrated that a high fat diet markedly upregulates CXCL14 serum protein concentration and its expression in white adipose tissue (Takahashi et al., 2007), whilst CXCL14 knockout mice are protected from HFD-induced obesity (Tanegashima et al., 2010), have improved insulin sensitivity and are protected from HFD-induced hyperinsulinemia and hyperglycaemia (Nara et al., 2007). CXCL14 has also been implicated in modifying insulin-dependent glucose uptake, albeit with differing effects, with attenuation of glucose uptake observed in monocytes (Hara and Nakayama, 2009), yet enhancement of glucose uptake is observed in adipocytes (Takahashi et al., 2007). According to the data revealed within this chapter, CXCL14 mRNA is expressed within both human and mouse islets, an observation that is consistent with results obtained by Suzuki *et al* who revealed by immunohistochemistry that CXCL14 is expressed within the secretory vesicles of δ-cells and not within α-, β- or PP cells (Suzuki and Yamamoto, 2015). It has therefore been postulated that CXCL14 may be co-released with somatostatin to modulate insulin secretion in a paracrine fashion (Suzuki and Yamamoto, 2015). However, the role of CXCL14 on islet function has not yet been assessed. The association of CXCL14 with metabolism and the demonstration that CXCL14 is expressed within islets makes it an attractive candidate for further investigation. The effects of CXCL14 on islet function will be explored in the following chapter.

Summary and future perspectives

The experiments performed within this chapter quantified and compared the mRNA expression profiles of 145 orthologue GPCR peptide ligands in human islets and in two strains of mouse islets. The expression profiles between ICR and C57 mice were remarkably similar despite C57 mice expressing 23 fewer GPCR peptide ligands. Human islets appear to be more similar to ICR mouse islets than to C57 islets, which is likely to be due to similarities in genetic variability, but the overall degree of expression similarity between human and mouse islets was low. Whilst similarities in peptide ligand expression was observed, with 71 (49%) peptide ligand genes expressed in both human and mouse islets, a degree of tissue-specific expression was also observed: human islets = 20, ICR = 10, C57 = 2 specific peptide ligands. In particular, the abundantly expressed CRH mRNA was shown to be expressed only in human islets, whilst PYY mRNA was expressed approximately 26,000 more abundantly in mouse islets compared to human islets.

The use of mouse islets as a translational model for predicting human islet GPCR peptide ligand function appears to be ligand-specific and needs to take into account not only the expression levels of the peptide ligand of interest but also the expression profile of the receptors responsible for mediating the function of the peptide. Furthermore, additional studies would need to be performed to elucidate the localisation of GPCR peptide ligand mRNA expression within islets due to the fact that the studies performed within this chapter reveal whole islet expression and not cell-specific expression, and it will also be necessary to confirm expression of the peptides themselves rather than just the mRNAs encoding them. Nevertheless, the results described provide detailed information into the expression profiles of 145

GPCR peptide ligand mRNAs in both human and mouse islets and, furthermore, they highlight the suitability of using mouse islets for assessing the function of GPCR peptide ligands in the human setting.

CHAPTER 5 - The effects of CXCL14 on islet function

5.1 Introduction

Analysis of the human and mouse islet 'Secretome' data generated in chapter 4 of this thesis revealed the expression of the CXC-family chemokine CXCL14 in both human and mouse islets. In recent years, CXCL14 has received interest from research groups studying its role in cancer, immunology and metabolism, but progress in understanding the mechanisms by which CXCL14 functions has been hindered by the orphan status of this chemokine, as no known receptor has been identified.

Typically, chemokines bind to receptors of their own class, of which there are four (C, CC, CXC, C3XC), and within each class some chemokines bind to many receptors and multiple receptors may bind to many chemokines (Kufareva et al., 2015). However, despite this class specific interaction between chemokine ligands and receptors, a receptor has yet to be identified for CXCL14. It has been proposed that CXCR4 is responsible for CXCL14 mediated function as determined by its ability to bind with high affinity to wild-type and stable CXCR4-overexpressing THP-1 cells in radioligand binding experiments (Tanegashima et al., 2013). In the same study, CXCL14 was also shown to inhibit CXCL12-mediated chemotaxis of THP-1 cells, a process which is facilitated by CXCR4. Conversely, a conflicting report demonstrated that CXCL14 did not alter CXCL12-induced CXCR4 phosphorylation, G-protein-mediated calcium mobilisation or CXCR4 internalisation in CXCR4 transfected HEK293 and Jurkat T cells, suggesting that CXCL14 is not a ligand for the CXCR4 receptor (Otte et al., 2014). As it stands, inconsistencies in the literature regarding the involvement of CXCR4, or any other receptor for that matter, in CXCL14 mediated function means CXCL14 will continue to maintain its orphan ligand status.

CXCL14 is currently being investigated by several research groups for its role in regulating metabolism. There is accumulating evidence demonstrating that obesity results in a state of low-grade chronic inflammation that promotes the release of pro-inflammatory cytokines, lipids and chemokines from adipose tissue, which consequently contributes to metabolic comorbidities such as type 2 diabetes mellitus (Xu et al., 2015). CXCL14 is a secreted chemokine that is expressed and secreted by the adipose tissue and contributes to inflammatory processes by recruiting monocytes to the site of inflammation. Studies in mice have demonstrated that a high fat diet markedly upregulates CXCL14 serum protein concentration and its expression in white adipose tissue (Takahashi et al., 2007), whilst CXCL14 knockout mice are protected from HFD-induced obesity (Tanegashima et al., 2010), have improved insulin sensitivity and are protected from HFD-induced hyperinsulinemia and hyperglycaemia (Nara et al., 2007). CXCL14 has also been shown to be implicated in modifying insulin-dependent glucose uptake, albeit with differing effects, with attenuation of glucose uptake observed in myocytes (Hara and Nakayama, 2009), whilst enhancement of glucose uptake is observed in adipocytes (Takahashi et al., 2007).

The association of CXCL14 with obesity, its subsequent effects on glucose homeostasis and its expression within the islets of Langerhans, as identified in the Secretome data (Figure 4.4.1), makes it an interesting target to study in relation to type 2 diabetes. Whilst most studies have focused on the role of CXCL14 on the regulation of glucose homeostasis in vivo, a direct effect of CXCL14 on islet function has yet to be explored. The experiments described in this chapter aim to explore the role of CXCL14 on islet and β-cell function and the underlying mechanisms mediating these effects, and to attempt to identify the GPCR/s through which it acts.

5.2 Aims

- Quantify CXCL14 mRNA expression in islets, β-cell lines and adipose tissue.
- Explore the effects of exogenous CXCL14 on islet and β-cell function.
- Identify the intracellular mechanisms involved in CXCL14-mediated effects on islets and β-cells.
- Using the islet GPCRome and Secretome data in Chapters 3 and 4, explore which receptor/s at which CXCL14 acts.

5.3 Methods

5.3.1 Gene expression analysis

mRNA was harvested from human islets, ICR mouse islets, MIN6 cells, Endoc-BH1 cells, mouse brown adipose tissue (BAT) and mouse gluteal white adipose tissue (GWAT) and reverse transcribed into cDNA as previously described (Sections 2.3.1, 2.3.3, 2.3.2 and 2.3.4). qPCR was performed using Qiagen's QuantiTect primer assays, Quantifast SYBR green master mix and the Roche LightCycler 480 under the settings described in section 2.3.5. Data were represented as expression relative to the expression of the housekeeping gene GAPDH. Confirmation of correct amplicon product was determined by agarose gel electrophoresis as described in section 2.3.6.

5.3.2 Static insulin secretion studies

The effects of acute CXCL14 exposure on insulin secretion from islets, MIN6 cells and INS-1 cells were carried out as described in section 2.4. In brief, islets, harvested as described in section 2.2, or monolayers of MIN6 cells and INS-1 cells were incubated with CXCL14 for 1 hour at 37^{o}C in physiological buffer supplemented with glucose. Following incubation, supernatant was retrieved and insulin content was determined by radioimmunoassay (Section 2.4.4).

5.3.3 Apoptosis protocol

Pro- or anti-apoptotic properties of CXCL14 were assessed by treating monolayers of MIN6 cells (25,000 cells/well) and INS-1 cells (15,000 cells/well) with exogenous CXCL14 in the absence or presence of pro-inflammatory cytokines (Section 2.5).

Enzymatic activity of the apoptotic enzymes Caspase 3 and 7 were determined using Promega's Capsase-Glo 3/7 assay.

5.3.4 Proliferation protocol

The proliferative effects of CXCL14 were assessed in MIN6 cells and INS-1 cells using a BrdU colorimetric ELISA as described in section 2.6. In brief, 20,000 MIN6 cells/well or 15,000 INS-1 cells/well were cultured in 96 well plates overnight in a humidified 37^{o}C incubator containing a 5% CO_2, 95% air atmosphere. The following day, the medium was changed to serum free medium supplemented with 2mM glucose and incubated overnight again to ensure the cells reached a quiescent state prior to experimentation. The following day, the medium was changed once more to medium containing either 0, 1, 2, 10, 20 or 40ng/ml of CXCL14 in the presence or absence of 10% serum. The cells were cultured for 48 hours at 37^{o}C before BrdU incorporation in newly synthesised cells was measured using the BrdU ELISA kit.

5.3.5 Intracellular cAMP assessment

In order to assess whether CXCL14 signals through agonism of Gαi-coupled receptors or inverse agonism of Gαs-coupled receptors, a cAMP assay using Cisbio's HTRF technology was developed. In brief, MIN6 cells were plated out in suspension in low volume 384 well white plates following flask detachment using enzyme-free dissociation buffer. CXCL14-mediated Gαi-coupling and Gαs-coupling was determined by treating MIN6 cells with exogenous CXCL14 in the presence or absence of forskolin respectively for a 1 hour incubation period in HBSS assay buffer

supplemented with IBMX. The plate was read on a BMG Pherastar and intracellular cAMP levels determined by extrapolating FRET values off of a standard curve.

5.3.5.1 Z factor calculation (Z')

To assess assay robustness, a Z' value was determined using the following calculation, where δ = standard deviation and μ = means of the positive (p) and negative (n) controls (Zhang et al., 1999).

$$Z' = 1 - \frac{3(\delta p + \delta n)}{|\mu p - \mu n|}$$

Z'	Interpretation
1	Ideal assay
Between 0.5 and 1	Excellent assay
Between 0 and 0.5	Marginal assay
0	No assay

5.3.6 Glucose uptake assessment

The effects of exogenous CXCL14 on glucose uptake in MIN6 cells were determined using the Promega glucose uptake kit as described in section 2.9. In brief, 30,000 MIN6 cells/well/100µl were plated out in fully complemented cell culture medium (as described in section 2.1.1) and cultured overnight in a humidified 37ºC incubator containing a 5% CO_2, 95% air atmosphere. The following day, the growth medium was replaced with fully complemented low glucose culture medium (no glucose DMEM supplemented with 2mM glucose, 10% FBS, 2mM L-glutamine and 100U/ml penicillin/100µg/ml streptomycin), in order to promote at state of quiescence prior to experimentation, before the cells were then incubated overnight in a humidified 37ºC

incubator containing a 5% CO_2, 95% air atmosphere. Following overnight incubation, the cell medium was removed from the plate and the cells were washed with 200µl/well of PBS. 50µl/well of treatment (CXCL14 or vehicle) was then added to each well of the plate and the cells were then incubated for 1 hour at 37ºC. 5µl of 10X 2DG solution prepared in PBS was added to each well and the cell plate was again incubated for 1 hour at 37ºC. Following incubation, 25µl of Stop buffer was added to each well in order to terminate glucose uptake and destroy intracellular NADPH. 25µl/well of Go buffer was added to the plate followed by 100µl of 2DG6P detection reagent and the plate was then incubated for 1 hour at room temperature. Luminescence was measured using a Veritas luminometer plate reader.

5.3.7 Intracellular ATP assessment

5.3.7.1 MIN6 cells

The effects of CXCL14 on intracellular ATP levels within MIN6 cells were determined using the CellTiter-Glo Viability kit as described in section 2.8.

Briefly, MIN6 (25,000 cells/well) cells were plated out in white walled, clear bottom plates and cultured overnight in a humidified 37ºC incubator containing a 5% CO_2, 95% air atmosphere. The following day, the medium was changed to low glucose medium (2mM glucose) with the aim of reducing glucose-induced basal intracellular ATP generation and thus increase the assay window. The next day, the medium was removed and the cells were incubated with 50µl/well of exogenous CXCL14 prepared in Gey and Gey buffer for 1 hour at 37ºC. 50µl/well of CellTiter-Glo reagent was added to each well and the plate was then incubated for 10 mins at room temperature before luminescence was measured using a Veritas Luminometer.

5.3.7.2 Islets

The effects of exogenous CXCL14 on intracellular ATP levels within ICR mouse islets were determined using the CellTiter-Glo 3D Viability kit.

Briefly, mouse islets were harvested as described in Section 2.2.2 and cultured overnight in RPMI medium (11.1mM glucose) supplemented with 10% FBS, 2mM L-glutamine and 100U/ml penicillin/100µg/ml streptomycin in a humidified 37^{o}C incubator containing a 5% CO_2, 95% air atmosphere. The following day, the islets were transferred to Gey & Gey physiological solution containing 2mM glucose and incubated for 2 hours within a humidified 37^{o}C incubator containing a 5% CO_2, 95% air atmosphere. The islets were then washed and 3 islets/well/25µl were handpicked under a microscope into a white 96 well plate and treated with 25µl of 2X treatment buffer in the presence of 2 or 20mM glucose for 1 hour at 37^{o}C. 50µl of luciferase reagent was added to each well and the plate was then incubated for 30mins at room temperature before the luminescent signal was measured.

5.3.8 β-Arrestin recruitment assays

The assessment of CXCL14 function at the CXCR4 and CXCR7 receptors was assessed using mouse CXCR4 and CXCR7 β-arrestin assay kits supplied by DiscoverX. Function of CXCL14 at these receptors was assessed in both agonist and antagonist mode, with CXCL12 used as the natural ligand and competing ligand to assess CXCL14 antagonism at both receptors. Detailed methodology can be found in section 2.10.

Briefly, 10,000 PathHunter cells/well were plated out and cultured for 48 hours in a humidified incubator at 37^{o}C supplemented with 5% CO_2. On the day of ligand

treatment, ligands were prepared at 2X concentration in assay buffer (HBSS, 10mM HEPES, 0.1% BSA, pH7.4 with NaOH). Agonism was assessed by adding 50µl/well of vehicle (antagonist diluent in assay buffer) followed by 50µl/well of 2X concentrated ligand in assay buffer. Antagonism was assessed by adding 50µl/well of 2X ligand (CXCL14), followed by 50µl of 2X agonist (CXCL12). The plate was incubated at 37ºC for 90 mins before 55µl/well of detection reagent was added. The plate was then incubated at room temperature for 60 mins and the luminescence signal measured using a Veritas luminometer.

5.4 Results

5.4.1 CXCL14 mRNA expression

qPCR analysis revealed the expression of CXCL14 mRNA in human islets, mouse islets, brown (BAT) and white (GWAT) adipose tissue but not in the Endoc-βH1 and MIN6 β-cell lines (Figure 5.4.1). Validation of the specificity of the qPCR product was confirmed by agarose gel electrophoresis (Figure 5.4.2).

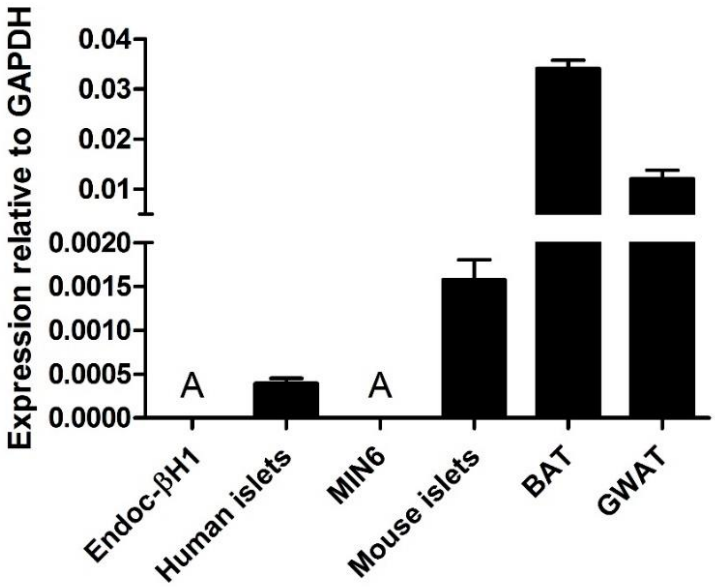

Figure 5.4.1. CXCL14 mRNA expression analysis in islets, β-cell lines and adipose tissue. Data expressed as mean + SEM relative to GAPDH mRNA expression, n=4. A = absent expression.

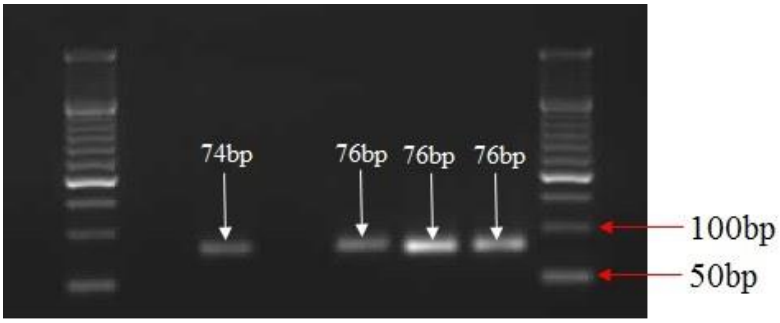

Figure 5.4.2. Agarose gel image of CXCL14 qPCR products. Wells are arranged in the following order from left to right: 50bp ladder, Endoc-βH1, human islet, MIN6, mouse islet, BAT, GWAT and 50bp ladder. Correct amplicon sizes for human (74bp) and mouse (76bp) samples were detected.

5.4.2 Exploring the effects of exogenous CXCL14 on islet function

5.4.2.1 The effects of CXCL14 on insulin secretion from MIN6 cells

The effects of exogenous CXCL14 on insulin secretion from MIN6 cells were assessed in order to identify whether CXCL14 modifies insulin secretion directly from β-cells. Acute exposure of MIN6 cells to exogenous CXCL14 for 1 hour resulted in a reduction in insulin secretion at both 2mM and 20mM glucose with greater statistical significance observed at 2mM glucose (Figure 5.4.3).

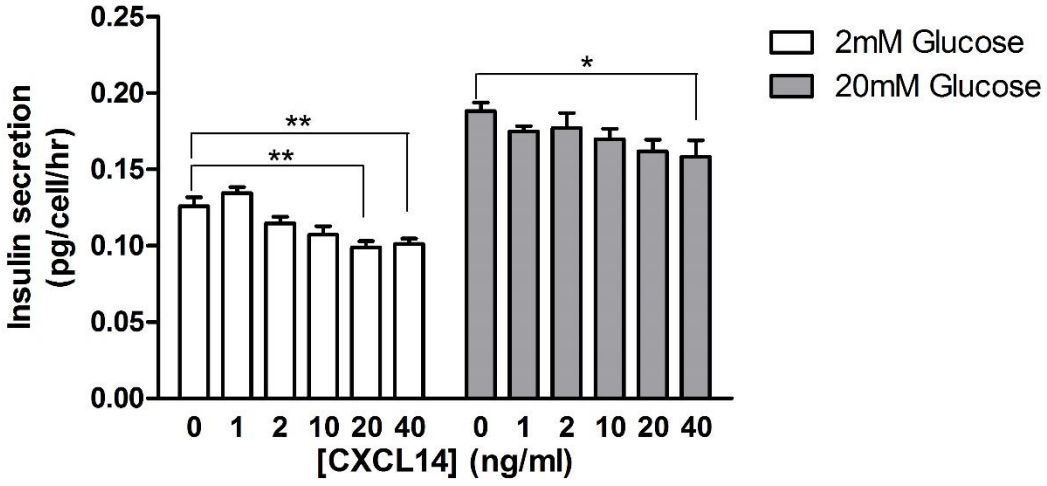

Figure 5.4.3 The effects of CXCL14 on insulin secretion from MIN6 cells. A dose dependent reduction in insulin secretion was observed with increasing concentrations of CXCL14. CXCL14 significantly reduced insulin secretion at both 2 and 20mM glucose. Data are expressed as mean + SEM, n=8 and represent three separate experiments. Statistics were performed using one-way ANOVA, *$p<0.05$, **$p<0.01$.

5.4.2.2 The effects of CXCL14 on insulin secretion from INS-1 cells

The effects of CXCL14 on insulin secretion from the INS-1 rat β-cell line were assessed to determine whether the effects of CXCL14 on insulin secretion from MIN6 cells could also be observed in an alternative rodent cell line. Data in Figure 5.4.4 indicates that 2 and 20ng/ml of CXCL14 was able to significantly inhibit insulin secretion. Like with MIN6 cells, a greater significance in the reduction of insulin secretion was observed at lower glucose concentrations.

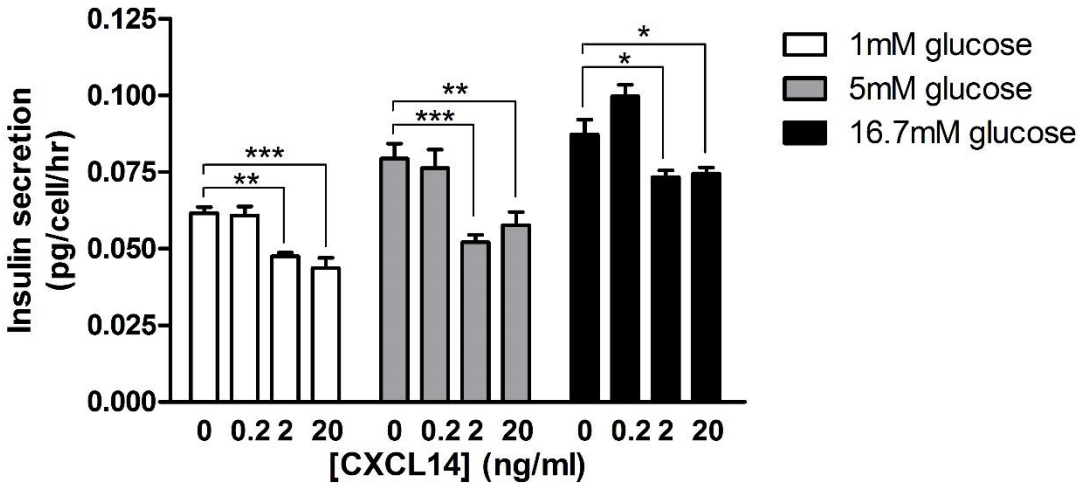

Figure 5.4.4 The effects of CXCL14 on insulin secretion from INS-1 cells. 2 and 20ng/ml of CXCL14 significantly inhibited insulin secretion independent of the glucose concentration. Data are expressed as mean + SEM, n=8 and represent two separate experiments. Statistics were performed using one-way ANOVA, *p<0.05, **p<0.01, ***p<0.001.

5.4.2.3 The effects of CXCL14 on insulin secretion from mouse islets

Following the revelation that CXCL14 inhibited insulin secretion from rodent β-cell lines, the effects of CXCL14 on insulin secretion from whole mouse islets were assessed. Mouse islets responded to glucose with a 15.03 fold increase in insulin secretion observed between 2mM (0.13±0.03ng/islet/hr) and 20mM (1.93±0.44) glucose. Acute exposure of mouse islets to exogenous CXCL14 resulted in a concentration dependent reduction in glucose-induced insulin secretion with increasing concentrations of CXCL14, with statistical significant observed with 40ng/ml of CXCL14. (Figure 5.4.5).

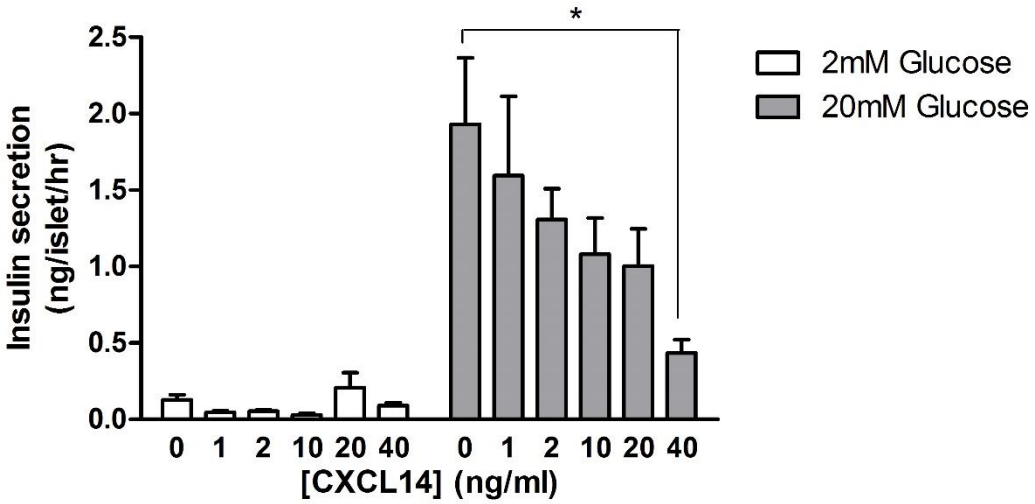

Figure 5.4.5 The effects of CXCL14 on insulin secretion from mouse islets. CXCL14 caused a dose dependent reduction in glucose-induced insulin secretion with statistical significance observed with 40ng/ml. Data are expressed as mean + SEM, n=8 and represent three separate experiments. Statistics were performed using one-way ANOVA, *p<0.05.

5.4.2.4 The effects of CXCL14 on insulin secretion from human islets

In order to determine whether the effects of CXCL14 on insulin secretion from mouse islets translated to human islets, a static insulin secretion experiment was also performed using human islets. Unlike with mouse islets and MIN6 cells, CXC14 did not significantly reduce insulin secretion from human islets (Figure 5.4.6).

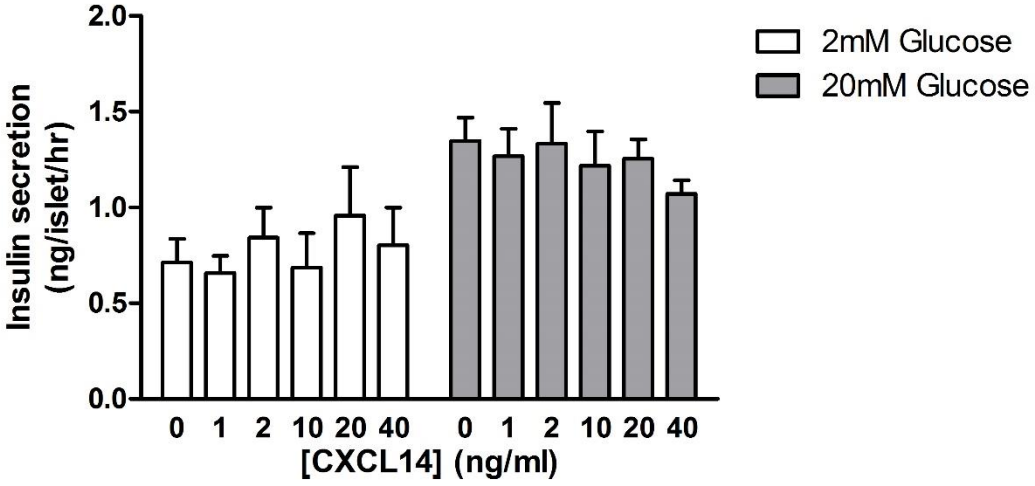

Figure 5.4.6 The effects of CXCL14 on insulin secretion from human islets. CXCL14 has no effect on human islet insulin secretion. Data are expressed as mean + SEM, n=8 and represent three separate experiments.

5.4.2.5 The effects of CXCL14 on β-cell line apoptosis

In order to assess whether CXCL14 could induce pro- or anti-apoptotic effects on β-cells, MIN6 cells and INS-1 cells were cultured with CXCL14 in the presence or absence of pro-apoptotic cytokines.

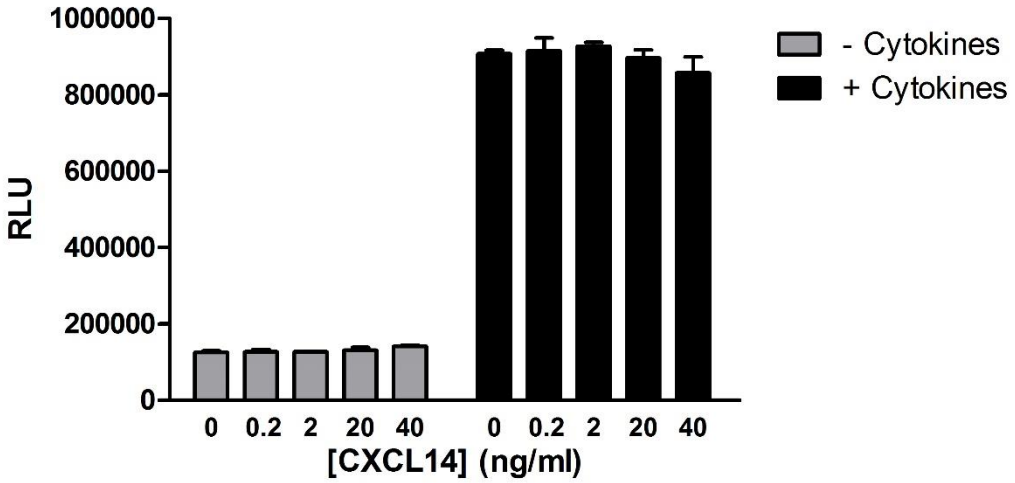

Figure 5.4.7 The effects of CXCL14 on MIN6 cell apoptosis. CXCL14 had no effect on MIN6 cell apoptosis. Data are expressed as mean + SEM, n=6 and represent three separate experiments. Statistics were performed using one-way ANOVA.

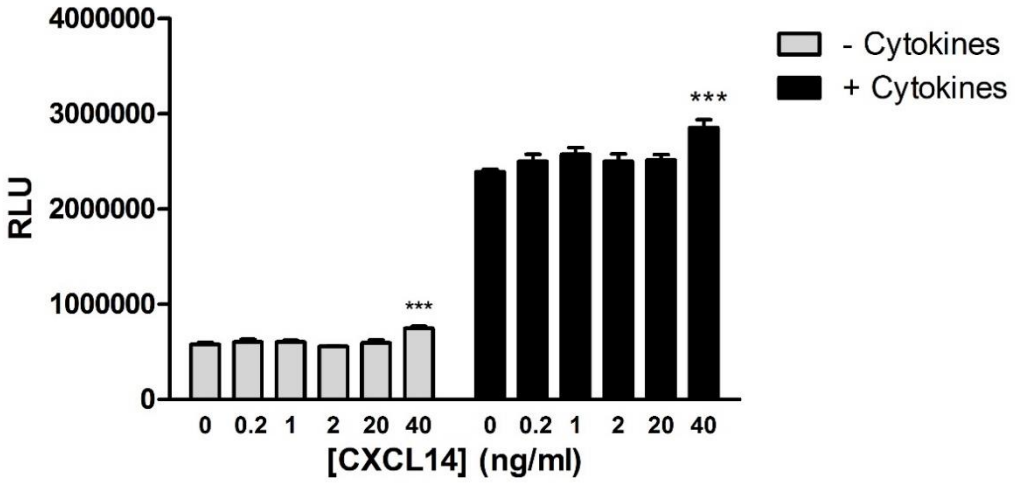

Figure 5.4.8 The effects of CXCL14 on INS-1 cell apoptosis. 40ng/ml CXCL14 promoted apoptosis in the absence and presence of pro-inflammatory cytokines. Data are expressed as mean + SEM, n=6 and represent two separate experiments. Statistics were performed using one-way ANOVA, ***$p<0.001$.

5.4.2.6 The effects of CXCL14 on β-cell proliferation

In order to assess whether CXCL14 could induce anti- or pro-proliferative effects on β-cells, MIN6 cells and INS-1 cells were cultured with CXCL14 in the presence or absence of serum (10% FCS).

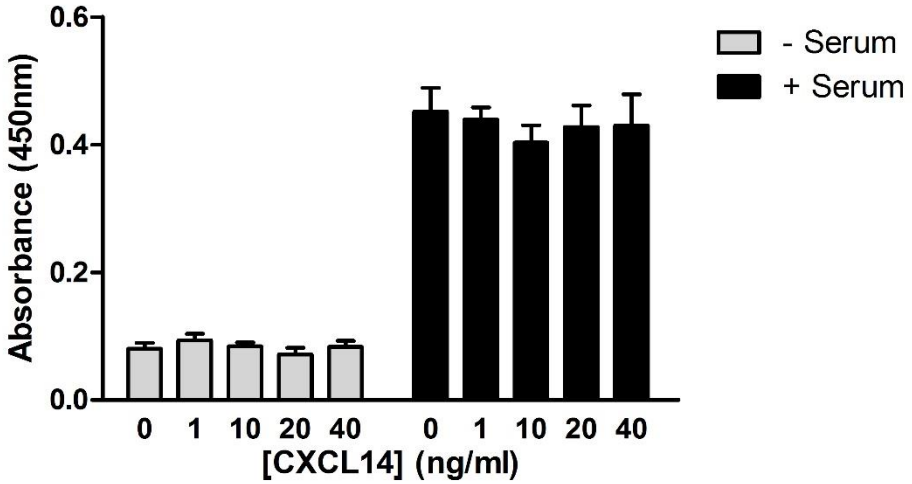

Figure 5.4.9 The effects of CXCL14 on MIN6 cell proliferation. CXCL14 had no effect on MIN6 cell proliferation in the presence or absence of serum. Data are expressed as mean + SEM, n=6 and represent two separate experiments. Statistics were performed using one-way ANOVA.

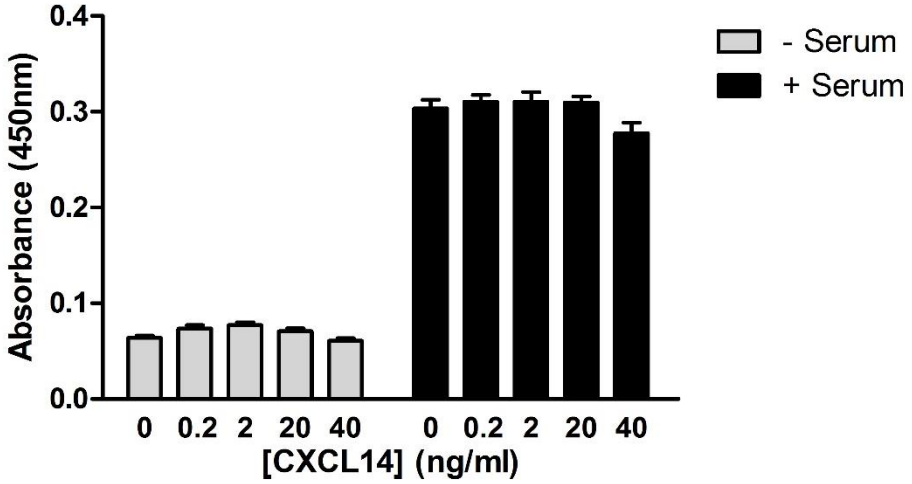

Figure 5.4.10 The effects of CXCL14 on INS-1 cell proliferation. CXCL14 had no effect on INS-1 cell proliferation in the presence or absence of serum. Data are expressed as mean + SEM, n=6 and represent two separate experiments. Statistics were performed using one-way ANOVA.

5.4.3 The mechanisms involved in CXCL14-mediated reduction in insulin secretion.

CXCL14 inhibited insulin secretion from both mouse islets and rodent β-cells lines, indicating that CXCL14 functions directly at the β-cell. Therefore, the MIN6 β-cell line was used for subsequent studies aimed at identifying the potential mechanisms involved in CXCL14-mediated regulation of insulin secretion. Potential mechanisms involved in the CXCL14-mediated inhibition of insulin secretion include a CXCL14-mediated reduction in intracellular cAMP, either by agonism of a Gαi-coupled GPCR or inverse agonism of a Gαs-coupled GPCR, or by inhibition of glucose uptake and/or glucokinase activity. The methods described below aim to explore which of these mechanisms may be involved in the inhibitory effect of CXCL14 on insulin secretion.

5.4.3.1 The effects of CXCL14 on intracellular cAMP production in MIN6 cells

The effects of CXCL14 on intracellular cAMP production in MIN6 cells was assessed using Cisbio's cAMP HTRF kit as described in section 5.3.5. The ability of CXCL14 to function as an inverse agonist of a Gαs-coupled GPCR was assessed by treating MIN6 cells with exogenous CXCL14 to see if a reduction in basal cAMP was observed. In order to assess whether CXCL14 functions as Gαi-coupled GPCR agonist, MIN6 cells were treated with CXCL14 in the presence of forskolin. Forskolin functions by activating the transmembrane enzyme adenylate cyclase, which is responsible for increasing intracellular cAMP levels by converting ATP to cAMP and pyrophosphate. In order to determine an appropriate concentration of stimulating concentration of forskolin and cell density to use for subsequent experiments, a dose response to forskolin using various MIN6 cell densities was performed.

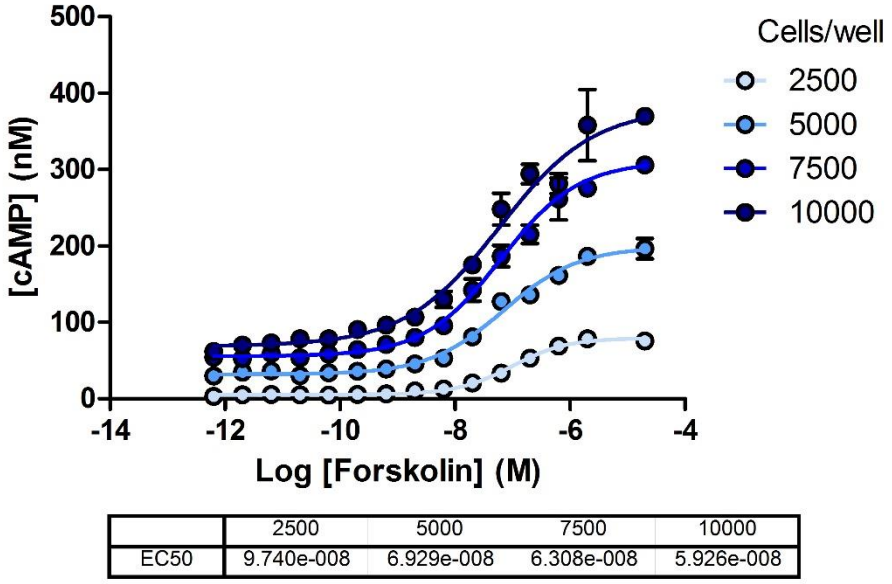

	2500	5000	7500	10000
EC50	9.740e-008	6.929e-008	6.308e-008	5.926e-008

Figure 5.4.11 Forskolin dose response curves with various seeded densities of MIN6 cells. A forskolin-induced increase in cAMP was observed for all cell densities tested. Data are expressed as mean ± SEM, n=3.

Table 5.4.1 HTRF-cAMP Z factor calculations.

Cell density	μp	μn	δp	δn	Z factor
2500	78.38	5.16	3.59	0.58	0.83
5000	186.35	23.91	3.81	2.66	0.88
7500	275.77	45.35	5.71	0.45	0.92
10000	358.13	65.81	46.58	2.34	0.50

As expected, an increase in basal intracellular cAMP was observed with increasing cell density. Forskolin dose response curves were generated for each cell density with a leftward shift in the EC_{50} values of forskolin observed with increasing cell density (Figure 5.4.11). Z factor calculations for each seeding density tested all fell within the 'excellent assay' range (Table 5.4.1). A comparison of the raw values generated for each cell density against the cAMP standard curve revealed that 2500 cells/well was suitable for further studies as all data points fell within the linear region of the cAMP standard curve (Figure 5.4.12).

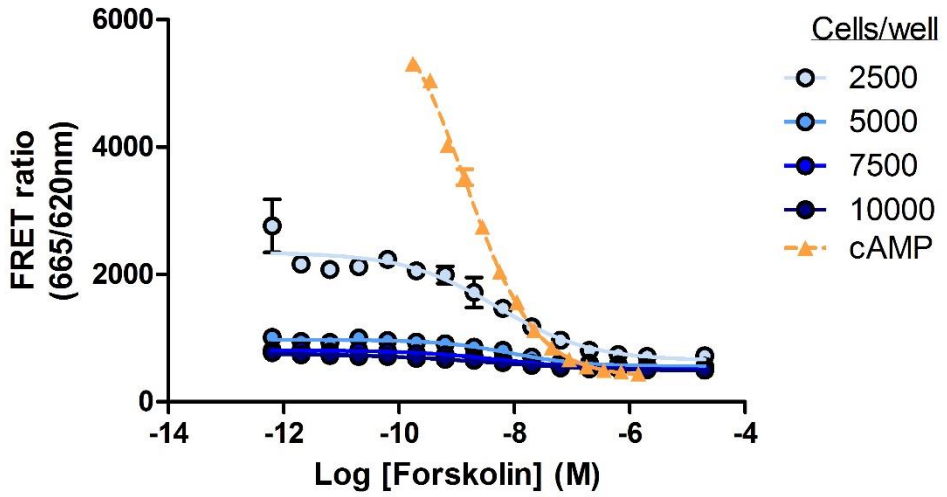

Figure 5.4.12 Assessment of cell density suitability. 2500 cells/well generated levels of cAMP that could be reliably detected within the linear sensitivity range. Data are expressed as mean ± SEM, n=3.

For the purpose of assessing CXCL14-mediated Gαi coupling in MIN6 cells, a stimulating forskolin concentration of 100nM was chosen. To determine that the correct concentration of stimulating forskolin was added to the assay, a forskolin dose response was performed on the same plate and the 'actual' stimulating concentration of forskolin added to the assay was determined by extrapolating the fluorescent signal from the forskolin dose response curve. For the represented Gαi assessment assay, the 'actual' stimulating concentration of forskolin was determined as 64.5nM (Figure 5.4.13), which was considered to be suitable. The stimulating forskolin concentration induced a cAMP response to a level within the assay's detection range. The α2-adrenergic agonist clonidine, which exerts its effects through Gαi coupling, was able to reduce a forskolin-induced increase in intracellular cAMP thus confirming assay proof of concept. CXCL14 however was unable to reduce a forskolin induced increase in cAMP (Figure 5.4.13B) and did not reduce basal cAMP levels (Figure 5.4.13C) in forskolin untreated MIN6 cells.

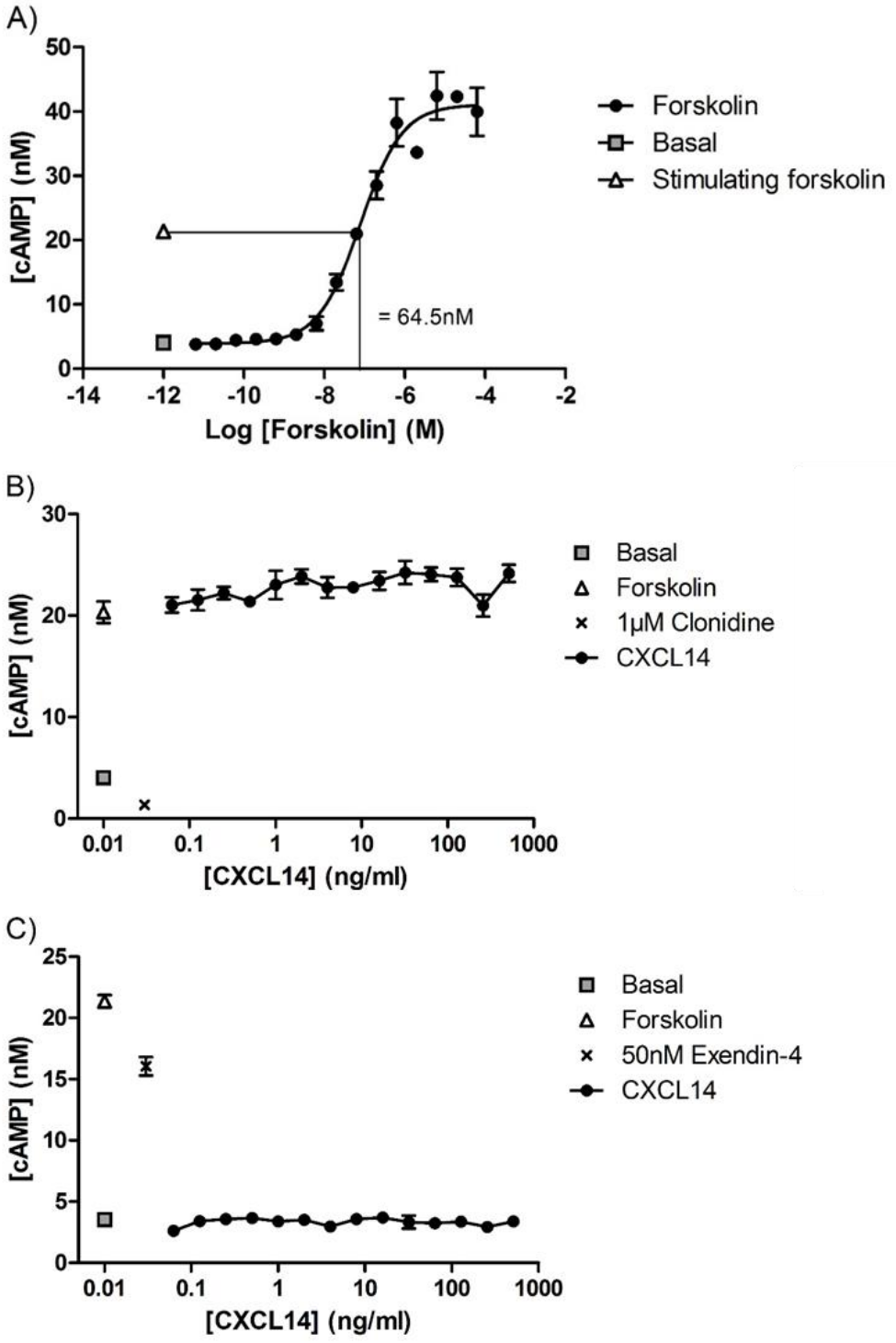

Figure 5.4.13 Assessment of CXCL14 on intracellular cAMP levels in MIN6 cells. Graphs depicted show A) a forskolin dose response, B) Gαi agonism assessment of CXCL14 function and C) Gαs inverse agonist assessment of CXCL14 function. CXCL14 did not inhibit a forskolin-induced increase in cAMP and did not inhibit or stimulate basal cAMP levels. Data are expressed as mean ± SEM, n=3 and represent three separate experiments.

5.4.3.2 The effects of CXCL14 on glucose uptake in MIN6 cells.

Previous studies have shown that CXCL14 both attenuates and promotes insulin-dependent glucose uptake in adipocytes and monocytes respectively. In mouse β-cells glucose uptake is insulin-independent and is mediated through the GLUT2 glucose transporter. As insulin secretion is dependent on the influx of glucose into the β-cell through the insulin-independent GLUT2 transporter, experiments were designed to explore whether the mechanism by which CXCL14 inhibits insulin secretion is via the attenuation of insulin-independent glucose uptake in MIN6 cells.

In order to assess the effect of CXCL14 on glucose uptake in MIN6 cells, assay conditions allowing for reliable assessment of glucose uptake needed to be optimised. Therefore, a matrix study assessing glucose uptake using various cell densities and 2-deoxy-D-glucose (2DG) concentrations was performed (Figure 5.4.14). An increase in 2DG uptake was observed with increasing concentration of 2DG and cell density. For the purpose of subsequent studies assessing the effect of CXCL14 on glucose uptake, a cell density of 30,000 MIN6 cells/well and 2DG concentrations of 2 and 20mM were chosen. CXCL14 appeared to reduce glucose uptake in MIN6 cells at both 2mM and 20mM of 2DG with statistical significance observed following treatment with 40 and 80ng/ml of CXCL14 (Figure 5.4.15). Similar to the effects of CXCL14 on insulin secretion from MIN6 cells, a greater degree of statistical significance was observed at lower concentrations of glucose/2DG.

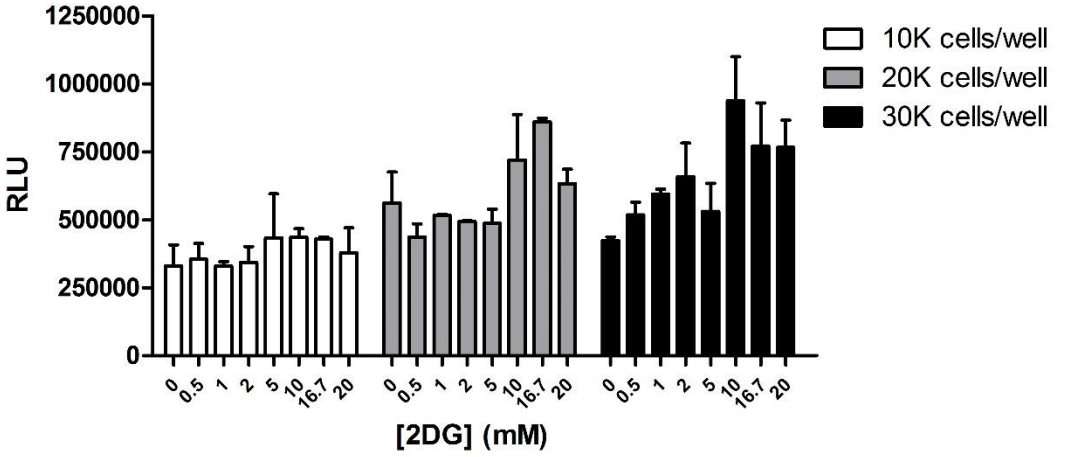

Figure 5.4.14 Glucose uptake assay optimisation with MIN6 cells. An increase in glucose uptake was observed with increasing cell density and 2DG concentration. Data are expressed as mean + range, n=2.

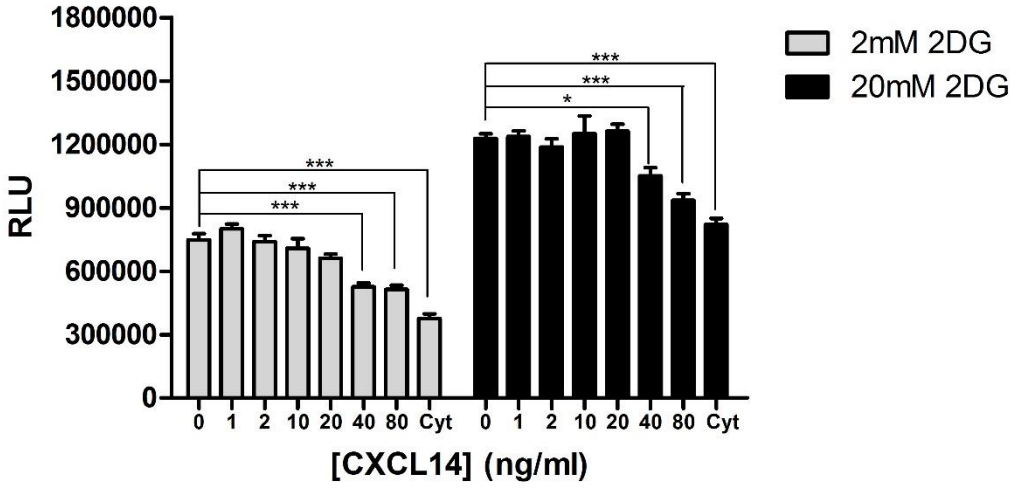

Figure 5.4.15 The effects of CXCL14 on glucose uptake in MIN6 cells. A significant reduction in glucose uptake was observed following treatment with 40 and 80ng/ml of exogenous CXCL14 at both 2 and 20mM 2DG. The glucose uptake transporter inhibitor cytochalasin-B ('Cyt' at 50µM) also significantly reduced glucose uptake. Data are expressed as mean + SEM, n=6 and represent two separate experiments. Statistics were performed using one-way ANOVA, *$p<0.05$, ***$p<0.001$.

5.4.3.3 The effects of CXCL14 on intracellular ATP generation

In order to confirm the effects of CXCL14 on glucose uptake, and thus a predicted subsequent reduction in intracellular ATP generation, the effects of CXCL14 on intracellular ATP generation were assessed in MIN6 cells.

Assay optimisation of cell density and glucose concentration was performed to ensure the levels of ATP generated by the MIN6 cells fell within the assay's sensitivity range.

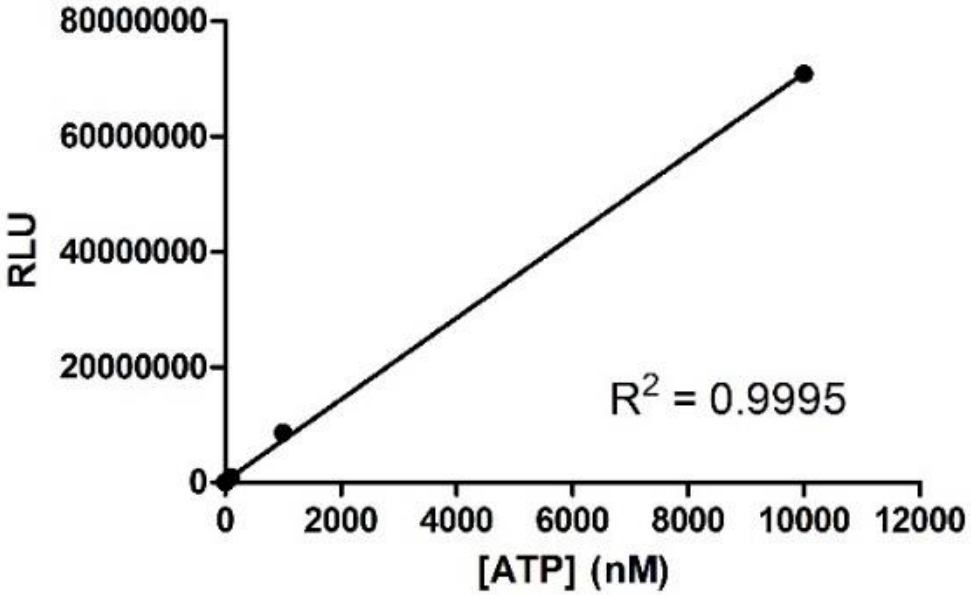

Figure 5.4.16 ATP standard curve. Data are expressed as mean ± range, n=2 and represent one experiment.

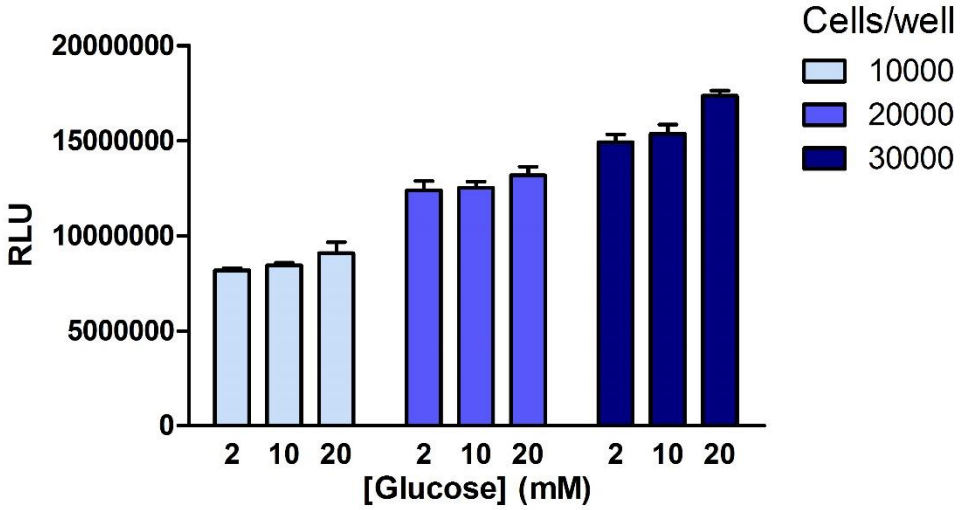

Figure 5.4.17 ATP assay MIN6 cell density study. Intracellular ATP concentration was directly proportional to cell density and glucose concentration. Data are expressed as mean + SEM of raw RLU, n=6 and represent one experiment.

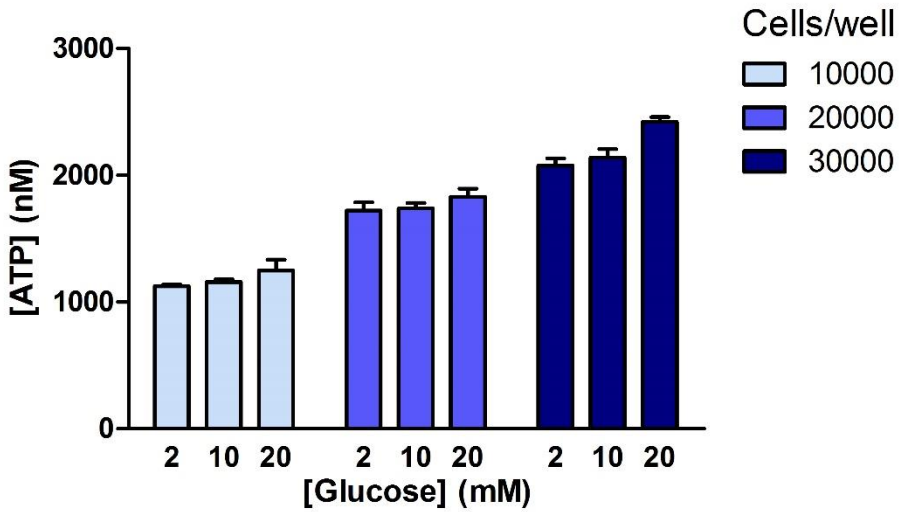

Figure 5.4.18 ATP assay MIN6 cell density study. An increase in generated ATP was directly proportional to cell density and glucose concentration. Data are expressed as mean + SEM (n=6) of extrapolated ATP concentration from the standard curve, and represent one experiment.

The concentrations of intracellular ATP generated at all cell densities fell within the kit's limit of sensitivity irrespective of the concentration of glucose. For the purpose of assessing the effects of CXCL14 on intracellular ATP levels within MIN6 cells, 30,000 cells/well were used.

Exogenous CXCL14 did not reduce intracellular ATP generation in MIN6 cells unlike the ATP synthase inhibitor, oligomycin (Figure 5.4.19).

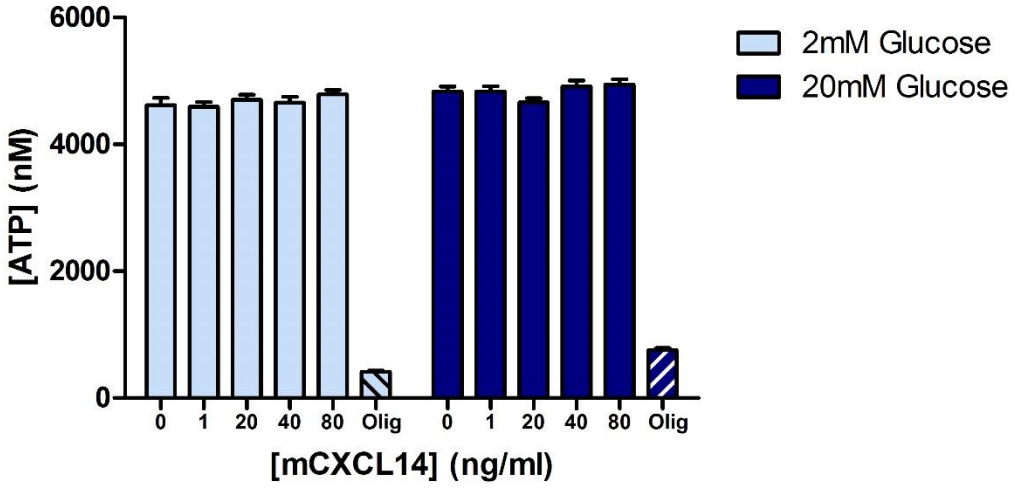

Figure 5.4.19 The effects of CXCL14 on intracellular ATP generation in MIN6 cells. CXCL14 did not affect intracellular ATP generation in MIN6 cells unlike 100ng/ml of the positive control oligomycin (Olig). Data are expressed as mean + SEM of extrapolated ATP concentration, n=6 and represent two experiments.

The effects of exogenous CXCL14 on intracellular ATP generation in mouse islets was also assessed (Figure 5.4.20). 20mM glucose promoted intracellular ATP generation above that of 2mM sub-stimulatory glucose concentration. The positive control oligomycon inhibited intracellular ATP generation at both 2 and 20mM glucose. In the presence of 20mM glucose, a dose responsive trend in the reduction of intracellular ATP generation was observed with increasing concentration of CXCL14, with statistical significance observed with <80ng/ml of CXCL14. At 2mM glucose,

CXCL14 did not significantly inhibit intracellular ATP production but a statistically non-sigificant reduction in ATP generation was observed with increasing CXCL14 concentration. The glucose-dependent effects of CXCL14 on ATP production in mouse islets exhibits a smilar trend to that observed with insulin secretion from mouse islets (Figure 5.4.5).

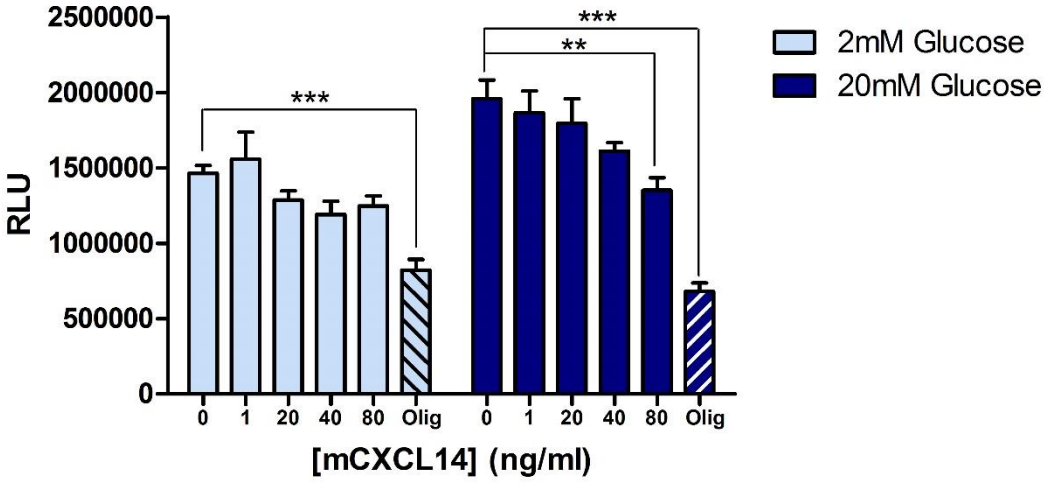

Figure 5.4.20 The effects of CXCL14 on intracellular ATP levels in mouse islets. 80ng/ml of CXCL14 significantly inhibited glucose-induced insulin secretion as did 100ng/ml of the positive control oligomycin (Olig). Data are expressed as mean + SEM, n=8 and represent two separate experiments. Statistics were performed using one-way ANOVA, **p<0.01, ***p<0.001.

5.4.4 Exploring the receptor/s responsible for CXCL14 function

One of the aims within this chapter was to identify the receptor/s responsible for mediating CXCL14 function. By combining current knowledge of CXC-family ligand-receptor interactions along with the 'GPCRome' and 'Secretome' data generated in the previous chapters, a targeted approach to identifying a CXCL14 receptor/s was employed.

5.4.4.1 CXC-chemokine family 'Interactome'

For the purpose of predicting which receptors may be responsible for mediating the function of CXCL14, an 'Interactome' of the CXC-chemokine family ligands and receptors was generated using data obtained from the IUPHAR database (Figure 5.4.21).

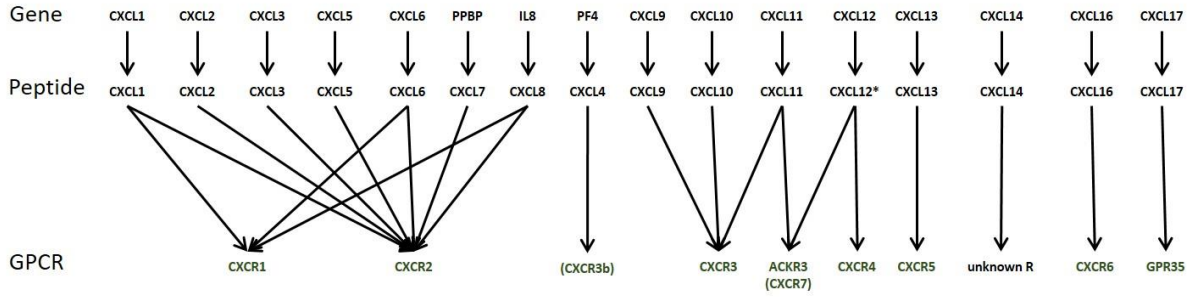

Figure 5.4.21 CXC-chemokine family 'Interactome'. Data were obtained from the IUPHAR/BPS guide to Pharmacology.

The 'Interactome' data indicates that all CXC-chemokine ligands interact with at least one CXC-chemokine receptor, thus suggesting that CXCL14 is likely to do so also.

5.4.4.2 CXC-family-chemokine receptor expression

In order to identify which CXC-receptor may be responsible for CXCL14 function, the mRNA expression profiles of all CXC-receptors in human islets, mouse islets and MIN6 cells were determined (Figure 5.4.22).

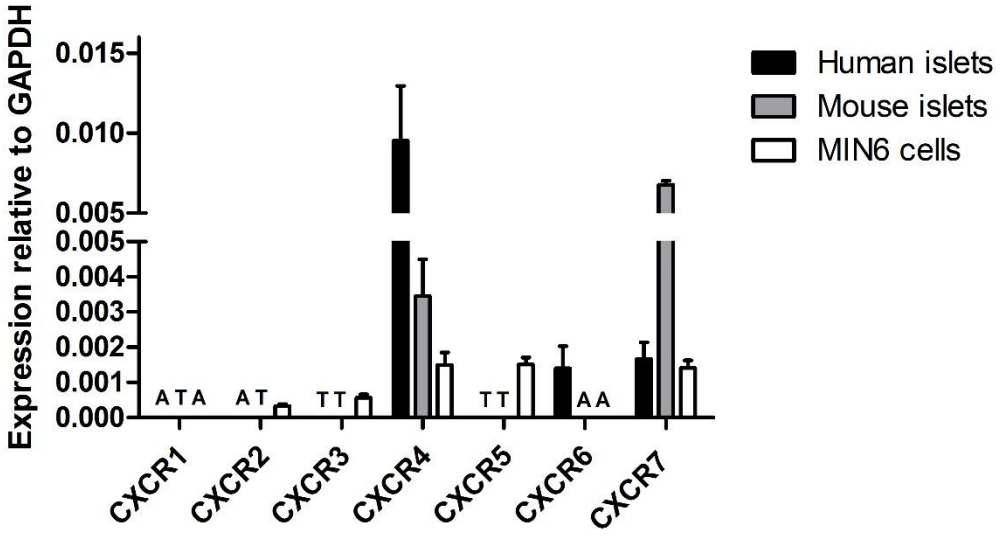

Figure 5.4.22 mRNA expression of CXC-family receptors in human islets, mouse islets and MIN6 cells. Data are expressed as mean + SEM expression relative to GAPDH, n=4. T = trace expression; A = absent expression.

mRNA expression analysis revealed that CXCR4 and CXCR7 are commonly expressed in human islets, mouse islets and MIN6 cells. This observation was particularly interesting as other groups have suggested that CXCL14 antagonises the actions of CXCL12 (Hara and Tanegashima, 2014), which functions at both the CXCR4 and CXCR7 receptors (Figure 5.4.21). According to the IUPHAR database, the principle signalling transduction pathways coupled to CXCR4 and CXCR7 are Gαi and β-arrestin respectively. Whilst we have already shown in section 5.4.3.1 that CXCL14 functions through a cAMP-independent mechanism, and thus unlikely to couple through a Gαi receptor, the fact that GPCRs are promiscuous and have the

ability to couple through atypical signalling pathways depending on which specific ligand interacts with the receptor (functional selectivity) justifies further exploration into the role of CXCR4 and CXCR7 in CXCL14 function.

5.4.4.3 Assessment of CXCL14 interactions with CXCR4 and CXCR7

For the purpose of assessing CXCL14 interaction at the CXCR4 and CXCR7 receptors, β-arrestin recruitment assays were used. The benefit of running β-arrestin assays to assess ligand function is that the technology allows for the detection of ligand function irrespective of the G-protein coupling mechanisms involved, which is particularly useful as many GPCRs couple through various signal transduction cascades, some of which are only activated by specific ligands for that receptor (functional selectivity). This phenomenon is commonly observed with chemokine receptors (Anderson et al., 2016) (Rajagopal et al., 2013) (Steen et al., 2014). CXCL14 function was assessed in agonist and antagonist mode at both the CXCR4 and CXCR7 receptors with CXCL12 used as the natural ligand for both receptors. For antagonism studies, a dose response to CXCL12 in the presence of increasing concentrations of CXCL14 was performed. The benefit of this approach is that not only can antagonism be determined but the mode of antagonism, (orthosteric or allosteric) and/or modulation (positive or negative) can also be elucidated. Due to the fact that CXCL14 inhibited insulin secretion from mouse islets and the mouse β-cell line, the MIN6 cell line, the mouse CXCR4 and CXCR7 β-arrestin assays were used to assess CXCL14 receptor interaction at these receptors.

5.4.4.3.1 Assessment of CXCR4 involvement in CXCL14 function

As expected, the natural ligand CXCL12 induced a dose dependent increase in β-arrestin recruitment at the mCXCR4 receptor (Figure 5.4.23). An EC_{50} of 15.86nM was determined and a Hill slope of 1.079 indicated a 1:1 stoichiometry (one ligand to one binding site) i.e. no co-cooperativity, no multiple binding sites. CXCL14 on the other hand did not to promote β-arrestin recruitment, thus indicating that it is not an agonist for the CXCR4 receptor.

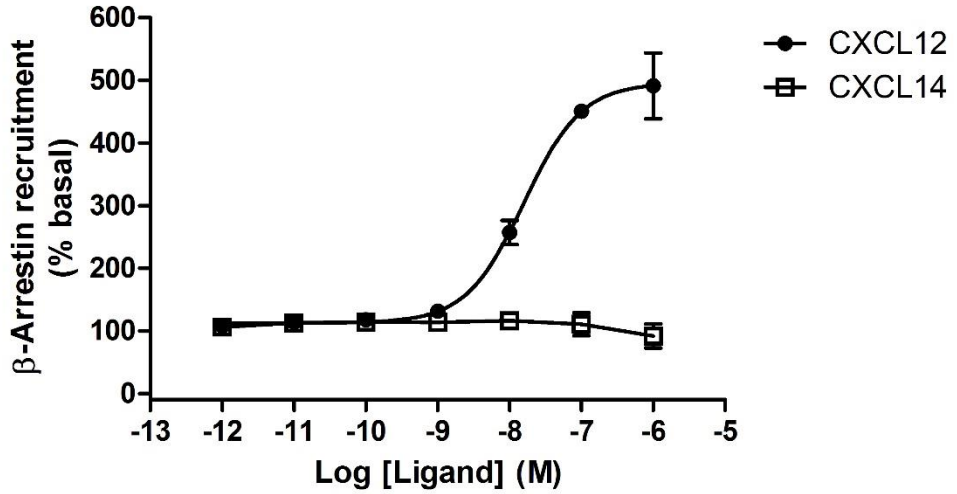

Figure 5.4.23 Assessment of CXCL14 agonism at the mouse CXCR4 receptor. CXCL12 induced β-arrestin recruitment at the mouse CXCR4 receptor with an EC_{50} of 15.86nM and a Hill slope of 1.079. CXCL14 did not promote β-arrestin recruitment. Data are expressed as mean±range, n=2 from one experiment.

The potential antagonistic properties of CXCL14 for the mCXCR4 receptor were assessed by performing dose responses to the natural agonist, CXCL12, in the presence of increasing concentrations of CXCL14 (Figure 5.4.24). The data revealed that, CXCL14 did not alter the EC_{50} of CXCL12 with EC_{50}s of 15.86, 13.98, 15.01, 15.99 and 13.96nM produced in the presence of 0, 0.3, 3, 30 and 300nM CXCL14 respectively. However, the Hill slope for the CXCL12 dose response did increase from

1.079 in the absence of CXCL14 to 1.720, 1.765, 1.593 and 1.996 in the presence of 0.3, 3 30 and 300nM of CXCL14 respectively. The E_{max} of the CXCL12 dose response also increased in the presence of CXCL14 and together with the increase in Hill slope may suggest a positive modulatory effect of CXCL14 on CXCL12 function. However, it is worth noting that neither of these effects were dose responsive within the tested range of CXCL14 (0.3-300nM).

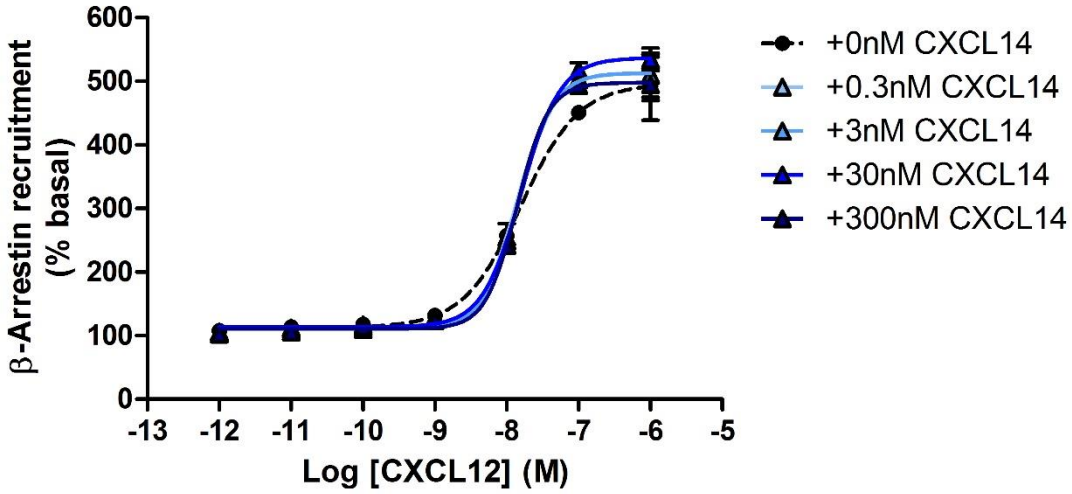

	+0nM CXCL14	+0.3nM CXCL14	+3nM CXCL14	+30nM CXCL14	+300nM CXCL14
Bottom	112.6	111.9	112.8	113.5	110.6
Top	496.1	512.8	513.2	536.8	497.7
LogEC50	-7.800	-7.854	-7.824	-7.796	-7.855
HillSlope	1.079	1.720	1.765	1.593	1.996
EC50	1.586e-008	1.398e-008	1.501e-008	1.599e-008	1.396e-008

Figure 5.4.24 The effects of CXCL14 on CXCL12 β-arrestin recruitment at the mouse CXCR4 receptor. CXCL14 increased both the Hill slope and the Emax of the CXCL12 dose response. Data are expressed as mean ± range, n=2 from one experiment.

5.4.4.3.2 Assessment of CXCR7 involvement in CXCL14 function

The study design for assessing whether CXCR7 is a receptor for CXCL14 was identical to that of the CXCR4 β-arrestin study as described above. To assess agonistic properties of CXCL14 at CXCR7, β-arrestin recruitment at CXCR7 following a 90minute treatment with CXCL14 was assessed. Whilst the natural ligand CXCL12 was able to induce β-arrestin recruitment, CXCL14 did not, thus concluding that CXCL14 is not an agonist for CXCR7 (Figure 5.4.25).

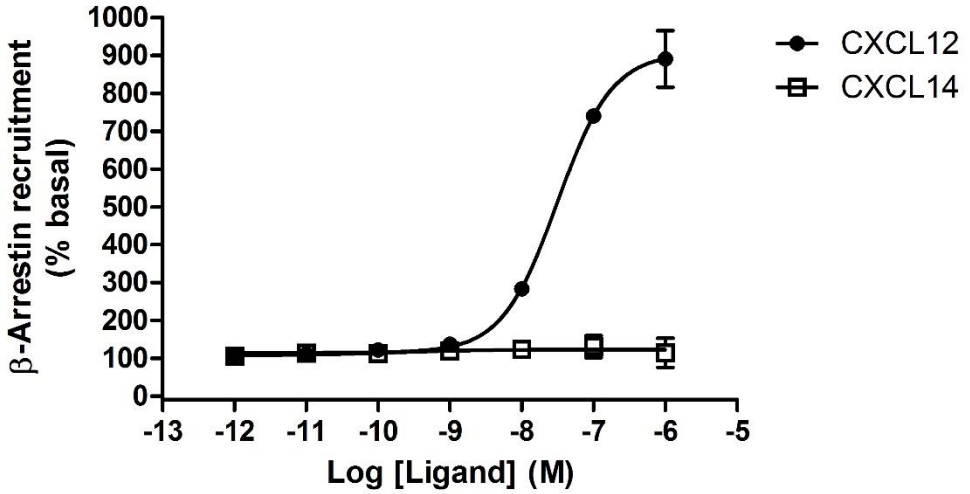

Figure 5.4.25 Assessment of CXCL14 agonism at the mouse CXCR7 receptor. CXCL12 induced β-arrestin recruitment at the mouse CXCR7 receptor with an EC_{50} of 31.29nM and a Hill slope of 1.134. CXCL14 did not promote β-arrestin recruitment. Data are expressed as mean ± range, n=2 from one experiment.

The potential antagonistic properties of CXCL14 at the CXCR7 receptor were assessed by observing the ability of CXCL14 to alter CXCL12-induced β-arrestin recruitment. As observed in Figure 5.4.26, CXCL14 did not alter the EC_{50} of CXCL12 with EC_{50}s of 31.29, 37.80, 35.59, 33.75 and 23.35nM determined in the presence of 0, 0.3, 3.0, 30 and 300nM of CXCL14. The Emax and Hill slope of the CXCL12 dose response were also unaffected, thus concluding that mouse CXCL14 is not an

antagonist for the mouse CXCR7 and that it does not modulate CXCL12 binding or efficacy to the mouse CXCR7 receptor.

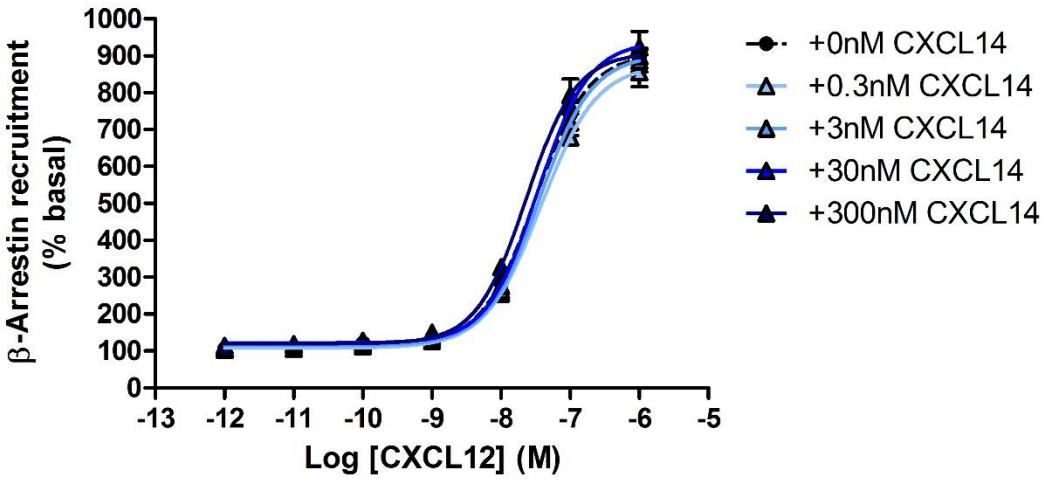

	+0nM CXCL14	+0.3nM CXCL14	+3nM CXCL14	+30nM CXCL14	+300nM CXCL14
Bottom	114.4	107.8	115.1	121.4	119.6
Top	907.2	877.9	903.5	939.0	908.9
LogEC50	-7.505	-7.422	-7.449	-7.472	-7.632
HillSlope	1.134	1.076	1.143	1.179	1.203
EC50	3.129e-008	3.780e-008	3.559e-008	3.375e-008	2.335e-008

Figure 5.4.26 The effect of CXCL14 on CXCL12 β-arrestin recruitment at the mouse CXCR7 receptor. CXCL14 had no effect on CXCL12-induced β-arrestin recruitment. Data are expressed as mean ± range, n=2 from one experiment.

5.5 Discussion

An association between obesity and CXCL14 upregulation, and its subsequent effects on glucose homeostasis, has recently been reported (Hara and Tanegashima, 2012). In the few publications to date, the overall trend regarding CXCL14's role in metabolism appears to be that of a detrimental one, with high fat diet fed CXCL14-knockout mice exhibiting improved insulin responsiveness, decreased hyperinsulinemia and decreased hyperglycaemia, (Nara et al., 2007) and protection from HFD-induced obesity (Tanegashima et al., 2010). Whilst these findings are interesting and present a justified rationale for exploring the effects of inhibiting CXCL14 expression or function as a possible therapeutic approach for T2DM, the revelation that CXCL14 mRNA is expressed within mouse and human islets, (Chapter 4), provided additional intrigue into its role at the islet level. Therefore, the experiments presented in this chapter aimed to identify the localisation of CXCL14 mRNA expression within islets, to assess the effects of CXCL14 on islet and β-cell function, to identify the mechanisms responsible for any observed functional effects and lastly to attempt to elucidate the receptors responsible for mediating CXCL14 function.

CXCL14 mRNA expression analysis, Chapter 4 (Figure 4.4.1), revealed that CXCL14 is expressed by human islets and by islets from both inbred and outbred mouse strains, with higher expression observed in mouse islets. In an attempt to further reveal the localisation of CXCL14 within islets, mRNA expression analysis of CXCL14 in the MIN6 cell and Endoc-βH1 β-cell lines was performed. Results revealed that CXCL14 mRNA expression was present in islets and adipose tissue but absent within both β-cell lines (Figure 5.4.1), indicating that CXCL14 is not expressed within mouse and human β-cells. This observation is consistent with results obtained by Suzuki *et al* revealing that CXCL14 is co-expressed with somatostatin within the secretory vesicles

of δ-cells and not within islet α-, β- or PP cells. It has therefore been postulated that CXCL14 may be co-released with somatostatin to modulate insulin secretion in a paracrine fashion (Suzuki and Yamamoto, 2015). In order to confirm this prediction, a series of experiments were designed to elucidate the role of CXCL14 on islet function.

One of the underlying characteristics of T2DM is β-cell dysfunction, which is characterised by a decrease in the secretion of insulin in response to glucose combined with a reduction in β-cell mass (Oh da and Olefsky, 2016). In order to assess the role of CXCL14 on β-cell dysfunction, the experiments described in this thesis were designed to observe the effects of exogenous CXCL14 on islet insulin secretion as well as CXCL14's effects on β-cell mass by investigating the proliferative and apoptotic properties of CXCL14 on rodent β-cell lines.

Insulin secretion experiments revealed that CXCL14 inhibited glucose-induced insulin secretion (20mM glucose) from mouse islets but not at sub-stimulatory (2mM) glucose concentrations (Figure 5.4.5), whereas a reduction in insulin secretion from MIN6 cells was observed at both 2 and 20mM glucose, with a more pronounced effect at 2mM glucose (Figure 5.4.3). A similar trend was observed with the rat INS-1 β-cell line, whereby CXCL14 also inhibited insulin secretion with a more pronounced effect observed at sub-stimulatory glucose concentrations (Figure 5.4.4). The observation that CXCL14 inhibits insulin secretion from both mouse islets and rodent β-cell lines, indicates that CXCL14 exerts its insulin reducing effects directly on the β-cell. However, the discrepancy in the effects of CXCL14 on insulin secretion at sub-stimulatory glucose concentrations between mouse islets and the rodent β-cell lines suggests that there may be additional non-β-cell specific mechanisms involved. Alternatively, a more simple explanation may be that the assay window with mouse

islets at sub-stimulatory glucose concentrations is not sufficient enough to observe the inhibitory effects of CXCL14, thus restricting the assessment of CXCL14-mediated function on mouse islet insulin secretion at sub-stimulatory glucose concentrations. Whilst these observations, in combination with the findings from other research groups, indicate a detrimental effect of CXCL14 on islet function, glucose homeostasis and obesity, the role of CXCL14 in humans has not yet been evaluated.

Our results indicate clear species differences in the effects of CXCL14 on insulin secretion between mouse and human islets. Data in Figure 5.4.6 reveal that, unlike with mouse islets, CXCL14 did not inhibit human islet insulin secretion at either sub-stimulatory or stimulatory glucose concentrations, thus questioning the translational relevance of studying CXCL14 in relation to T2DM. One obvious explanation for the observed species difference may be due to a difference in the expression level of the receptor responsible for CXCL14 function. The absence of the receptor responsible for CXCL14 function in human islet β-cells would explain the species difference observed, as would a reduced receptor expression in human islets, but due to the fact that CXCL14 is an orphan ligand i.e. its receptor is unknown, this question cannot be easily resolved.

In addition to the effects of CXCL14 on insulin secretion, the effects of CXCL14 on β-cell mass were studied using the MIN6 and INS-1 β-cell lines. Acute exposure to CXCL14 for 1 hour had no effect on MIN6 cell proliferation (Figure 5.4.9) nor apoptosis (Figure 5.4.7), whereas an anti-proliferative effect (Figure 5.4.10), which may be due to a pro-apoptotic effect (Figure 5.4.8), was observed with 40ng/ml of CXCL14 in INS-1 cells. CXCL14 is a homeostatic chemokine whose role is to regulate monocyte infiltration and thus regulate inflammatory processes (Takahashi et al., 2007), and therefore an ability to promote β-cell apoptosis through inflammatory

processes may well be possible, especially in a state where circulating CXCL14 is upregulated e.g. in obesity. However, such pro-apoptotic effects would be expected to be secondary to monocyte infiltration, yet the pro-apoptotic effects observed with CXCL14 on INS-1 cells suggests a direct effect of CXCL14 on β-cell apoptosis. Interestingly, it has been reported that overexpression of CXCL14 promotes apoptosis of HepG2 cells through caspase-dependent pathways (Wang et al., 2013). Such data suggest that CXCL14 is able to promote cell apoptosis independent of monocyte infiltration.

An important consideration when assessing the effects of CXCL14 on islet function is the exposure time. Whilst 1 hour exposure of exogenous CXCL14 had no effect on insulin secretion from human islets at the concentrations tested, the chronic effects of CXCL14 on insulin secretion from human or mouse islets have not been assessed. It has been shown that serum levels of CXCL14 are upregulated in mice fed a high fat diet (Takahashi et al., 2007) and therefore chronic exposure of islets to increased circulating levels of CXCL14 may well have additional detrimental effects on islet function. Studies designed to assess the chronic effects of CXCL14 on islet function, which include the effects on both insulin secretion and β-cell mass, should be performed to gain a full insight into the role of CXCL14 on islet function and also to fully evaluate the species difference effects that we have observed.

According to the data in this chapter, the predominant functional effect of acute exposure of islets to CXCL14 is an inhibition of insulin secretion through direct interaction with the β-cells. In order to identify the underlying mechanisms by which CXCL14 inhibits insulin secretion, mechanistic studies were performed in MIN6 cells. An obvious mechanism responsible for CXCL14 function on insulin secretion is through a reduction in intracellular cAMP, a process mediated either by agonist

activation of a Gαi-coupled GPCR or inverse agonism of a Gαs-coupled GPCR. Interestingly, it has been proposed that CXCL14 binds to the Gαi-coupled CXCR4 receptor in THP-1 cells (Tanegashima et al., 2013), which provided additional justification for assessing the function of CXCL14 as a Gαi-coupled receptor agonist. However, our data revealed that CXCL14, unlike the positive control clonidine, was unable to reduce a forskolin-induced increase in intracellular cAMP in MIN6 cells indicating that it does not function through a Gαi-coupled receptor (Figure 5.4.13). Likewise, the data also revealed that CXCL14 did not reduce basal cAMP levels in MIN6 cells indicating that CXCL14 does not function as an inverse agonist for a Gαs-coupled GPCR (Figure 5.4.13). These results conclude that the effects of CXCL14 on insulin secretion are mediated via a cAMP-independent mechanism.

Another mechanism involved in the regulation of insulin secretion from β-cells is glucose uptake. Insulin secretion is regulated by glucose uptake through membrane localised GLUTs and intracellular glucokinase activity. Studies have shown that CXCL14 enhances insulin-dependent glucose uptake into adipocytes (Takahashi et al., 2007) but conversely attenuates glucose uptake in cultured myocytes (Nara et al., 2007). Whilst it appears that CXCL14 has contrasting effects on insulin-dependent glucose uptake depending on tissue type, the question remained whether CXCL14 could modulate glucose uptake into β-cells, an insulin-independent mechanism. The results reveal that CXCL14 inhibits glucose uptake in MIN6 cells at both 2 and 20mM 2DG with a more pronounced effect observed at 2mM 2DG, a trend which is remarkably similar to the effect of CXCL14 on insulin secretion from MIN6 cells and INS-1 cells. However, the glucose uptake assay used for the experiments described in this thesis does not distinguish between glucose transporter and glucokinase activity, so whether the observed effects of CXCL14 is due to an inhibition of glucose uptake

via the predominantly expressed GLUT-2 or an inhibition of glucokinase activity remains unclear. The mechanism by which CXCL14 enhances glucose uptake, and insulin sensitivity, in cultured adipocytes is proposed to be due to increased tyrosine phosphorylation of the insulin receptor and IRS-1, which is speculated to increase GLUT-4 translocation (Takahashi et al., 2007). However, the predominant GLUT in MIN6 cells is GLUT-2, which unlike GLUT-4, is an insulin-independent facilitative transporter that does not undergo translocation in β-cells. Therefore, whether CXCL14 could interact directly with GLUT-2 to reduce glucose uptake and subsequent insulin secretion remains unclear. It is however worth noting that GLUT subtype expression differs between mouse and human β-cells where GLUT-1, -2 and -3 have been shown to be expressed in human β-cells, whilst GLUT-2 is the predominant transporter in mouse β-cells (Thorens, 2015). If CXCL14 does in fact inhibit GLUT-2 directly then the GLUT subtype expression differences between mouse and human β-cells may explain the species difference effect of CXCL14 on insulin secretion.

The modulation of glucokinase activity by ligands that function through GPCRs has been demonstrated with the GLP-1 receptor. A study by Ding *et al* demonstrated that activation of the GLP-1 receptor by GLP-1 augmented glucose-dependent rises in NADPH in both βTC3 insulinoma cells and mouse islets in a manner that was consistent with post-translation activation of glucokinase by enhancing S-nitrosylation of the V367 amino acid of glucokinase (Ding et al., 2011). Whilst there is no confirmed evidence to suggest that CXCL14 does in fact function through a GPCR, the fact that all other CXC-family chemokine ligands couple through GPCRs and that glucokinase activity can be modulated through GPCR-mediated mechanisms, suggests that CXCL14 may possibly inhibit glucokinase activity through a GPCR-mediated mechanism.

In order to confirm the effects of CXCL14 on MIN6 cell glucose uptake, an assay was developed to assess ATP generation in MIN6 cells (Figure 5.4.18). In theory, intracellular ATP generation should be directly proportional to glucose uptake within a cell and therefore, inhibitors of glucose uptake should affect intracellular ATP generation. However, CXCL14 did not inhibit intracellular ATP levels in MIN6 cells (Figure 5.4.19) unlike the positive control oligomycin. An explanation for this absent effect could partly be due to the narrow assay window of ATP generation following glucose treatment, which suggests that MIN6 cells are highly metabolically active. However, the assessment of CXCL14-mediated effects on intracellular ATP generation in mouse islets revealed that CXCL14 significantly inhibited intracellular ATP generation in mouse islets at 20mM but not at 2mM glucose (Figure 5.4.20), a trend that is similar to the effects observed on insulin secretion from mouse islets. Whilst glucose uptake could not be confirmed in mouse islets due to technical limitations (data not shown), the data so far indicate that the observed inhibitory effect of CXCL14 on insulin secretion is likely to be due to an inhibition of glucose uptake and or/glucokinase activity, which consequently results in a reduction in intracellular ATP production and reduced insulin release. The discrepancy in the glucose-dependent effects of CXCL14 on insulin secretion between MIN6 cells and mouse islets may suggest that CXCL14 exerts additional non-β-cell specific effects that also influence insulin secretion.

The final aim of this chapter was to attempt to identify the receptor/s responsible for CXCL14 function. Using information obtained from the IUPHAR database, an interactive map, an ‘Interactome’, of all CXC-family ligands with their respective CXC-family receptors was generated (Figure 5.4.21). The Interactome information revealed that all CXC-family ligands function through at least one CXC-family

receptor, thus suggesting that CXCL14 is likely to do so also. mRNA expression analysis of the CXC-family receptors in human islets, ICR mouse islets and MIN6 cells revealed abundant expression of the CXCR4 and CXCR7 receptors, which are the cognate receptors for CXCL12. Tanegashima *et al* reported that CXCL14 antagonises CXCL12-mediated chemotaxis of $CD34^+$ hematopoietic progenitor cells and binds with high affinity to the CXCR4 receptor in CXCR4 over-expressing THP-1 cells (Tanegashima et al., 2013). However, a conflicting study reported that CXCL14 did not affect the dose response profiles of CXCL12-induced CXCR4 phosphorylation, calcium mobilisation, ERK1/2 phosphorylation or CXCR4 internalisation in CXCR4 transfected HEK293 and Jurkat T cells (Otte et al., 2014). Despite conflicting evidence, we studied whether CXCL14 functioned as an agonist, antagonist or allosteric modulator at the CXCR4 receptor, in addition to the CXCR7 receptor, using β-arrestin technology. β-arrestin technology was chosen to allow the detection of ligand function irrespective of the G-protein mechanisms involved following receptor activation, thus providing the opportunity to measure unpredicted pathway activation as a result of functional selectivity. The β-arrestin studies were designed to elucidate mechanism of action i.e. agonism, antagonism or modulation, in addition to potential mode of binding i.e. orthosteric or allosteric binding. Our studies revealed that CXCL14 did not induce β-arrestin recruitment at either the CXCR4 (Figure 5.4.23) or CXCR7 (Figure 5.4.25) receptors, indicating that CXCL14 is not an agonist at these receptors. Likewise, antagonist studies revealed that CXCL14 did not antagonise or modulate CXCL12 affinity or efficacy at the CXCR7 receptor, indicating that CXCL14 is not an antagonist or modulator of CXCL12 activity at the CXCR7 receptor. However, an increase in the Hill slope and Emax of the CXCL12 dose response curve at the CXCR4 receptor was observed following co-treatment with

CXCL14, suggesting that CXCL14 positively modulates both the binding and efficacy of CXCL12 at the CXCR4 receptor. It is however worth noting that these observed effects were minor and not dose responsive, suggesting that such observed effects are unlikely to be due to CXCL14 specifically, but more likely due to variability within the assay.

The assumption that CXCL14 function is GPCR-mediated is speculative and is based on the GPCR receptor-activity relationships of fellow CXC-family ligands along with inconsistent literature data. Whether CXCL14 does in fact bind to a GPCR is debateable as CXCL14 homologs in all vertebrates differ structurally from all other chemokines by possessing an uncharacteristically short amino-terminus of only two amino acids located before the first disulphide bridge, a region which is typically required for triggering GPCR activation (Benarafa and Wolf, 2015). This evidence suggests that unlike its fellow CXC-family ligands, CXCL14 function may not be GPCR-mediated and thus efforts to elucidate the target responsible for mediating CXCL14 function should also consider alternative target classes.

Summary and future perspectives

It is clear from published studies that CXCL14 plays a role in rodent glucose homeostasis and the data within this chapter provides additional information into CXCL14's role in inhibiting insulin secretion from rodent islets and β-cell lines, yet due to the absence of effect in human islets, the translational relevance of these observations remains unclear. Further studies are required to assess the chronic effects of CXCL14 on both mouse and human islet function to conclusively state whether

species differences exist and whether CXCL14 should be pursued further as a target of interest in relation to T2DM.

The mechanism by which CXCL14 inhibits insulin secretion from MIN6 cells and mouse islets appears to be at least in part due to a reduction in glucose uptake leading to a subsequent reduction in ATP synthesis, but whether this is due to a direct effect on GLUT2 or glucokinase activity requires further clarification. The discrepancy in the glucose-dependent effects of CXCL14 on insulin secretion from MIN6 cells and mouse islets suggests that CXCL14 may also mediate functional effects on alternative cell types within islets. It may therefore be worth investigating the effects of CXCL14 on somatostatin and glucagon release.

Should CXCL14 function through a GPCR it may well be possible that the inhibitory effect of CXCL14 on glucose uptake could be due to a GPCR-mediated inhibition of glucokinase activity, but exploring this remains challenging due to CXCL14's orphan status. Contrasting reports combined with the results obtained within this chapter suggest that, unlike other CXC-family chemokines, CXCL14 is unlikely to function through a CXC-family receptor. There is evidence to suggest inter-chemokine-family ligand-receptor interactions exist (Huang, 2002) (Kufareva et al., 2015) and the GPCRome data revealed within this thesis could identify potential receptor candidates that are worth of exploring, such as CCR2, CCR3, CCR5 and CCR10. It is however also possible that CXCL14 does not function through a GPCR-mediated mechanism and therefore alternative target classes should also be considered.

CHAPTER 6 - General discussion

T2DM is a metabolic disorder that accounts for approximately 90% of all diabetes cases and is estimated to affect 371 million people worldwide (Guariguata, 2012). It is characterised by hyperglycaemia, which is a consequence of insufficient insulin secretion, insulin resistance in metabolically active tissues and inadequate suppression of glucagon production (Spellman, 2010). The principle causal factors contributing to the increase in incidence of T2DM worldwide include relative over-nutrition and sedentary activity, both of which are a result of a global transition to a more modern westernised lifestyle (Zimmet, 1999). In the UK alone, approximately 9% of the NHS budget is spent on treating diabetes and its associated complications, equating to approximately £10 billion per year (Meetoo et al., 2007). This figure is certain to rise further with projected increases in incidences, and therefore efforts are being made to develop suitable therapies to treat T2DM and to prevent its associated complications.

The primary aim of T2DM therapies is to maintain glucose homeostasis for as long as possible following diagnosis, thereby reducing the onset of associated complications (Kahn et al., 2014). Numerous therapies with varying mechanisms of action have been developed but limitations in drug safety profiles and efficacy mean that the search for improved therapies are ongoing. One particular target class that is receiving such attention is the GPCR family. Historically, GPCRs have proven to be a successful target class for many indications accounting for approximately 17% of all approvals since 1982 (Rask-Andersen et al., 2011). However, despite this success for a variety of conditions, only one GPCR, the GLP-1 receptor, has proven to be clinically successful in treating T2DM. Part of the issue contributing the limited success of targeting GPCRs for T2DM is the poor functional characterisation of the majority of islet-expressed GPCRs. This issue is further exacerbated by the limited availability of human islets required to study GPCR function, and as a result rodent islets, particularly

mouse islets, are relied upon as translational models. Structural differences between rodent and human islets are well documented (Steiner et al., 2010), which poses a question of the suitability of using rodent islets, in particular mouse islets, as translational models for predicting GPCR-mediated regulation of human islet function. Therefore, the experiments described in this thesis aimed to quantify and compare the mRNA expression levels of non-odorant GPCRs and GPCR peptide ligands in mouse and human islets in order to assess the suitability of using mouse islets to predict GPCR and GPCR peptide ligand function in human islets. Furthermore, this thesis also highlights how such gene expression data can be utilised to identify islet-expressed GPCR peptide ligands whose role in islet function is yet to be characterised, and how both the Secretome and GPCRome data can be employed to explore the mechanism of action of such peptides in islet function, as exemplified by CXCL14.

6.1 GPCRome comparison

GPCR mRNA expression analyses detailed in Chapter 3 revealed that a high proportion of non-odorant GPCRs are expressed within both human and mouse islets of Langerhans. Of the 376 GPCRs assessed for expression within human islets, 284 GPCR mRNAs (75%) were shown to be expressed by human islets, whereas of the 335 mouse orthologue GPCR genes screened in mouse islets, 281 (84%) and 230 (67%) GPCRs were expressed in ICR and C57 mouse islets respectively. This high proportion of GPCR expression is unsurprising given the fact that GPCRs play an important role in regulating islet function, that islets are comprised of numerous cell types and that islet function is regulated by various GPCR-dependent inputs such as,

neural input from the CNS, by gastrointestinal peptides, bile acids and also circulating nutrients, fatty acids and amino acids (Reimann and Gribble, 2016).

Despite the fact that a large proportion of the total GPCRs quantified were shown to be expressed in both human and mouse islets, regression analysis (r^2) revealed that GPCR expression levels differed between human islets and mouse islets: human vs. ICR = 0.360 and human vs. C57 = 0.304. Part of the cause of this variation is likely to be the difference in the proportions of endocrine cells between human and mouse islets. However, this does not explain the exclusive expression of certain GPCRs within each islet group.

The observation that the degree of overall GPCR expression in human islets is more similar to that of the ICR mouse strain than the C57 strain is likely to be due the degree of genetic variability between the two mouse strains, as one would presume that a greater degree of gene expression variability is likely to be observed within the outbred ICR strain. This degree of genetic variability between biological replicates of the ICR strain could result in a greater degree of inconsistency in expression compared to the C57 strain, thus preferentially skewing the data in favour of using ICR islets as suitable surrogate models for human islet studies. Furthermore, the use of outbred models is likely to introduce a degree of genetic variability consistent with the human situation, and thus be more translationally relevant.

The data within Chapter 3 suggest that mouse islets can be utilised to predict the involvement of GPCRs in human islet function, but that suitability is receptor-specific. For example, the expression levels of the 14 selected GPCRs that exhibit functional characteristics appropriate for the treatment of T2DM indicate that mouse islets would indeed be suitable ($r^2 = 0.531$). However, whilst it can be postulated that mouse islets

are suitable surrogate models based on mRNA expression analysis, further functional studies are required confirm such claims. For example, assessment on whether the GPCR mRNA is translated into protein, whether the receptor localises to the plasma membrane or whether the cellular machinery required for protein function is present in islets should be determined, in addition to assessing which endocrine cell types express which GPCRs.

6.2 Secretome comparison

A high proportion of GPCR peptide ligand mRNAs are expressed within both human and mouse islets. Of the 159 GPCR peptide ligands screened for expression in human islets, 128 (81%) were shown to be expressed, whilst of the 145 mouse orthologues screened, 109 (75%) and 86 (59%) were expressed in ICR and C57 mouse islets respectively. This expression of a variety of peptide ligands is likely to be expected of endocrine cells whose primary function is to secrete a multitude of factors which regulate not only processes within the islet microenvironment but also the processes of other body tissues through delivery via the systemic circulation (Brereton et al., 2015).

However, similar with GPCR expression, despite the fact both human and mouse islets express a multitude of peptide ligands, the degree of mRNA expression of those peptide ligands varies between human and mouse islets. This is highlighted by regression analysis (r^2), which indicates that human vs. ICR = 0.245 and human vs. C57 = 0.225. As discussed previously, the disparity in expression level is likely to be due to differences in the proportion of endocrine cells present within islets between the species. Interestingly, the number of GPCR peptide mRNAs expressed within C57

mouse islets was less than in ICR mouse islets, a trend that was also observed for GPCR expression (Figure 3.4.4, Figure 3.4.5). This trend is likely to be attributed to the greater genetic variability of the outbred ICR strain compared to the more homogeneous inbred C57 mouse strain, where expression between biological replicates is more consistent. As previously mentioned, the use of outbred models, such as ICR mice, is more comparable with the human situation and thus more translationally relevant. This fact that is further reinforced by the regression analysis data which revealed that human islets are more similar to ICR mouse islets than C57 mouse islets with regards to GPCR peptide ligand gene expression (human vs. ICR = 0.245 and human vs. C57 = 0.225).

While the principal aim of the Secretome comparison was to highlight similarities and differences in peptide ligand expression between human and mouse islets, the data generated also offered the opportunity to identify islet-expressed GPCR peptide ligands whose role in islet function has yet to be determined. Such examples include, C1QL1, EDN3 and CXCL14. Interestingly, CXCL14 has been shown to play a role in rodent glucose metabolism and obesity, yet the role of CXCL14 on islet function is not understood. Furthermore, the receptor to which CXCL14 binds is also unknown. Therefore, the final results chapter in this thesis aimed to reveal not only the role of CXCL14 in islet function but also to explore which receptors may be responsible for CXCL14 function.

6.3 The effects of CXCL14 on islet function

An association between obesity and CXCL14 upregulation, and its subsequent effects on glucose homeostasis, has recently been reported (Hara and Tanegashima, 2012). In the few publications to date, the overall trend regarding CXCL14's role in metabolism appears to be that of a detrimental one, with high fat diet fed CXCL14-knockout mice exhibiting improved insulin responsiveness, decreased hyperinsulinaemia and decreased hyperglycaemia (Nara et al., 2007), while also being protected from HFD-induced obesity (Tanegashima et al., 2010). Whilst these findings are interesting and present a justified rationale for exploring the effects of inhibiting CXCL14 expression or function as a possible therapeutic approach for T2DM, the revelation that CXCL14 mRNA is expressed within mouse and human islets, (Chapter 4), provided additional intrigue into its role at the islet level.

Prior to undertaking this project, the localisation of CXCL14 within islets was not known. According to the data presented in this thesis, CXCL14 mRNA is not expressed within β-cells as indicated by the absence of mRNA expression in the Endoc-βH1 and MIN6 human and mouse β-cell lines. During the course of performing such studies, a recently published study revealed that CXCL14 is co-expressed with somatostatin within mouse δ-cells but not expressed within α-, β- and PP cells (Suzuki and Yamamoto, 2015), a finding which was consistent with the expression data in this thesis. It was therefore postulated that CXCL14 may be co-released with somatostatin to regulate insulin secretion, so functional studies assessing the role of CXCL14 on insulin secretion and β-cell mass were performed.

Treatment of both MIN6 cells and INS-1 cells with CXCL14 resulted in a significant inhibition of insulin secretion with a more pronounced effect observed at sub-

stimulatory glucose concentrations. Interestingly, CXCL14 also inhibited insulin secretion from mouse islets, but only at stimulatory glucose levels. The differences in effects seen with the cell lines and islets suggests that whilst the inhibitory effects of CXCL14 appear to be β-cell-specific, it may also act at other cell types in whole islets. In order to confirm the translational relevance of such findings, the effects of CXCL14 on insulin secretion from human islets were studied. Unlike the data obtained with mouse islets, CXCL14 did not inhibit insulin secretion indicating a clear species-specific effect, which is likely to be explained by a disparity in the expression of the receptor responsible for CXCL14 function. However, due to the orphan status of CXCL14, this cannot be easily determined.

In addition to assessing the effects of CXCL14 on insulin secretion, effects on β-cell mass were also explored. CXCL14 did not modulate MIN6 cell proliferation or apoptosis but a decrease in INS-1 cell proliferation and an increase in INS-1 cell apoptosis were observed at the highest concentration of CXCL14 tested (40ng/ml). Interestingly, it has been reported that overexpression of CXCL14 promotes apoptosis of a liver cell line (HepG2) through caspase-dependent pathways (Wang et al., 2013), thus suggesting that CXCL14 exhibits pro-apoptotic properties. Such published findings, in addition to the data generated in this thesis, suggest that CXCL14 may impact β-cell mass through the promotion of apoptosis, but further experiments are required to establish whether these observations in INS-1 cells are also seen in primary islets.

Exploration of the mechanisms involved in CXCL14's regulation of insulin secretion indicate that it does not function through a cAMP-dependent mechanism but instead inhibits either glucose uptake via GLUT2 or β-cell glucokinase activity. Such a mode of action was further reinforced following the observation that acute treatment (1 hour)

with exogenous CXCL14 inhibited ATP production in mouse islets. Furthermore, the effects of CXCL14-mediated inhibition of ATP production in mouse islets appear to be glucose-dependent, an effect also observed for its effects on insulin-secretion from mouse islets. The combination of such functional data suggests that CXCL14 inhibits insulin secretion by impairing glucose uptake or glucokinase activity, thus reducing glucose metabolism through the glycolytic and TCA pathways and resulting in a reduction intracellular ATP production. However, whether such effects are due to GLUT-2 or glucokinase inhibition are unclear. Should CXCL14 function via a GPCR, like fellow members of its chemokine class, it could be postulated that glucokinase activity may be the underlying factor involved as GPCR-mediated modulation of glucokinase activity has been previously been demonstrated, such as with GLP1R (Ding et al., 2011). If inhibition of GLUT-2 activity was the underlying factor then this may explain the species-selective effect of CXCL14 on insulin secretion due to the GLUT subtype expression differences observed between human and mouse β-cells (Thorens, 2015). Further studies are required to distinguish between GLUT-2 and glucokinase involvement in CXCL14-mediated reduction in insulin secretion and whether such effects are in fact facilitated by a GPCR mechanism.

The experiments within this thesis rule out the involvement of both CXCR4 and CXCR7 in CXCL14 function in β-cells, despite reports suggesting that CXCR4 interacts with CXCL14 (Tanegashima et al., 2013). There is evidence to suggest the existence of inter-chemokine-family ligand-receptor interactions (Huang, 2002) (Kufareva et al., 2015) and the GPCRome data revealed within this thesis could identify potential receptor candidates that are worth exploring, such as CCR2, CCR3, CCR5 and CCR10. However, whether CXCL14 does in fact bind to a GPCR is debateable as CXCL14 homologues in all vertebrates differ structurally from all other

chemokines by possessing an uncharacteristically short amino-terminus of only two amino acids located before the first disulphide bridge, a region which is typically required for triggering GPCR activation (Benarafa and Wolf, 2015). This evidence suggests that unlike its fellow CXC-family ligands, CXCL14 function may not be GPCR-mediated and thus efforts to elucidate the mechanism responsible for mediating CXCL14 function should also consider alternative target classes.

6.4 Concluding remarks

The islet GPCR and peptide ligand mRNA quantifications described in this thesis reveal a large amount of data that can be evaluated to assess the suitability of utilising mouse islets to study GPCR and peptide ligand involvement in human islet function. Understanding translation model suitability is fundamental to the research work flow before time and resources are committed. This point is exemplified by the limited success of strategies directed at developing GPR119 agonists as T2DM therapeutics, which has been attributed to efficacy differences between rodent and human species (Ritter et al., 2016). Furthermore, gene expression data also provide a resource of information that can be utilised to identify receptors and peptides whose role in islet function are yet to be characterised, for example, CXCL14, thus furthering our understanding of islet function and offering additional opportunities to identify novel targets for T2DM.

7 Reference

AHREN, B. 2000. Autonomic regulation of islet hormone secretion--implications for health and disease. *Diabetologia,* 43**,** 393-410.

AHREN, B. & LARSSON, H. 1996. Peptide YY does not inhibit glucose-stimulated insulin secretion in humans. *Eur J Endocrinol,* 134**,** 362-5.

AMERICAN DIABETES, A. 2014. Standards of medical care in diabetes--2014. *Diabetes Care,* 37 Suppl 1**,** S14-80.

AMERICAN DIABETES, A. 2016. 2. Classification and Diagnosis of Diabetes. *Diabetes Care,* 39 Suppl 1**,** S13-22.

AMISTEN, S., SALEHI, A., RORSMAN, P., JONES, P. M. & PERSAUD, S. J. 2013. An atlas and functional analysis of G-protein coupled receptors in human islets of Langerhans. *Pharmacol Ther,* 139**,** 359-91.

ANDERSON, C. A., SOLARI, R. & PEASE, J. E. 2016. Biased agonism at chemokine receptors: obstacles or opportunities for drug discovery? *J Leukoc Biol,* 99**,** 901-9.

APARICIO, L. M., VILLAAMIL, V. M., CALVO, M. B., RUBIRA, L. V., ROIS, J. M., VALLADARES-AYERBES, M., CAMPELO, R. G., BOLOS, M. V. & PULIDO, E. G. 2010. Glucose transporter expression and the potential role of fructose in renal cell carcinoma: A correlation with pathological parameters. *Mol Med Rep,* 3**,** 575-80.

ARIYASU, H., TAKAYA, K., TAGAMI, T., OGAWA, Y., HOSODA, K., AKAMIZU, T., SUDA, M., KOH, T., NATSUI, K., TOYOOKA, S., SHIRAKAMI, G., USUI, T., SHIMATSU, A., DOI, K., HOSODA, H., KOJIMA, M., KANGAWA, K. & NAKAO, K. 2001. Stomach is a major source of circulating ghrelin, and feeding state determines plasma ghrelin-like immunoreactivity levels in humans. *J Clin Endocrinol Metab,* 86**,** 4753-8.

ASHCROFT, F. M. & RORSMAN, P. 2012. Diabetes mellitus and the beta cell: the last ten years. *Cell,* 148**,** 1160-71.

BACHA, F. & KLINEPETER BARTZ, S. 2015. Insulin resistance, role of metformin and other non-insulin therapies in pediatric type 1 diabetes. *Pediatr Diabetes.*

BARRETT, J. C., CLAYTON, D. G., CONCANNON, P., AKOLKAR, B., COOPER, J. D., ERLICH, H. A., JULIER, C., MORAHAN, G., NERUP, J., NIERRAS, C., PLAGNOL, V., POCIOT, F., SCHUILENBURG, H., SMYTH, D. J., STEVENS, H., TODD, J. A., WALKER, N. M., RICH, S. S. & TYPE 1 DIABETES GENETICS, C. 2009. Genome-wide association study and meta-analysis find that over 40 loci affect risk of type 1 diabetes. *Nat Genet,* 41**,** 703-7.

BAYNES, K. C. 2010. The evolving world of GLP-1 agonist therapies for type 2 diabetes. *Ther Adv Endocrinol Metab,* 1**,** 61-7.

BELL, G. I., PICTET, R. L., RUTTER, W. J., CORDELL, B., TISCHER, E. & GOODMAN, H. M. 1980. Sequence of the human insulin gene. *Nature,* 284**,** 26-32.

BENARAFA, C. & WOLF, M. 2015. CXCL14: the Swiss army knife chemokine. *Oncotarget,* 6**,** 34065-6.

BENNER, C., VAN DER MEULEN, T., CACERES, E., TIGYI, K., DONALDSON, C. J. & HUISING, M. O. 2014. The transcriptional landscape of mouse beta cells compared to human beta cells reveals notable species differences in long non-coding RNA and protein-coding gene expression. *BMC Genomics,* 15**,** 620.

BENNETT, K., JAMES, C. & HUSSAIN, K. 2010. Pancreatic beta-cell KATP channels: Hypoglycaemia and hyperglycaemia. *Rev Endocr Metab Disord,* 11**,** 157-63.

BENNETT, S. T., LUCASSEN, A. M., GOUGH, S. C., POWELL, E. E., UNDLIEN, D. E., PRITCHARD, L. E., MERRIMAN, M. E., KAWAGUCHI, Y., DRONSFIELD, M. J., POCIOT, F. & ET AL. 1995. Susceptibility to human type 1 diabetes at IDDM2 is determined by tandem repeat variation at the insulin gene minisatellite locus. *Nat Genet,* 9**,** 284-92.

BERGMAN, R. N. 2005. Minimal model: perspective from 2005. *Horm Res,* 64 Suppl 3**,** 8-15.

BJARNADOTTIR, T. K., GLORIAM, D. E., HELLSTRAND, S. H., KRISTIANSSON, H., FREDRIKSSON, R. & SCHIOTH, H. B. 2006. Comprehensive repertoire and phylogenetic analysis of the G protein-coupled receptors in human and mouse. *Genomics,* 88**,** 263-73.

BOEY, D., LIN, S., KARL, T., BALDOCK, P., LEE, N., ENRIQUEZ, R., COUZENS, M., SLACK, K., DALLMANN, R., SAINSBURY, A. & HERZOG, H. 2006. Peptide YY ablation in mice leads to the development of hyperinsulinaemia and obesity. *Diabetologia,* 49**,** 1360-70.

BOHME, I. & BECK-SICKINGER, A. G. 2009. Illuminating the life of GPCRs. *Cell Commun Signal,* 7**,** 16.

BOLLIGER, M. F., MARTINELLI, D. C. & SUDHOF, T. C. 2011. The cell-adhesion G protein-coupled receptor BAI3 is a high-affinity receptor for C1q-like proteins. *Proc Natl Acad Sci U S A,* 108**,** 2534-9.

BONNEVIE-NIELSEN, V., SKOVGAARD, L. T. & LERNMARK, A. 1983. beta-Cell function relative to islet volume and hormone content in the isolated perfused mouse pancreas. *Endocrinology,* 112**,** 1049-56.

BOSI, E. 2009. Metformin--the gold standard in type 2 diabetes: what does the evidence tell us? *Diabetes Obes Metab,* 11 Suppl 2**,** 3-8.

BOTTCHER, G., AHREN, B., LUNDQUIST, I. & SUNDLER, F. 1989. Peptide YY: intrapancreatic localization and effects on insulin and glucagon secretion in the mouse. *Pancreas,* 4**,** 282-8.

BOUTENS, L. & STIENSTRA, R. 2016. Adipose tissue macrophages: going off track during obesity. *Diabetologia,* 59**,** 879-94.

BOWE, J. E., FOOT, V. L., AMIEL, S. A., HUANG, G. C., LAMB, M. W., LAKEY, J., JONES, P. M. & PERSAUD, S. J. 2012. GPR54 peptide agonists stimulate insulin secretion from murine, porcine and human islets. *Islets,* 4**,** 20-3.

BOWE, J. E., KING, A. J., KINSEY-JONES, J. S., FOOT, V. L., LI, X. F., O'BYRNE, K. T., PERSAUD, S. J. & JONES, P. M. 2009. Kisspeptin stimulation of insulin secretion: mechanisms of action in mouse islets and rats. *Diabetologia,* 52**,** 855-62.

BRERETON, M. F., VERGARI, E., ZHANG, Q. & CLARK, A. 2015. Alpha-, Delta- and PP-cells: Are They the Architectural Cornerstones of Islet Structure and Co-ordination? *J Histochem Cytochem,* 63**,** 575-91.

BROWN, A. E., PALSGAARD, J., BORUP, R., AVERY, P., GUNN, D. A., DE MEYTS, P., YEAMAN, S. J. & WALKER, M. 2015. p38 MAPK activation upregulates proinflammatory pathways in skeletal muscle cells from insulin-

resistant type 2 diabetic patients. *Am J Physiol Endocrinol Metab,* 308**,** E63-70.

BRUNICARDI, F. C., ATIYA, A., MOLDOVAN, S., LEE, T. C., FAGAN, S. P., KLEINMAN, R. M., ADRIAN, T. E., COY, D. H., WALSH, J. H. & FISHER, W. E. 2003. Activation of somatostatin receptor subtype 2 inhibits insulin secretion in the isolated perfused human pancreas. *Pancreas,* 27**,** e84-9.

BURGE, M. R., CASTILLO, K. R. & SCHADE, D. S. 1997. Meal composition is a determinant of lispro-induced hypoglycemia in IDDM. *Diabetes Care,* 20**,** 152-5.

BUTEAU, J. 2008. GLP-1 receptor signaling: effects on pancreatic beta-cell proliferation and survival. *Diabetes Metab,* 34 Suppl 2**,** S73-7.

BUTEAU, J., FOISY, S., JOLY, E. & PRENTKI, M. 2003. Glucagon-like peptide 1 induces pancreatic beta-cell proliferation via transactivation of the epidermal growth factor receptor. *Diabetes,* 52**,** 124-32.

BUTEAU, J., RODUIT, R., SUSINI, S. & PRENTKI, M. 1999. Glucagon-like peptide-1 promotes DNA synthesis, activates phosphatidylinositol 3-kinase and increases transcription factor pancreatic and duodenal homeobox gene 1 (PDX-1) DNA binding activity in beta (INS-1)-cells. *Diabetologia,* 42**,** 856-64.

BUTLER, A. E., JANSON, J., BONNER-WEIR, S., RITZEL, R., RIZZA, R. A. & BUTLER, P. C. 2003. Beta-cell deficit and increased beta-cell apoptosis in humans with type 2 diabetes. *Diabetes,* 52**,** 102-10.

CABRERA, O., BERMAN, D. M., KENYON, N. S., RICORDI, C., BERGGREN, P. O. & CAICEDO, A. 2006. The unique cytoarchitecture of human pancreatic islets has implications for islet cell function. *Proc Natl Acad Sci U S A,* 103**,** 2334-9.

CAMPBELL, J. E. & DRUCKER, D. J. 2015. Islet alpha cells and glucagon--critical regulators of energy homeostasis. *Nat Rev Endocrinol,* 11**,** 329-38.

CARLSSON, P. O., STRIDSBERG, M. & JANSSON, L. 1995. Influence of corticotropin-releasing factor on pancreatic and islet blood flow in different regions of the rat pancreas. *Digestion,* 56**,** 242-5.

CHU, Z. L., CARROLL, C., ALFONSO, J., GUTIERREZ, V., HE, H., LUCMAN, A., PEDRAZA, M., MONDALA, H., GAO, H., BAGNOL, D., CHEN, R.,

JONES, R. M., BEHAN, D. P. & LEONARD, J. 2008. A role for intestinal endocrine cell-expressed g protein-coupled receptor 119 in glycemic control by enhancing glucagon-like Peptide-1 and glucose-dependent insulinotropic Peptide release. *Endocrinology,* 149**,** 2038-47.

CRESPIN, S. R., GREENOUGH, W. B., 3RD & STEINBERG, D. 1973. Stimulation of insulin secretion by long-chain free fatty acids. A direct pancreatic effect. *J Clin Invest,* 52**,** 1979-84.

CURRIE, K. P. 2010. G protein modulation of CaV2 voltage-gated calcium channels. *Channels (Austin),* 4**,** 497-509.

DA ROCHA FERNANDES, J., OGURTSOVA, K., LINNENKAMP, U., GUARIGUATA, L., SEURING, T., ZHANG, P., CAVAN, D. & MAKAROFF, L. E. 2016. IDF Diabetes Atlas estimates of 2014 global health expenditures on diabetes. *Diabetes Res Clin Pract,* 117**,** 48-54.

DAI, C., BRISSOVA, M., HANG, Y., THOMPSON, C., POFFENBERGER, G., SHOSTAK, A., CHEN, Z., STEIN, R. & POWERS, A. C. 2012. Islet-enriched gene expression and glucose-induced insulin secretion in human and mouse islets. *Diabetologia,* 55**,** 707-18.

DANEMAN, D. 2006. Type 1 diabetes. *Lancet,* 367**,** 847-58.

DANESHIAN, M., AKBARSHA, M. A., BLAAUBOER, B., CALONI, F., COSSON, P., CURREN, R., GOLDBERG, A., GRUBER, F., OHL, F., PFALLER, W., VAN DER VALK, J., VINARDELL, P., ZURLO, J., HARTUNG, T. & LEIST, M. 2011. A framework program for the teaching of alternative methods (replacement, reduction, refinement) to animal experimentation. *ALTEX,* 28**,** 341-52.

DASCAL, N. 2001. Ion-channel regulation by G proteins. *Trends Endocrinol Metab,* 12**,** 391-8.

DATE, Y., NAKAZATO, M., HASHIGUCHI, S., DEZAKI, K., MONDAL, M. S., HOSODA, H., KOJIMA, M., KANGAWA, K., ARIMA, T., MATSUO, H., YADA, T. & MATSUKURA, S. 2002. Ghrelin is present in pancreatic alpha-cells of humans and rats and stimulates insulin secretion. *Diabetes,* 51**,** 124-9.

DAVIDSON, H. W. & HUTTON, J. C. 1987. The insulin-secretory-granule carboxypeptidase H. Purification and demonstration of involvement in proinsulin processing. *Biochem J,* 245**,** 575-82.

DE CARLO, E., MILANESI, A., MARTINI, C., MAFFEI, P., SICOLO, N. & SCANDELLARI, C. 2000. Endothelin-1 and endothelin-3 stimulate insulin release by isolated rat pancreatic islets. *J Endocrinol Invest,* 23**,** 240-5.

DEL PRATO, S., MARCHETTI, P. & BONADONNA, R. C. 2002. Phasic insulin release and metabolic regulation in type 2 diabetes. *Diabetes,* 51 Suppl 1**,** S109-16.

DEWIRE, S. M., AHN, S., LEFKOWITZ, R. J. & SHENOY, S. K. 2007. Beta-arrestins and cell signaling. *Annu Rev Physiol,* 69**,** 483-510.

DEZAKI, K. & YADA, T. 2012. Islet beta-cell ghrelin signaling for inhibition of insulin secretion. *Methods Enzymol,* 514**,** 317-31.

DING, S. Y., NKOBENA, A., KRAFT, C. A., MARKWARDT, M. L. & RIZZO, M. A. 2011. Glucagon-like peptide 1 stimulates post-translational activation of glucokinase in pancreatic beta cells. *J Biol Chem,* 286**,** 16768-74.

DOLENSEK, J., RUPNIK, M. S. & STOZER, A. 2015. Structural similarities and differences between the human and the mouse pancreas. *Islets,* 7**,** e1024405.

DRAKE, M. T., SHENOY, S. K. & LEFKOWITZ, R. J. 2006. Trafficking of G protein-coupled receptors. *Circ Res,* 99**,** 570-82.

DRUCKER, D. J. 2015. Deciphering metabolic messages from the gut drives therapeutic innovation: the 2014 Banting Lecture. *Diabetes,* 64**,** 317-26.

DUAN, H., NING, M., ZOU, Q., YE, Y., FENG, Y., ZHANG, L., LENG, Y. & SHEN, J. 2015. Discovery of Intestinal Targeted TGR5 Agonists for the Treatment of Type 2 Diabetes. *J Med Chem,* 58**,** 3315-28.

DUBOIS, M., VANTYGHEM, M. C., SCHOONJANS, K. & PATTOU, F. 2002. [Thiazolidinediones in type 2 diabetes. Role of peroxisome proliferator-activated receptor gamma (PPARgamma)]. *Ann Endocrinol (Paris),* 63**,** 511-23.

EASOM, R. A. 1999. CaM kinase II: a protein kinase with extraordinary talents germane to insulin exocytosis. *Diabetes,* 48**,** 675-84.

EDFALK, S., STENEBERG, P. & EDLUND, H. 2008. Gpr40 is expressed in enteroendocrine cells and mediates free fatty acid stimulation of incretin secretion. *Diabetes,* 57**,** 2280-7.

ELMORE, S. 2007. Apoptosis: a review of programmed cell death. *Toxicol Pathol,* 35**,** 495-516.

ERGUL, A. 2011. Endothelin-1 and diabetic complications: focus on the vasculature. *Pharmacol Res,* 63**,** 477-82.

FANG, P., SHI, M., ZHU, Y., BO, P. & ZHANG, Z. 2016. Type 2 diabetes mellitus as a disorder of galanin resistance. *Exp Gerontol,* 73**,** 72-7.

FEKETE, E. M. & ZORRILLA, E. P. 2007. Physiology, pharmacology, and therapeutic relevance of urocortins in mammals: ancient CRF paralogs. *Front Neuroendocrinol,* 28**,** 1-27.

FENG, Y., GUAN, X. M., LI, J., METZGER, J. M., ZHU, Y., JUHL, K., ZHANG, B. B., THORNBERRY, N. A., REITMAN, M. L. & ZHOU, Y. P. 2011. Bombesin receptor subtype-3 (BRS-3) regulates glucose-stimulated insulin secretion in pancreatic islets across multiple species. *Endocrinology,* 152**,** 4106-15.

FILIPPATOS, T. D., PANAGIOTOPOULOU, T. V. & ELISAF, M. S. 2014. Adverse Effects of GLP-1 Receptor Agonists. *Rev Diabet Stud,* 11**,** 202-30.

FOULIS, A. K. & STEWART, J. A. 1984. The pancreas in recent-onset type 1 (insulin-dependent) diabetes mellitus: insulin content of islets, insulitis and associated changes in the exocrine acinar tissue. *Diabetologia,* 26**,** 456-61.

FREDRIKSSON, R., LAGERSTROM, M. C., LUNDIN, L. G. & SCHIOTH, H. B. 2003. The G-protein-coupled receptors in the human genome form five main families. Phylogenetic analysis, paralogon groups, and fingerprints. *Mol Pharmacol,* 63**,** 1256-72.

FULLERTON, M. D., GALIC, S., MARCINKO, K., SIKKEMA, S., PULINILKUNNIL, T., CHEN, Z. P., O'NEILL, H. M., FORD, R. J., PALANIVEL, R., O'BRIEN, M., HARDIE, D. G., MACAULAY, S. L., SCHERTZER, J. D., DYCK, J. R., VAN DENDEREN, B. J., KEMP, B. E. & STEINBERG, G. R. 2013. Single phosphorylation sites in Acc1 and Acc2 regulate lipid homeostasis and the insulin-sensitizing effects of metformin. *Nat Med,* 19**,** 1649-54.

GARLAND, S. L. 2013. Are GPCRs still a source of new targets? *J Biomol Screen,* 18**,** 947-66.

GILLIES, P. S., FIGGITT, D. P. & LAMB, H. M. 2000. Insulin glargine. *Drugs,* 59**,** 253-60; discussion 261-2.

GOVERS, R. 2014. Molecular mechanisms of GLUT4 regulation in adipocytes. *Diabetes Metab,* 40**,** 400-10.

GOYVAERTS, L., SCHRAENEN, A. & SCHUIT, F. 2016. Serotonin competence of mouse beta cells during pregnancy. *Diabetologia,* 59**,** 1356-63.

GREEN, J. A., SCHMID, C. L., BLEY, E., MONSMA, P. C., BROWN, A., BOHN, L. M. & MYKYTYN, K. 2016. Recruitment of beta-Arrestin into Neuronal Cilia Modulates Somatostatin Receptor Subtype 3 Ciliary Localization. *Mol Cell Biol,* 36**,** 223-35.

GREGERSEN, S., THOMSEN, J. L. & HERMANSEN, K. 2000. Endothelin-1 (ET-1)-potentiated insulin secretion: involvement of protein kinase C and the ET(A) receptor subtype. *Metabolism,* 49**,** 264-9.

GRIBBLE, F. M. 2012. The gut endocrine system as a coordinator of postprandial nutrient homoeostasis. *Proc Nutr Soc,* 71**,** 456-62.

GRODSKY, G. M., CURRY, D., LANDAHL, H. & BENNETT, L. 1969. [Further studies on the dynamic aspects of insulin release in vitro with evidence for a two-compartmental storage system]. *Acta Diabetol Lat,* 6 Suppl 1**,** 554-78.

GROOP, L. C., BONADONNA, R. C., DELPRATO, S., RATHEISER, K., ZYCK, K., FERRANNINI, E. & DEFRONZO, R. A. 1989. Glucose and free fatty acid metabolism in non-insulin-dependent diabetes mellitus. Evidence for multiple sites of insulin resistance. *J Clin Invest,* 84**,** 205-13.

GUARIGUATA, L. 2012. By the numbers: new estimates from the IDF Diabetes Atlas Update for 2012. *Diabetes Res Clin Pract,* 98**,** 524-5.

HALBAN, P. A. 1991. Structural domains and molecular lifestyles of insulin and its precursors in the pancreatic beta cell. *Diabetologia,* 34**,** 767-78.

HAN, J., ZHANG, M., FROESE, S., DAI, F. F., ROBITAILLE, M., BHATTACHARJEE, A., HUANG, X., JIA, W., ANGERS, S., WHEELER, M. B. & WEI, L. 2015. The Identification of Novel Protein-Protein Interactions in Liver that Affect Glucagon Receptor Activity. *PLoS One,* 10**,** e0129226.

HARA, T. & NAKAYAMA, Y. 2009. CXCL14 and insulin action. *Vitam Horm,* 80**,** 107-23.

HARA, T. & TANEGASHIMA, K. 2012. Pleiotropic functions of the CXC-type chemokine CXCL14 in mammals. *J Biochem,* 151**,** 469-76.

HARA, T. & TANEGASHIMA, K. 2014. CXCL14 antagonizes the CXCL12-CXCR4 signaling axis. *Biomol Concepts,* 5**,** 167-73.

HAUGE-EVANS, A. C., RICHARDSON, C. C., MILNE, H. M., CHRISTIE, M. R., PERSAUD, S. J. & JONES, P. M. 2006. A role for kisspeptin in islet function. *Diabetologia,* 49**,** 2131-5.

HAUNER, H. 2002. The mode of action of thiazolidinediones. *Diabetes Metab Res Rev,* 18 Suppl 2**,** S10-5.

HERMANSEN, K., DAVIES, M., DEREZINSKI, T., MARTINEZ RAVN, G., CLAUSON, P. & HOME, P. 2006. A 26-week, randomized, parallel, treat-to-target trial comparing insulin detemir with NPH insulin as add-on therapy to oral glucose-lowering drugs in insulin-naive people with type 2 diabetes. *Diabetes Care,* 29**,** 1269-74.

HOLST, J. J. 1994. Glucagonlike peptide 1: a newly discovered gastrointestinal hormone. *Gastroenterology,* 107**,** 1848-55.

HOLST, J. J. 2007. The physiology of glucagon-like peptide 1. *Physiol Rev,* 87**,** 1409-39.

HORN, F., WEARE, J., BEUKERS, M. W., HORSCH, S., BAIROCH, A., CHEN, W., EDVARDSEN, O., CAMPAGNE, F. & VRIEND, G. 1998. GPCRDB: an information system for G protein-coupled receptors. *Nucleic Acids Res,* 26**,** 275-9.

HOYER, S. 1990. Brain glucose and energy metabolism during normal aging. *Aging (Milano),* 2**,** 245-58.

HUANG, G. C., ZHAO, M., JONES, P., PERSAUD, S., RAMRACHEYA, R., LOBNER, K., CHRISTIE, M. R., BANGA, J. P., PEAKMAN, M., SIRINIVSAN, P., RELA, M., HEATON, N. & AMIEL, S. 2004. The development of new density gradient media for purifying human islets and islet-quality assessments. *Transplantation,* 77**,** 143-5.

HUANG, Z. 2002. Structure, function and modulation of chemokine receptors: members of the g-protein-coupled receptor superfamily. *Mini Rev Med Chem,* 2**,** 373-83.

HUGHES, S. J., SMITH, H. & ASHCROFT, S. J. 1993. Characterization of Ca2+/calmodulin-dependent protein kinase in rat pancreatic islets. *Biochem J,* 289 (Pt 3)**,** 795-800.

HUISING, M. O., VAN DER MEULEN, T., VAUGHAN, J. M., MATSUMOTO, M., DONALDSON, C. J., PARK, H., BILLESTRUP, N. & VALE, W. W. 2010. CRFR1 is expressed on pancreatic beta cells, promotes beta cell

proliferation, and potentiates insulin secretion in a glucose-dependent manner. *Proc Natl Acad Sci U S A,* 107**,** 912-7.

HUR, E. M. & KIM, K. T. 2002. G protein-coupled receptor signalling and cross-talk: achieving rapidity and specificity. *Cell Signal,* 14**,** 397-405.

HUTTON, J. C. 1982. The internal pH and membrane potential of the insulin-secretory granule. *Biochem J,* 204**,** 171-8.

INTERNATIONAL HYPOGLYCAEMIA STUDY, G. 2015. Minimizing Hypoglycemia in Diabetes. *Diabetes Care,* 38**,** 1583-91.

IPP, E., DOBBS, R. E., ARIMURA, A., VALE, W., HARRIS, V. & UNGER, R. H. 1977. Release of immunoreactive somatostatin from the pancreas in response to glucose, amino acids, pancreozymin-cholecystokinin, and tolbutamide. *J Clin Invest,* 60**,** 760-5.

IRWIN, N. & FLATT, P. R. 2009. Therapeutic potential for GIP receptor agonists and antagonists. *Best Pract Res Clin Endocrinol Metab,* 23**,** 499-512.

IRWIN, N. & FLATT, P. R. 2015. New perspectives on exploitation of incretin peptides for the treatment of diabetes and related disorders. *World J Diabetes,* 6**,** 1285-95.

IWANAGA, T., MIKI, T. & TAKAHASHI-IWANAGA, H. 2011. Restricted expression of somatostatin receptor 3 to primary cilia in the pancreatic islets and adenohypophysis of mice. *Biomed Res,* 32**,** 73-81.

IWASAKI, K., HARADA, N., SASAKI, K., YAMANE, S., IIDA, K., SUZUKI, K., HAMASAKI, A., NASTESKA, D., SHIBUE, K., JOO, E., HARADA, T., HASHIMOTO, T., ASAKAWA, Y., HIRASAWA, A. & INAGAKI, N. 2015. Free fatty acid receptor GPR120 is highly expressed in enteroendocrine K cells of the upper small intestine and has a critical role in GIP secretion after fat ingestion. *Endocrinology,* 156**,** 837-46.

JACKSON, S., LE ROUX, C. W. & DOCHERTY, N. G. 2014. Bariatric surgery and microvascular complications of type 2 diabetes mellitus. *Curr Atheroscler Rep,* 16**,** 453.

JANSSON, L., BARBU, A., BODIN, B., DROTT, C. J., ESPES, D., GAO, X., GRAPENSPARR, L., KALLSKOG, O., LAU, J., LILJEBACK, H., PALM, F., QUACH, M., SANDBERG, M., STROMBERG, V., ULLSTEN, S. & CARLSSON, P. O. 2016. Pancreatic islet blood flow and its measurement. *Ups J Med Sci,* 121**,** 81-95.

JASTRZEBSKA, B. 2013. GPCR: G protein complexes--the fundamental signaling assembly. *Amino Acids,* 45**,** 1303-14.

JIANG, G. & ZHANG, B. B. 2003. Glucagon and regulation of glucose metabolism. *Am J Physiol Endocrinol Metab,* 284**,** E671-8.

JO, J., CHOI, M. Y. & KOH, D. S. 2007. Size distribution of mouse Langerhans islets. *Biophys J,* 93**,** 2655-66.

JONES, P. M. & PERSAUD, S. J. 1998. Ca(2+)-induced loss of Ca2+/calmodulin-dependent protein kinase II activity in pancreatic beta-cells. *Am J Physiol,* 274**,** E708-15.

JONES, P. M., PERSAUD, S. J. & HOWELL, S. L. 1992. Ca2(+)-induced insulin secretion from electrically permeabilized islets. Loss of the Ca2(+)-induced secretory response is accompanied by loss of Ca2(+)-induced protein phosphorylation. *Biochem J,* 285 (Pt 3)**,** 973-8.

KAHN, S. E., COOPER, M. E. & DEL PRATO, S. 2014. Pathophysiology and treatment of type 2 diabetes: perspectives on the past, present, and future. *Lancet,* 383**,** 1068-83.

KAILEY, B., VAN DE BUNT, M., CHELEY, S., JOHNSON, P. R., MACDONALD, P. E., GLOYN, A. L., RORSMAN, P. & BRAUN, M. 2012. SSTR2 is the functionally dominant somatostatin receptor in human pancreatic beta- and alpha-cells. *Am J Physiol Endocrinol Metab,* 303**,** E1107-16.

KATO, T. & NODE, K. 2014. Therapeutic potential of alpha-glucosidase inhibitors to prevent postprandial endothelial dysfunction. *Int Heart J,* 55**,** 386-90.

KATZ, L. B., GAMBALE, J. J., ROTHENBERG, P. L., VANAPALLI, S. R., VACCARO, N., XI, L., SARICH, T. C. & STEIN, P. P. 2012. Effects of JNJ-38431055, a novel GPR119 receptor agonist, in randomized, double-blind, placebo-controlled studies in subjects with type 2 diabetes. *Diabetes Obes Metab,* 14**,** 709-16.

KAWAI, K., YOKOTA, C., OHASHI, S., WATANABE, Y. & YAMASHITA, K. 1995. Evidence that glucagon stimulates insulin secretion through its own receptor in rats. *Diabetologia,* 38**,** 274-6.

KELLY, T. N., BAZZANO, L. A., FONSECA, V. A., THETHI, T. K., REYNOLDS, K. & HE, J. 2009. Systematic review: glucose control and cardiovascular disease in type 2 diabetes. *Ann Intern Med,* 151**,** 394-403.

KHARROUBI, A. T. & DARWISH, H. M. 2015. Diabetes mellitus: The epidemic of the century. *World J Diabetes,* 6**,** 850-67.

KIM, A., MILLER, K., JO, J., KILIMNIK, G., WOJCIK, P. & HARA, M. 2009. Islet architecture: A comparative study. *Islets,* 1**,** 129-36.

KOLAKOWSKI, L. F., JR. 1994. GCRDb: a G-protein-coupled receptor database. *Receptors Channels,* 2**,** 1-7.

KRISTIANSEN, O. P., LARSEN, Z. M. & POCIOT, F. 2000. CTLA-4 in autoimmune diseases--a general susceptibility gene to autoimmunity? *Genes Immun,* 1**,** 170-84.

KROEZE, W. K., SHEFFLER, D. J. & ROTH, B. L. 2003. G-protein-coupled receptors at a glance. *J Cell Sci,* 116**,** 4867-9.

KUFAREVA, I., SALANGA, C. L. & HANDEL, T. M. 2015. Chemokine and chemokine receptor structure and interactions: implications for therapeutic strategies. *Immunol Cell Biol,* 93**,** 372-83.

KUTLU, B., BURDICK, D., BAXTER, D., RASSCHAERT, J., FLAMEZ, D., EIZIRIK, D. L., WELSH, N., GOODMAN, N. & HOOD, L. 2009. Detailed transcriptome atlas of the pancreatic beta cell. *BMC Med Genomics,* 2**,** 3.

LAMOS, E. M., YOUNK, L. M. & DAVIS, S. N. 2013. Canagliflozin , an inhibitor of sodium-glucose cotransporter 2, for the treatment of type 2 diabetes mellitus. *Expert Opin Drug Metab Toxicol,* 9**,** 763-75.

LEETE, P., WILLCOX, A., KROGVOLD, L., DAHL-JORGENSEN, K., FOULIS, A. K., RICHARDSON, S. J. & MORGAN, N. G. 2016. Differential Insulitic Profiles Determine the Extent of beta-Cell Destruction and the Age at Onset of Type 1 Diabetes. *Diabetes,* 65**,** 1362-9.

LETURQUE, A., BROT-LAROCHE, E. & LE GALL, M. 2009. GLUT2 mutations, translocation, and receptor function in diet sugar managing. *Am J Physiol Endocrinol Metab,* 296**,** E985-92.

LI, C., BOWE, J. E., JONES, P. M. & PERSAUD, S. J. 2010. Expression and function of cannabinoid receptors in mouse islets. *Islets,* 2**,** 293-302.

LI, C., CHEN, P., VAUGHAN, J., BLOUNT, A., CHEN, A., JAMIESON, P. M., RIVIER, J., SMITH, M. S. & VALE, W. 2003. Urocortin III is expressed in pancreatic beta-cells and stimulates insulin and glucagon secretion. *Endocrinology,* 144**,** 3216-24.

LI, C., CHEN, P., VAUGHAN, J., LEE, K. F. & VALE, W. 2007. Urocortin 3 regulates glucose-stimulated insulin secretion and energy homeostasis. *Proc Natl Acad Sci U S A,* 104**,** 4206-11.

LIH, A., HIBBERT, E., WONG, T., GIRGIS, C. M., GARG, N. & CARTER, J. N. 2010. The role of insulin glulisine to improve glycemic control in children with diabetes mellitus. *Diabetes Metab Syndr Obes,* 3**,** 403-12.

LIU, B., HASSAN, Z., AMISTEN, S., KING, A. J., BOWE, J. E., HUANG, G. C., JONES, P. M. & PERSAUD, S. J. 2013. The novel chemokine receptor, G-protein-coupled receptor 75, is expressed by islets and is coupled to stimulation of insulin secretion and improved glucose homeostasis. *Diabetologia,* 56**,** 2467-76.

LOHSE, M. J., MAIELLARO, I. & CALEBIRO, D. 2014. Kinetics and mechanism of G protein-coupled receptor activation. *Curr Opin Cell Biol,* 27**,** 87-93.

LUDVIGSEN, E., OLSSON, R., STRIDSBERG, M., JANSON, E. T. & SANDLER, S. 2004. Expression and distribution of somatostatin receptor subtypes in the pancreatic islets of mice and rats. *J Histochem Cytochem,* 52**,** 391-400.

LYSSENKO, V., LUPI, R., MARCHETTI, P., DEL GUERRA, S., ORHO-MELANDER, M., ALMGREN, P., SJOGREN, M., LING, C., ERIKSSON, K. F., LETHAGEN, A. L., MANCARELLA, R., BERGLUND, G., TUOMI, T., NILSSON, P., DEL PRATO, S. & GROOP, L. 2007. Mechanisms by which common variants in the TCF7L2 gene increase risk of type 2 diabetes. *J Clin Invest,* 117**,** 2155-63.

MA, X., GUAN, Y. & HUA, X. 2014. Glucagon-like peptide 1-potentiated insulin secretion and proliferation of pancreatic beta-cells. *J Diabetes,* 6**,** 394-402.

MACDONALD, M. J. & KOWLURU, A. 1982. Calcium-calmodulin-dependent myosin phosphorylation by pancreatic islets. *Diabetes,* 31**,** 566-70.

MATSCHINSKY, F. M. 1996. Banting Lecture 1995. A lesson in metabolic regulation inspired by the glucokinase glucose sensor paradigm. *Diabetes,* 45**,** 223-41.

MEETOO, D., MCGOVERN, P. & SAFADI, R. 2007. An epidemiological overview of diabetes across the world. *Br J Nurs,* 16**,** 1002-7.

MENGE, B. A., TANNAPFEL, A., BELYAEV, O., DRESCHER, R., MULLER, C., UHL, W., SCHMIDT, W. E. & MEIER, J. J. 2008. Partial pancreatectomy in adult humans does not provoke beta-cell regeneration. *Diabetes,* 57**,** 142-9.

MESSAGER, S., CHATZIDAKI, E. E., MA, D., HENDRICK, A. G., ZAHN, D., DIXON, J., THRESHER, R. R., MALINGE, I., LOMET, D., CARLTON, M. B., COLLEDGE, W. H., CARATY, A. & APARICIO, S. A. 2005. Kisspeptin directly stimulates gonadotropin-releasing hormone release via G protein-coupled receptor 54. *Proc Natl Acad Sci U S A,* 102**,** 1761-6.

METZ, S., VANROLLINS, M., STRIFE, R., FUJIMOTO, W. & ROBERTSON, R. P. 1983. Lipoxygenase pathway in islet endocrine cells. Oxidative metabolism of arachidonic acid promotes insulin release. *J Clin Invest,* 71**,** 1191-205.

METZ, S. A., MURPHY, R. C. & FUJIMOTO, W. 1984. Effects on glucose-induced insulin secretion of lipoxygenase-derived metabolites of arachidonic acid. *Diabetes,* 33**,** 119-24.

MIYAZAKI, J., ARAKI, K., YAMATO, E., IKEGAMI, H., ASANO, T., SHIBASAKI, Y., OKA, Y. & YAMAMURA, K. 1990. Establishment of a pancreatic beta cell line that retains glucose-inducible insulin secretion: special reference to expression of glucose transporter isoforms. *Endocrinology,* 127**,** 126-32.

MOLLER, S., VILO, J. & CRONING, M. D. 2001. Prediction of the coupling specificity of G protein coupled receptors to their G proteins. *Bioinformatics,* 17 Suppl 1**,** S174-81.

MOREIRA, I. S. 2014. Structural features of the G-protein/GPCR interactions. *Biochim Biophys Acta,* 1840**,** 16-33.

MORGAN, N. G., LEETE, P., FOULIS, A. K. & RICHARDSON, S. J. 2014. Islet inflammation in human type 1 diabetes mellitus. *IUBMB Life,* 66**,** 723-34.

MUECKLER, M. 1994. Facilitative glucose transporters. *Eur J Biochem,* 219**,** 713-25.

MUIR, A. I., CHAMBERLAIN, L., ELSHOURBAGY, N. A., MICHALOVICH, D., MOORE, D. J., CALAMARI, A., SZEKERES, P. G., SARAU, H. M., CHAMBERS, J. K., MURDOCK, P., STEPLEWSKI, K., SHABON, U., MILLER, J. E., MIDDLETON, S. E., DARKER, J. G., LARMINIE, C. G., WILSON, S., BERGSMA, D. J., EMSON, P., FAULL, R., PHILPOTT, K. L. & HARRISON, D. C. 2001. AXOR12, a novel human G protein-coupled receptor, activated by the peptide KiSS-1. *J Biol Chem,* 276**,** 28969-75.

NARA, N., NAKAYAMA, Y., OKAMOTO, S., TAMURA, H., KIYONO, M., MURAOKA, M., TANAKA, K., TAYA, C., SHITARA, H., ISHII, R., YONEKAWA, H., MINOKOSHI, Y. & HARA, T. 2007. Disruption of CXC motif chemokine ligand-14 in mice ameliorates obesity-induced insulin resistance. *J Biol Chem,* 282**,** 30794-803.

NESHER, R. & CERASI, E. 1987. Biphasic insulin release as the expression of combined inhibitory and potentiating effects of glucose. *Endocrinology,* 121**,** 1017-24.

NESHER, R. & CERASI, E. 2002. Modeling phasic insulin release: immediate and time-dependent effects of glucose. *Diabetes,* 51 Suppl 1**,** S53-9.

NESSA, A., RAHMAN, S. A. & HUSSAIN, K. 2016. Hyperinsulinemic Hypoglycemia - The Molecular Mechanisms. *Front Endocrinol (Lausanne),* 7**,** 29.

NOTKINS, A. L. & LERNMARK, A. 2001. Autoimmune type 1 diabetes: resolved and unresolved issues. *J Clin Invest,* 108**,** 1247-52.

NYMAN, L. R., WELLS, K. S., HEAD, W. S., MCCAUGHEY, M., FORD, E., BRISSOVA, M., PISTON, D. W. & POWERS, A. C. 2008. Real-time, multidimensional in vivo imaging used to investigate blood flow in mouse pancreatic islets. *J Clin Invest,* 118**,** 3790-7.

OH DA, Y. & OLEFSKY, J. M. 2016. G protein-coupled receptors as targets for anti-diabetic therapeutics. *Nat Rev Drug Discov,* 15**,** 161-72.

OH, D. Y., TALUKDAR, S., BAE, E. J., IMAMURA, T., MORINAGA, H., FAN, W., LI, P., LU, W. J., WATKINS, S. M. & OLEFSKY, J. M. 2010. GPR120 is an omega-3 fatty acid receptor mediating potent anti-inflammatory and insulin-sensitizing effects. *Cell,* 142**,** 687-98.

OHARA-IMAIZUMI, M., KIM, H., YOSHIDA, M., FUJIWARA, T., AOYAGI, K., TOYOFUKU, Y., NAKAMICHI, Y., NISHIWAKI, C., OKAMURA, T., UCHIDA, T., FUJITANI, Y., AKAGAWA, K., KAKEI, M., WATADA, H., GERMAN, M. S. & NAGAMATSU, S. 2013. Serotonin regulates glucose-stimulated insulin secretion from pancreatic beta cells during pregnancy. *Proc Natl Acad Sci U S A,* 110**,** 19420-5.

ORCI, L., VASSALLI, J. D. & PERRELET, A. 1988. The insulin factory. *Sci Am,* 259**,** 85-94.

OTTE, M., KLIEWER, A., SCHUTZ, D., REIMANN, C., SCHULZ, S. & STUMM, R. 2014. CXCL14 is no direct modulator of CXCR4. *FEBS Lett,* 588**,** 4769-75.

PERSAUD, S. J. & BEWICK, G. A. 2014. Peptide YY: more than just an appetite regulator. *Diabetologia,* 57**,** 1762-9.

PERSAUD, S. J. & JONES, P. M. 1993. The involvement of protein kinase C in glucose-stimulated insulin secretion. *Biochem Soc Trans,* 21**,** 428S.

PERSAUD, S. J., JONES, P. M. & HOWELL, S. L. 1991. Activation of protein kinase C is not required for glyceraldehyde-stimulated insulin secretion from rat islets. *Biochim Biophys Acta,* 1095**,** 183-5.

PERSAUD, S. J., LIU, B., SAMPAIO, H. B., JONES, P. M. & MULLER, D. S. 2011. Calcium/calmodulin-dependent kinase IV controls glucose-induced Irs2 expression in mouse beta cells via activation of cAMP response element-binding protein. *Diabetologia,* 54**,** 1109-20.

PFAFFL, M. W. 2001. A new mathematical model for relative quantification in real-time RT-PCR. *Nucleic Acids Res,* 29**,** e45.

PRASAD-REDDY, L. & ISAACS, D. 2015. A clinical review of GLP-1 receptor agonists: efficacy and safety in diabetes and beyond. *Drugs Context,* 4**,** 212283.

QUESADA, I., TUDURI, E., RIPOLL, C. & NADAL, A. 2008. Physiology of the pancreatic alpha-cell and glucagon secretion: role in glucose homeostasis and diabetes. *J Endocrinol,* 199**,** 5-19.

RAHIER, J., GUIOT, Y., GOEBBELS, R. M., SEMPOUX, C. & HENQUIN, J. C. 2008. Pancreatic beta-cell mass in European subjects with type 2 diabetes. *Diabetes Obes Metab,* 10 Suppl 4**,** 32-42.

RAJAGOPAL, S., BASSONI, D. L., CAMPBELL, J. J., GERARD, N. P., GERARD, C. & WEHRMAN, T. S. 2013. Biased agonism as a mechanism for differential signaling by chemokine receptors. *J Biol Chem,* 288**,** 35039-48.

RANKOVIC, Z., BRUST, T. F. & BOHN, L. M. 2016. Biased agonism: An emerging paradigm in GPCR drug discovery. *Bioorg Med Chem Lett,* 26**,** 241-50.

RASK-ANDERSEN, M., ALMEN, M. S. & SCHIOTH, H. B. 2011. Trends in the exploitation of novel drug targets. *Nat Rev Drug Discov,* 10**,** 579-90.

REGARD, J. B., SATO, I. T. & COUGHLIN, S. R. 2008. Anatomical profiling of G protein-coupled receptor expression. *Cell,* 135**,** 561-71.

REIMANN, F. & GRIBBLE, F. M. 2016. G protein-coupled receptors as new therapeutic targets for type 2 diabetes. *Diabetologia,* 59**,** 229-33.

RITTER, K., BUNING, C., HALLAND, N., POVERLEIN, C. & SCHWINK, L. 2016. G Protein-Coupled Receptor 119 (GPR119) Agonists for the Treatment of Diabetes: Recent Progress and Prevailing Challenges. *J Med Chem,* 59**,** 3579-92.

ROBERTSON, N., JAZAYERI, A., ERREY, J., BAIG, A., HURRELL, E., ZHUKOV, A., LANGMEAD, C. J., WEIR, M. & MARSHALL, F. H. 2011. The properties of thermostabilised G protein-coupled receptors (StaRs) and their use in drug discovery. *Neuropharmacology,* 60**,** 36-44.

RODERIGO-MILNE, H., HAUGE-EVANS, A. C., PERSAUD, S. J. & JONES, P. M. 2002. Differential expression of insulin genes 1 and 2 in MIN6 cells and pseudoislets. *Biochem Biophys Res Commun,* 296**,** 589-95.

ROHRBORN, D., WRONKOWITZ, N. & ECKEL, J. 2015. DPP4 in Diabetes. *Front Immunol,* 6**,** 386.

ROMERO-ZERBO, S. Y., RAFACHO, A., DIAZ-ARTEAGA, A., SUAREZ, J., QUESADA, I., IMBERNON, M., ROSS, R. A., DIEGUEZ, C., RODRIGUEZ DE FONSECA, F., NOGUEIRAS, R., NADAL, A. & BERMUDEZ-SILVA, F. J. 2011. A role for the putative cannabinoid receptor GPR55 in the islets of Langerhans. *J Endocrinol,* 211**,** 177-85.

RUTTER, G. A. 2014. Dorothy Hodgkin Lecture 2014. Understanding genes identified by genome-wide association studies for type 2 diabetes. *Diabet Med,* 31**,** 1480-7.

RUTTER, G. A., PULLEN, T. J., HODSON, D. J. & MARTINEZ-SANCHEZ, A. 2015. Pancreatic beta-cell identity, glucose sensing and the control of insulin secretion. *Biochem J,* 466**,** 203-18.

RYAN, E. A., LAKEY, J. R., RAJOTTE, R. V., KORBUTT, G. S., KIN, T., IMES, S., RABINOVITCH, A., ELLIOTT, J. F., BIGAM, D., KNETEMAN, N. M., WARNOCK, G. L., LARSEN, I. & SHAPIRO, A. M. 2001. Clinical outcomes and insulin secretion after islet transplantation with the Edmonton protocol. *Diabetes,* 50**,** 710-9.

RYS, P., PANKIEWICZ, O., LACH, K., KWASKOWSKI, A., SKRZEKOWSKA-BARAN, I. & MALECKI, M. T. 2011. Efficacy and safety comparison of rapid-acting insulin aspart and regular human insulin in the treatment of type 1 and type 2 diabetes mellitus: a systematic review. *Diabetes Metab,* 37**,** 190-200.

SANLIOGLU, A. D., ALTUNBAS, H. A., BALCI, M. K., GRIFFITH, T. S. & SANLIOGLU, S. 2013. Clinical utility of insulin and insulin analogs. *Islets,* 5**,** 67-78.

SCHEEN, A. J. 2015. Safety of dipeptidyl peptidase-4 inhibitors for treating type 2 diabetes. *Expert Opin Drug Saf,* 14**,** 505-24.

SCHIOTH, H. B. & FREDRIKSSON, R. 2005. The GRAFS classification system of G-protein coupled receptors in comparative perspective. *Gen Comp Endocrinol,* 142**,** 94-101.

SEINO, S., TAKAHASHI, H., TAKAHASHI, T. & SHIBASAKI, T. 2012. Treating diabetes today: a matter of selectivity of sulphonylureas. *Diabetes Obes Metab,* 14 Suppl 1**,** 9-13.

SESTI, G. 2000. Insulin receptor substrate polymorphisms and type 2 diabetes mellitus. *Pharmacogenomics,* 1**,** 343-57.

SKELIN, M., RUPNIK, M. & CENCIC, A. 2010. Pancreatic beta cell lines and their applications in diabetes mellitus research. *ALTEX,* 27**,** 105-13.

SLADEK, R., ROCHELEAU, G., RUNG, J., DINA, C., SHEN, L., SERRE, D., BOUTIN, P., VINCENT, D., BELISLE, A., HADJADJ, S., BALKAU, B., HEUDE, B., CHARPENTIER, G., HUDSON, T. J., MONTPETIT, A., PSHEZHETSKY, A. V., PRENTKI, M., POSNER, B. I., BALDING, D. J., MEYRE, D., POLYCHRONAKOS, C. & FROGUEL, P. 2007. A genome-wide association study identifies novel risk loci for type 2 diabetes. *Nature,* 445**,** 881-5.

SONI, A., AMISTEN, S., RORSMAN, P. & SALEHI, A. 2013. GPRC5B a putative glutamate-receptor candidate is negative modulator of insulin secretion. *Biochem Biophys Res Commun,* 441**,** 643-8.

SPELLMAN, C. W. 2010. Pathophysiology of type 2 diabetes: targeting islet cell dysfunction. *J Am Osteopath Assoc,* 110**,** S2-7.

STEEN, A., LARSEN, O., THIELE, S. & ROSENKILDE, M. M. 2014. Biased and g protein-independent signaling of chemokine receptors. *Front Immunol,* 5**,** 277.

STEINER, D. J., KIM, A., MILLER, K. & HARA, M. 2010. Pancreatic islet plasticity: interspecies comparison of islet architecture and composition. *Islets,* 2**,** 135-45.

STIENSTRA, R., DUVAL, C., MULLER, M. & KERSTEN, S. 2007. PPARs, Obesity, and Inflammation. *PPAR Res,* 2007**,** 95974.

STONE, V. M., DHAYAL, S., BROCKLEHURST, K. J., LENAGHAN, C., SORHEDE WINZELL, M., HAMMAR, M., XU, X., SMITH, D. M. & MORGAN, N. G. 2014. GPR120 (FFAR4) is preferentially expressed in pancreatic delta cells and regulates somatostatin secretion from murine islets of Langerhans. *Diabetologia,* 57**,** 1182-91.

STROWSKI, M. Z., PARMAR, R. M., BLAKE, A. D. & SCHAEFFER, J. M. 2000. Somatostatin inhibits insulin and glucagon secretion via two receptors subtypes: an in vitro study of pancreatic islets from somatostatin receptor 2 knockout mice. *Endocrinology,* 141**,** 111-7.

SUDHOF, T. C. & ROTHMAN, J. E. 2009. Membrane fusion: grappling with SNARE and SM proteins. *Science,* 323**,** 474-7.

SUZUKI, H. & YAMAMOTO, T. 2015. CXCL14-Like Immunoreactivity Exists in Somatostatin-Containing Cells of Mouse Pancreas. *Acta Histochem Cytochem,* 48**,** 173-8.

TAKADA, I. & MAKISHIMA, M. 2015. PPARgamma ligands and their therapeutic applications: a patent review (2008 - 2014). *Expert Opin Ther Pat,* 25**,** 175-91.

TAKAHASHI, K., GHATEI, M. A., LAM, H. C., O'HALLORAN, D. J. & BLOOM, S. R. 1990. Elevated plasma endothelin in patients with diabetes mellitus. *Diabetologia,* 33**,** 306-10.

TAKAHASHI, M., TAKAHASHI, Y., TAKAHASHI, K., ZOLOTARYOV, F. N., HONG, K. S., IIDA, K., OKIMURA, Y., KAJI, H. & CHIHARA, K. 2007. CXCL14 enhances insulin-dependent glucose uptake in adipocytes and is related to high-fat diet-induced obesity. *Biochem Biophys Res Commun,* 364**,** 1037-42.

TANEGASHIMA, K., OKAMOTO, S., NAKAYAMA, Y., TAYA, C., SHITARA, H., ISHII, R., YONEKAWA, H., MINOKOSHI, Y. & HARA, T. 2010. CXCL14 deficiency in mice attenuates obesity and inhibits feeding behavior in a novel environment. *PLoS One,* 5**,** e10321.

TANEGASHIMA, K., SUZUKI, K., NAKAYAMA, Y., TSUJI, K., SHIGENAGA, A., OTAKA, A. & HARA, T. 2013. CXCL14 is a natural inhibitor of the CXCL12-CXCR4 signaling axis. *FEBS Lett,* 587**,** 1731-5.

TANG, C., AHMED, K., GILLE, A., LU, S., GRONE, H. J., TUNARU, S. & OFFERMANNS, S. 2015. Loss of FFA2 and FFA3 increases insulin secretion and improves glucose tolerance in type 2 diabetes. *Nat Med,* 21**,** 173-7.

TANG, X. L., WANG, Y., LI, D. L., LUO, J. & LIU, M. Y. 2012. Orphan G protein-coupled receptors (GPCRs): biological functions and potential drug targets. *Acta Pharmacol Sin,* 33**,** 363-71.

TATULIAN, S. A. 2015. Structural Dynamics of Insulin Receptor and Transmembrane Signaling. *Biochemistry,* 54**,** 5523-32.

TENGHOLM, A. 2012. Cyclic AMP dynamics in the pancreatic beta-cell. *Ups J Med Sci,* 117**,** 355-69.

THORENS, B. 2001. GLUT2 in pancreatic and extra-pancreatic gluco-detection (review). *Mol Membr Biol,* 18**,** 265-73.

THORENS, B. 2015. GLUT2, glucose sensing and glucose homeostasis. *Diabetologia,* 58**,** 221-32.

TODD, J. A., BELL, J. I. & MCDEVITT, H. O. 1987. HLA-DQ beta gene contributes to susceptibility and resistance to insulin-dependent diabetes mellitus. *Nature,* 329**,** 599-604.

TOMKIN, G. H. 2014. Treatment of type 2 diabetes, lifestyle, GLP1 agonists and DPP4 inhibitors. *World J Diabetes,* 5**,** 636-50.

TRAN, L., ZIELINSKI, A., ROACH, A. H., JENDE, J. A., HOUSEHOLDER, A. M., COLE, E. E., ATWAY, S. A., AMORNYARD, M., ACCURSI, M. L., SHIEH, S. W. & THOMPSON, E. E. 2015. Pharmacologic treatment of type 2 diabetes: oral medications. *Ann Pharmacother,* 49**,** 540-56.

TRUJILLO, J. M. & NUFFER, W. 2014. GLP-1 receptor agonists for type 2 diabetes mellitus: recent developments and emerging agents. *Pharmacotherapy,* 34**,** 1174-86.

TSUNEKAWA, S., YAMAMOTO, N., TSUKAMOTO, K., ITOH, Y., KANEKO, Y., KIMURA, T., ARIYOSHI, Y., MIURA, Y., OISO, Y. & NIKI, I. 2007. Protection of pancreatic beta-cells by exendin-4 may involve the reduction of endoplasmic reticulum stress; in vivo and in vitro studies. *J Endocrinol,* 193**,** 65-74.

TUTEJA, N. 2009. Signaling through G protein coupled receptors. *Plant Signal Behav,* 4**,** 942-7.

VAN DE LAAR, F. A., LUCASSEN, P. L., AKKERMANS, R. P., VAN DE LISDONK, E. H., RUTTEN, G. E. & VAN WEEL, C. 2005. Alpha-glucosidase inhibitors for type 2 diabetes mellitus. *Cochrane Database Syst Rev***,** CD003639.

VAN DER MEULEN, T., DONALDSON, C. J., CACERES, E., HUNTER, A. E., COWING-ZITRON, C., POUND, L. D., ADAMS, M. W., ZEMBRZYCKI, A., GROVE, K. L. & HUISING, M. O. 2015. Urocortin3 mediates somatostatin-dependent negative feedback control of insulin secretion. *Nat Med,* 21**,** 769-76.

VAN GENUGTEN, R. E., VAN RAALTE, D. H. & DIAMANT, M. 2012. Dipeptidyl peptidase-4 inhibitors and preservation of pancreatic islet-cell function: a critical appraisal of the evidence. *Diabetes Obes Metab,* 14**,** 101-11.

VASILAKOU, D., KARAGIANNIS, T., ATHANASIADOU, E., MAINOU, M., LIAKOS, A., BEKIARI, E., SARIGIANNI, M., MATTHEWS, D. R. & TSAPAS, A. 2013. Sodium-glucose cotransporter 2 inhibitors for type 2 diabetes: a systematic review and meta-analysis. *Ann Intern Med,* 159**,** 262-74.

VIKMAN, J. & AHREN, B. 2009. Inhibitory effect of kisspeptins on insulin secretion from isolated mouse islets. *Diabetes Obes Metab,* 11 Suppl 4**,** 197-201.

VOLANTE, M., ALLIA, E., GUGLIOTTA, P., FUNARO, A., BROGLIO, F., DEGHENGHI, R., MUCCIOLI, G., GHIGO, E. & PAPOTTI, M. 2002. Expression of ghrelin and of the GH secretagogue receptor by pancreatic islet cells and related endocrine tumors. *J Clin Endocrinol Metab,* 87**,** 1300-8.

WALSH, M. F. & PEK, S. B. 1984. Effects of lipoxygenase and cyclooxygenase inhibitors on glucose-stimulated insulin secretion from the isolated perfused rat pancreas. *Life Sci,* 34**,** 1699-706.

WANG, P., FIASCHI-TAESCH, N. M., VASAVADA, R. C., SCOTT, D. K., GARCIA-OCANA, A. & STEWART, A. F. 2015. Diabetes mellitus--advances and challenges in human beta-cell proliferation. *Nat Rev Endocrinol,* 11**,** 201-12.

WANG, W., HUANG, P., ZHANG, L., WEI, J., XIE, Q., SUN, Q., ZHOU, X., XIE, H., ZHOU, L. & ZHENG, S. 2013. Antitumor efficacy of C-X-C motif chemokine ligand 14 in hepatocellular carcinoma in vitro and in vivo. *Cancer Sci,* 104**,** 1523-31.

WATSON, S. J., BROWN, A. J. & HOLLIDAY, N. D. 2012. Differential signaling by splice variants of the human free fatty acid receptor GPR120. *Mol Pharmacol,* 81**,** 631-42.

WEIR, G. C. & BONNER-WEIR, S. 2011. Finally! A human pancreatic beta cell line. *J Clin Invest,* 121**,** 3395-7.

WETTSCHURECK, N. & OFFERMANNS, S. 2005. Mammalian G proteins and their cell type specific functions. *Physiol Rev,* 85**,** 1159-204.

WRIGHT, E. M., LOO, D. D. & HIRAYAMA, B. A. 2011. Biology of human sodium glucose transporters. *Physiol Rev,* 91**,** 733-94.

XU, L., KITADE, H., NI, Y. & OTA, T. 2015. Roles of Chemokines and Chemokine Receptors in Obesity-Associated Insulin Resistance and Nonalcoholic Fatty Liver Disease. *Biomolecules,* 5**,** 1563-79.

YANG, S. N. & BERGGREN, P. O. 2006. The role of voltage-gated calcium channels in pancreatic beta-cell physiology and pathophysiology. *Endocr Rev,* 27**,** 621-76.

ZAMBRE, Y., LING, Z., CHEN, M. C., HOU, X., WOON, C. W., CULLER, M., TAYLOR, J. E., COY, D. H., VAN SCHRAVENDIJK, C., SCHUIT, F., PIPELEERS, D. G. & EIZIRIK, D. L. 1999. Inhibition of human pancreatic islet insulin release by receptor-selective somatostatin analogs directed to somatostatin receptor subtype 5. *Biochem Pharmacol,* 57**,** 1159-64.

ZHANG, D., ZHAO, Q. & WU, B. 2015. Structural Studies of G Protein-Coupled Receptors. *Mol Cells,* 38**,** 836-42.

ZHANG, J. H., CHUNG, T. D. & OLDENBURG, K. R. 1999. A Simple Statistical Parameter for Use in Evaluation and Validation of High Throughput Screening Assays. *J Biomol Screen,* 4**,** 67-73.

ZHOU, L., CHEN, H., XU, P., CONG, L. N., SCIACCHITANO, S., LI, Y., GRAHAM, D., JACOBS, A. R., TAYLOR, S. I. & QUON, M. J. 1999. Action of insulin receptor substrate-3 (IRS-3) and IRS-4 to stimulate translocation of GLUT4 in rat adipose cells. *Mol Endocrinol,* 13**,** 505-14.

ZIMMET, P. Z. 1999. Diabetes epidemiology as a tool to trigger diabetes research and care. *Diabetologia,* 42**,** 499-518.

ZINMAN, B., FULCHER, G., RAO, P. V., THOMAS, N., ENDAHL, L. A., JOHANSEN, T., LINDH, R., LEWIN, A., ROSENSTOCK, J., PINGET, M. & MATHIEU, C. 2011. Insulin degludec, an ultra-long-acting basal insulin, once a day or three times a week versus insulin glargine once a day in patients with type 2 diabetes: a 16-week, randomised, open-label, phase 2 trial. *Lancet,* 377**,** 924-31.

ZINMAN, B., TILDESLEY, H., CHIASSON, J. L., TSUI, E. & STRACK, T. 1997. Insulin lispro in CSII: results of a double-blind crossover study. *Diabetes,* 46**,** 440-3.